

CHARACTERISTIC ANALYSIS OF VANADIUM OXIDE FOR ENERGY AND SENSING APPLICATION

Thesis Submitted for the Award of the Degree of

DOCTOR OF PHILOSOPHY

in
Physics

By
KM Neetu Vishwakarma

Registration Number: 12021120

Supervised By

Dr. Mukesh Kumar (11512)
Department of Physics (Professor)
Lovely Professional University,
Phagwara, Punjab, India

Co-Supervised by

Dr. Ajit Kumar Sharma (24338)
Department of Chemistry (Professor)
Lovely Professional University,
Phagwara, Punjab, India



LOVELY PROFESSIONAL UNIVERSITY, PUNJAB
2025

DECLARATION

I, hereby declare that the presented work in the thesis entitled "**Characteristic Analysis of Vanadium Oxide for Energy and Sensing Application**" in fulfilment of the degree of **Doctor of Philosophy (Ph.D.)** in Physics to the Lovely Professional University Phagwara is the result of my original and independent work under the supervision of **Dr. Mukesh Kumar** and co-supervision of **Dr. Ajit Kumar Sharma**. This work has not previously formed the basis for the award of any degree, fellowship, diploma or other similar titles in this or any other University.

Dated – 25-05-2024



KM Neetu Vishwakarma

Registration No – 12021120

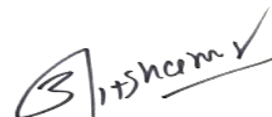
CERTIFICATE

This is to certify that the work reported on the Ph.D. thesis entitled “**Characteristic Analysis of Vanadium Oxide for Energy and Sensing Application**” submitted in fulfilment of the requirement for the award of the degree of Doctor of Philosophy Ph.D. in the Department of Physics, School of Chemical Engineering and Physical Sciences, Lovely Professional University, is a research work carried out by KM Neetu Vishwakarma (12021120) is a bonafide record of her original work carried out under my supervision and that no part of the thesis has been submitted for any other degree, diploma and equivalent course.



Signature of supervisor

Dr. Mukesh Kumar
Professor
Department of Physics
Lovely Professional University
Phagwara, Punjab



Signature of Co-supervisor

Dr. Ajit Kumar Sharma
Professor
Department of Chemistry
Lovely Professional University
Phagwara, Punjab

ABSTRACT

The field of electrochemical energy storage is a fast-moving area of technological innovation, driven by its crucial function in powering many of today's technologies. From making daily life easier with automated locks to enabling the use of common portable devices like laptops and phones, its uses are widespread. Moreover, it plays a vital part in the progress of sustainable transportation, especially in hybrid vehicles. In this dynamic field, lithium-ion batteries and, more and more, supercapacitors have become the leading technologies for meeting current energy storage needs.

Supercapacitors, also called ultracapacitor, offer a powerful middle ground in energy storage technology, sitting between the high energy of batteries and the high power of conventional capacitors. Their key strengths include rapid power delivery, extremely long lifespan in terms of charge-discharge cycles, very fast charging and discharging, and high capacitance. These devices are classified into three main types based on their charge storage methods: Electric Double Layer Capacitors (EDLCs), which store charge electrostatically at the electrode-electrolyte interface; Pseudocapacitor, which use fast, reversible chemical reactions for charge storage; and Hybrid Capacitors, which combine both electrostatic and chemical storage mechanisms for enhanced performance. While they offer many benefits, a major hurdle is increasing their energy density so they can function as the primary energy storage in challenging applications.

This PhD dissertation, "CHARACTERISTIC ANALYSIS OF VANADIUM OXIDE FOR ENERGY AND SENSING APPLICATION" explores the creation and thorough examination of potential materials for electrodes. It details how graphene oxide (GO) was made, along with the synthesis of vanadium oxide (V_2O_5) and its combination with graphene oxide (V_2O_5 -GO). The resulting V_2O_5 -graphene oxide composite underwent in-depth analysis using various techniques: Field Emission Scanning Electron Microscopy (FESEM) to study its shape, Energy Dispersive X-ray Spectroscopy (EDS) to determine its elemental makeup, Fourier Transform Infrared Spectroscopy (FTIR) to identify its functional groups, X-ray Diffraction (XRD) to analyze its crystal structure, and Raman Spectroscopy to investigate its vibrational properties. The findings from these analyses are thoroughly discussed in the thesis. The synthesized composite was then used to create electrodes, which

were rigorously tested for their electrochemical performance (using Cyclic Voltammetry - CV, Galvanostatic Charge-Discharge - GCD, and Electrochemical Impedance Spectroscopy - EIS with a Ni foam current collector) and their ability to sense gases. Later parts of the dissertation provide a complete account of these investigations.

Energy storage and gas sensing are presented in the first chapter as essential pillars of contemporary science and engineering, particularly for managing energy and monitoring the environment. The chapter illustrates the necessity of energy storage devices, such as batteries and supercapacitors, for capturing and storing energy. It then focuses on a key challenge: the development of next-generation energy storage solutions that are light, flexible, and high-performing to satisfy growing energy demands. This challenge is the primary reason researchers are investigating advanced technologies like supercapacitors (SCs), lithium-ion batteries (LIBs), and sodium-ion batteries (SIBs).

The second chapter is dedicated to a thorough review of the existing scientific literature pertinent to the research area, establishing the context and identifying knowledge gaps addressed by this work.

The third chapter dives deep into the characterization methods used in this research. It explains how the different analytical instruments work, which were crucial for evaluating the synthesized samples. These advanced tools and techniques allowed for a thorough assessment of the materials' properties, confirming that the synthesized nanoparticles met the required specifications and had the necessary characteristics for their intended use in supercapacitors and gas sensors. This detailed characterization process provided the insights needed to predict how the materials would behave and to optimize device design, ultimately leading to more efficient and dependable energy storage and sensing technologies.

The fourth chapter outlines a key objective of this doctoral research: the synthesis of V_2O_5 nanostructures via three distinct methods – Hydrothermal, Mechanochemical, and Microwave-assisted synthesis. It focuses on the comparative electrochemical analysis of these V_2O_5 samples when fabricated into electrodes and tested in a 3 M Potassium Hydroxide (KOH) aqueous electrolyte. This comparative study revealed that V_2O_5 nanoparticles synthesized using the microwave method exhibited the most promising electrochemical performance, achieving the highest specific capacitance of 122 Fg^{-1} among the three preparation routes explored.

The fifth chapter presents a comparative investigation focused on gas sensing capabilities. It analyzes sol-gel spin-coated V_2O_5 nanostructured thin films, synthesized using materials derived from both the mechanochemical and microwave methods previously explored. These films were tested for their ability to detect volatile organic compounds (VOCs) – specifically acetone, methanol, and isopropanol (IPA) – electrochemically at room temperature. The experimental findings revealed a P-type semiconductor-like behavior and demonstrated notably high sensitivity and selectivity of the V_2O_5 sensor towards acetone vapor compared to IPA or methanol vapors. Impressively fast response and recovery times were recorded: 4 seconds response and 2 seconds recovery for acetone, 12 s and 2 s for IPA, and 6 s and 3 s for methanol, respectively. This study provides valuable insights for engineering high-performance, ultrafast, and highly selective industrial-grade acetone vapor sensors.

Expanding on previous optimization efforts, the sixth chapter focuses on the preparation of V_2O_5 /graphene oxide (GO) nanostructures using a specifically optimized microwave technique. This investigation systematically explores the impact of GO loading (5, 10, and 15 wt %) on the electrochemical properties of the resulting composites. The optimized nanostructures demonstrated outstanding performance as supercapacitor electrodes, reaching a maximum specific capacitance of 737 Fg^{-1} at 1 Ag^{-1} and a remarkably low charge transfer resistance of $0.5 \text{ }\Omega$, crucial for high-power applications. Furthermore, the study reports the successful integration of a carbon coating onto the V_2O_5 through a combined microwave process. This strategically designed V_2O_5 -GO nanorod architecture exhibits highly desirable capacitive features, including high specific capacitance and low internal resistance. This work builds on earlier findings where a V_2O_5 -GO composite, prepared with microwave-derived V_2O_5 and GO via a hydrothermal route, achieved a significant specific capacitance of 736 Fg^{-1} in 3 M KOH, surpassing that of pure V_2O_5 .

In conclusion, this thesis directly compares the supercapacitor performance of pure V_2O_5 and V_2O_5 /GO electrodes, evaluated through comprehensive electrochemical testing in a 3 M KOH electrolyte. Furthermore, it revisits gas sensing measurements to clarify how post-synthesis treatments (sonication and microwave assistance) affect the resistance change and response times of the sensor materials, explicitly demonstrating the impact of these treatments on surface modification and gas detection capabilities.

ACKNOWLEDGEMENT

The acknowledgement section is the sole opportunity to thank everyone who contributed selflessly to the creation of this work, even though it was written and read at the last moment. The invaluable efforts of several people allowed this task to be completed in time. First, I owe and express my deep gratitude and heartfelt respect to God for continuously providing spiritual energy that has inspired me on this level.

I am heartily thankful to my supervisor **Dr. Mukesh Kumar**, Professor, Department of Physics and co-supervisor **Dr. Ajit Kumar Sharma**, Professor, Department of Chemistry, School of Chemical Engineering and Physical Sciences, Lovely Professional University, Phagwara, Punjab, for his scholastic guidance, innovative suggestions, constant supervision and motivation, valuable advice, and helpful criticism in carrying out the research work and preparation of this manuscript.

I am extremely grateful to **Dr. Kailash Juglan**, Head of School of Chemical Engineering and Physical Sciences, Lovely Professional University, Phagwara, Punjab, for his valuable suggestions, constant guidance, and immeasurable support, encouragement rendered during the entire course period.

I take this opportunity to extend my heartfelt thanks to the Assistant Professors, **Dr. Amar Srivastava**, of the Department of Physics, School of Chemical Engineering and Physical Sciences, Lovely Professional University, Phagwara, Punjab. I am sincerely grateful for his inspiring guidance, Constant inspiration, Encouragement, Support, and talented versatile advice during my research work.

I am thankful to Mr. Nitin Kumar Yadav, Laboratory Technician, School of Chemical Engineering and Physical Sciences Lovely Professional University for his wholehearted cooperation, support, and kindness.

I would like to express my heartfelt thanks to my batchmates for their selfless help, cooperation, support, and encouragement during my research work.

I am expressing my Special thanks to my parents Mr. Amarnath Vishwakarma and Mrs. Parwati Devi and my brothers Mr. Raj Kumar and Rajkishor Vishwakarma for their moral support and blessings, who stood behind me, as a great source of energy against all odds and showed me immense love, support, and encouragement throughout my course of instruction.

I am thankful to **Lovely Professional University** for allowing me to study in this Prestigious Institution and for letting me do my research in a well-equipped Laboratory, which provides an excellent learning environment.

Neetu Vishwakarma

Table of Contents

Chapters	Title	Page no
1.	Introduction	1
	1.1.Need of energy storage system	1-3
	1.2.Different types of energy storage system	4-6
	1.3. Supercapacitor	7-16
	1.4. Gas sensor in daily life	18-24
	1.5. Vanadium Oxide (V ₂ O ₅)	25-26
2.	Literature Review	24
	2.1.A brief view of relevant literature	28-42
	2.2. Research Gap	42
	2.3. Objective of the Research Work	43
3.	Research Design, Materials and Methods	44
	3.1.Methods used for the synthesized V ₂ O ₅	45
	3.1.1. Hydrothermal technique	46-47
	3.1.2. Microwave technique	48-49
	3.1.3. Mechanochemical technique	50
	3.2.Characterization	50
	3.2.1. Scanning Electron Microscope (SEM)	51-52
	3.2.2. X-ray diffraction (XRD) spectroscopy	53
	3.2.3. Fourier transform infrared (FTIR) spectroscopy	54
	3.2.4. Raman Spectroscopy	55
	3.3.Supercapacitor Performance	56
	3.3.1. Three Electrode System	56-57
	3.3.2. Preparation of working the electrode	58
	3.4.Electrochemical Study	58
	3.4.1. Cyclic voltammetry	59
	3.4.2. Galvanostatic charge/discharge test	59-60

	3.4.3. Electrochemical impedance spectroscopy	61
	3.4.4. Gas Sensing Measurement	62
4.	Synthesis and Electrochemical Characterization of V₂O₅	63
	4.1. Introduction	63
	4.2. Preparation of V ₂ O ₅ by different method	64
	4.2.1. Hydrothermal Synthesis Technique	64
	4.2.2. Mechanochemical Synthesis Technique	65
	4.2.3. Microwave Synthesis Technique	66
	4.3. Characterization of synthesized V ₂ O ₅ nanoparticles	66-68
	4.4. Electrochemical analysis of prepared Sample	69-72
5.	Properties and Performance of V₂O₅ as a Gas Sensor	73
	5.1. Introduction	73-74
	5.2. Materials and methods	74
	5.2.1. Synthesis of V ₂ O ₅ by Solvent-thermal and microwave method	75
	5.2.2. Thin film Preparation of V ₂ O ₅	76
	5.2.3. Gas sensing Measurement	77
	5.3. Result and discussion	78
	5.3.1. Gas sensing Measurement	81
	5.4. Gas sensing Mechanism	82-83
6.	Electrochemical Applications of Microwave Assisted V₂O₅-Graphene Oxide Composites	84
	6.1.Introduction	84-85
	6.2.Materials and methods	85
	6.2.1. Synthesis of V ₂ O ₅ microwave method	86
	6.2.2. Synthesis of V ₂ O ₅ -graphene oxide nanocomposite	87
	6.3.Result and Discussion	87
	6.3.1. Crystallographic study	87
	6.3.2. Morphological study	88
	6.3.3. FTIR Spectral analysis	89

	6.3.4. Raman Analysis	90
	6.3.5. Electrochemical Measurement	91-94
	6.3.6. Energy Storage Mechanism	95-97
	7. Summery and Conclusion	
	7.1.1. Conclusion	98-99
	7.1.2. Future Scope	100
	8. References	101-127
	9. List of publications and conferences attended	
	9.1.1. List of Publications	128
	9.1.2. Conferences and Workshops	128-129
	9.1.3. Award	129

List of Figure

- Figure 1.1 Source of Energy Storage
- Figure 1.2 Representing different energy storage systems
- Figure 1.3 Ragone plot of power density against energy density
- Figure 1.4 Schematic representation of conventional capacitors
- Figure 1.5 Electrical double layer (EDL) is an electrode surface that is used in the procedure of supercapacitors to collect ions from the electrolyte.
- Figure 1.6 Systematic diagram of Electrochemical Double Layered Supercapacitor
- Figure 1.7 Systematic diagram of Pseudocapacitor
- Figure 1.8 Schematic representation of hybrid or lithium-ion capacitor
- Figure 1.9 Human organs act like sensors.
- Figure 1.10 Schematic representation of MOS-based gas sensor's Chemiresistive gas detecting mechanism
- Figure 1.11 Schematic representation of gas sensing mechanism for n-type semiconductors
- Figure 1.12 Graphical representation of chemiresistive gas sensing curve of response gas
- Figure 1.13 Graphical representation of the selectivity of MOS-based gas sensors towards various gases
- Figure 1.14 Graphical representation of the recovery time analysis with respect to resistance ($k\Omega$) and time (s)
- Figure 1.15 Crystal structure of V_2O_5
- Figure 3.1 Hydrothermal reactor
- Figure 3.2 Schematic diagram of microwave oven
- Figure 3.3 Schematic of FESEM
- Figure 3.4 Schematic of XRD
- Figure 3.5 Schematic of FTIR
- Figure 3.6 Schematic of RAMAN
- Figure 3.7 Three electrode system: WE - working electrode, RE – reference electrode, CE – Counter electrode
- Figure 3.8 Cyclic voltammogram of (a) ideal capacitor and (b) real capacitor
- Figure 3.9 Galvanostatic charge discharge plot of pseudocapacitive material
- Figure 3.10 Graphical representation of Nyquist impedance

Figure 4.1	Flow chart of synthesis of V_2O_5 nanoparticles by hydrothermal method
Figure 4.2	Flow chart of synthesis of V_2O_5 nanoparticles by mechanochemical method
Figure 4.3	Flow chart of synthesis of V_2O_5 nanoparticles by microwave method
Figure 4.4	XRD data of hydrothermal, mechanochemical and microwave method of V_2O_5
Figure 4.5	FTIR data of hydrothermal, mechanochemical and microwave method of V_2O_5
Figure 4.6	SEM and EDX data of V_2O_5 prepared by (a & d) hydrothermal method, (b & e) mechanochemical method and (c & f) microwave method
Figure 4.7	CV curve of the V_2O_5 electrode at different scan rates for mechanochemical, hydrothermal and microwave method
Figure 4.8	The GCD curve of the V_2O_5 electrodes are depicted for hydrothermal, mechanochemical and microwave method
Figure 4.9	Electrochemical impedance spectroscopy (EIS) plot of V_2O_5 electrode of different method
Figure 5.1	Flow diagram of V_2O_5 synthesized by solvent thermal and Microwave method
Figure 5.2	Flow chart of fabricate V_2O_5 thin films based on the sol gel spin coating process.
Figure 5.3	Experimental setup for the gas sensing measurement
Figure 5.4	Response and Recovery time for the (a and b) acetone, (c and d) methanol (e and f) IPA vapor gases.
Figure 5.5	Gas sensing mechanism of V_2O_5 in air and in acetone
Figure 6.1	Flow chart of synthesis of V_2O_5 -graphene oxide composite by hydrothermal method
Figure 6.2	XRD pattern of V_2O_5 , GO and VG10
Figure 6.3	FESEM image and EDS analysis of (a, d) V_2O_5 microspheres (b, e) GO nanosheet and (c, f) VG10 composite
Figure 6.4	FTIR spectrum of V_2O_5 , GO and VG10 composite
Figure 6.5	RAMAN spectrum of V_2O_5 , GO, VG10
Figure 6.6	CV curve of (a) V_2O_5 , (b) VG5, (c) VG10 and (d) VG15

- Figure 6.7 GCD curve of (a) V_2O_5 , VG5, VG10 and VG15, (b) VG10 at the different current density (c) Specific capacitance of VG10 as a function of current density from GCD. (d) Specific capacitance of pure V_2O_5 and Composites as a function of scan rate from CV curves.
- Figure 6.8 Nyquist plots of pure V_2O_5 and various VG10 electrode (insets are the corresponding equivalent circuit)
- Figure 6.9 (a) The graph of relationship between the log of the peak current and the log of scan rate of VG10 for the anodic peaks, (b) percentage of diffusion contribution by VG10 at different scan rate (c) the distribution of percentage contribution from capacitive and diffusion currents at a fixed scan rate of 10 mV/s of VG10

Chapter 1

Introduction

1.1. Need of energy storage system

Energy is essential for human society's growth because it supports so many different demands and projects, including those related to food, clothes, housing, health, education, and the economy. Global energy consumption rose by 2.3% in 2018 [1]. The world's energy usage saw a significant uptick in 2018, with a 2.3% increase marking the largest growth in a decade. Meanwhile, global electricity demand jumped by 4%, reaching a record high of over 23,000 terawatt-hours. If this trend continues, energy demand is expected to skyrocket to over 35,000 terawatt-hours within the next few decades.

According to the World Energy Outlook 2019 – Analysis, 2019 figure 1.1, fossil fuels included coal, gases and petroleum now account for 68% sources of energy, nuclear power for 14%, hydropower for 15%, and other renewable energy sources for 3%. Therefore, fossil fuels are the primary source of energy; but, their supply is limited, they are finite, and as they break down, they flow pollutants into the environment, including carbon dioxide [1]. Only half of the CO₂ produced by burning fossil fuels is absorbed by natural processes, leaving the earth with a net annual increase of about 10.5 billion tons of CO₂. Therefore, it is important that we look for advanced, less expensive, and pollution-free renewable energy sources.

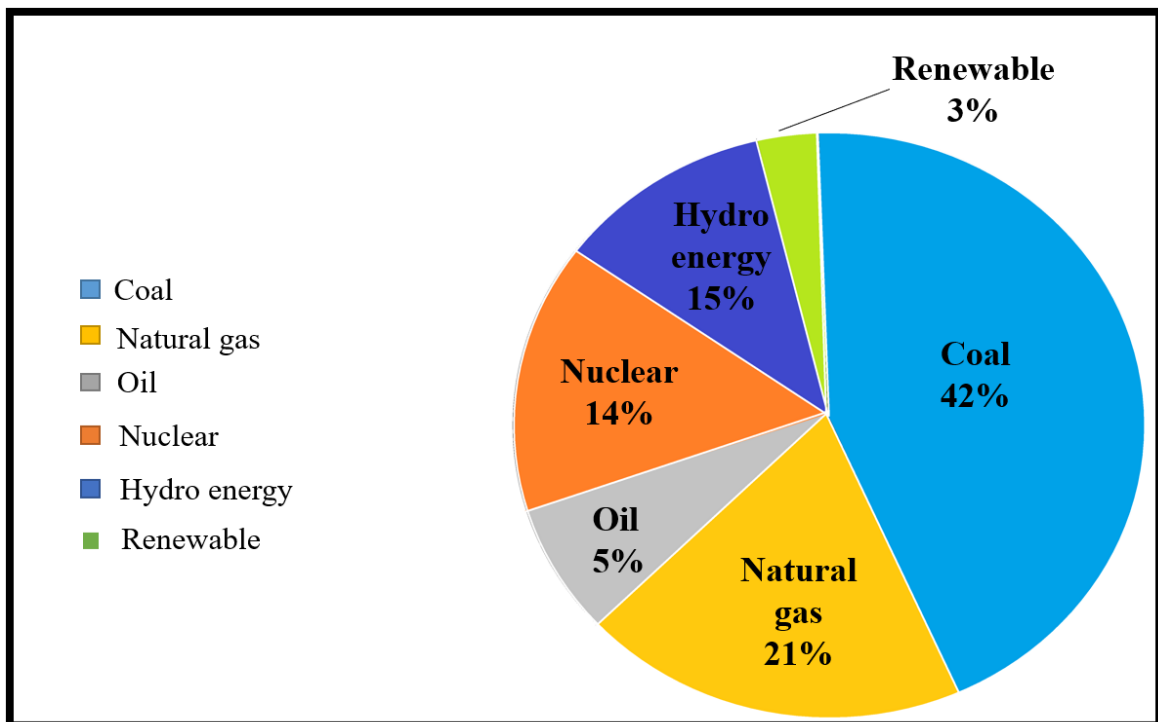


Figure 1.1 Source of Energy Storage

Solar energy, geothermal energy, biomass, hydropower, wind energy, and biofuels are some examples of sustainable energy sources. For fulfilling the global energy requirements, these sources cannot be completely utilized at all times nor have the necessary technologies been created. Because energy storage systems must be able to provide energy on demand whenever needed, energy management is a crucial undertaking that necessitates giving energy storage the same priority as energy production. Energy storage systems that are affordable, versatile, lightweight, and environmentally friendly are necessary in today's world. As seen in figure 1.2, a large number of scientists and researchers are studying energy storage systems, which include supercapacitors, batteries, fuel cells, and capacitors [2].

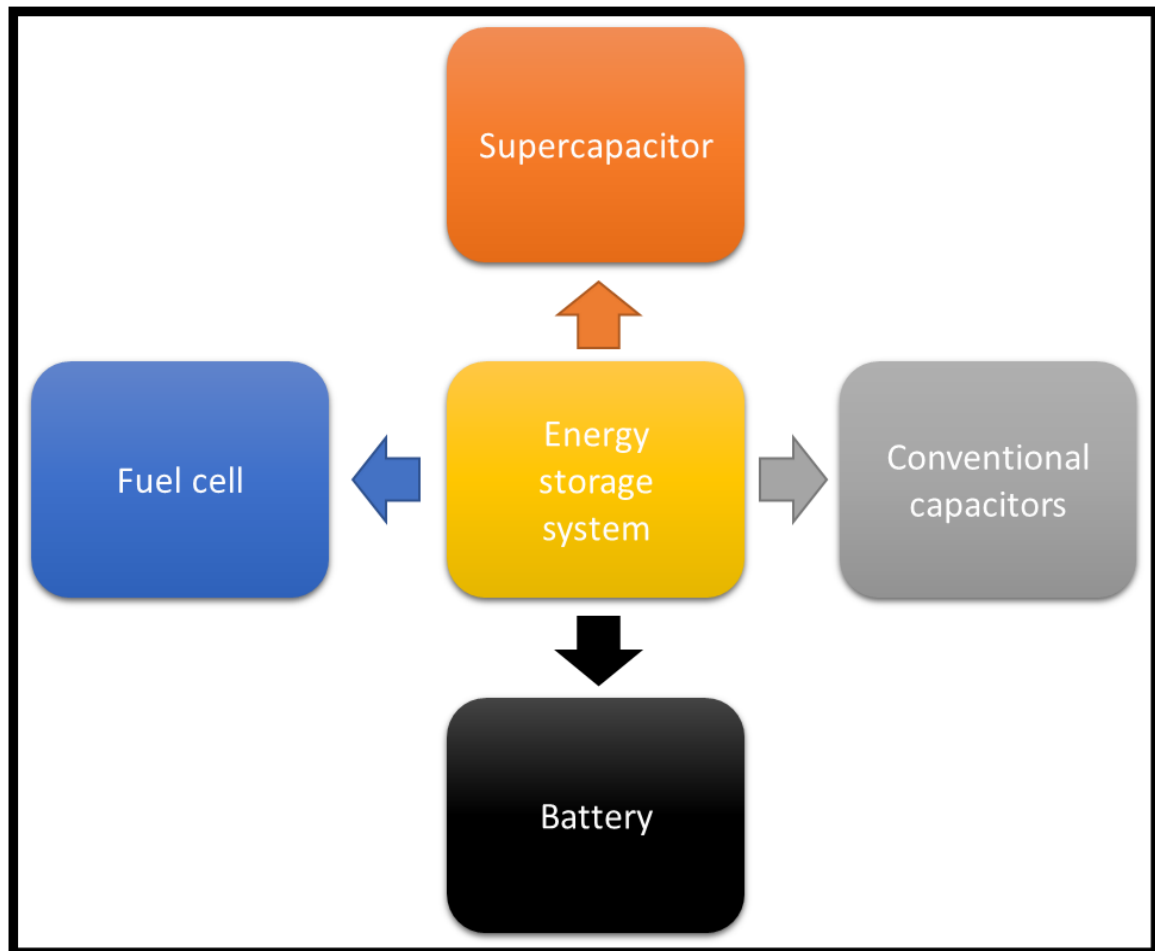


Figure 1.2 Representing different energy storage systems

Battery is the mostly used for energy storage application, despite a number of disadvantages, such as a slow charge-discharge rate, a short lifespan, and a heavy weight. The application of supercapacitors is one possible resolution for these problems. Supercapacitors have

several important features, fast charging and discharging rates, high power density, long cycle stability and light weight. These attributes make them suitable for a range of applications, including power backup, hybrid vehicles, portable electronics, and military usage.

An electrical energy storage device's energy density and power density have a strong association with its performance. An effective way to measure an electrochemical device's performance or potential is to plot its energy density compared to power density, or Ragone plot.

A Ragone plot, which compares power density to energy density, is seen in Figure 1.3. Specific energy and specific power are significantly impacted by supercapacitors. Because supercapacitors have high energy density than regular capacitors and high power density than lithium-ion batteries, which is the most effective way to meet the growing demands of energy storage systems in the twenty-first century [3].

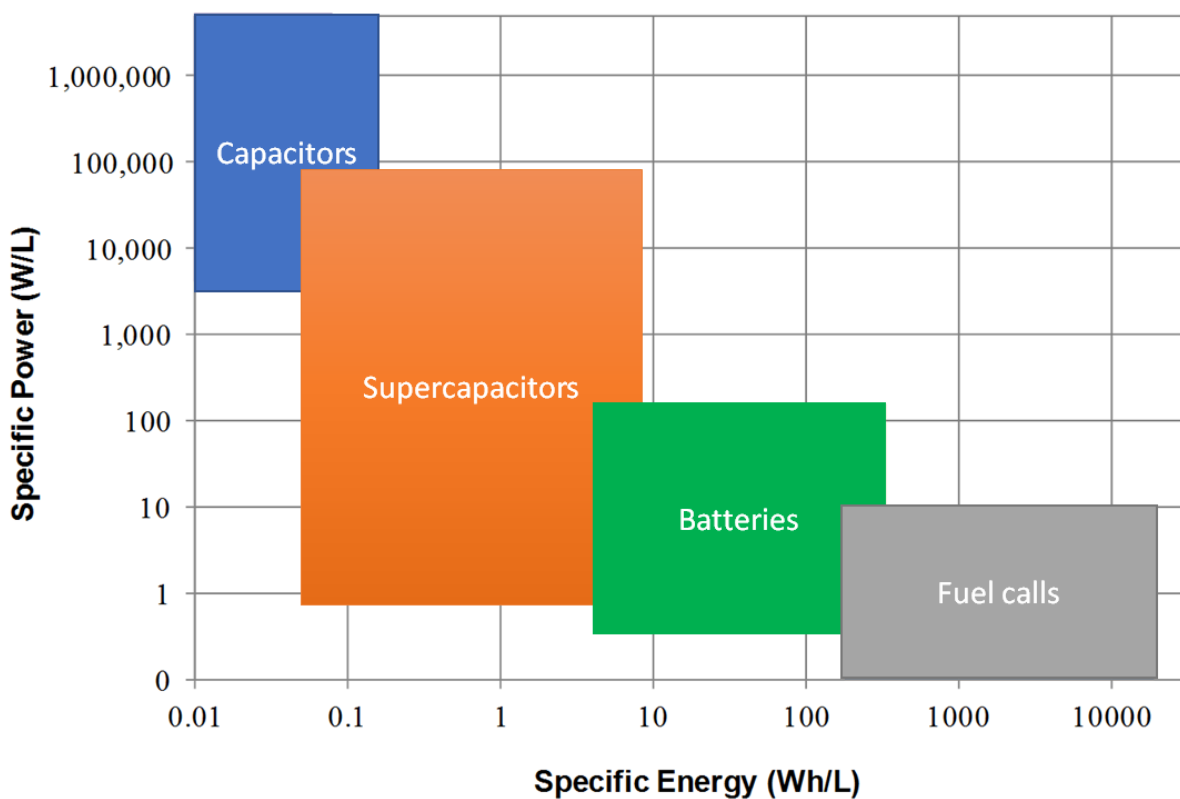


Figure 1.3 Ragone plot of power density against energy density

Supercapacitors may be broadly classified into two categories based on the way they store energy. Electrostatic charge that forms at the electrode/electrolyte contact is the only kind of capacitance found in an EDLC. Wide-surface-area, carbon-based compounds that are

obtainable by the electrolyte ions are typically employed. The expected energy density of EDLCs is 5 Wh/kg, and they are capable of supporting millions of cycles since the electrodes do not physically change while they are charged or discharged. A distinctive kind of capacitor is the pseudo capacitor, which operates on fast and reversible faradaic redox processes using TMOs and electrically conductive polymers as material of electrode. This pseudocapacitance can be covered using an electric double-layer capacitance. Higher energy densities have been achieved by pseudocapacitance-based devices than by EDLCs; however, phase changes carried on by the faradaic processes occurring within the electrode limit their lifetime and power density. To provide the necessary synergistic effect, these two processes can occur at the same time depending on the electrode materials' composition.

Different types of energy storage system

Different type of energy storage system such as fuel cell, battery, conventional capacitor and supercapacitor. Supercapacitor will be discuss in detail.

1.1.1. Fuel cell

Fuel cells are devices that use redox reactions to transform fuel's chemical energy into electrical energy. It is made up of an electrolyte and two electrodes, just like batteries. Hydrogen gas (H_2) given to the anode and gaseous oxygen (O_2 - often acquired directly from ambient air) pumped to the cathode are used to produce the fuel for fuel cells. Electricity, water, and heat are the reaction products of a pair of redox processes at the two electrodes. The electrodes comprise porous catalysts with excellent electron conductivities but no proton conductivity. These are typically comprised of carbon sheets that have been lightly coated with platinum nanoparticles. An electrolyte is a substance having strong proton conductivity and a zero or extremely low electron conductivity [4]. Fuel cells may create electricity constantly for as long as fuel is available, but they require a constant supply of fuel to maintain the chemical reaction. Fuel cells have high energy density but very low power density, and they lack any harmful by products or electronic waste.

1.1.2. Battery

According to Tarascon and Armand (2010) and Caillon-Caravanier et al. (2002), An electrolyte-electrolyte interface involves faradic reactions (oxidation and reduction) that transform chemical energy into electrical energy, which is essentially batteries perform. A

negative electrode, positive electrode, electrolyte, and separator make up each of the several cells that comprise a battery. When electrodes are attached by an external load, free electron movement from negative to positive potential and ion migration across the electrolyte take place, generating electrical energy while maintaining charge neutrality [5]. In the area of energy storage, batteries are well-known and have seen significant development since they were widely available in the 1980s. Numerous electronic equipment, such as laptops, cell phones, remote alarm systems, solar power storage, and even hybrid electric automobiles, use batteries as portable energy sources. However, several difficulties prevent their excessive usage, including their heavy weight, low power density, short shelf life, and the fact that they produce a significant amount of environmentally toxic electronic trash [6].

Table 1. Comparing the basic characteristics of batteries, conventional capacitors and supercapacitors [7].

Sr. No.	Factors	Capacitors	Batteries	Supercapacitors
1.	Cyclability (cycle life)	Almost infinite	~500 – 2000	> 5,00,000
2.	Specific power (W kg ⁻¹)	>10,000	~50 – 200	~1000 - 2000
3.	Specific energy (Wh kg ⁻¹)	< 0.1	~20 – 100	~1 - 10
4.	Charging time	ps - ms	H	ms to s
5.	Discharging time	ps - ms	H	ms to s
6.	Charge- discharge efficiency (%)	~ 100	~70 – 85	Up to 99

1.1.3. Conventional capacitor

An insulating material separates the two parallel conducting metal plates (electrodes) that make up a capacitor as shown in figure 1.4. Electricity is stored in capacitors in the form of electrical charges that create a voltage across their plates.

When DC voltage is delivered across a capacitor, an equal amount of positive and negative charge develops up on each plate. The capacitance of the capacitor, which is dependent on the surface area and spacing of the conducting plates and a gap that acts as a dielectric between them, is connected to the charge that is deposited on the plates, the applied voltage across the capacitor plates, and the applied voltage across the capacitor plates [8].

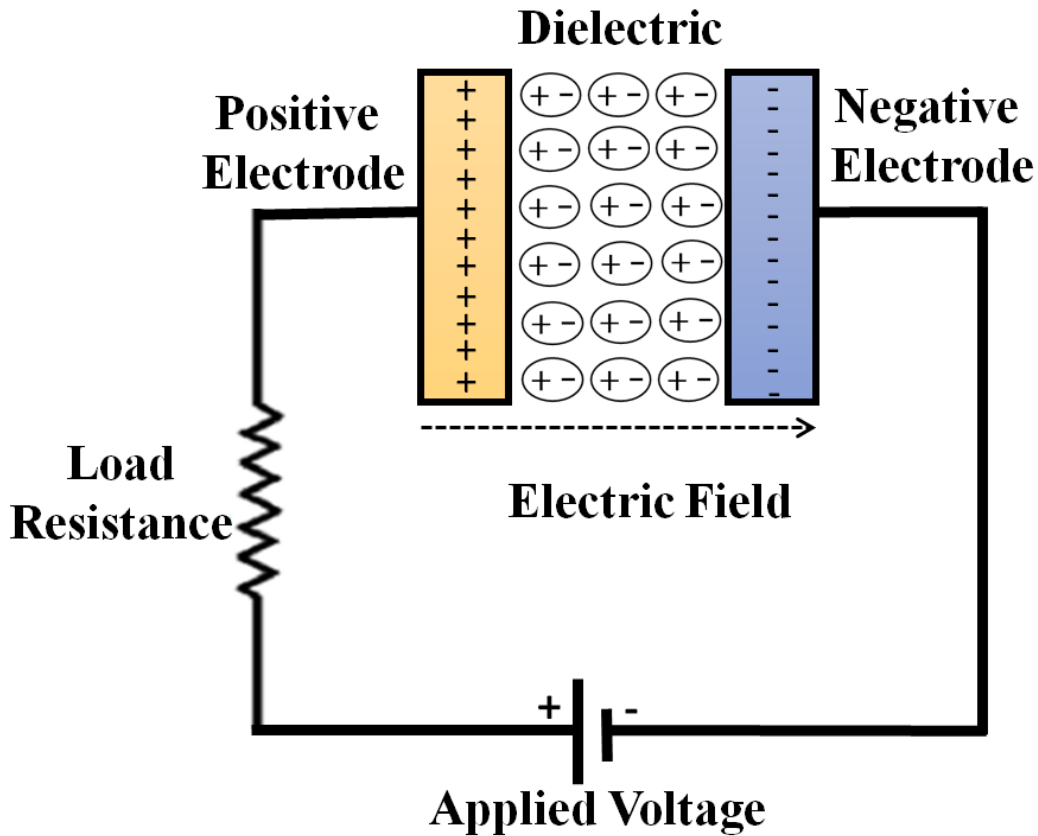


Figure 1.4 Schematic representation of conventional capacitors

In the equation no (1) capacitance (C) is shown as where the area of cross sections is A, d is distance, and ϵ is the medium's permittivity.

$$C = \frac{\epsilon A}{d} \quad \dots\dots 1$$

The charge (Q) that remain on the plates is determined by multiplying the applied voltage by the capacitance, as shown below:

$$Q = CV$$

The power (P) and energy (U) of a capacitor is expressed as

$$P = V^2 / 4R$$

$$E = \frac{1}{2} CV^2$$

Where R is the equivalent series resistance.

1.3 Supercapacitor

Air pollution, climate change, dwindling fossil fuel supplies and rising oil costs, restricted natural resource availability in the global ecosystem, and other factors are pushing the globe towards the development of environmentally benign, high-power energy sources. Development of clean, safe and environmentally friendly energy sources is necessary for solving these problems. Today, high electric energy may be produced by transforming natural energy sources like the sun, wind, and sea tides into sustainable and renewable ones. However, humans have limited power over events of nature as renewable resources are dependent on geographic and environmental factors including location, temperature, and the gravitational pull of the sun and moon on Earth. It is more crucial to use these renewable energy sources for continuous energy production rather than only using them to replace fossil fuels. Additionally, storing energy in a variety of forms is a crucial component that can address the issues [9]. Electrical energy storage devices are essential to many applications. The development of electric vehicles and the storage of renewable energy both depend significantly on advanced technology.

Future energy demands must be achieved; hence it is essential to create lightweight, flexible, high-performance energy storage technology. This situation has encouraged researchers to investigate improved energy storage technologies, such as supercapacitors, lithium-ion batteries (LIBs), and sodium-ion batteries. Recently, supercapacitors have garnered a lot of attention due to their huge potential for a wide range of applications. Supercapacitors offer better energy storage properties than conventional capacitor due to their rapid charge/discharge efficiency, extended cycling life ($> 500,000$ cycles), and high power density ($> 10 \text{ kW kg}^{-1}$) [9]. The positive and negative electrodes of a supercapacitor are electrically separated by a separator (such as an aqueous and non-aqueous electrolyte, porous membrane, etc.). The electrical double layer (EDL) is an electrode surface that is used in the procedure of supercapacitors (figure 1.5) to collect ions from the electrolyte. The usage of supercapacitors is common in hybrid cars, telecommunications equipment (remote communication, mobile phones, walkie-talkies, satellites, etc.), memory backup systems, pacemakers, portable electronic gadgets, etc.

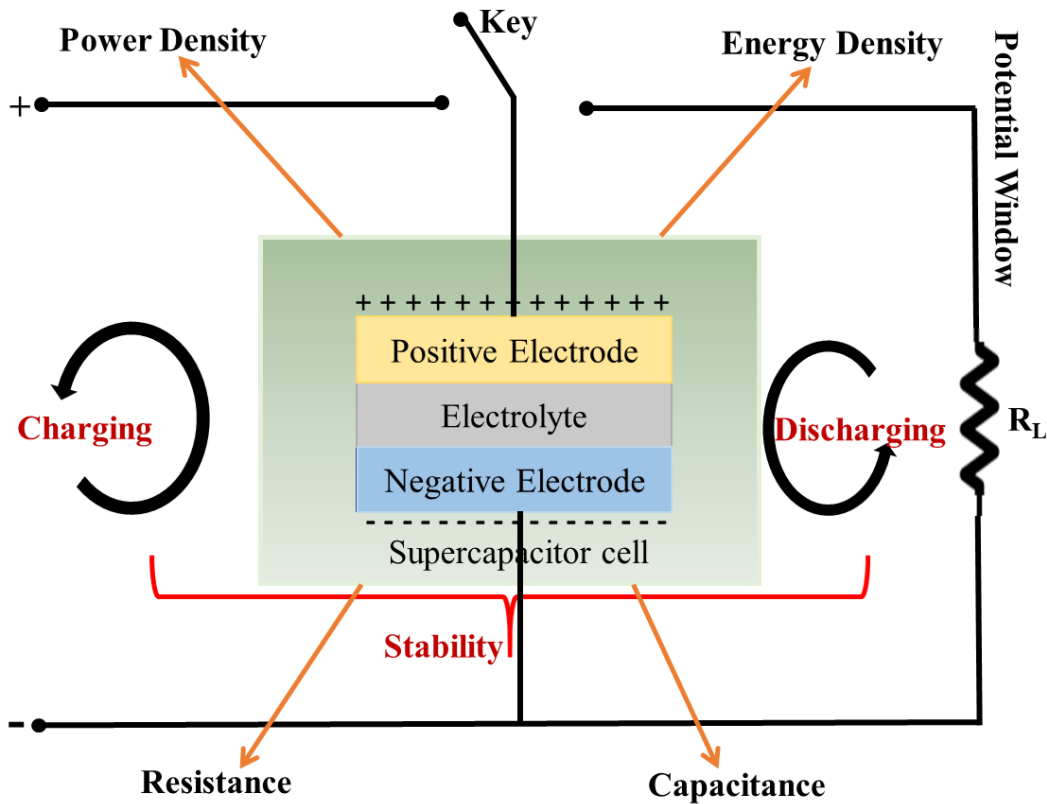


Figure 1.5 Electrical double layer (EDL) is an electrode surface that is used in the procedure of supercapacitors to collect ions from the electrolyte.

Table 1 highlights the differences in performance between different energy storage technologies (supercapacitors, batteries, and regular capacitors). Researchers have focused a lot of their attention on batteries among the many energy storage systems that are now on sale because of their capacity to store large amounts of energy and deliver sufficient power for a wide range of applications. However, during the charge-discharge cycles of batteries, irreversible redox processes typically arise by the electrode-electrolyte interfaces, changing the molecular pattern of the active materials. Because of this, batteries typically only have a limited lifespan of a few hundred to a thousand charge-discharge cycles, which results in lower cyclic performance [10]. Contrarily, since supercapacitor active materials are not involved in redox processes, there are no substantial chemical changes in electrode materials during cycling. As a result, this highly reversible storage system usually achieves a nearly infinite cyclability [11]. In addition, supercapacitors provide substantially greater power distribution for brief periods. Charge-discharge mechanisms in batteries, however, are substantially slower than those in supercapacitors due to faradaic processes [12]. Furthermore, batteries need at least several hours or longer to release their energy and

recharge while supercapacitors may be charged and drained in a matter of seconds [13]. Supercapacitors' fundamental strength, meanwhile, is that they have an equivalently lower energy capacity than batteries [14]. Supercapacitors have been proven to be a developing strategy to combat the rising power demand in multi-functional gadgets in the twenty-first century because to their high power.

Supercapacitor performance

The formula of specific capacitance for a supercapacitor

$$C_s = \frac{Q}{mV} \quad \dots$$

(2)

Where Q is the stored charge in coulombs, V is the voltage in volts, and m is the weight of the active material applied to the electrode expressed in grams. If the Q charge flows in time t, the current will be.

$$i(V) = \frac{Q(V)}{t}$$

Or

$$Q(V) = i(V) \times t \quad \dots$$

(3)

Putting equation (3) into equation (2) result in

$$C_s = \frac{i(V) \times t}{mV}$$

The above equation can be rewritten as

$$C_s = \frac{i(V)}{m \frac{V}{t}}$$

Where V/t is scan rate of cyclic voltammetry in Volt/sec and V/t represented by k:

$$C_s = \frac{i(V)}{mk}$$

Or

$$i(V) = C_s \times m \times k \quad \dots(4)$$

The area that is encircled by the CV curve is represented by in figure.

$$A = \int_{V_1}^{V_2} i(V) dV = \int_{V_1}^{V_2} (C_s \times m \times k) dV$$

Or

$$A = (V_2 - V_1) C_s \times m \times k$$

Or

$$C_s = \frac{A}{(V_2 - V_1) \times m \times k} \quad \dots\dots (5)$$

Where V is the whole voltage range, V/t is the scan rate in V/s , C_s is the specific capacitance expressed in F/g , and m is the weight deposited on the electrode in gm . The area that the curve encloses is A .

In relation to this, cyclic voltammetry is utilized to determine the specific capacitance C_s of a supercapacitor using equation (5).

1.3.1 Types of Supercapacitors

Electrochemical supercapacitors may be categorized into three kinds based on the electrodes and the mechanism of energy storage used: hybrid capacitor, EDLC and pseudocapacitor.

Electrochemical Double Layer Capacitors (EDLC)

An EDLC's electrode surface and electrolyte contact exhibits an accumulation of charge when a voltage is applied across them due to electrostatic interactions. To enhance EDLC storage capacity, the electrode materials need to possess a substantial specific surface area [15]. In this situation, electrodes typically constructed of carbon materials with large porosities are utilised as shown in figure 1.6.

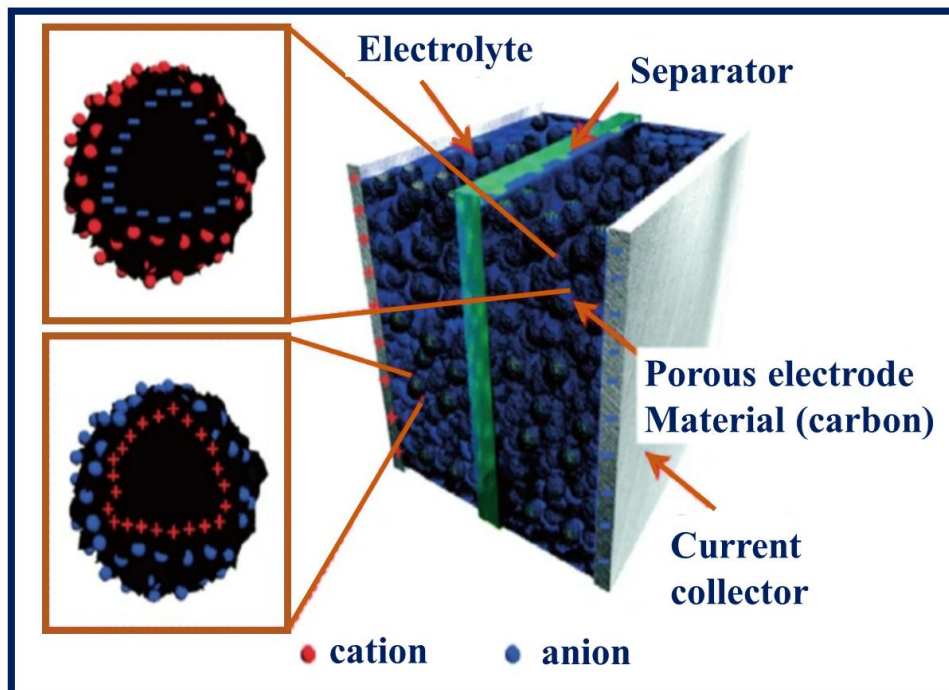


Figure 1.6 Systematic diagram of Electrochemical Double Layered Supercapacitor

An EDLC may achieve high power densities, quick charge-discharge cycles, and great cycle stability because the electrical energy is stored via ion adsorption, which is a completely

electrostatic process that excludes Faradaic charge transfer [16]. By using the use of an external load, electrons are transferred from the negative to the positive electrode when the system is charged. At the interface of the electrode and electrolyte, two layers develop when anions travel toward the positive electrode and cations migrate toward the negative electrode in the bulk electrolyte. The procedures change, however, when the system discharges. No net ion exchanges or charge transfers across the interface of electrode and electrolyte occur through this process between the electrodes and the electrolyte. This suggests that during the cycles of charging and discharging, the concentration of electrolyte stays constant [17].

Pseudocapacitor

The energy-storing capability of a pseudocapacitor is derived from reversible redox processes, sometimes referred to as the faradic process, which occur at or close to the surface of an electrode material. The electrochemical parameters of the device have a close connection to a carbon-based capacitor with a significantly higher capacitance due to the rapid redox process. The energy storage mechanism of pseudocapacitor, in contrast to EDLCs supercapacitor, is based on a transfer of charges through reversible faradaic interactions between electrode and electrolyte. An oxidation/reduction process in a pseudocapacitor is schematically represented in Figure 1.7. Pseudocapacitor materials often include metal oxides, sulphides, conducting polymers, and phosphates [18]. Pseudocapacitor create 10 times more capacitance and have a better energy density than EDLCs because their electrode surface has a higher capacity for storing charges than EDLCs.

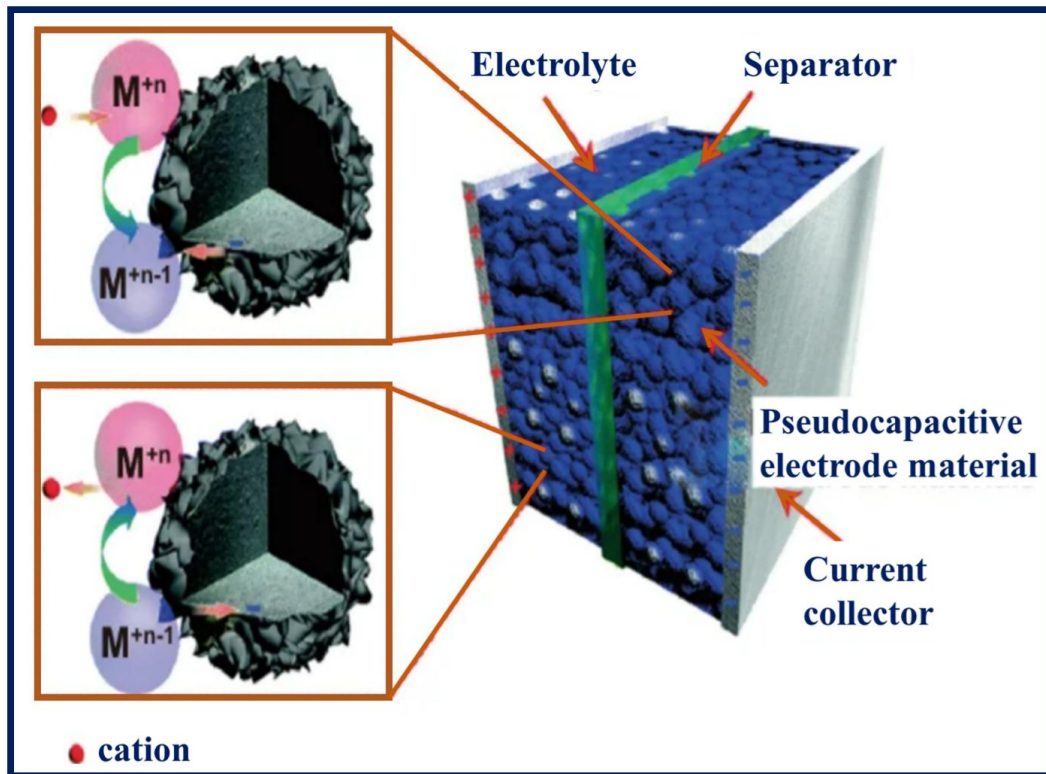


Figure 1.7 Systematic diagram of Pseudocapacitor

However, Pseudocapacitor properties include the size of the particle, the conductivity and porosity of the materials, the electrode's surface area, etc. Pseudocapacitor also have a shorter lifespan than EDLCs because the active material delaminates as a result of electrochemical redox processes. However, pseudocapacitive materials are becoming more and more popular because of their high specific capacitance, high energy density, and rapid and reversible redox processes.

Hybrid Capacitor

A hybrid capacitor is a device that simultaneously uses electrostatic and faradaic energy storage methods display in figure 1.8. Asymmetric designs are employed in hybrid capacitors, which give an expanded operating potential window while the cathode and anode materials are different. This improvement results from combining two distinct active electrode materials, each operating efficiently within different potential windows. This synergy enhances the device's overall working voltage, boosting its performance. One battery-type electrode (usually composed of metals like lithium, PbO_2 , TiO_2 , and $Ni(OH)_2$, among others) and one EDLC electrode (usually made of activated carbons) are commonly

used in asymmetric systems [19]. Examples of typical hybrid capacitors constructed using carbon and electrodes similar to those found in batteries include carbon// $\text{RuO}_2/\text{TiO}_2$ [20], carbon//titania nanotubes [21], and carbon// $\text{Ni}(\text{OH})_2$ [22]. The newest types of hybrid capacitors are battery-type hybrid devices, such as carbon/ PbO_2 and lithium-ion capacitors (LIC). It is also possible to construct asymmetrical hybrid capacitors by using one pseudocapacitive positive electrode (such as MnO_2) and one electrode that resembles a rechargeable battery (such as Li metal) [23].

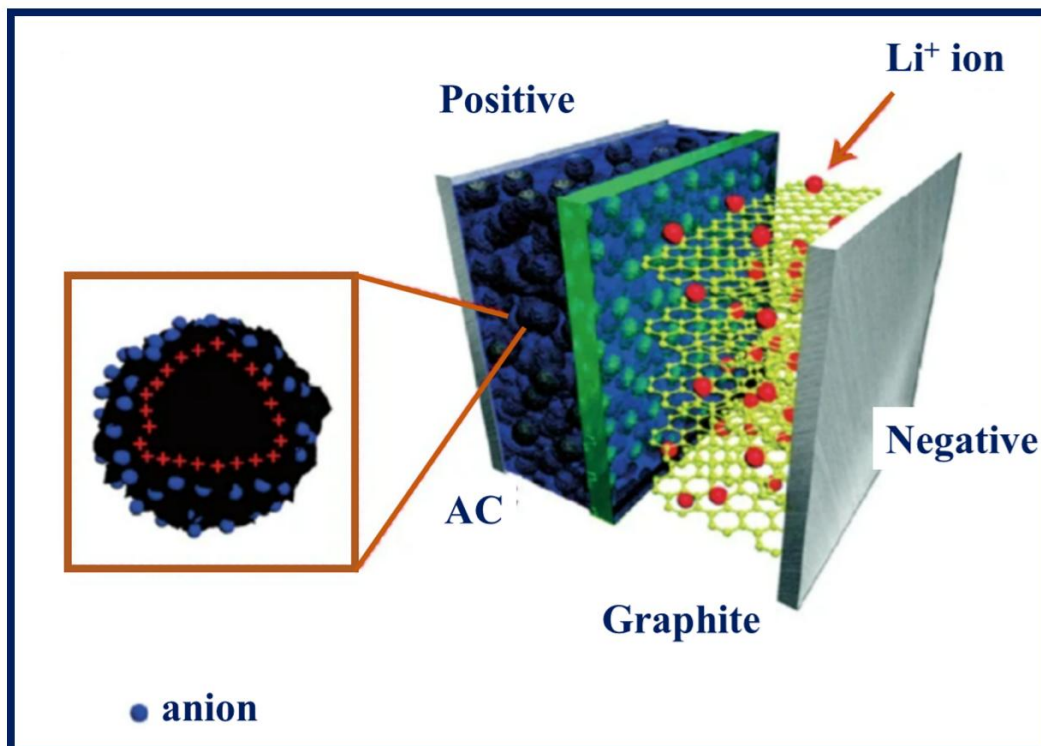


Figure 1.8 Schematic representation of hybrid or lithium-ion capacitor

1.3.2 Supercapacitor Design

Three fundamental parts make up a supercapacitor: the separator, the electrolyte, and the electrode. The electrochemical characteristics of SCs are mostly determined by the electrode and electrolyte. However, the electrode is the main source of energy both delivery and storage. The details of a supercapacitor system's different parts are provided in the following sections.

1.3.2.1 Electrode materials

The fast growth of supercapacitor technology has been possible for several years by the change of new smart electrode materials with higher specific capacitance. The electrode material is the factor that has the biggest impact on a supercapacitor system's electrochemical performance. There are three different types of electrode materials that are employed and advantageous for the supercapacitor application. These consist of carbon-oriented compounds, polymers, and TMOs.

Carbon based material

For supercapacitor electrode applications, high surface area carbon and carbon-based compounds are frequently used. The chemical and physical characteristics of carbon materials are generally advantageous. Because of their many advantages, such as their natural abundance, affordability, ultrahigh specific surface area, high conductivity, porous structure, high corrosion resistance, process ability, and improved compatibility, carbon-based materials are a preferred choice for supercapacitor electrode applications. Carbon cryogels, carbon aerogels carbon nanotubes, carbon nanofibers graphene, and activated carbon are just a few of the several forms of carbon that are utilized as SC electrodes [24].

The carbon-based products made from natural resources, such as wood, animal waste, and others, have significant impurity/ash content, which lowers the performance of the supercapacitor system [25]. Additionally, the pores have a limited number of diameters and differ between sources. As a result, "activation" is the process of increasing the surface area and porosity of carbons by heat or chemical treatments, which leads to the creation of activated carbon (AC) [26]. The unique porous structure of the activated carbons (ACs) consists of macropores larger than 50 nm in diameter, mesopores ranging in dimension from 2 to 50 nm, and micropores smaller than 2 nm. As electrodes for supercapacitors, the AC and their composites are widely used [27]. Higher capacitance values are often produced by electrode materials that include a significant number of mesopores (2–50 nm). The specific capacitance of the ACs is affected by the limited availability of mesopores because of the decreased ion accessibility with improved surface area of the ACs [28].

Since the 1990s, most of the research has focused on the use of carbon nanotubes (CNTs) as supercapacitor electrode materials. It has several advantageous characteristics, including a small pore size distribution PSD, a big surface area, low resistivity, and unique stability [29]. These benefits make CNT an attractive material for supercapacitor electrodes [30]. However, because to their expensive manufacture, CNTs are not practical for large-scale

production. But it's also crucial to remember that they usually act as conductivity enhancers and take the role of carbon black and activated carbons in supercapacitor electrodes [31].

The high electrical conductivity and enormous intrinsic surface area of graphene make it a suitable electrode material for supercapacitors [32]. In addition, graphene has great heat conductivity, low mass density, more stability in terms of chemicals, and remarkable intrinsic strength [33]. Because of these appealing qualities, graphene offers a superior platform for ion and electron storage and transit [34].

Numerous researchers have used graphene extensively for supercapacitor electrode applications [35].

Conducting Polymer

The conducting polymers are a special type of electrode materials for supercapacitor applications because of their unique three-dimensional (3D) porous structure, high capacitance, high energy density, scalable production methods, and light weight [36]. The most common conducting polymers used for SCs are polyaniline, polypyrrole and poly[3,4ethylenedioxythiophene] (PEDOT) and its variants [37]. Regarding their potential in supercapacitor applications, many attractive papers based on conducting polymer electrodes have been reported [38]. Conducting polymers may be used in supercapacitor electrode applications, but there are some major drawbacks, including low cyclic stability, active material removing off from collector, bulging of the electrolyte on increased cycling, and oxidative degradation of active material [39].

Metal Oxides

The transition metal oxides and nanostructures based on them are used as smart options for supercapacitor electrode applications because of their attractive redox chemistry. To identify a few materials that have been studied as supercapacitor electrodes are nanostructured ruthenium oxide (RuO_2) [40], titanium oxide (TiO_2), manganese oxide (MnO_2) and nickel oxide (NiO) [41], iron oxide (Fe_2O_3), cobalt oxide, and vanadium pentoxide (V_2O_5). Furthermore, studies have concentrated on integrating TMOs with conductive or carbon oriented polymers, mixed metal oxides, and ternary composites to increase the electrochemical performance [42].

RuO_2 is a desirable material for energy storage applications because of its range of oxidation states. It features rapid proton transport across water, a low electrical resistivity, and great

theoretic specific capacitance of up to 1450 Fg^{-1} . This interesting material has gone through substantial research in relation to applications for supercapacitor electrodes.

However, the greater price, environmental concerns, and limited supply of this precious substance prevent its widespread use. Several research organizations all over the globe have focused their efforts on finding alternatives to RuO_2 for use in energy storage applications [43]. When it comes to supercapacitor electrode applications, MnO_2 is seen to be a superior substitute for RuO_2 . MnO_2 has garnered significant attention in supercapacitor development because of its distinct characteristics. Among these are an extensive potential window in aqueous electrolytes, cost-effectiveness, and environmental friendliness, with a large specific capacitance in theory is 1370 Fg^{-1} . Various researchers have utilized MnO_2 as an electrode material for electrochemical performance, highlighting its potential in enhancing energy storage performance [44], [45]. However, its practical use is limited by its low specific surface area and manganese ion solubility in aqueous conditions [46], [47], [48], [49], [50], [51].

Supercapacitor electrodes made of Co_3O_4 and TiO_2 nanostructures have also been tested because of their cost-effectiveness, better theoretical capacitance, and environmental friendliness. With the help of charge-discharge processes, TiO_2 has high structural stability. Additionally, applications for both electrodes in supercapacitor devices were investigated [52], [53], [54], [55], [56], [57].

Among the metal oxides that have been researched the most for use as supercapacitor electrodes is NiO . This material is also inexpensive, has excellent thermal and chemical durability, and has a high theoretical specific capacitance (2573 Fg^{-1}) in the 0.5 V potential range. Because of these special qualities, NiO is widely employed for supercapacitor electrode applications [58], [59], [60].

Fe_2O_3 has attracted the interest of several researchers since it is less harmful and abundant naturally. Fe_2O_3 also has the ability to be non-combustible and environmentally friendly, which are significant characteristics. Fe_2O_3 nanostructures' performance in supercapacitor electrode applications has recently been widely reported by researchers [61], [62], [63], [64]. Metal oxides have also been observed to increase electrochemical performance in SCs in addition to metal oxide nanostructures [65], [66], [67].

1.3.2.2 Electrolyte

An important component of an SC system, electrolytes connected to the two electrodes and provides charge transfer. Aqueous electrolytes, organic electrolytes, and ionic solutions are the three main types of electrolytes that are frequently used. Each of these electrolytes has advantages and drawbacks of each one. For example, neutral aqueous electrolytes used in SCs have increased conductivity and capacitance. But because of the low decomposition voltage of aqueous electrolytes, its operating voltage is constrained (up to 1.2 V) [68]. However, organic electrolytes function at much greater voltages but have poor ionic conductivity. Although the fact that ionic liquids at room temperature produce the optimum working voltage, their expensive price makes them unsuitable. The electrolyte's ionic conductivity and stability within the applied potential window are the main factors influencing the selection of electrolytes.

Aqueous electrolytes

Energy storage applications frequently utilise the use of aqueous electrolytes. For example, aqueous electrolytes were utilised in 84.8% of published studies in 2014 [69]. Additionally, aqueous electrolytes are affordable and simple to handle, which greatly simplifies the device production process. In SCs, neutral aqueous electrolytes have strong ionic conductivity, are inexpensive, and are non-flammable. The dissolved ions in aqueous electrolytes are smaller in size, and their dielectric constants are larger. These two characteristics increase a supercapacitors capacitance. Increased conductivities of aqueous electrolytes up to $\sim 1 \text{ Scm}^{-1}$ lead to increased power delivery [70]. However, its use is restricted by the low working window value (1.2V). An inverse square connection exists between a supercapacitors energy density and cell voltage. Supercapacitors can have much higher energy densities by extending the electrolyte's voltage window [71].

Organic electrolytes

Currently leading the market are commercial supercapacitor devices with organic electrolytes because of their enhanced voltage range of 1V to 2.7V. These devices are more efficient because the increased cell voltage greatly improves electrochemical characteristics like specific capacitance and energy density. Additionally, organic electrolytes allow for the use of packaging and electrodes made of cheap materials, such as aluminium. To create stable electrolytes with greater conductivity and a wider potential window, several research projects are being undertaken. Before using it as an electrolyte for SC applications,

researchers should carefully examine its high cost, reduced ionic conductivity, flammability, volatility, and toxicity.

Ionic liquid electrolytes

Ionic liquids are another category of electrolytes for SCs that are solvent free. Ionic liquids are used as electrolytes, which increase the potential window to over 3V [72]. The electrolytes that are used most frequently include (fluoromethanesulphonyl) imide (FSI) and bis (trifluoromethanesulphonyl) imide (TFSI). At ambient temperature, these ionic liquids have a relatively low conductivity. However, energy storage devices are employed between -30°C and +60°C. To enhance the stability and conductivity of ionic liquids at ambient temperatures, further modifications are necessary. Despite their potential, these liquids need additional adjustments to optimize their performance and ensure reliable operation under standard conditions. The expensive price of these components prevents many people from using ionic liquids, despite their effectiveness.

1.3.2.3 Separator

A supercapacitor system includes the separator as one of its components. The Separators are ion-permeable, preventing both electrical and physical contact while allowing the transfer of ion charges. Separators in supercapacitors need to have greater ionic conductivity and be smaller to function effectively. Supercapacitor typically use nonwoven paper/polymer separators with aqueous electrolytes [73].

1.4 Gas sensors in daily life

Humans now enjoy a high quality of living thanks to the industrial revolution [74]. The need for energy sources has grown as a result of the transportation, industrial, and agricultural sectors developing quickly. Regular energy sources, like as petroleum products and fossil fuels, have been used in recent years to meet energy needs, but their stocks are finite. To meet the need for energy, these conventional sources must be replaced. Air pollution is the main issue with these old energy sources. The amount of air pollution rises as a result of the huge amount of pollutants produced into the environment. Air pollution has been an international issue in recent years due to the release of hazardous chemicals into the atmosphere, which results in acid rain, greenhouse effects, and ozone layer depletion [75].

Numerous hazardous gases, including ammonia (NH_3), acetone, nitrogen oxides (NO_x), xylene, methanol (CH_3OH), carbon dioxide (CO_2), ethanol ($\text{C}_2\text{H}_5\text{OH}$), amines, and many more, are continuously released from the transportation of vehicles, the industrial sector, the production of electricity, the combustion of fossil fuels, and many other sources. The amount of toxic contaminants in the atmosphere is rising daily, endangering both human health and the ecosystem [76].

There have been reports of the poisonous gas disaster from all across the world in recent years. The Union Carbide India Limited (UCIL) office was relocated from Mumbai to Bhopal in 1968. Bhopal is a stunning and ancient city in India. Sevin Technical Concentrate was imported from the United States of America and work on grinding and mixing was completed at the Bhopal factory, which was established in 1969 as a formulation plant. Methyl isocyanate (MIC) was used to begin the manufacturing of sevin insecticide in 1980. However, following four years of trouble-free operations, 30 metric tonnes of MIC gas unintentionally spilled from the factory on December 2, 1984. Nearly 200,000 individuals were directly exposed to this very deadly MIC gas at Bhopal, where almost 20,000 people perished. Following this catastrophe, the factory closed down [77]. Other than Delhi, Gwalior, and Allahabad, these cities are among the most polluted in the world, which presents a serious risk to public health. The eye, nose, ear, fingers, tongue, and other sensory organs function as sensors for light, sound, smell, touch, and taste. The human sensory organs that function as distinct sensors are shown in figure 1.9. The human nose is the most effective sensor of all these organs; it can identify and differentiate between a wide range of gases, although it cannot detect odourless gases or gases at very low concentrations [78].

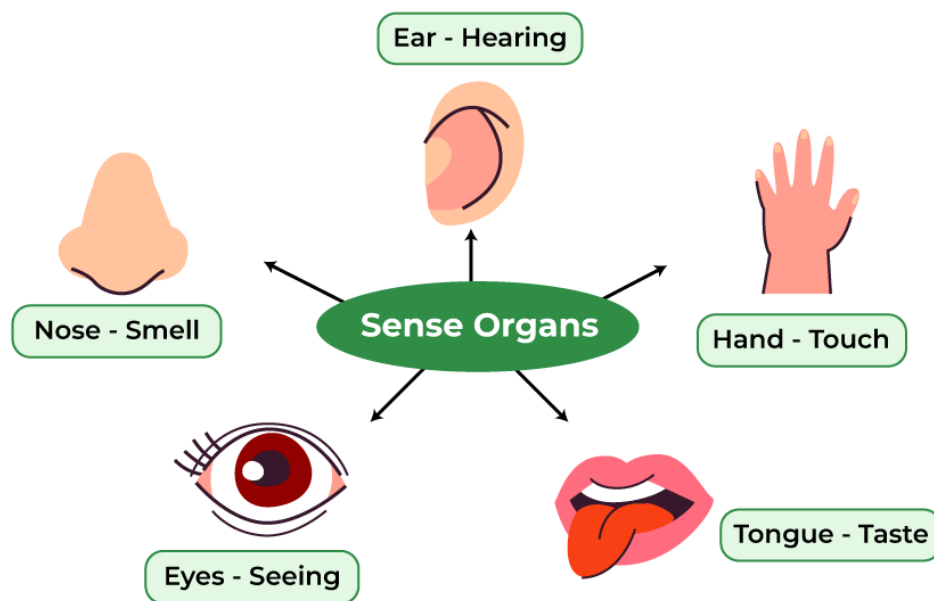


Figure 1.9 Human organs act like sensors.

Therefore, a more advanced, reasonably priced, and reliable gas sensor is required. The last several decades have seen a sharp rise in the need for portable, reliable gas sensors that can differentiate between different gases at low concentrations. In the past, coal mining was the first application for gas sensors [79]. The earliest gas sensor was the screaming canary, which was employed in mining operations to detect the dangerous gas methane. Later, Davey's lamp was also employed as a gas sensor. When Bardeen and Brattain originally published on the concept of the sensor in 1953, it marked as a significant development in the field of gas sensors. Taguchi first developed a metal oxide semiconductor (MOS)-based gas sensor in 1968. In general terms, detectors are electronic transducers that can transform signals—mechanical, electrical, magnetic, chemical, optical, thermal, etc into readable forms and provide information about the gases present in the surrounding atmosphere [80]. The most important characteristics of an exceptional gas sensor are its high sensitivity, low working temperature, and fast reaction and recovery time [81]. MOS-based gas sensors include those found in TiO_2 [82], SnO_2 [83], WO_3 [84], V_2O_5 [85], ZnO [86] and several other materials.

1.4.1 Types of gas sensor

It's important to understand the actual significance of gas sensors before talking about different kinds of sensors. A substance that reacts to its surroundings and produces a signal is a MOS-based gas sensor. The reaction is subsequently read by the electronic device and transformed into sensible and quantitative terms. To put it another way, a gas sensor is an electrical device that can identify gases in the environment. Gas sensors are classified into a number of types that are described below based on their basic principles of operation.

Chemiresistive Gas Sensor

Semiconducting materials are typically used in its construction, and charge carrier density changes are sensed. To put it another way, it measures how a semiconductor's conductivity changes when it relates with the gas under study. Mostly used the metal oxides, which include SnO₂, TiO₂, WO₃, and others. These materials are sensitive to carbon hydroxide, CO₂, H₂S, NH₃, NO_x, and O₃. Typically, an illuminating substrate is used to create this kind of gas sensor, which is connected to Au, Pt (conductive wires). The component is included in the circuit. When the target gases interact with the O₂ and become adsorbed on the sensor element, there is a significant change in energy levels, which highly contributes to gas detection [87].

Potentiometric gas sensor

It depends on Nernst's finding that materials with high ionic conductivity may be used to create an electrochemical cell even while they are still electrically insulating. An example of such a substance is a solid electrolyte. The working electrode and reference electrode voltage, or potential difference, is used to measure the signal. The potential of the working electrode is influenced by the analyte concentration in the gas phase. In recorded history, stabilized zirconia has been the most expert and well-known ion conductor [88]. Doping the material with cations (Ca²⁺, Y³⁺, Yb³⁺, etc.) has improved its oxygen ion conductivity. Due to its superior ability to regulate the emission of air-polluting gases from automobile exhaust, the automotive exhaust system is where it is most commonly used.

Chemical field effect transistor

It makes use of semiconductor characteristics by means of a metal oxide semiconductor field effect transistor (MOSFET), which detects changes in the threshold voltage of the gate electrode.

Acoustic wave-based sensor

An acoustic wave-based sensor is a device that employs acoustic waves to monitor and examine variations in its environment. By using these waves, the sensor can detect and analyze changes around it, providing valuable information about its surroundings. These sensors typically consist of a transducer, which generates and detects acoustic waves, and a sensing element that interacts with the target substance or property being measured. When the target substance or property interacts with the sensing element, it causes changes in the acoustic wave characteristics, such as frequency, phase, or amplitude [89]. These changes are then analysed to determine the presence, concentration, or other relevant parameters of the target substance or property. Acoustic wave-based sensor is commonly used in various application, including gas sensing, liquid sensing, and bio-sensing, because of their high sensitivity, fast response time, and compatibility with miniaturization.

Calorimetric based sensor

By measuring the temperature increase produced on by the process of oxidation on a catalyst, the concentration of combustible gas is determined. Calorimetric based sensor is also known as Pellistor. Typically, the functions of temperature measurement and heating are integrated. The initial concept consisted of Pt wires that worked at 800-1000°C. According to enhanced oxygen porosity and better catalyst dispersion, recent developments have decreased the operating temperature and achieved acceptable combustion. The low explosion limit (LEL), represented as a percentage, and of flammable gases may be found using this process. As such, it's extremely effective for methane, carbon monoxide, and hydrogen detection.

Optical gas sensor

An optical gas sensor is a device that employs light to detect and analyze specific gases in its environment. A light source, optical elements for focusing and adjusting the light, and a sensing device that connects with the target gas are commonly included in these sensors. When the gas interacts with the sensing element, it alters the optical properties of the element—such as through absorption, scattering, or fluorescence. The existence, concentration, and other properties of the gas are then determined by measuring and analyzing these changes. Because of their excellent sensitivity, selectivity, and quick reaction, optical gas sensors are useful in a variety of applications, including industrial safety, medical diagnostics, and environmental monitoring.

1.4.3. Principal of gas sensing

The oxygen from the atmosphere is first deposited on the surface of MOS during gas sensing. Adsorption occurs in two different forms: chemical adsorption and physical adsorption. A space charge area is created when oxygen is adsorbed, which also takes one or more electrons from MOS. Figure 1.10 displayed the different oxygen species, including O_2^- ($<100^\circ\text{C}$), O^- ($100\text{-}300^\circ\text{C}$), and O^{2-} ($>300^\circ\text{C}$) [90], are formed on the surface of MOS depending on temperature. The following reaction represents the adsorption of oxygen species.

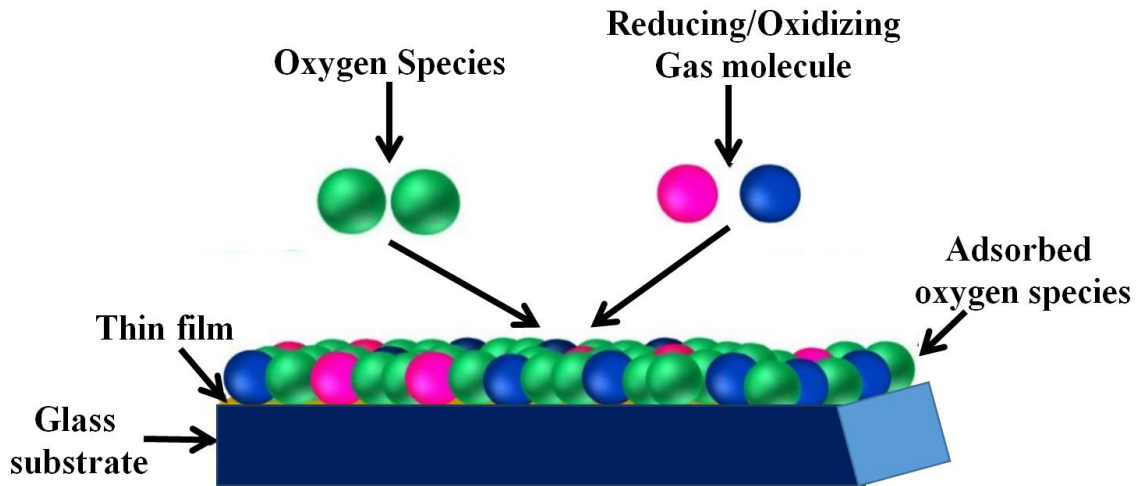


Figure 1.10 Schematic representation of MOS-based gas sensor's Chemiresistive gas detecting mechanism

Electron transit may be impeded by the resistance present in the space charge area. Depending on the kind of MOS (n-type/p-type) and gas (reducing/oxidizing gas), when this MOS is exposed to the target gas, it either grabs an electron from MOS or delivers an electron to MOS. As a result, the breadth of the space charge area either rises or decreases. As a result, the potential barrier's height varies, providing information on a variety of gas sensing characteristics, including sensitivity, selectivity, reaction time, recovery time, and many more. A schematic illustration of an n-type semiconductor's gas detecting mechanism is shown in figure 1.11. Adsorbed oxygen species generate the space charge area by collecting one or more electrons, as seen in the early portion of figure 1.11 from the n-type

MOS's conduction band, which causes band bending. The MOS exposed to the oxidising gas in the second portion of the figure 1.10 causes the breadth of the space charge area to rise because of the electrons that are gained from the MOS, which raises the potential barrier's height. Like this, in the third section of figure 1.10 the MOS is exposed by decreasing gas, which causes the height of the potential barrier to drop due to the gas's loss of one electron to the MOS's conduction band. Like this, but in the complete opposite way, is gas detection by the p-type MOS. below table. The behaviour of resistance to n-type and p-type MOS for both oxidising and reducing gas is shown in figure 1.10.

Table 2. Response of MOS towards different gases.

Type of semiconductor	Oxidising gases	Reducing gases
p-type semiconductor	Resistance decrease	Resistance increase
n-type semiconductor	Resistance increase	Resistance decrease

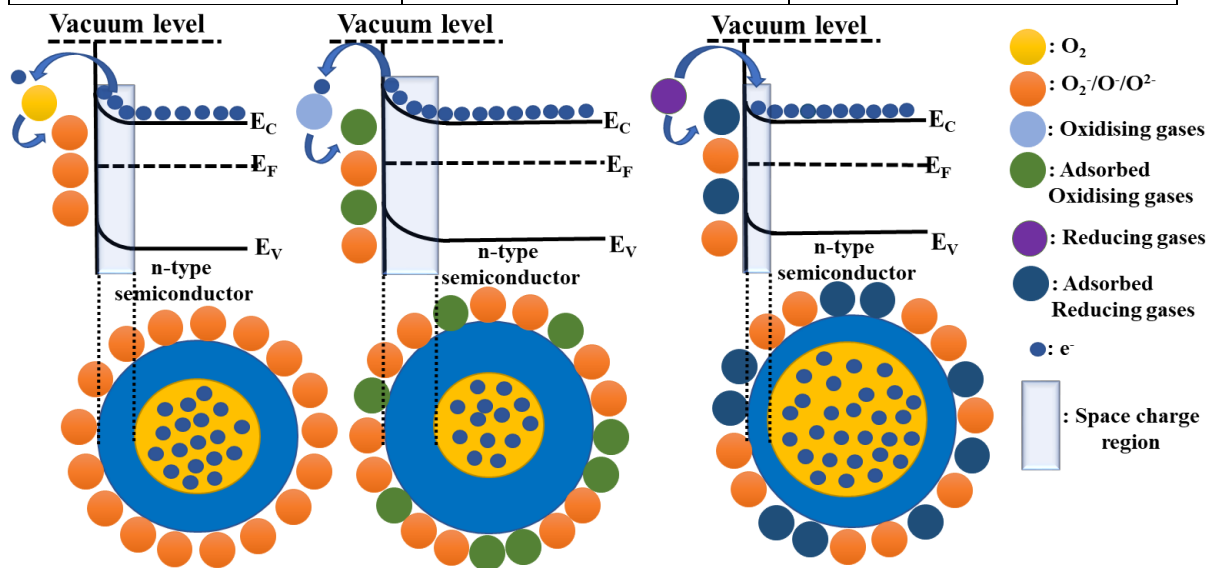


Figure 1.11 Schematic representation of gas sensing mechanism for n-type semiconductors

1.4.3 Gas sensing parameter

The gas sensors' actual performance is determined by the following parameters:

Gas response

It is a gas sensor's reaction to a change in gas concentration of one unit. The response curve (figure 1.12) expressed in terms of optical absorbance, capacitance, resistance, or many other

signals. The following formulas [91] can be used to represent the sensitivity of a chemiresistive type gas sensor:

$$S = \frac{R_G - R_0}{R_0}, R_G > R_0 \text{ (Oxidizing gas) } \dots\dots\dots 1.5$$

$$S = \frac{R_0 - R_G}{R_G}, R_G < R_0 \text{ (Reducing gas) } \dots\dots\dots 1.6$$

Where the resistance of the sensor both before and after gas exposure is represented by R_0 and R_G .

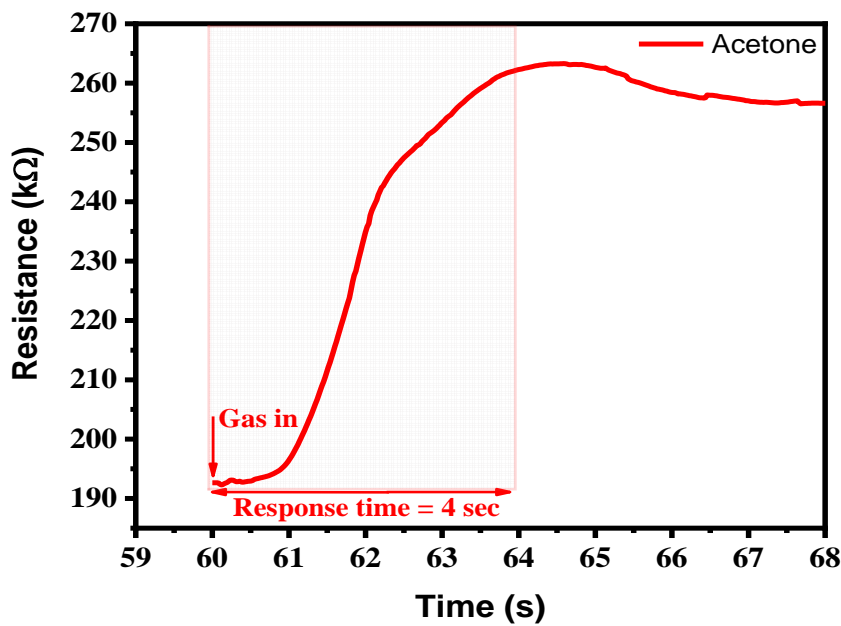


Figure 1.12 Graphical representation of chemiresistive gas sensing curve of response gas.

Selectivity

Only the most sensitive gas present in the environment is shown by the gas sensor in figure 1.13. The ratio of a particular gas's reactivity to that of other ambient gases can be used to determine the selectivity of a gas sensor.

$$\text{Selectivity of gas sensor} = \frac{\text{Response of particular gas}}{\text{Response of other gases}}$$

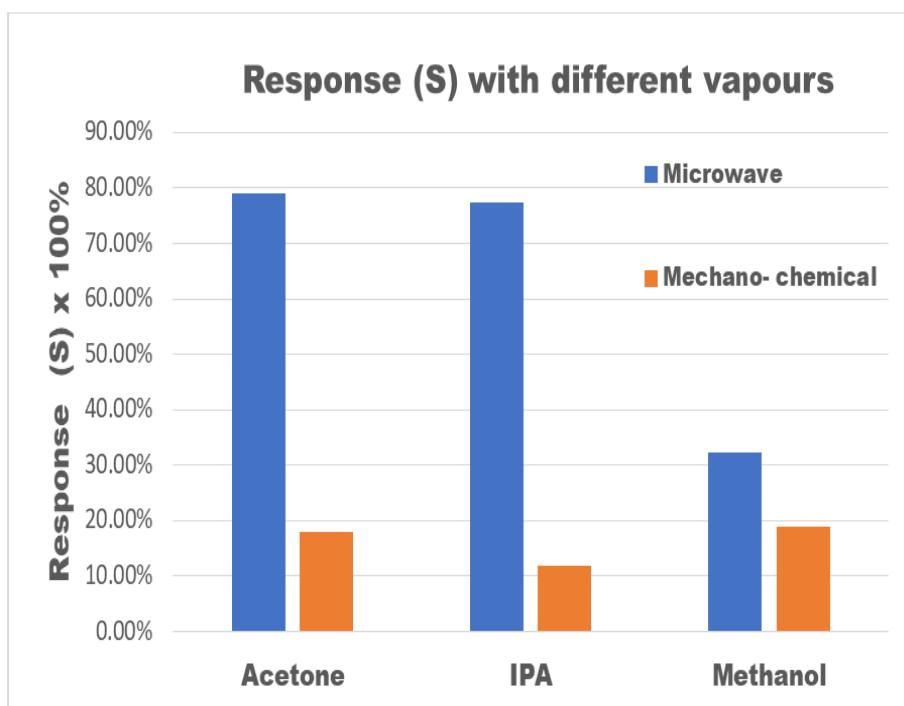


Figure 1.13 Graphical representation of the selectivity of MOS-based gas sensors towards various gases

Response and Recovery time

When a sensor is exposed to the target gas, its reaction time is the amount of time it takes for it to attain 90% of its maximum response. This can be expressed in terms of resistance, absorbance, capacitance, or other pertinent properties. The amount of time needed for the sensor to release the target gas and restore 90% of its original signal is called the recovery time. Response and recovery times are critical during gas sensing operations.

An important feature of a good sensor is its quick reaction and recovery time. The gas sensing curve is displayed in figure 1.14 and is used to calculate response and recovery times.

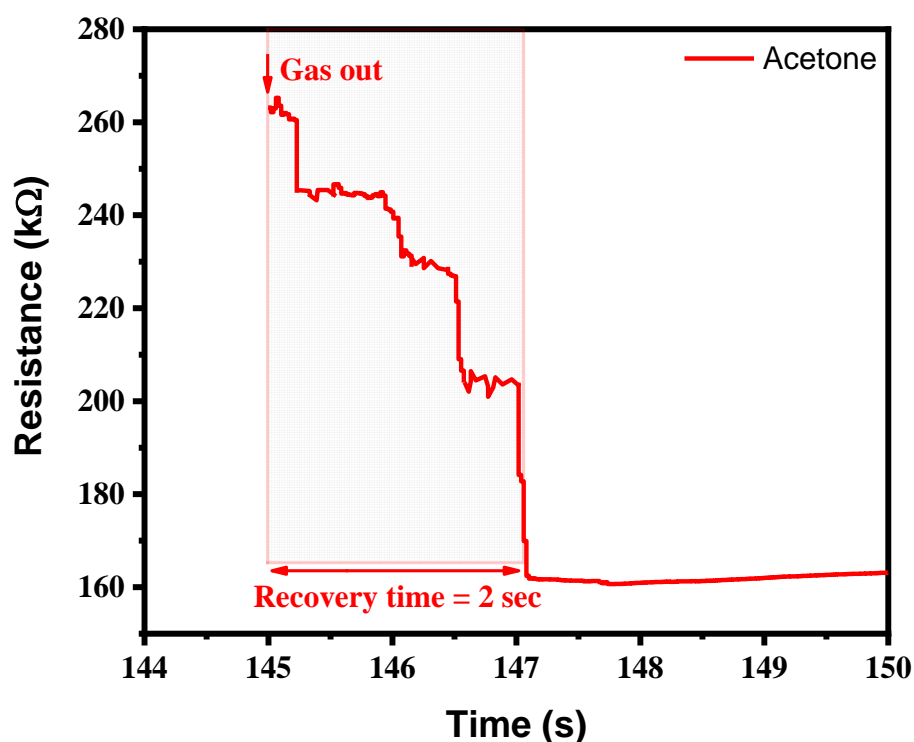


Figure 1.14 Graphical representation of the recovery time analysis with respect to resistance ($k\Omega$) and time (s)

Stability

Stability denotes to a sensor's capacity to continue sensing gases for a predetermined amount of time. For sensors, high stability is a crucial gas sensing feature.

Working Temperature

Gas sensors need low operating temperatures, and research is still being done to find the lowest operating temperature at which the maximum response may be obtained.

Detection Time

The lowest target gas concentration that a sensor at a low operating temperature can detect.

1.5 Vanadium pentoxide (V_2O_5)

Vanadium oxides have become a lot of interest nowadays due to their remarkable pattern, physical, and chemical characteristics. The crystal structure of V_2O_5 as shown in figure 1.15. Vanadium, the fifth transition metal and the nineteenth most popular part in the earth crust, is essential for many uses [92]. In addition, V_2O_5 is thought to be the most stable form of

V_2O_5 because of its greatest oxidation state. It has a multilayer architecture and an orthorhombic unit cell with a Pmmn space group. The measurements for V_2O_5 's lattice parameters are $a = 11.510\text{\AA}$, $b = 3.563\text{\AA}$, and $c = 4.369\text{\AA}$. The oxygen atoms around the vanadium atoms form trigonal bipyramidal coordination polyhedra, which exhibit some distortion [93].

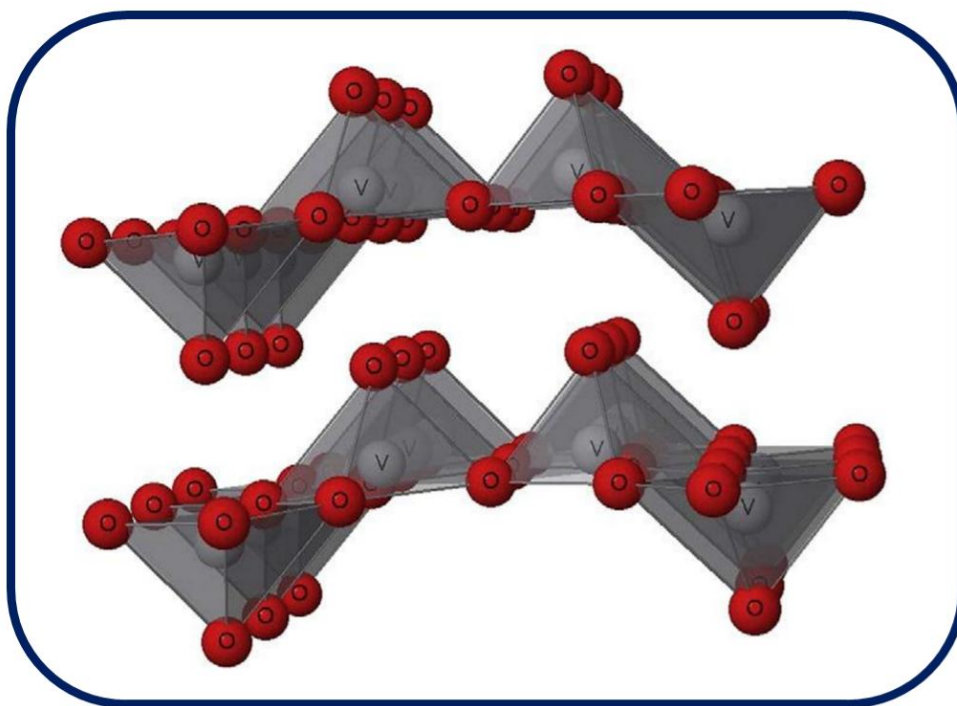


Figure 1.15 Crystal structure of V_2O_5

V_2O_5 is still an excellent catalyst because of the range of oxidation states (V^{2+} to V^{5+}) and variously arranged coordinate oxygen shape. This compound's unique structure offers strategies to regulate its surface and physical characteristics. V_2O_5 displays rich due to its open/layered structure, numerous oxidation states, and crystal chemistry.

Since its initial publication by Whittingham et al. [94], vanadium pentoxide (V_2O_5) has received a lot of interest among the many vanadium-based materials. V_2O_5 has a lower conductivity than ruthenium oxides as an electrode, but its numerous oxidation states allow for more redox processes. V_2O_5 is numerous and less costly than RuO_2 . V_2O_5 can be used as an alternative electrode material to RuO_2 due to simple production techniques. In this context, the significant advancement of nanostructured materials has sped up the development of energy storage technologies. When utilized as supercapacitor electrodes, nanostructured materials' unique mechanical, structural, and surface properties significantly

increase performance [94]. Importantly, materials with nano architecture provide the following attractive properties.

- The contact area per unit mass of the electrolyte ion has been significantly increased by decreasing the active electrode material. Effective charge transfer processes considerably increase the density of ion adsorption sites.
- The nanostructured electrodes have shorter ion diffusion periods because there are few ion diffusion routes. It offers increased energy density and rate capacity.
- The cyclic stability of the material is decreased by the volumetric variations of the electrode active materials. Improved ion intercalation/deintercalation tolerance is shown in electrodes at the nanoscale. It's possible that the nanostructured electrodes will have more cycle stability.

Nanostructured electrode materials can be used to create transparent, flexible, and lightweight energy storage devices.

Chapter 2

Literature Review

2.1. A brief view of relevant literature

Zhang et al. [95] examine that the affordable way to create films and nanoparticles of VO₂ (M) with superior thermochromic characteristics. By using the precursor NH₄VO₃ and C₂H₆O₂ They synthesized the VO₂ (M) high crystalline powder by using facile method. These VO₂ (M) nanoparticles produced composite thin films with superior thermochromics qualities. Liu et al. [96] Create metastable VO₂ nanobelts using a hydrothermal process. The monoclinic phase VO₂ (B) was present in the XRD index of typical samples, and XPS data indicated that V (IV) was unique to V₂O₅. SEM and TEM images revealed the dimensions of the VO₂ (B) nanobelts: 20–30 nm in thickness, 70–180 nm in width, and 0.6–2.2 µm in length. Wu et al. [97] synthesized the VO₂ nanoparticles by hydrothermal calcination method. The VO₂ (M) nanoparticles were produced at a temperature of 300°C during vacuum annealing. This work discusses how the phase transition characteristic of VO₂ (M) nanoparticles is affected by temperature and particle shape.

In this article Liang et al. [31] Develop the VO₂ nanorods by one step hydrothermal method to provide their application in smart window. The W-doped VO₂ (M) nanocomposite film was made flexible on PET by utilizing a simple roller coating technique. This nanocomposite film showed a phase transition temperature of around 37.3°C and a notable middle-infrared transmission reverse of up to 31%. Using a one-step hydrothermal treatment of the hydrolysed precipitate from V₂O₅, where N₂H₄, in this study Karahan et al. [98] presented the synthesis and characterisation of different morphologies of VO₂ (M) nanocrystals. Water is used as a reducing agent. By using this method, it was possible to synthesise extremely crystalline and homogeneous monoclinic vanadium dioxide nanostructures with asterisk, urchin, and multifaceted spherical shapes. This led to the synthesis of superior, guided, and well-organized VO₂ nanotubes with a consistent size distribution.

Chen et al. [99] creates the multistep structure VO₂ (M) from the VO₂ (D) precursor using an annealing and hydrothermal procedure. Measurements of reflection loss reveal that the VO₂ (M) sample, which has a multi-step petaloid laminated structure, has remarkable microwave absorption capabilities. The sample had an effective absorption bandwidth (RL < -10 dB) reaching up to 4.01 GHz at 1.3 mm and a peak reflection loss of -37.99 dB at 3.5 mm after being annealed at 570 °C. This review describes how Li et al [100] synthesised VO₂ polymorphs by hydrothermal synthesis and emphasises the one- and two-step

hydrothermal approaches used to create thermochromic VO₂ (M). It is evident that hydrothermal synthesis yields VO₂ polymorphs with regulated shape and size, particularly when generating VO₂ (M) nanoparticles on a large scale for nano thermochromic applications. Modern approaches that should improve the thermochromic property and enable VO₂ energy-efficient smart windows to perform a variety of tasks are described.

The VO₂ (B) nanobelts were designed by Wang et al. [101] and can be ball milled at room temperature to produce VO₂ (M) nanoparticles that can be released into the atmosphere. The phase change occurs by pressure, in contrast to the typical thermally generated phase transition. By reducing the ball's diameter, without producing VO₂ (M), the weak grinding ball's impact pressure may convert VO₂ (B) into VO₂ (A).). The researcher suggested quick and easy hydrothermal method to synthesize vanadium dioxide B polymorph. To generate VO₂ (B) platelets, we employed a unique, combination of precursors, citric acid and V₂O₅. In order to propose an indirect, quick preparation approach for VO₂ (M1), Popuri et al. [102] shown in this study that testing of the VO₂ (B) phase transition conducted in vacuum indicate a one-step conversion into VO₂ (M1). Wang et al. [103] fabricate the VO₂ (D) nanobelts by using hydrothermal method and changed in VO₂ (M) by using annealing process at the temperature of 250-400°C for 0.5-5h. In this article they explain the grain size increased from 20nm to 30nm when the increase the temperature from 250°C to 400°C.

Zhu et al. [104] examine the VO₂ (B) nanoparticles' Hydrothermal production for gas sensing applications. In this paper they characterized the composition and microstructure of VO₂ (B) nanoparticles in the application of gas sensing. At the ideal working temperature of 300 °C, the VO₂ (B) nanoparticles showed a significant sensitivity to alcohols (isopropanol, ethanol and butanol) and acetone. Simo et al. [105] fabricate the high crystalline VO₂ nanorods by using facile hydrothermal sol-gel method. In this study, they provide a combination of monoclinic phases that significantly boost the material's resistance and enable its strong performance as a formaldehyde sensor at low concentrations and as a room temperature resistive methanol sensor at high concentrations. Pan et al. [106] V₂O₅ with diameters range from 190 to 560 nm were created using a simple method, and the result was superior electrochemical performance of 440 nm hollow spheres with improved cycle stability, showing a maximum specific discharge capacity.

Simo et al. [107] highlighted the surprisingly boosted hydrogen sensing properties of a specific phase of vanadium dioxide in the form of nanobelt at room temperature. Compared

to CO and CO₂, this sensing provides a high gas selectivity and a detection concentration limit of 0.17 ppm H₂. By using a hydrothermal technique, Liang et al. [108] created VO₂ nanorods. These nanorods were then successfully annealed at 450 °C to adorn them with Ag nanoparticles. After exposed to 5 ppm NO₂ at ambient high temperature, Ag-modified VO₂ nanorods sample that was annealed at 450 °C had the greatest response (2.54) of all the samples. With VO₂, the greatest quantity of Ag nanoparticles demonstrated efficient adherence in the T450 sample.

Vanadium oxide nanotubes were produced with a high yield by Chandrappa et al. [109] by adding hexadecylamine to V₂O₅•nH₂O gels and then hydrothermally treating the mixture at 150–180 °C for two to seven days. Transmission electron microscopy (TEM) was used to examine the nanotubes' morphology, while XRD and SEM were used to modify the reaction duration and temperature needed to synthesize VO_x-NT. Kamila et al. examined the energy storage properties of these electrode materials by employing both symmetric and asymmetric supercapacitor devices. Their research highlights the evaluation of these materials' performance in various supercapacitor configurations [110]. The hybrid material exhibits the 737 Fg⁻¹ specific capacitance when used in a symmetric supercapacitor device. Additionally, the performance of both symmetric and asymmetric supercapacitor configurations was evaluated with potential range of 2 V, highlighting the effectiveness of the energy storage system. The V₂O₅ nanoparticles were made by Menezes et al. [111] using a simple process that involved heating a layered vanadium oxide that resembled bariandite. The nanoparticles have a normal width of 15 nm and a high degree of crystallinity, as shown by TEM studies. Starting with a solution made by ultrasonic treatment, the nanoparticles were electro-phoretically deposited to create a V₂O₅ nanostructured film. FESEM pictures indicate that this film has a fibrous quality. This electrode is electroactive in an ionic liquid-based electrolyte, according to cyclic voltammetry tests. Nanoparticle addition increased discharge capacity values by about 50% as compared to an electrode prepared by casting a V₂O₅ xerogel.

Zhang et al. [112] created this work has developed a facile and efficient synthesis technique to manufacture Na_{1.08}V₃O₈ nanorods. At the ideal working temperature of 260°C, With S = 3.45, the Na_{1.08}V₃O₈ nanorods demonstrated good sensitivity towards 100 ppm ethanol, according to the gas sensing measurement.

Chu et al. [113] provide a simple method to produce an electrochromic film using V_2O_5 nanorods. The results of this study indicate that the development of lithium-ion secondary batteries and smart window technologies can greatly benefit from the use of synthesized V_2O_5 . Li et al. [114] employ the hydrothermal approach to synthesize V_2O_5 nanosheets with the aim of enhancing the powder's electrochemical characteristics by structural modification. According to the findings of electrochemical tests, the V_2O_5 nanosheet functions well in the 0.5M K_2SO_4 electrolyte. At 0.5 A/g of current density, the specific capacitance may reach 375 F/g. Furthermore, the material retains 96.8% of its capacitance even after 1000 cycles. The V_2O_5 nanoparticles were created by Sutrave et al. [115] and are successfully synthesised using a low-cost fuel and solution combustion synthesis. The generated nanoparticle's pseudo-capacitive characteristics are displayed using cyclic voltammograms. The GCD technique gives the specific capacitance 310 F/g, and a modified Randel's circuit is fitted to get the system parameters. The generated electrode would be suitable for industrial application, according to the results. Shah et al. have outlined various solution-based techniques for integrating vanadium pentoxide (V_2O_5) with graphene oxide (GO) nanosheets [116]. The composite's enhanced hybrid super capacitive performance has been examined. The electrochemical performance of the V_2O_5 nanocomposite is significantly enhanced upon the addition of GO. The composite materials exhibit notably elevated specific capacitance, reaching 438.1 Fg^{-1} at 1 Ag^{-1} .

The V_2O_5 /rGO/PCL nanofiber was created by Chanu et al. [117] employing the electrospinning procedure after the chemical reduction approach. In the cyclic voltammetry investigation, the highest specific capacitance of 702 Fg^{-1} at a scan rate 10 mVs^{-1} and the smallest equivalent series resistance at current density of 2 Ag^{-1} are $44.25 \text{ } \Omega$. The solution resistance and charge transfer resistance were determined to be $19.8 \text{ } \Omega$ and $442.56 \text{ } \Omega$, respectively, using the Nyquist plot analysis. In this work, Gupta et al. [118] used a simple, one-step hydrothermal method to manufacture electroactive electrodes made of graphene nanoribbons/nanosheets and vanadium oxide nanobelts (VNB) composites with varying weight ratios. Electrochemical characteristics revealed that the specific capacitance of composites was larger than that of components, and as expected, it declined with increasing scan rate.

A binder-free type of flexible wrinkling thin film electrode was created by Hu et al. [119] using an affordable, quick, easy and environmentally friendly synthesis method. At a current

density of 5 A/g, the VG8 composite thin film electrode retains 98% of its capacitance after 2000 cycles, exhibiting remarkable cycling stability once created. At 1 A/g of current density, it also shows a high specific capacitance of 397 F/g. Synergistic effects between V_2O_5 and graphene oxide (GO) are responsible for this remarkable performance. Applying the sol-gel process, Reddy et al. [120] produced porous structured V_2O_5 , which showed 214 Fg^{-1} specific capacitance in a 2 M KCl electrolyte at a scan rate of 5 mVs^{-1} . For up to 100 cycles, this porous V_2O_5 maintains its initial capacitance. The main cause of capacitance fading in materials based on V_2O_5 was attributed by the authors to the structural instability of V_2O_5 during ion intercalation. Qu et al. [121] synthesised V_2O_5 nanoribbons via a hydrothermal process, and they investigated its potential as supercapacitor electrode applications. The specific capacitance of V_2O_5 nanoribbon has 181 Fg^{-1} in 0.5M K_2SO_4 electrolyte. Furthermore, this substance showed excellent stability over 100 cycles. The performance of an asymmetric type supercapacitor device that the scientists made using this material as the electrode was also reported.

V_2O_5 nanofibers were produced by Wee et al. [122] using an electrospinning process and heat treatment at various temperatures. Using propylene carbonate electrolyte and annealed at 400°C, the scientists were able to achieve the highest specific capacitance of 250 Fg^{-1} in 1M LiClO_4 and 190 Fg^{-1} in 2 M KCl. They also discussed how the material shape varied with different annealing temperatures. Chen and colleagues [123] employed the melt quenching process to manufacture the AC/ V_2O_5 composite and then examined its electrochemical characteristics. This material has a 33 Fg^{-1} maximum specific capacitance at a current density of 200 mA g^{-1} in a 2 M NaNO_3 solution. The performance of the composite in several electrolytes, including NaNO_3 , KNO_3 , LiNO_3 , Na_2SO_4 , K_2SO_4 , and Li_2SO_4 , was investigated by the authors. NaNO_3 electrolyte was one of them mentioned.

The low-cost spray pyrolysis approach used by Wang et al. [124] to synthesise the V_2O_5 /carbon composite powder produced a specific capacitance of 295 Fg^{-1} in an electrolyte of 2 M KCl. The authors noted that varying the annealing temperature caused variations in the electrochemical performance. Regrettably, the authors did not carry out stability, charge-discharge, or impedance experiments to fully comprehend the electrochemical characteristics. Perera et al. [125] used the physical vapour deposition (PVD) technique to create spherical clusters of V_2O_5 nanotubes. The diameter of the V_2O_5 nanotubes that were PVD-deposited was 70 nm. For electrochemical studies, the authors used 1M LiTFSI

organic electrolyte (in acetonitrile). This material exhibited outstanding stability, with no discernible fading even after 50 charge-discharge cycles.

Mesopores activated carbon nanofibers were created by Kim et al. [126] using an electrospinning method. This produced 74 Fg^{-1} specific capacitance in the electrolyte, acetonitrile. The authors also varied the V_2O_5 content in the composite and examined changes in its electrochemical features. Porous structured V_2O_5 /carbon nanofibers composites were prepared by Kim et al. [127] using an electrospinning technique. In order to investigate the materials application in supercapacitor electrodes, they looked at its electrochemical characteristics. This material shows a specific capacitance of up to 150 F/g , an energy density of 8.8 Wh/kg , and a power density of about 400 W/kg . Chen et al. [128] used a easy in-situ hydrothermal method to create V_2O_5 nanowires. The nanowires were found to have 440 Fg^{-1} and 200 Fg^{-1} specific capacitances at 0.25 and 10 Ag^{-1} , respectively. The authors used carbon as the electrode and V_2O_5 nanowires to create an asymmetric supercapacitor. Using a specific capacitance of 45 Fg^{-1} at 0.62 mAcm^{-2} and a power density of 75 Wkg^{-1} , this asymmetric device provided 16 Whkg^{-1} energy density. Additionally, this device retains 90% of its capacity even after 100 charges and discharges.

Using a self-anodization process, Yang et al. [129] created V_2O_5 - TiO_2 mixed oxide nanostructures that had an energy density of 19.56 Whkg^{-1} and a specific capacitance of 220 Fg^{-1} . Up to 600 rounds of cyclic stability testing were reported by other authors. Jayalakshmi et al. [130] produced nanostructured SnO_2 - V_2O_5 mixed oxide by a hydrothermal method. In an aqueous solution containing 0.1 M KCl , the mixed oxide composite material has the maximum specific capacitance of 121 Fg^{-1} . Vanadium oxide/ordered mesoporous carbon composites were made by Hao et al. [131] using a liquid phase approach and calcinations. With 5 M LiNO_3 , this hybrid nanocomposite had a maximum specific capacitance of 257 Fg^{-1} at 0.5 Ag^{-1} and endured at 77.3% at 8 Ag^{-1} . Afterward 5000 cycles, this composite lost 20% of its original capacity. Shakir and colleagues [132] produced hybrid composites of V_2O_5 with multiwall carbon nanotubes using a bottom-up construction method. In 2 M KCl electrolyte, this nano composite may show the specific capacitance of 510 Fg^{-1} . Using a hydrothermal process, Perera et al. [133] created flexible paper electrodes made of graphene and V_2O_5 nanowire composites without the need for binders. Using this hybrid composite material, the scientists created a device of supercapacitor, demonstrating 80 Fg^{-1} specific

capacitance in 1 M Lithium bistrifluoromethane sulfonimide (LiTFSI) in an aqueous organic electrolyte.

In LiPF_6 organic electrolyte, Zhao et al. [134] created nanostructured V_2O_5 /reduced graphene oxide composite and explored its potential for supercapacitor and Li-Ion battery applications. For the creation of this composite electrode material, the authors combined a low temperature pyrolysis technique with a hydrothermal process, and they methodically examined the electrochemical performance. RGO/ V_2O_5 hydrogel was created by Zhang et al. [135] and evaluated for usage in wave absorbent and super capacitor applications. This nanocomposite electrode provided 320 F/g of specific capacitance at a current density of 1 A/g. additionally, this material exhibits very low specific capacitance ($\sim 170 \text{ Fg}^{-1}$ at 8 Ag^{-1}) at higher current rates. Up to 1000 cycles, this composite material maintains 70% of its capacitance. Reduced graphene oxide and V_2O_5 nanocrystals were created by Li et al. [136] and their applicability as supercapacitor electrodes was investigated. At a current density 1 Ag^{-1} , this nanocomposite demonstrated 537 Fg^{-1} specific capacitance. Furthermore, up to 1000 cycles, 84% of the capacitance in this composite is retained.

Qu et al. [137] created core-shell structured PPy grown on V_2O_5 nanoribbons by hydrothermally treating the material with dodecyl benzene sulfonate (DBS) as a surfactant. The specific capacitance of this composite material is 308 Fg^{-3} at 100 mAg^{-3} in $0.5 \text{ M K}_2\text{SO}_4$. Activated carbon and PPy/ V_2O_4 were used as electrodes in the development and analysis of a supercapacitor device by the researchers. Bai et al. [138] employed the co-deposition process to prepare the V_2O_5 /polypyrrole composite. This nanocomposite has 412 Fg^{-1} specific capacitance at 4.5 mA/cm^2 in a 5 M LiCl aqueous solution. This study's usage of organic electrolyte provides an extra potential window of up to 2V.

Yang et al. [139] produced hollow spherical V_2O_5 particles by utilising a solvothermal technique. It may show up as much as 479 Fg^{-1} of specific capacitance in 5 mVs^{-1} of organic electrolyte with 5 M LiNO_3 . The specific capacitance of the PPy-coated V_2O_5 spheres is 559 Fg^{-1} at 5 mVs^{-1} . Despite having a higher specific capacitance, this material loses its capacitance after 100 cycles. In 1 M LiClO_4 in propylene carbonate electrolyte, the Ni doped V_2O_5 thin films made by Jayalakshmi et al. [140] employing spray pyrolysis process show 417 Fg^{-1} specific capacitance at 5 mVs^{-1} . Hydrothermally treated V_2O_5 nanoribbons were synthesised by Wei et al. [141] In a 2 M NaCl solution, these nanoribbons have a specific capacitance of 453 Fg^{-1} at a scan rate of 2 mVs^{-1} . The authors skipped the charge/discharge,

cycle stability, or impedance tests to gain a complete understanding of the material's electrochemical capabilities.

Through the creative combination of hydrothermal, nano casting and freeze-drying methods, Cao et al. [142] created 3D $\text{V}_2\text{O}_5@\text{PPy}$. At 0.25 Ag^{-1} and 10 Ag^{-1} , this material showed specific capacitances of 502 and 244 Fg^{-1} . What's more intriguing is that the scientists created an asymmetric supercapacitor and used it to power a light-emitting diode. An important study on the V_2O_5 -based supercapacitor was described by Zhu et al. [143] This study described the hydrothermal method's creation of three-dimensional V_2O_5 nanosheets. The authors achieved 451 Fg^{-1} higher specific capacitance at 0.5 Ag^{-1} . This material retains 230 Fg^{-1} at 10 Ag^{-1} and has a charge transfer resistance of 10Ω . Wu et al. [144] employed an easy sol gel technique to produce hybrid aerogels of graphene and V_2O_5 . It was discovered that this composite has 250 Wkg^{-1} power density, 68 Whkg^{-1} energy density of, and 486 Fg^{-1} specific capacitance. It is possible to sustain 180 Fg^{-1} with this composite material at a higher current rate of 10 Ag^{-1} . Hydrothermal process was used by Lee et al. [31] to create graphene-decorated V_2O_5 nanobelts. In an aqueous electrolyte containing $1 \text{ M Na}_2\text{SO}_4$, they were able to achieve 288 Fg^{-1} specific capacitance using the nanocomposite material. Materials based on V_2O_5 have the physical and electrochemical characteristics summarised in the following table. Large-scale long $(\text{NH}_4)_0.5\text{V}_2\text{O}_5$ nanowires were synthesised by Wu et al. [145] using a hydrothermal process. The produced nanowires' conductivity at room temperature was 10^{-3} Scm^{-1} , according to electrical investigations. Furthermore, heat treatment turned the $(\text{NH}_4)_0.5\text{V}_2\text{O}_5$ nanowires into V_2O_5 nanowires.

Qiao et al. [146] produced $\text{V}_3\text{O}_7 \cdot \text{H}_2\text{O}$ nanobelts efficiently by hydrothermally processing store-bought V_2O_5 powder at relatively low temperatures. The resulting nanobelts had an average thickness of 20 nm and were many tens to hundreds of micrometres in length and length. It was shown that the nanobelts' electrochemical characteristics included a high discharge specific capacity of 253 mAhg^{-1} in the potential range of 3.8-1.7V. By using a thermolysis technique, Peng et al. [147] generated well-crystallized, narrowly distributed nanopowder of vanadium dioxide and tungsten doped vanadium dioxide. The change of the tetragonal structure from the monoclinic one during the heating process resulted in the observation of the semiconductor-metal transition. The W-doped powders had an 8°C heating-cooling hysteresis and a decreased transition temperature of 26.46°C , as indicated by the resistance temperature curve and DSC measurements. Gao et al. [148] effectively

synthesised single-crystalline $V_3O_7 \cdot H_2O$ nanobelts using a hydrothermal technique. The resulting nanobelts had a thickness of 30 nm and a width of 50 nm. A discharge capacity of 409 mAhg^{-1} was demonstrated by the $V_3O_7 \cdot H_2O$ nanobelts electrode, which equivalent to 4.32 mol Li^+ is intercalating into 1 mol of $V_3O_7 \cdot H_2O$ nanobelts. Zhai et al. [149] used a hydrothermal process to synthesise high-quality, large-quantity centimeter-long V_2O_5 nanowires. The diameter range of the single crystal orthorhombic nanowire structure that was developed is 80-120 nm. The nanowires showed a high capacity of 351 mAhg^{-1} together with a high coulomb performance of 99%.

Mai et al. [150] shown that annealing and electrospinning may be used to create ultralong structured V_2O_5 nanowires have a thickness of 100–200 nm and an average length of several millimetres. The 100 nm-long and around 50 nm-diameter vanadium oxide nanorods that were joined together to form the hierarchical nanowires. Within the potential window of 1.75 to 4.0V, the vanadium oxide nanowire cathodes' initial and 50th discharge capacities were 390 and 201 mAhg^{-1} . At contrast, at the potential window of 2.0 and 4.0V, ultralong hierarchical vanadium oxide nanowires showed initial and 50th discharge capacities of 275 and 187 mAhg^{-1} , respectively. Using commercial V_2O_5 powder as a precursor, Zhang et al. [151] shown the simple fabrication of large-scale nanobelts of vanadium oxide hydrate. For the manufacture of $V_3O_7 \cdot H_2O$ nanobelts, the Hydrating-Reducing-Exfoliating-Splitting (HRES) process was employed. Through the initial discharge capacity of 373 mAhg^{-1} , the $V_3O_7 \cdot H_2O$ nanobelts that were developed showed tremendous potential as cathode materials for batteries. High purity V_2O_5 ultralong nanobelts were created by Li et al. [152] using a hydrothermal process. The length of the straight nanobelts can reach a millimetre or more, and their width ranges from 30 to 200nm. The growth mechanism of directed attachment provided an explanation for the formation of ultralong nanobelts of V_2O_5 . Zhang Y et al. [153] used the hydrothermal technique to synthesise vanadium oxides with various morphologies. In comparison to the VO_2 nanobelts, which are long between 1 and 2.7 μm , broad between 80 and 140 nm, and thick between 2 and 8 nm, the synthesized $V_3O_7 \cdot H_2O$ are long up to 10 micrometres, wide between 60 and 150 nm, and thick between 5 and 10 nm. The $V_3O_7 \cdot H_2O$ and VO_2 (B) nanobelts showed the discharge capacity of 296-247 mAhg^{-1} at 0.2 mAcm^{-2} current density. Zhang et al. [154] successfully synthesized $V_3O_7 \cdot H_2O$ @C core-shell nanocomposites using an ambient hydrothermal method, using glucose as carbon and $V_3O_7 \cdot H_2O$ as the cores in the presence of sodium lauryl sulphate. However, by thermally

processing $\text{V}_3\text{O}_7 \cdot \text{H}_2\text{O}@\text{C}$ at 400 °C for two hours in an argon environment, $\text{V}_3\text{O}_7@\text{C}$ composites were created. $\text{V}_3\text{O}_7@\text{C}$ has a far higher discharge capacity than pure $\text{V}_3\text{O}_7 \cdot \text{H}_2\text{O}$, with a capacity of 151.2 mAhg^{-1} after 45 cycles, compared to 100 mAhg^{-1} after 30 cycles. This illustrates the improved cycle stability of the $\text{V}_3\text{O}_7@\text{C}$ composites. Using a hydrothermal technique, homogeneous starfruit-like V_2O_5 was first made by Shao et al. [155] the microstructural research revealed the hexangular starfruit-like construction mechanism. The starfruit-like vanadium oxide structures offered great cycle stability and a high-power capability (19 Whkg^{-1} specific energy at the specific power of 3.4 kWkg^{-1}) for supercapacitor applications. $\text{V}_3\text{O}_7 \cdot \text{H}_2\text{O}$ and VO_2 (B) nanobelts were successfully synthesised by Zhang et al. [156] using a moderate, direct hydrothermal process without the need for a template. The resulting $\text{V}_3\text{O}_7 \cdot \text{H}_2\text{O}$ nanobelts are between 100 and 300 nm wide and have lengths in the few tens of micrometre range. Comparably, the length of VO_2 nanobelts ranges from hundreds to several micrometres, while their breadth falls between 100 and 200nm. The synthesized $\text{V}_3\text{O}_7 \cdot \text{H}_2\text{O}$ and VO_2 nanobelts demonstrated 350 mAhg^{-1} initial discharge capacity and 190 mAhg^{-1} at a current density of 30 mA g^{-1} .

Zhu et al. demonstrated the wide-ranging production of 3D V_2O_5 constructs using hydrothermal and freeze-drying techniques. The resultant V_2O_5 structures have a 133 m^2g^{-1} surface area and include narrow walls, multilayer pores, and remarkable flexibility. At a current density of 0.5 Ag^{-1} , these special structures demonstrated a high specific capacitance of 451 Fg^{-1} , and at a high-power density of 9.4 KWKg^{-1} , they demonstrated an energy density of 107 Whkg^{-1} . High-quality MoV_2O_8 nanowires were successfully synthesised by Shahid et al. [157] by spin coating and thermal annealing. Synthetic nanowires range in length from 1 to 5 meters and have an average diameter of 100 nm. The electrochemical properties of the synthesized nanowires yielded a 56 Fg^{-1} specific capacitance at 5 mVs^{-1} scan rate using cyclic voltammetry.

Tang et al. [158] explored the electrochemical performance of vanadium pentoxide nanoflowers. The hydrothermally produced $\text{V}_{10}\text{O}_{24} \cdot n\text{H}_2\text{O}$ samples were annealed to get the porous V_2O_5 nanoflowers. The V_2O_5 nanoflowers' pore volume and surface area are 22.7 m^2g^{-1} and 0.12 cm^3g^{-1} , respectively. The V_2O_5 nanoflowers offered 275 mAhg^{-1} initial discharge capacity at a 50 mA g^{-1} current density with high cycle stability. Sun et al. [159] effectively created hydrated vanadium pentoxide nanoribbons modified with decreased graphene oxide by the use of a hydrothermal process. Li ions have low diffusion lengths and

effective electron conduction channels because to the interweaving network of free-standing VO_x/RGO film. The VO_x/RGO film's electrochemical studies revealed a 160 mAhg⁻¹ discharge capacity and strong cycle stability in the voltage range of 2.0 to 3.5V.

Mjejri et al. [160] used a straightforward and elegant method to hydrothermally synthesise Mesoporous V₃O₇ nanorods with cross section from a combination of V₂O₅ and hydroquinone. V₃O₇ has a surface area of 18 m²g⁻¹, a mean width of 130 nm, a mean thickness of 70 nm, and high degree of crystallinity in its rod-like nanostructures. Hydrogen nanorods showed potential as cathode materials in batteries, most likely because of their charge-discharge cycling-induced reversible redox behaviour. Li et al. [67] used a hydrothermal method to create a V₃O₇.H₂O/CNT nanocomposite that included functionalized CNTs. The V₃O₇.H₂O nanobelts had a width of a few hundred nanometres and a length of several micrometres. The nanocomposite electrode indicated the 186.4 mAhg⁻¹ discharge capacity at 200 mA g⁻¹ current density with good cycle stability. Applying a basic green methodology, Perera et al. [133] created V₂O₅ nanowires on graphene sheets. At a consistent discharge current of 0.5Ag⁻¹, the developed hGO-VNW paper electrode demonstrated the 38.8 Whkg⁻¹ energy density and 465Wkg⁻¹ power density. But at this moment, the electrode's estimated specific capacitance was 80 Fg⁻¹.

V₂O₅ nanowires were produced on graphene sheets by Perera et al. [161] use an easy green technique. Using a fixed discharge current of 0.5Ag⁻¹, the developed hGO-VNW paper electrode demonstrated the 38.8 Whkg⁻¹ energy density and 465 Wkg⁻¹ power density. But at this moment, the electrode's estimated specific capacitance was 80Fg⁻¹. The hydrothermally synthesised Co₃V₂O₈ nanoplates for supercapacitors were studied by Cheng et al. [162]. The morphological analysis of the synthesised Co₃V₂O₈ thin nanoplates, which has a thickness of 40 nm and a diameter between 150 and 200 nm. The synthesised Co₃V₂O₈ nanoplates showed good cycling stability even after 2000 cycles, with 739 Fg⁻¹ specific capacitance at 0.5 Ag⁻¹ current density.

The ultra-thin nanobelts arrays of metastable VO₂ (B) were created by Qin et al. [163] these arrays may be transformed into porous V₂O₅ nanobelts arrays by calcining VO₂ (B) in air for duration of one hour at 400°C. The V₂O₅ nanobelt arrays offered the 142 mAhg⁻¹ discharge capacity at 50mA g⁻¹ current density with high cycle stability. Additionally, they showed remarkable capacity retention and a 130 mAh⁻¹ discharge capacity at a 1Ag⁻¹ current density. Zhu et al. [164] created V₂O₅ micro/nanorods by electrospinning NH₄VO₃ and

H₂C₂O₄ composite fibres and then heat treating the result. The resulting micro/nanorods had an average diameter of 300 nm and a length-to-diameter ratio of 5–10. Their composition was orthorhombic V₂O₅. On the other hand, the cathode electrodes of vanadium oxide demonstrated excellent stability in structure and an excellent capacity for discharge of 418.8 mAhg⁻¹ at a current density of 50 mA g⁻¹.

A novel and simple method for creating a CoV₂O₆/natural graphite electrode with sodium alginate binder was created by Ni et al. [165] The generated electrodes have 902 mAhg⁻¹ discharge and charge capacity at 110 mA g⁻¹ current density. The CoV₂O₆/NG electrode's remarkable cycle performance and high specific capacity demonstrated the material's considerable promise as a Li-ion battery.

A hydrated vanadium oxide nanocomposite coated with graphene was described by An et al. [166] as an effective cathode material for magnesium storage with a longer cycle life. The nanocomposite showed remarkable performance of electrochemical with 320 mAhg⁻¹ specific capacity at 0.05 Ag⁻¹ current density and fast cycling for 200 cycles. Additionally, the nanocomposite demonstrated a wide working temperature, ranging from -30°C (~ 40 mAhg⁻¹) to 55°C (200 mAhg⁻¹). Chiku et al. initially employed an amorphous vanadium oxide/carbon composite as the positive electrode in rechargeable aluminium batteries [167]. 200 mAhg⁻¹ initial discharge capacity was achieved by the composite electrode. The redox of the vanadium ion in the composite electrode was examined using XPS during charging and discharging. The average valence of V ranged between 4.14 and 4.85, according to the data.

Wang et al. [168] used an easy solvothermal process to successfully manufacture a novel V₂O₅/graphene mesoporous composite that resembles a sandwich. Graphene sheets were used to support the nanostructured vanadium oxide particles in a sandwich-like manner. The novel structural composite demonstrated 1006 mAhg⁻¹ high reversible capacity at 0.5 Ag⁻¹ current density after 300 cycles. Li et al. [169] examined the hydrothermal procedure after employing the sol-gel method to create a novel 2Li₃V₂(PO₄)₃.LiV₃O₈ nanocomposite with the morphology of thin plate. The prepared composite exhibits a high initial capacity of 162.8 mAhg⁻¹ at a voltage of 2.0–4.3V and a current density of 100 mA g⁻¹. Using the galvanostatic intermittent titration method, the diffusion coefficient of lithium ions inside the composite was found to be between 10⁻¹¹ and 10⁻⁹ cm²s⁻¹.

The authors Song et al. [170] Mesoporous V_2O_5 nanosheets were successfully produced by a hydrothermal procedure that involves rapid heating and annealing in air. The prepared V_2O_5 nanosheets are collected from different nanosheets and have a highly mesoporous nanosheet structure. The high specific capacity of 147 mAhg^{-1} and current density of 100 mA g^{-1} indicate that the mesoporous V_2O_5 nanosheets utilized as the cathode materials in batteries have great rate capability.

A unique method of preparing porous vanadium pentoxide for use as a cathode material in lithium ion batteries was disclosed by Su et al. [171]. Ketjen black, porous carbon composites were used as stiff templates to allow precursor species to fit into their openings. At 100 mA g^{-1} current density, the porous V_2O_5 electrodes displayed excellent rate capability, cycling stability and 141.1 mAhg^{-1} initial discharge capacity. Wei et al. [172] Vanadium pentoxide nanowires were produced by using the vapor-solid technique of thermal evaporation. V_2O_5 nanowires are longer than 10 nm and have a diameter of 100 nm , giving them an orthorhombic structure. Peak excitation spectra of V_2O_5 nanowires have been measured at 400 , 560 , and 710 nm . These spectra are the consequence of discrete interband transition from the O $2p$ valence band to the V $3d$ conduction band. The electrochemical properties of V_2O_5 nanowires and their electrical resistivity of 64.62 demonstrated their suitability as cathode materials for secondary batteries. Using cetyltrimethylammonium bromide as a soft template, Umeshbabu et al. [173] produced distinct V_2O_5 hierarchical one-dimensional nanochains. It was the hydrothermal process that made this possible. For the V_2O_5 -ctab samples, the determined BET unique surface area was 68 mg^{-1} . At a current density of 0.5 Ag^{-1} , the V_2O_5 nanoclusters displayed a highest unique capacitance of 631 Fg^{-1} . Moreover, after 1200 charge-discharge cycles, they maintained 75% of the capacitance, demonstrating outstanding cyclic stability.

Li et al.'s effective synthesis of porous vanadium pentoxide (V_2O_5) nanotubes [174] used a simple electrospinning technique followed by an annealing step. The generated vanadium oxide nanotubes produced 114.9 mAhg^{-1} capacity at a rate of 10 C within the $2.5 - 4.0 \text{ V}$ potential range. However, the nanotubes of porous V_2O_5 demonstrated excellent cycling performance and 96.4% capacity retention after 200 cycles at a rate of 50 C . B.M. Babar et al. [175] The hydrothermal method was successful in synthesizing the nanostructure of the V_2O_5 -rGO nanocomposite. To verify the presence of oxygen vacancies or abnormalities, they employ PL spectroscopy. The maximum gas response, or around 121.85% , is shown

by a calcined product with the ideal surface area and pore size when it is subjected to 100 ppm of NO₂ gas at 150°C. The constructed composite has response and recovery periods of approximately 39 and 262 s, respectively.

By using ultrathin LiV₃O₈ nanoflakes and graphene nanosheets to self-assemble sheet to sheet, Wang et al. [176] a novel LiV₃O₈/graphene nanocomposite was produced. The graphene nanosheets can maintain the structural integrity of LiV₃O₈, improve electrical conductivity, and prevent the nanoflakes from clumping together after repeatedly adding and removing lithium ions. As a result, the novel composite generated 328.7 mAhg⁻¹ high discharge capacity at 2C current density.

Tang et al. [177] created a free-standing, highly conductive VO/VO_x/CNF composite electrode via heat treatment and electrospinning. The electrode's specific capacitance was 325.7 Fg⁻¹ at a current density of 1 Ag⁻¹ of nanocomposite. Even after 5000 cycles, the electrode of a symmetric two-electrode capacitor retained 92% of its original capacitance at a current density of 4 Ag⁻¹. Wang et al. [178] used a hydrothermal technique to make a composite comprising V₂O₅, carbon nanotubes, and highly activated carbon. The novel nanocomposite had 357.5 Fg⁻¹ specific capacitance at 10 Ag⁻¹ current density. Additionally, after 200 cycles, the capacitance rose to 128.7% of its starting value, and after 1000 cycles, it maintained 99.5% of its highest value.

Pandey et al. [179] used a two-step solvothermal approach to create an efficient mesoporous hybrid composite of V₂O₅ attached on reduced graphene oxide nanosheets. In a symmetric supercapacitor cell, the rGO-V₂O₅ electrodes exhibit great cycle stability, a high specific capacitance of 466 Fg⁻¹ and good rate capability. 295 mAhg⁻¹ specific capacity at C/9 rate was provided by the hybrid cathode electrode rGO-V₂O₅ in LIB. According to Zhang et al. [180], commercial V₂O₅, ethanol (EtOH), and H₂O materials were used in a straightforward hydrothermal process to create V₂O₅ nanoparticles with a irregular surface. The best parameters for producing V₂O₅ were a ratio of EtOH/H₂O = 10/25 and two to four hours of calcination at 400°C. At 0.5Ag⁻¹ current density, the synthesised V₂O₅ nanomaterials established a specific capacitance of 423 Fg⁻¹, and they were able to maintain 327 Fg⁻¹ at a high current density of 10Ag⁻¹. Li et al. [181] first developed wet-spinning method to make hybrid fiber electrodes based on vanadium pentoxide. Asymmetric V₂O₅/SWCNT/RGO/SWCNT solid-state nanofiber supercapacitors demonstrated a 90% retention rate and a volumetric energy density of 1.95 mWhcm⁻³. Additionally, they

displayed a 7.5 mWcm^{-3} volumetric power density. It does, however, show good mechanical behaviour and flexibility; 97% of the capacitance was preserved after 500 cycles of 90° bending. For Amperometric dopamine sensing and lithium ion battery applications, Yang et al. [182] examined the electrochemical characteristics of an electrode made from a combination of smaller-crystalline melt-quenched vanadium oxide and graphene oxides generated hydrothermally. With the maximum sensitivity of $25.02 \text{ AmM}^{-1} \text{ cm}^{-2}$ and the lowest detection limit of 0.07 M , the composite electrode excelled. In comparison, the electrode used in the lithium-ion battery application demonstrated excellent cycle stability and a 200 mAhg^{-1} discharge capacity at a 0.1 C current density.

By employing the seed-assisted hydrothermal approach, Xu et al. [183] were able to effectively build a 3D free-standing V_6O_{13} nanostructure made of linked nanosheets. The electrode exhibited a specific capacity of 170 mAhg^{-1} at 0.3 Ag^{-1} current density. But even after 300 cycles at 0.3 Ag^{-1} current density, the electrode covered with carbon nanotubes retained 74% of its initial capacity. Park et al. [184] used the radio frequency sputtering technique to create vanadium oxide thin films with varying thicknesses from V_2O_5 (ceramic) and V (metal) targets. The V_2O_5 ceramic target was used to create 500 nm-thick films, which showed suitable cycle performance and discharge capacity. However, the electrochemical properties of the film become invisible when its thickness surpasses 500 nm. As the film thickness rose, so did the discharging capacity and cycle performance of the V_2O_5 thin films produced from the vanadium metals target. Lopez et al. reported that reactive sputtering with a vanadium metal target produced thin films of vanadium pentoxide without the requirement for post-annealing treatment [185]. The films with a $2.4 \text{ }\mu\text{m}$ thickness showed a constant capacity of 75 Ah/cm^2 at 100 A/cm^2 current density after 100 cycles within a potential window of $3.8/2.8 \text{ V}$. Furthermore, the discharge capacity was increased to 130 Ah/cm^2 in the potential range of $3.8/2.15 \text{ V}$.

Orthorhombic V_2O_5 thin films were investigated by Wang et al. [186] via Sol electrophoretic deposition and post-treatment at 500°C . At current density of 50 Acm^{-2} , the synthesised V_2O_5 thin films demonstrated high capacities of 300 mAhg^{-1} in the 0.4 to 1.6 V potential window and 110 mAhg^{-1} in the potential window of 0.4 to 1.1 V . Using a metallic Ag target and a V_2O_5 target, Gies et al. [187] created $\text{Ag}_y\text{V}_2\text{O}_5$ thin films by radiofrequency magnetron co-sputtering in either pure argon or a mixed argon/oxygen environment with 14% of oxygen partial pressure. The produced amorphous $\text{Ag}_{0.32}\text{V}_2\text{O}_{4.6}$ thin films had a smooth surface,

were dense, and demonstrated strong cycle stability and discharge capacity. Because silver ions are participating in the redox processes in addition to crystallised V_2O_5 , the deposited amorphous $\text{Ag}_{0.26}\text{V}_2\text{O}_5$ thin films are porous and have shown improved discharge capabilities. Yu et al. [188] applied the sol-gel technique to create Mn-doped V_2O_5 thin films, employing H_2O_2 and V_2O_5 as precursors and adding Mn^{2+} right away during the sol production process. At 68 mA g^{-1} current density, Mn-doped V_2O_5 thin films had 283 mAh g^{-1} discharge capacity also the exceptional cycle stability, fading at a rate of less than 0.06% each cycle.

The relationship between the electrochemical behaviour and capacity fading of LiV_3O_8 thin-film positive electrodes and cycle performance was examined by Shi et al. [189]. The electrode deteriorated after 400 cycles, losing 44% of its initial capability, according to the extended cycling test. Capacity fading was mostly caused by the exfoliation of the active components and the creation of a surface layer. Reactive ballistic deposited nanostructured V_2O_5 thin film performance was investigated by Wu et al. [190] using LiPF_6 /diethyl carbonate + ethylene carbonate and LiClO_4 /propylene carbonate (PC) electrolytes in electrochemical processes. Electrochemical and Raman experiments revealed a 32% drop in capacity between both cycles in films cycled in LiPF_6 /DEC+EC as compared to the cycled in LiClO_4 /PC. This is because redox alters the form and content of the surface. The V_2O_5 cycled in LiPF_6 /DEC+EC had a greater atomic fluoride concentration (16.18%) than the V_2O_5 cycled in LiClO_4 /PC, according to XPS analysis.

Boukhalfa et al. [191] created a novel method for supercapacitor applications using atomic layer deposition, such as the deposition of nanostructured vanadium oxide on the surface of electrodes made of carbon nanotubes. Excellent electrical conductivity, high capacitance of 1550 F g^{-1} , and cycle stability were demonstrated by the 10 nm thick composite electrode. Its porosity was adjusted as well. Using a spray pyrolysis process, Mousavi et al. [192] created S-doped (0 to 40 at. %) vanadium oxide thin films. Both optical band gap and sheet resistance increased, rising from 2.41 to 2.7 eV and 940 to $4015 \text{ k}^\Omega/\text{square}$, respectively. Expanded and sharper anodic and cathodic peaks are visible in the cyclic voltammogram data of the undoped and 20 at. % of S-doped films, respectively.

For the first time, hot-wall chemical vapour deposition was used by Jampani et al. to create carbon nanotube (CNT) supported vanadium oxide nanospheres for supercapacitor applications. Vanadium oxide nano-droplets interacted with the electrolyte on a three-

dimensional electron transport channel made possible by the electrical conductivity of carbon nanotubes. As a result of this interaction, the nanocomposite showed good charge retention for up to 200 cycles, a high capacitance of 1400Fg^{-1} , and robust rate capability. Jayalakshmi et al. looked at the behaviour of sol-gel spin coated vanadium oxide films with different thicknesses [193] in relation to supercapacitors. The produced films feature V_2O_5 phase with 6-12 layered films, and the optical band gap was 2.2-2.5eV, according to microstructural and optical investigations. On the other hand, at a scan rate of 5mVs^{-1} , the eight-layered V_2O_5 film with 202 nm thickness of provided 346Fg^{-1} specific capacitance. The microstructural and electrochemical characteristics of Vanadium pentoxide thin films that were generated on flexible Kapton substrates covered with indium tin oxide by the use of the reactive evaporation process were examined by Hari Krishna et al. [194]. As deposited, V_2O_5 thin films demonstrated a consistent $60\text{Ah}/(\text{cm}^2\text{-}\mu\text{m})$ discharge capacity over 10 cycles at ambient temperature within the potential window of 4.0-2.5V. Furthermore, the multi-layered $\text{V}_2\text{O}_5/\text{Ag}/\text{V}_2\text{O}_5$ thin films showed improved cyclability and a discharge capacity of $75\text{Ah}/(\text{cm}^2\text{-}\mu\text{m})$.

Yin et al. [195] used a chemical vapour deposition approach to successfully synthesise three distinct types of V_2O_5 micro/nano-structures as hierarchical wires, rod and porous tubes by varying the oxidation temperature. Their hollow structure creation, increased pore quantity, and decreased particle size resulted in a considerable rise in their surface-to-volume ratio. Furthermore, studies on lithium-ion storage in aqueous electrolyte demonstrate that by inhibiting irreversible phase shift, a surface area increase can greatly improve stability, storage capacity, and electrochemical kinetics. Yu et al. [196] Using a simple anodic electrodeposition method, homogenous Vanadium pentoxide nanostructured materials thin sheets looking like mica were produced. Mica-like V_2O_5 thin films with 596mAhg^{-1} an initial discharge capacity at 1080mAg^{-1} current density were produced using nanosheets that were less than 50 nm thick. Moreover, V_2O_5 thin-films showed exceptional cycling stability with 1% of fading rate per cycle at 1080mAg^{-1} of current density. Bilayer structure of nano crystalline V_2O_5 (cathode) produced electrochemically on steel substrate in VOSO_4 solution for sodium-ion batteries was described by Li et al. [197]. The structure's two-dimensional V_2O_5 stacks were separated by an interlayer spacing of 11.6\AA , which is ideal for holding Na^+ ions. As a result, the electrode's high capacity (220mAhg^{-1}) and exceptional stability were attained.

2.2 Research Gap

- A need for more effective room temperature sensing as key limitations, thus presenting significant research gaps. Furthermore, a deeper understanding of the synthesis-structure-property relationship and strategies for enhanced response and recovery time offer additional avenues for future research in V_2O_5 -based gas sensors.
- A critical research gap involves exploring and optimizing microwave-assisted synthesis of V_2O_5 nanostructures specifically tailored for high-performance supercapacitor applications. This includes investigating how microwave synthesis parameters influence key material properties such as surface area, electrical conductivity, and ion diffusion pathways, ultimately impacting capacitance, energy density, and power density.
- Further research is needed to develop energy-efficient and scalable microwave-assisted synthesis protocols for V_2O_5 based electrode materials for supercapacitors. This includes optimizing reaction times, precursor concentrations, and microwave parameters to minimize energy consumption while achieving high yields and consistent material quality suitable for cost-effective device fabrication.

2.3 Objective of the Research Work

- Synthesis of vanadium oxide using mechano-chemical process, hydrothermal process and microwave process
- Modification of synthesized vanadium oxide using graphene oxide
- Comparative characteristic analysis of synthesized vanadium oxide
- Preparing the electrode of vanadium oxide for supercapacitor applications
- Device fabrication for sensing application of synthesized vanadium oxide

Chapter 3

Research Design, Materials and Methods

There are many synthesis techniques have been developed over time for creating electrode materials specifically designed for supercapacitors, as discussed in introduction part. The portion of the appropriate synthesis method is critical when working with nanoparticles. This is because nanoparticles are highly sensitive to the synthesis method and the precursor materials used, which can significantly affect their final properties and performance.

This chapter provides a detailed explanation of experimental methods which is used to synthesize vanadium oxide nanoparticles and their composites with GO. Three main synthesis techniques were employed: hydrothermal synthesis and mechanochemical and the microwave method. Using high-temperature aqueous solutions at high vapor pressures during hydrothermal synthesis helps to create well-defined nanostructures. The microwave synthesis method offers rapid and uniform heating, which significantly reduces reaction times and enhances the control over nanoparticle size and morphology. This technique also improves energy efficiency and often results in higher purity and yield of the synthesized materials. The mechanochemical synthesis method offers the advantage of being an environmentally friendly process that often requires less solvent and energy, while also enabling the production of nanomaterials with unique properties due to the high-energy mechanical forces involved.

Characterization of the synthesized materials is a crucial step. It makes it possible for researchers to have an extensive knowledge of the characteristics, behaviour, morphology, and other important factors that affect how the material is used in supercapacitors. There are various characterization techniques available for investigating the properties of nanosized particles. These techniques help in determining critical attributes such as size, shape, porosity, crystal structure, and the degree of agglomeration.

Identifying the modified properties during synthesis is essential. Therefore, nanoparticles must be thoroughly characterized to understand how they have changed due to the synthesis process. This includes assessing parameters like size and shape, which affect the surface area and reactivity, and crystal structure, which influences the mechanical and electrical properties. One of the major issues in nanoparticle synthesis is achieving reproducibility and maintaining the desired properties throughout the processing stages. Nanoparticles can exhibit different behaviours when subjected to various environments, which can change in their properties. Hence, researchers must recognize and address these unexpected

challenges. Understanding how different characterization techniques can minimize synthesis surprises and property changes is vital for advancing the field.

This chapter also discusses the various characterization techniques in detail, along with descriptions of the different instruments used for characterizing the samples. These instruments and methods provide the necessary tools to evaluate and ensure that the synthesized nanoparticles meet the desired specifications and perform as expected in their intended applications. By thoroughly characterizing the materials, researchers can better predict their performance and tailor them for specific uses in supercapacitors, leading to more efficient and reliable energy storage devices.

3.1. Methods used for the synthesized V_2O_5

There are many technique to synthesize V_2O_5 nanoparticles like sol-gel, auto combustion method, hydrothermal method, mechanochemical method and the microwave method. Among these methods hydrothermal, mechanochemical and the microwave method used to prepare the V_2O_5 nanoparticles.

3.1.1. Hydrothermal Technique

The term "hydrothermal method" encompasses various techniques utilized in hydrothermal synthesis, where compounds are crystallized from high-temperature aqueous solutions under elevated vapor pressures. This approach has geological roots, as "hydrothermal" pertains to research in geology. Since the early 1900s, mineralogists and geochemists have studied hydrothermal phase equilibria. Percy W. Bridgman at Harvard University and George W. Morey at the Carnegie Institution made important contributions to develop the guidelines for handling reactive media at the temperatures and pressures typical of hydrothermal processes.

The hydrothermal synthesis method makes use of the solubility in hot water under high pressure to create single crystals. The autoclave, a steel pressure vessel that carries water and nutrients, is the apparatus used to carry out the crystal formation process. The ends of the growth chamber are maintained at distinct temperatures. To develop the desired crystal, the nutrient solute is dissolved at the hotter end and put on a seed crystal at the cooler. In 1845, Karl Emil von Schafhäütl, a German geologist (1803–1890) reported the first instance

of hydrothermal crystal development. Using a pressure cooker, he created tiny quartz crystals.

The hydrothermal approach has shown very adaptable in the synthesis of different kinds of chemicals. This comprises, among other things, elements, tungstate, molybdates, carbonates, silicates, germinates, and simple and complicated oxides. Notably, the production of synthetic quartz, gemstones, and other single crystals of economic value is largely dependent on hydrothermal synthesis. This technique has been effectively used to develop a variety of crystals, including emeralds, rubies, quartz, and alexandrite. Hydrothermal synthesis is also a highly useful technique for identifying new mixtures with detailed physical properties and for conducting regular research of complex systems at high pressures and temperatures.

Design of Hydrothermal reactor

Autoclaves are the crystallization containers that are employed in figure 3.1. These are typically steel cylinders with strong walls and hermetic seals that must endure high pressure and temperatures for extended periods of time. In addition, the material to be autoclaved needs to be solvent-inert. The autoclave's sealing is by far its most crucial component. Several seal designs have been created, the most well-known of which being the Bridgman seal. Hydrothermal tests often utilize steel-corroding solutions. Protective inserts are often used to stop corrosion within the autoclave's interior cavity.



Figure 3.1 Hydrothermal reactor

Temperature-difference method

Hydrothermal synthesis and crystal growth are commonly performed using this technique. The process involves creating a temperature gradient within the crystal growth zone to induce super saturation. In this procedure, the nutrient is placed at the bottom of an autoclave that has a certain amount of solvent inside. A temperature gradient created by heating the autoclave causes the nutrient to dissolve in the hotter bottom part. The saturated solution is then moved upward by the solution's convective currents. The solution comes into contact with colder temperatures at the top of the autoclave as it rises. The cooling causes the solution to become supersaturated in the upper region, initiating the crystallization process.

Temperature-reduction technique

In this method, crystallization may be induced without the need for the temperature gap between the dissolution and growth areas. Instead, the temperature of the autoclave solution is progressively reduced to achieve super saturation. However, the challenge of managing the growth process and adding seed crystals is a significant drawback of this technique. These difficulties explain why this method is still very uncommon.

Metastable-phase technique

The solubility difference between the starting phase and the phase suitable for growth is the basis for this technique. During the growth process, the molecules in the nutrient phase are thermodynamically unstable. As the metastable phase dissolves, which is more soluble compared to the stable phase, the stable phase begins to crystallize. Typically, this approach is used alongside one of the other two methods previously mentioned.

Advantage of hydrothermal synthesis for nanoparticles synthesis

The hydrothermal technique of crystal development has an advantage over other methods since it may produce phases of crystals which are not reliable at the melting point. High vapour pressure materials that are near to their melting temperatures can also be produced via the hydrothermal process. Controlling the composition of large, superior crystals during their development is another area in which the approach excels. The usage of a steel tube will prevent the crystal shape from being visible, as well as the need for expensive autoclaves, are the method's shortcomings. Autoclaves with robust glass walls can be used at pressures of up to 10 bar and temperatures of up to 300 °C.

3.1.2. Microwave Technique

The study of using microwave radiation (systematic diagram of microwave oven as depicted in figure 3.2) to accelerate chemical processes is known as microwave chemistry. Any

material having electric charges, such as conducting ions in a solid or polar molecules in a liquid, will often be heated by microwaves, which operate as high frequency electric fields. When molecules in polar liquids collide and are compelled to spin with the field, they heat up. Because of the electrical resistance of the material, ions or electrons within conducting or semiconducting samples lose energy and generate an electric current, which causes them to heat up. After publications in 1986, microwave heating in the lab started to become widely accepted. Even though chemical modification has been using microwave heating since the 1950s. These acronyms, which are often referred to as microwave-assisted organic synthesis, microwave-enhanced chemistry or microwave-organic reaction enhancement, have not gained much traction outside of a select few organizations.

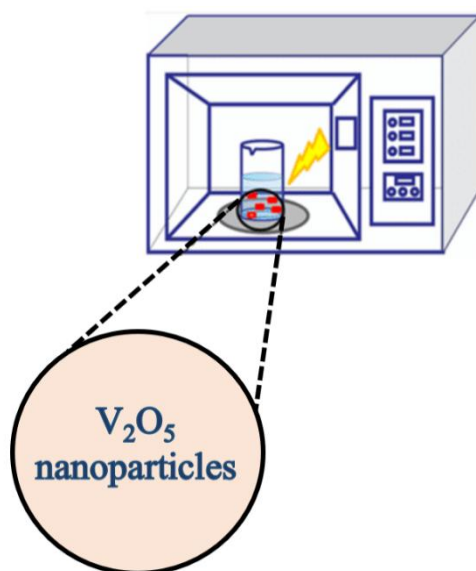


Figure 3.2 systematic diagram of microwave oven

Microwave absorption may heat the target compounds without heating the oil bath or furnace overall, saving time and energy since it functions as an internal heat source. Additionally, it may heat thin things sufficiently across their volume rather than only across their outside, which should result in more even heating. However, due to uneven absorption by the object being heated and the non-uniform nature of most microwave oven designs, localized superheating often arises in the microwave field. To counteract the uneven absorption, microwave volumetric heating (MVH) applies a strong, consistent microwave field. The rate at which various substances convert microwave radiation into heat changes. The reaction vessel in particular benefits from this selectivity, which enables certain areas of the item to heat more slowly or faster than others.

Compared to traditional ovens, microwave heating can offer the following advantages: Acceleration of the response rate, milder circumstances for the response, high chemical, output with less energy used, distinct selectivities of reactions and both organic and inorganic chemistry are utilized to microwave chemistry

Advantage of microwave synthesis method

Using microwave radiation to heat inorganic nanomaterial production has shown to be a very successful method. It provides the following benefits:

- effective way to heat anything (superheat), which raises reaction rates and speeds up synthesis
- regulation of form and size by simple adjustment of instrumental or reaction parameters
- selective heating using the idea that various materials react to microwaves in different ways
- Higher repeatability of chemical reactions compared to traditional heating because to more consistent heating and improved process parameter control.
- Potential combinations of microwave chemistry with other proven liquid-phase synthesis techniques, such as Sono chemical and solvothermal techniques.

3.1.3. Mechanochemical Technique

Mechanochemistry has a very long background. The mortar and pestle were first used as a grinding instrument back in the Stone Age. Subsequently, more advanced tools that may be used to produce materials for study and many real-world applications took the place of these basic tools. Using a variety of mechanical forces, including friction, shear strain, compression, and others, the reactant species undergoes a chemical change as part of the mechanochemical process. Theophrastus discovered that this procedure was written down as early as 315 BC in his work "On Stones". Although the fundamentals of Mechanochemistry remain mostly enigmatic, systematic research on the subject began in the 19th century and made great strides in the 1960s.

Cement clinker, ores, and powder metallurgy processes are a few significant industrial applications of mechanochemistry that date from the 19th century. These processes use fine grinding as a mechanochemical technique. Mechanochemistry is still a subject of study, although its initial slow progress was sped up with the development of mechanical alloying.

These days, mechanochemical synthesis is becoming more and more common in several disciplines, including organic, inorganic, and materials chemistry. A reaction of mechanochemical is "a chemical reaction that is induced by the direct absorption of mechanical energy," according to the definition provided by IUPAC in 2003 due to the rising popularity of Mechanochemistry.

Advantage of Mechanochemical method

One of the most secure methods for creating nanomaterials is mechanochemical synthesis. Comparing this synthesis to wet chemical processing, it is safer. The following are this synthesis's main benefits:

- Mesoporous materials may be synthesized by mechanical grinding with the use of templates. Furthermore, mechanochemical may be used to create nanoporous materials using nano-casting synthesis.
- The active sites on the surface, size, functionality, and surface-to-volume ratio of nanomaterials all play a significant part in their activity. Doping NPs can change their surface characteristics, which is frequently done to improve their antibacterial, catalytic, and other qualities.
- Conventional synthesis takes longer than mechanochemical processes. In traditional synthesis, it takes 70 hours to reduce particle size from 2-3 mm diameters to 3 μm , whereas a planetary ball mill can do the same task in 3 minutes.
- This method assists in producing nanoparticles with a limited distribution of particle sizes.

3.2. Characterization Techniques

Their characterisation may be used to identify the crystalline structure, size, and shape of the produced nanoparticles and nanocomposites. The electrochemical performance of supercapacitor electrodes was examined by means of electrochemical techniques such as electrochemical impedance spectroscopy, galvanostatic charge/discharge experiments, and cyclic voltammetry. The three primary metrics used to evaluate the performance of supercapacitors are specific capacitance, power density, and energy density.

3.2.1. Scanning Electron Microscope (SEM)

The morphological structure of the produced nanoparticles was investigated using a field emission scanning electron microscope (FESEM, JOEL). Figure 3.3 displayed the

Schematic of SEM. A scanning electron microscope, in contrast to conventional optical microscopes, produces pictures by use of a concentrated electron beam. A metal filament within the electron cannon is heated to produce this electron beam at the upper of the electron microscope. The electron ray descends the column of the microscope vertically. The beam is focused and directed onto the sample by use of electromagnetic lenses. As the sample comes into contact with the electron beam, secondary electrons are released from its surface. Following their collection, the secondary electrons are transformed into a signal that may be measured by detectors. This signal is used to generate an image displayed on a computer screen [198].

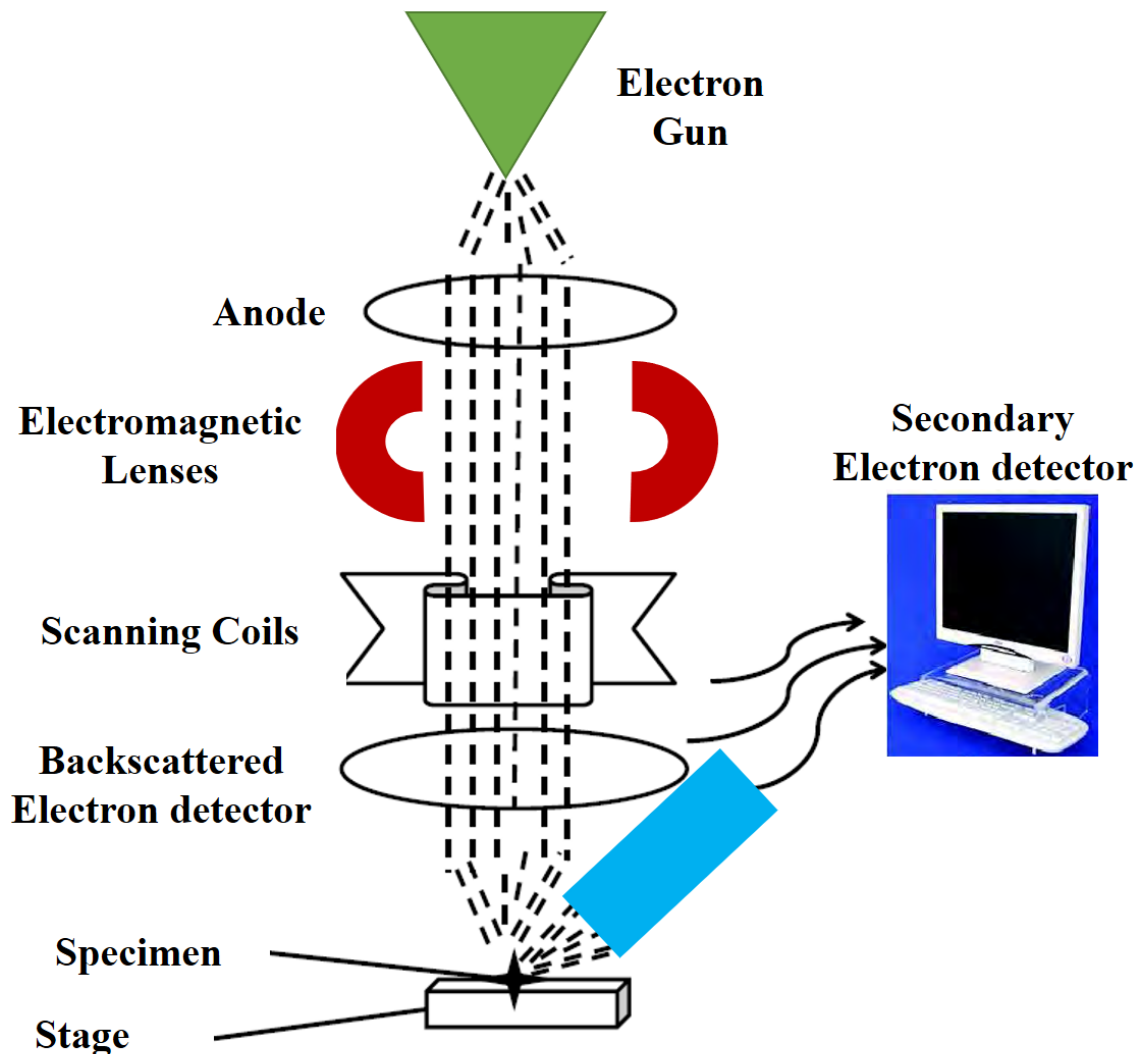


Figure 3.3 Schematic of SEM.

One of the significant advantages of FESEM is the use of a field emission cathode in the electron gun. This cathode produces a narrow, finely focused probing beam with a high degree of electron energy control. This precise beam reduces the risk of charging or damaging the sample during imaging, making FESEM particularly suitable for delicate applications. Additionally, the narrow beam enhances spatial resolution, allowing for detailed visualization of the sample's morphology. Additionally, an energy-dispersive X-ray analytical system can be added on FESEM. The fundamental composition of the nanoparticles may be identified because of their addition. Typical X-rays released as end of the sample and electron beam interacting. These X-rays are detected and analyzed by the EDX system, providing information about the elements present in the sample and their relative abundances. This dual capability of imaging and compositional analysis makes FESEM a powerful tool for the comprehensive study of nanomaterials [199]

To visualize a sample, a scanning electron microscope collects scattered electrons by scanning the electron beam across the surface of the sample. Since the picture is generated using backscattered signals compared to forward-transmitted signals, a high electron beam energy (less than 40 keV) is not necessary, nor does the sample need to have electronic transparency or an appropriate level of conductivity to avoid charging [199].

3.2.2. X-ray Diffraction (XRD) spectroscopy

X-ray diffraction is a powerful method used to determine various quality attributes of a sample, such as its crystal structure, atomic arrangement, particle size, crystalline texture, and overall perfection. Figure 3.4 represent the Schematic diagram of XRD. Because the atomic spacing in crystals falls within the angstrom range, which is extremely small, X-rays are employed due to their similarly small wavelengths, typically in the angstrom (Å) range.

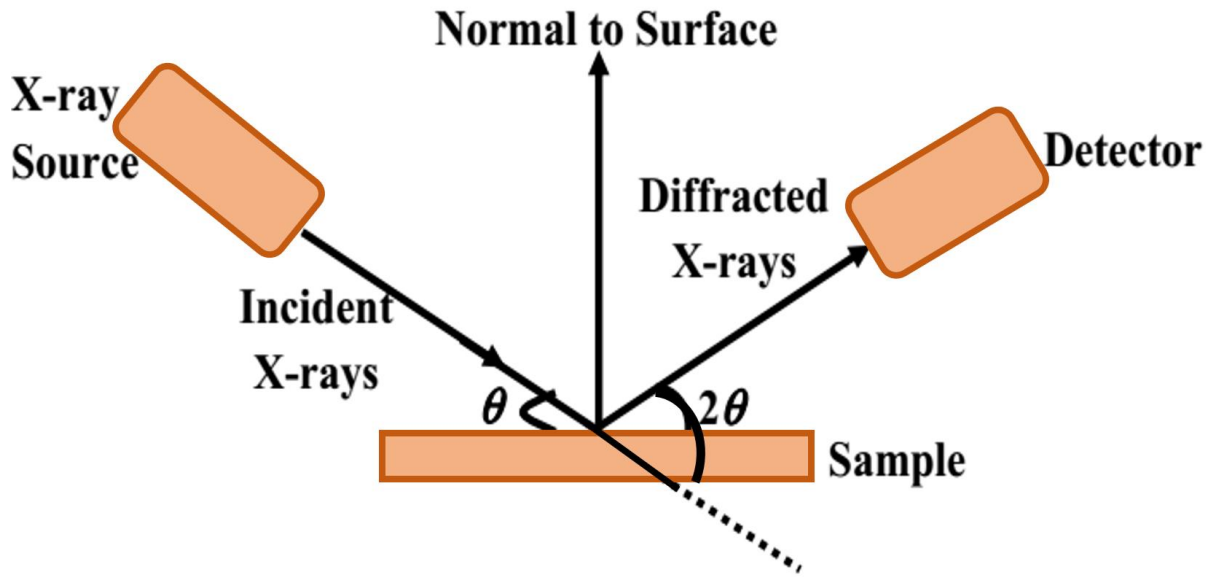


Figure 3.4 Schematic of XRD.

These X-rays can penetrate the atomic arrays and provide detailed insights into the sample's internal structure. In an XRD analysis, X-rays are directed onto the sample from a fixed point. As the X-rays interact with the sample, they are diffracted in specific directions, depending on the arrangement of the atoms within the crystal. Bragg's Law, which is written as ($2d \sin\Theta = n\lambda$), governs this diffraction pattern. The variables in this equation are (n) the order of diffraction, (d) the distance between the atomic planes in the crystal, (Θ) the angle of incidence at which the X-rays impact the sample, and (λ) the wavelength of the incoming X-rays. The wavelengths of $\text{CuK}\alpha_1$ (1.54056 Å) and $\text{CuK}\alpha_2$ (1.5444 Å) are often utilized in XRD.

The diffracted X-rays are detected over a range of angles (θ), creating a diffraction pattern. By analyzing this pattern, one can infer a variety of properties about the sample. For instance, the positions of the peaks in the diffraction pattern indicate the crystal structure and atomic arrangement, while the intensities of these peaks provide information about the crystallographic texture and the degree of perfection within the crystal. The broadening of the peaks in the diffraction pattern is inversely related to the particle size, according to the Scherrer equation. This means that smaller particles will cause broader peaks, allowing researchers to estimate their size based on the diffraction data [200].

Debye-Scherrer's formula of has been used to analyze the crystallite size (D) from the line broadening.

$$D = \frac{k\lambda}{\beta \cos \theta}$$

Where,

D = Crystalline size (nm),

K = 0.9 (Scherrer Constant),

λ = Wavelength of x-rays (0.15406 nm)

β = FWHM (Radians),

θ = Peak position.

In the present study, X-ray diffraction of all samples was analysed with a diffractometer [Brand: BRUKER] with X-ray radiation of wavelength 1.54056 Å. The scattering angle covered was from 20° to 80°.

3.2.3. Fourier transform infrared (FTIR) spectroscopy

It is an essential and essential characterization method for explaining the molecular-scale structure of the substance (Figure 3.5). Infrared spectroscopy is use to identify the chemical structure and the bonding structure of the material's basic parts. [201]. In order to get the infrared spectrum, FTIR spectrometers convert the Fourier signal from a moving mirror interferometer to an optical IR signal transform. In order to determine the chemical structure, IR spectroscopy entails identifying the individual components or groups of atoms absorbed at certain IR frequencies [202].

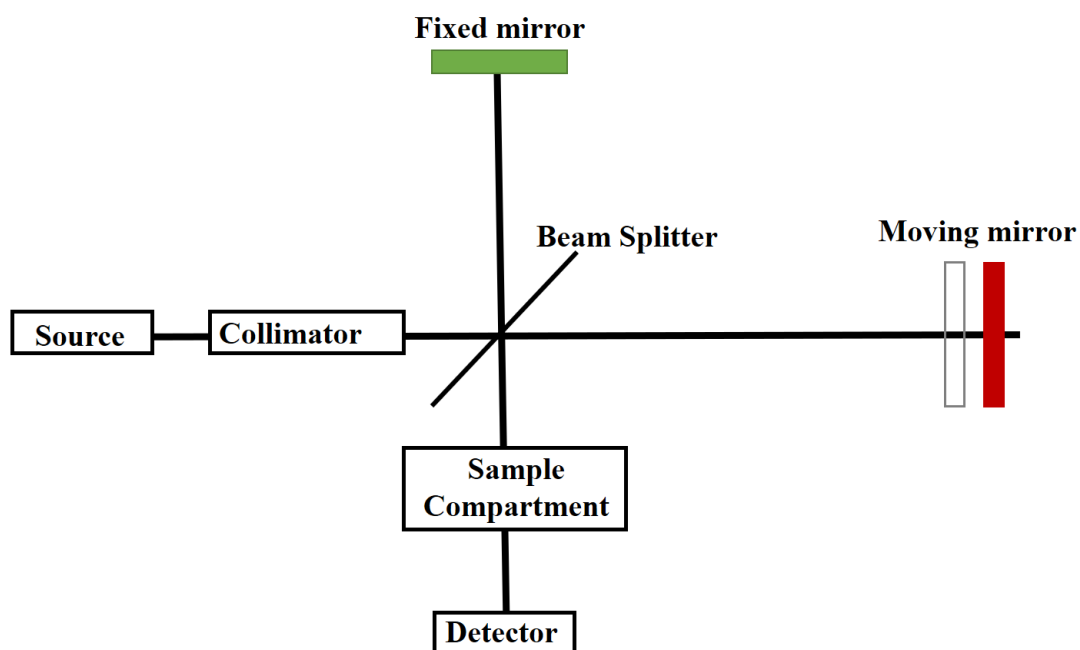


Figure 3.5 Schematic of FTIR.

This approach is impartial when it comes to chemical analysis. Furthermore, it is possible to compute molecular strain, crystallinity, and tacticity.

The frequencies observed in the infrared field are linked to the vibrational movements of the chemically bound components of matter. Matter may couple with an infrared electromagnetic radiation beam and share energy with it once the frequencies are within resonance when certain vibrational modes cause oscillations. In infrared testing, the sample is utilized as an action of light frequency, ν , to measure the intensity of an IR radiation beam before to (I_0) and following (I) interaction [203]. On a graph of I/I_0 vs frequency, we have the IR spectrum. It is most likely possible to identify the types, conditions, and concentrations of the chemical bonds that are present.

3.2.4. Raman Spectroscopy

This high spatial resolution vibrational spectroscopy method is non-destructive, non-contact, and offers insights into crystal structure and molecule vibrations (diagram shown in the figure 3.6). Through interactions with the molecules, a laser light with a frequency of ν_0 modifies the electron cloud, creating a virtual state in this spectroscopy. The photon is reemitted as scattered light because the virtual state is unstable. Depending on the kind of scattering, the light can either have the same frequency ($\nu_s = \nu_0$) as the different frequencies or incident light.

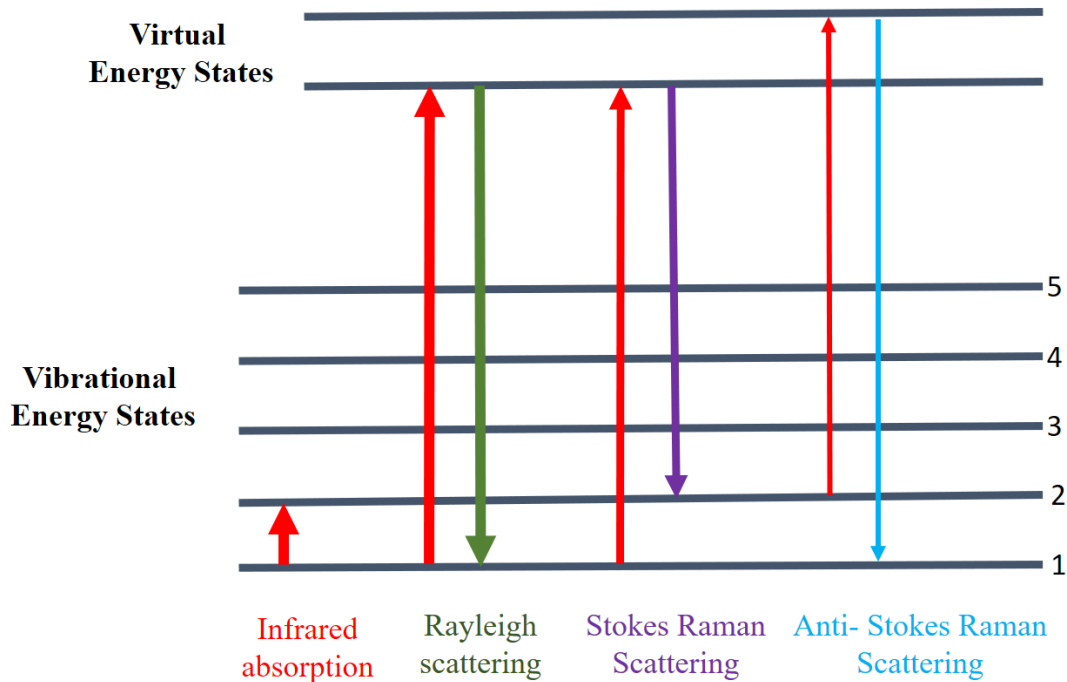


Figure 3.6 Schematic of RAMAN.

Stokes scattering refers to light dispersed at a frequency lower than the incident light ($\nu_s = \nu_o - \nu_t$), whereas anti-Stokes scattering refers to light scattered at a frequency higher than the incoming light ($\nu_s = \nu_o + \nu_t$). The Raman shift, defined as ($\Delta\nu = \nu_o \pm \nu_t$), is the difference in frequency between the Stokes or anti-Stokes line and the approaching beam. One in every 106–108 dispersed photons are subject to the extremely weak Raman scattering process, in contrast to the dominant Rayleigh scattering process. The Raman scattered light is captured as a Raman spectrum using a camera that has a charge-coupled device (CCD) attached to it. To identify materials specific orientation, crystallinity and stress, a specific Raman spectrum is employed [204].

In Raman instruments, a filter removes Rayleigh light, leaving single Stokes Raman dispersed light that can be verified at room temperature. Single Stokes light is detected at room temperature because the intensity of the Stokes Raman scattered light is greater than the concentration of the anti-Stokes light. But unlike Stokes light, anti-Stokes Raman light's intensity rises with temperature, hence anti-Stokes light may also be measured [205]. In the current study, a Renishaw Raman microscope is used to get the Raman spectra in the 100–1500 cm^{-1} wavenumber range with a laser excitation of 514 nm. To avoid sample damage from the laser's heating, measurements are made at low laser incident power.

1.3 Supercapacitor Performance

The research apparatus was divided into two categories—two and three-electrode systems—for the purpose of evaluating supercapacitors. The three-electrode system is designed to evaluate electrode materials by screening them with small quantities of the active ingredient. The two-electrode method, which is similar to the design of fully built supercapacitors, assesses a cell's efficiency in less-than-ideal conditions.

3.3.1. Three Electrode System

A potentiostat is attached to a working electrode, reference electrode, and counter electrode in the three-electrode method shown in figure 3.7. As the current flowing through the electrode is captured or controlled, there is a shift in the electrode potential and current. This potentiostat is used to control the electrode potential after measuring variations in the current and electrode potential. The active material is usually covered on the outside surface of a fixed electrode, which can be either platinum metal or glassy carbon, to create the working electrode.

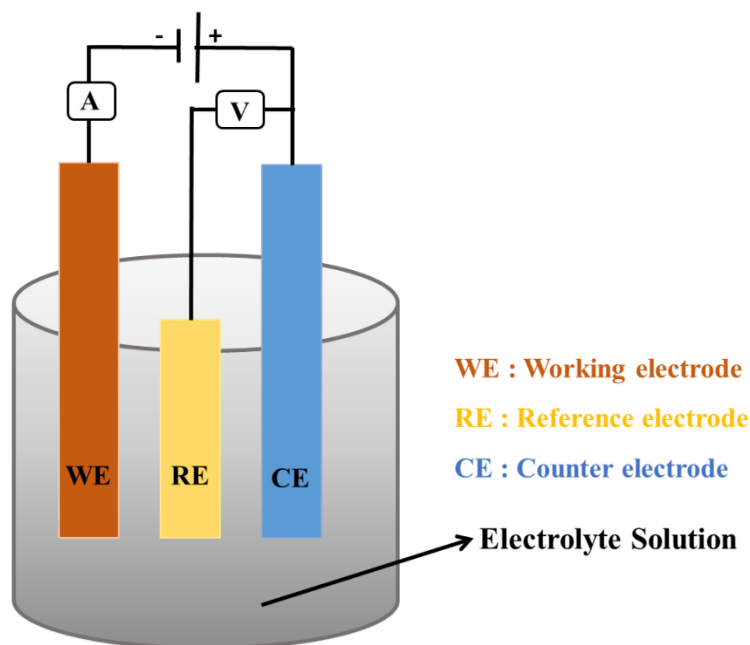


Figure 3.7 three electrode system; WE-working electrode, RE-reference electrode, and CE-counter electrode

Before the ink is equally distributed, a chosen solvent is used to dissolve the working substance (such as water, ethanol, or isopropanol). If the active ingredient in this ink is conductively insufficient carbon supplements are added. The previously polished electrode surface is then pipetted with the necessary amount of ink. To prevent the ink from leaking into the electrolyte, a small quantity of polymeric binder, such as Nafion, is frequently added after the ink has been deposited. The reference electrode in the three-electrode setup creates a foundation potential by establishing a stable potential.

Single fixed potential reference electrodes are available in a variety of shapes. Traditional hydrogen electrodes (NHE), Ag/AgCl silver chloride electrodes, and saturated calomel electrodes (SCE) are examples of common reference electrodes. Finally, by changing their potential, a counter electrode, sometimes referred to as an auxiliary electrode, balances the reaction that occurs in the working electrode. Graphitic rods or platinum mesh, which are highly conductive but inert, were most likely utilized as reference electrodes for this purpose.

3.3.2. Preparation of working the electrode

Carbons, polyvinylidene fluoride (PVDF), and the required weight percentage of as-produced V_2O_5 nanoparticles were mixed (80:10:10, respectively) to make electrodes for electrochemical studies. The resulting slurry was uniformly applied to a nickel foam foundation of approximately 1 cm^2 , and then allow to dry for 12 hours at $60\text{ }^\circ\text{C}$. Ultimately, it is seen as a functional electrode. The KOH was used as the electrolyte solution in the electrochemical workstation (CHI660E) during the electrochemical testing. A three-electrode cell is powered by a cyclic voltammeter, the reference electrode functions as the Ag electrode and the counter electrode as the Pt electrode in the above case.

3.4. Electrochemical study

Supercapacitors' electrochemical performance may be examined by utilizing parameters including series resistance, capacitance, energy density, operating voltage, and time. To find out the essential characteristics of the supercapacitors, the electrochemical workstation [Brand: Biologic, Model: VSP Potentiostat, France] was used in the current study project. There are usually three ways to assess a supercapacitors performance. The primary goal of three approaches to analyze the electrochemical properties of energy storage system.

Cyclic voltammetry uses a defined scan rate and potential to calculate current density, whereas Electrochemical Impedance Spectroscopy uses capacitance or impedance, and Galvanostatic Charge and Discharge usages for current density and fixed potentials. The most accurate way to assess the electrochemical performance of supercapacitors is by GCD.

3.4.1. Cyclic voltammetry

In the study of electrochemistry, cyclic voltammetry, or CV, is an invaluable instrument. The performance of several electrical energy storage devices, including supercapacitors, whole cells, and batteries, may be interpreted using it extensively. Electrodes that change frequently and linearly with time are subjected to an electrical potential during a CV test. A measurement is made of the resultant electrical current. By integrating the electrical current concerning time, the total charge generated on the electrode surface is ascertained. The total charge divided by the potential window is the final formula for the capacitance [206].

Capacitance is commonly evaluated at various scan rates to assess the supercapacitors efficiency. Although they are closer to the ideal form, the capacitance values are larger at lower scan rates as compared to higher scanning levels [207] . Furthermore, it was usual to figure out the electrochemical processes behind the charging and discharging of supercapacitors from the structure of CV curves.

As an example, while charging supercapacitors from zero potential, the current increases initially and decreases as the electrical potential rises further. Therefore, it is typical to see a "hump" in the CV curves. A perfect rectangular form and scan rate-dependent behaviour are indicated by the CV of an ideal capacitor that has low resistance, as seen in figure 3.8(a). As seen in figure 3.8(b). Deviations from the rectangular form are observed in the case of actual capacitors and are represented as the series combination of internal resistance R and total capacitance C [208].

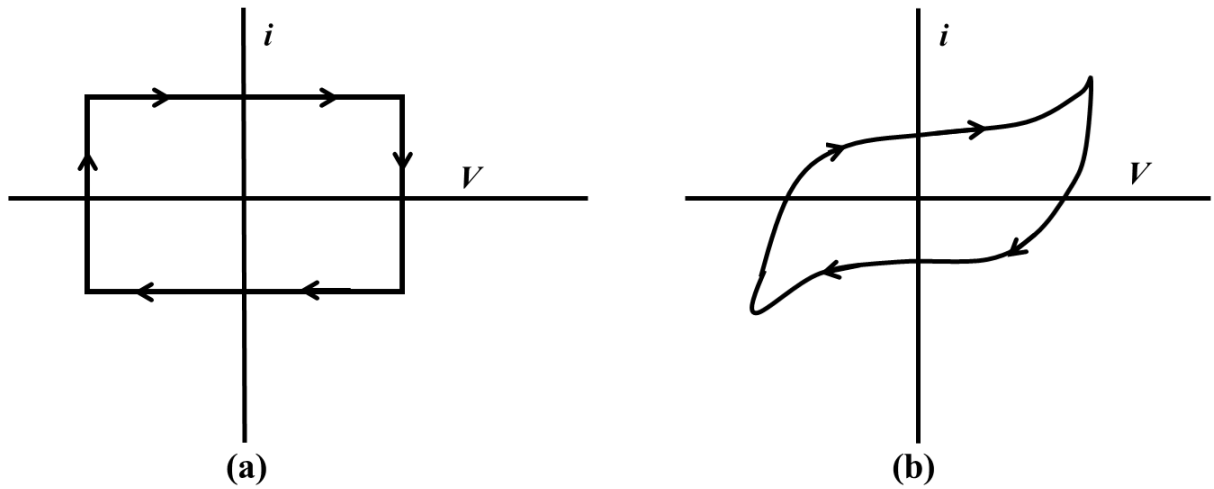


Figure 3.8 Cyclic voltammogram of (a) ideal capacitor and (b) real capacitor

Using the following equation, the specific capacitances were determined from the CV data.

$$C_s = \frac{1}{mv(V_1 - V_2)} \int_{V_2}^{V_1} I(V) dV$$

Where I , is the current being discharged (A), $V_1 - V_2$ is the potential window (in V), m is the mass (g) of one electrode, C is the specific capacitance in (Fg^{-1}), and v is the scan rate (in Vs^{-1}).

3.4.2. Galvanostatic charge/discharge test

An effective technique for determining electrochemical capacitance under regulated conditions is galvanostatic charge-discharge or GCD. Because the current is controlled and the voltage is measured, this approach is different from cyclic voltammetry. Due to its extension from a laboratory size to an industrial one, this is one of the most widely used supercapacitor methods [209]. A set of supercapacitor properties, including capacitance, ESR, and cycle stability, are obtained by this method, which is also known as chronopotentiometry.

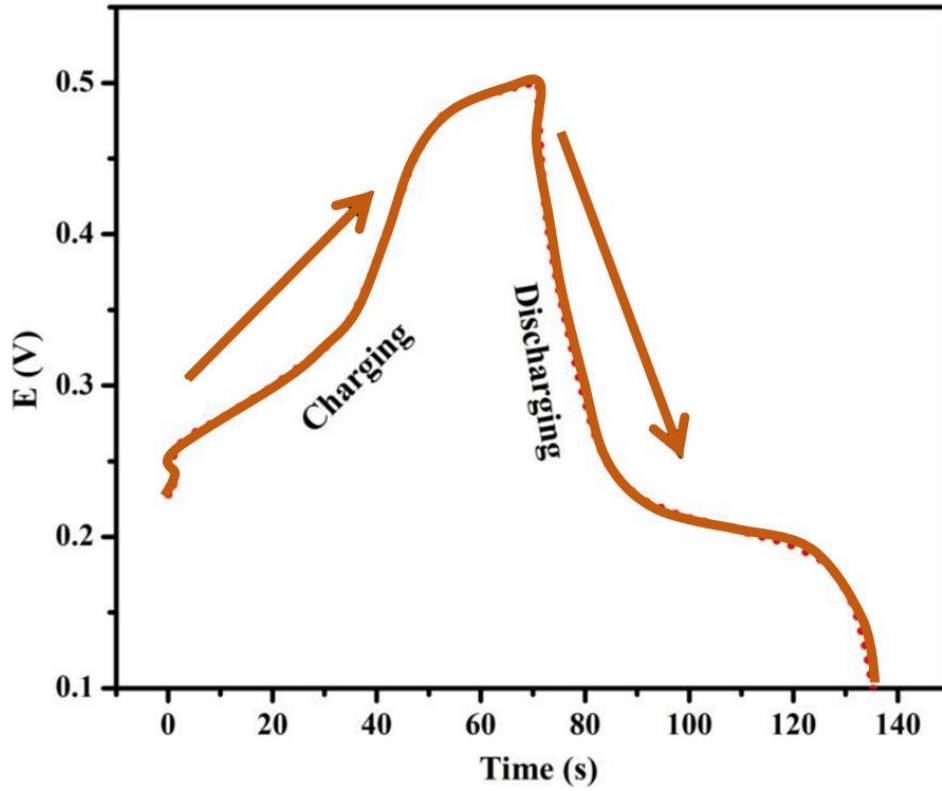


Figure 3.9 Galvanostatic charge-discharge plot of pseudocapacitive material

This test involves applying a continuous current to the working electrode and measuring the potential generated with a reference electrode as a function of time. The following equation was used to measure the specific capacitance (C_s) using the charge-discharge technique.

$$C_s = \frac{I \times \Delta t}{\Delta V \times M}$$

Where mass of the active material is M , potential window is ΔV , discharge time is Δt , current during the discharge process is I , and C_s is the specific capacitance.

Series resistance is seen when there is a voltage drop across the current inversion. For an inverse current, the resistance of the cell is directly related to the voltage drop [210]. Furthermore, by measuring capacitance and resistance repeatedly over a significant number of cycles, one can evaluate the cyclic stability of supercapacitors (also known as redox capacitors or EDLCs).

3.4.3. Electrochemical impedance spectroscopy

The EIS test provides supercapacitor impedance data at open circuit potential using changing potential for a wide frequency range (e.g. from 0.01 to 100 kHz) at a narrow amplitude (e.g., ± 5 to ± 10 mV). Apply the Bode plot's linear portion of a $\log |Z|$ vs. $\log f$ curve, the capacitance is calculated using $C=1/(2\pi f |Z|)$ from the EIS test, where f is the frequency and $|Z|$ is the imaginary component of impedance [211]. The Bode plot makes it clear that capacitance dropped as frequency increased. At higher frequencies, supercapacitors are made completely of resistance. This suggests that the electrolyte ions will be unable to penetrate the electrode's micropores at higher frequencies [212].

An additional technique for determining the impedance from the EIS test is the Nyquist chart (Graphical representation of Nyquist impedance has been in Figure 3.10). A curve is developed by plotting the imaginary ($Z(f)''$) and real ($Z(f)'$) components of impedance against each other. By determining the semicircle diameter, the charge transfer resistance may also be calculated from the Nyquist plot.

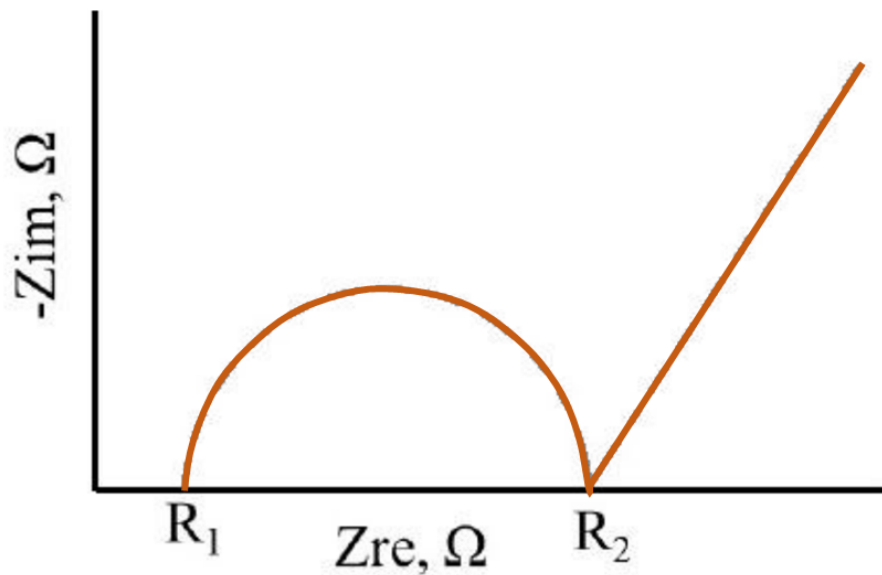


Figure 3.10 Graphical representation of Nyquist impedance

In the same way, the pseudo capacitor's charge transfer resistance is determined between high and low frequencies. In contrast, the impedance plot's primary component is the pure capacitive performance at extremely low frequencies. EIS testing may be done over a extensive range of frequency, from 10 mHz to 100 kHz.

3.4.4. Gas Sensing Measurement

Response and Recovery Time

Response time is the amount of time desired used for a sensor to attain 90% of its entire response after being exposed to the target gas in terms of resistance, absorbance, capacitance, etc. The recovery time is the amount of time desired to remove the target gas from it and restore 90% of the initial signal. During gas sensing performance, response and recovery times are crucial. An important feature of a good sensor is its quick reaction and recovery time.

Chapter 4

Synthesis and Electrochemical Characterization of V₂O₅

Chapter 4

Synthesis and Electrochemical Characterization of V_2O_5

4.1. Introduction

Energy storage has become increasingly critical in various aspects of modern life, reflecting its essential role in several key areas. This includes harnessing renewable energy sources, powering electric vehicles, generating electricity, and ensuring the efficient operation of portable electronic devices such as computers and mobile phones [213]. The growing reliance on these technologies underscores the need for advanced energy storage solutions. Supercapacitors (SCs), commonly referred to as electrochemical capacitors (ECs), are a major energy storage technology that can be identified by their high energy density, quick charging and discharging speeds, and extended lifespan [214]. These characteristics make SCs particularly attractive for a wide range of applications, from powering electric vehicles to stabilizing renewable energy sources and enhancing the performance of portable electronics.

The improvement of advanced materials is pivotal in advancing these energy storage technologies. A diverse array of materials has been investigated for this purpose, with metal oxides like Co_3O_4 , RuO_2 , MnO_2 , CuO , NiO , and V_2O_5 showing great promise due to their excellent electrochemical properties. Among these, vanadium pentoxide (V_2O_5) is especially noteworthy for pseudocapacitor applications [215]. V_2O_5 is favoured because of its multiple valence states, high potential window, low cost, versatility in forming multiple structures, and relatively low toxicity [216], [217]. These inherent properties make V_2O_5 an excellent candidate for energy storage devices. To capitalize on these advantageous characteristics, various synthesis methods have been employed to produce vanadium oxide nanoparticles. These methods include sol–gel techniques, hydrothermal synthesis, microwave-assisted processes, and solvent-thermal methods. Recent research has highlighted the impressive performance of V_2O_5 nanofibers produced through electrospinning, which exhibit a significant capacitance of 190 F/g [218]. Another study demonstrated that V_2O_5 nanostructures could attain a maximum capacitance of 155 F/g [219].

Despite these promising results, challenges remain. Inadequate conductivity and difficulties in precisely controlling the morphology, shape, and valence states of V_2O_5 contribute to its

relatively low specific capacitance values. Overcoming these challenges is crucial for developing more efficient and durable energy storage technologies.

This research aims to investigate the electrochemical characteristics of V_2O_5 synthesized with distinct morphologies using hydrothermal mechanochemical and microwave methods. By assessing and comparing their performance, this study seeks to address the existing challenges and enhance the understanding of how different synthesis techniques impact the electrochemical properties of V_2O_5 . In final analysis, this research may contribute to the development of better energy storage systems by utilizing V_2O_5 's full potential as a supercapacitor material.

4.2. Preparation of V_2O_5 by different method

4.2.1. Hydrothermal Synthesis Technique

To synthesize V_2O_5 nanoparticles using the hydrothermal technique (Figure 4.1), this process begins with dissolving 1 gram of ammonium metavanadate (NH_4VO_3) in 60 ml of de-ionized water. This is done under continuous stirring to ensure complete dissolution and uniform mixing. Next, 1.27 grams of oxalic acid ($C_2H_2O_4$) is mixed in the solution. Stirring continues for another 15 minutes to ensure that the oxalic acid is thoroughly mixed with the solution. For the hydrothermal method, the resultant solution is then transferred into a 100 ml Teflon-lined hydrothermal reactor. The reactor, containing the solution, is placed in hot air oven and heated at $150^\circ C$ for 7 h. This controlled heating process facilitates the formation of V_2O_5 nanoparticles under high pressure and temperature conditions.

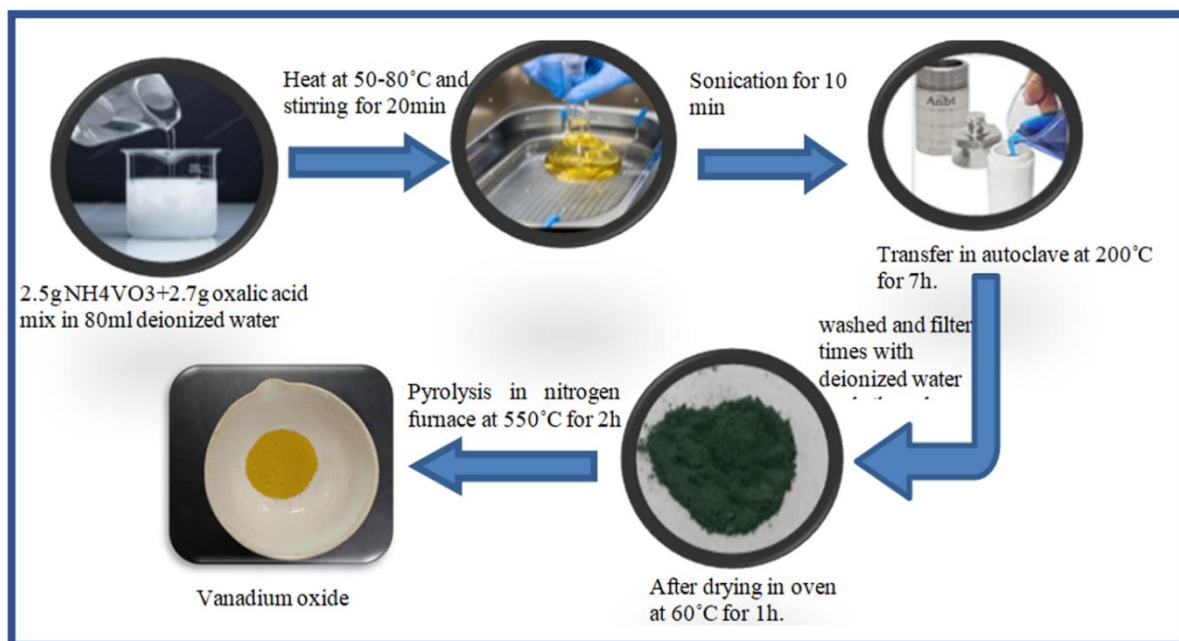


Figure 4.1 Flow chart of synthesis of V_2O_5 nanoparticles by hydrothermal method

4.2.2. Mechanochemical Synthesis Technique

For the mechanochemical method, first NH_4VO_3 mixed with the ethylene glycol and the mixture was stirred for an extra 1 hour and 30 minutes. This continued stirring ensures better interaction and reaction between the components, potentially leading to different morphological or structural properties in the final nanoparticles. The filtered nanoparticles are then washed multiple times with ethanol and de-ionized water. This washing process is crucial to remove any residual impurities or unreacted precursors that might be present.

The washed nanoparticles are then dried in a hot air oven at $45^\circ C$ for 30 minutes. This drying step helps to remove any remaining moisture, resulting in dry vanadium oxide nanoparticles. To further enhance the crystalline structure and purity of the nanoparticles, they are subjected to calcination. Calcination involves heating the dried nanoparticles at $550^\circ C$ for 2 hours. This high-temperature treatment helps in stabilizing the crystal structure and improving the material's properties for various applications. The detailed process of preparing V_2O_5 nanoparticles by mechanochemical methods is summarized in a flow chart, as shown in figure 4.2.

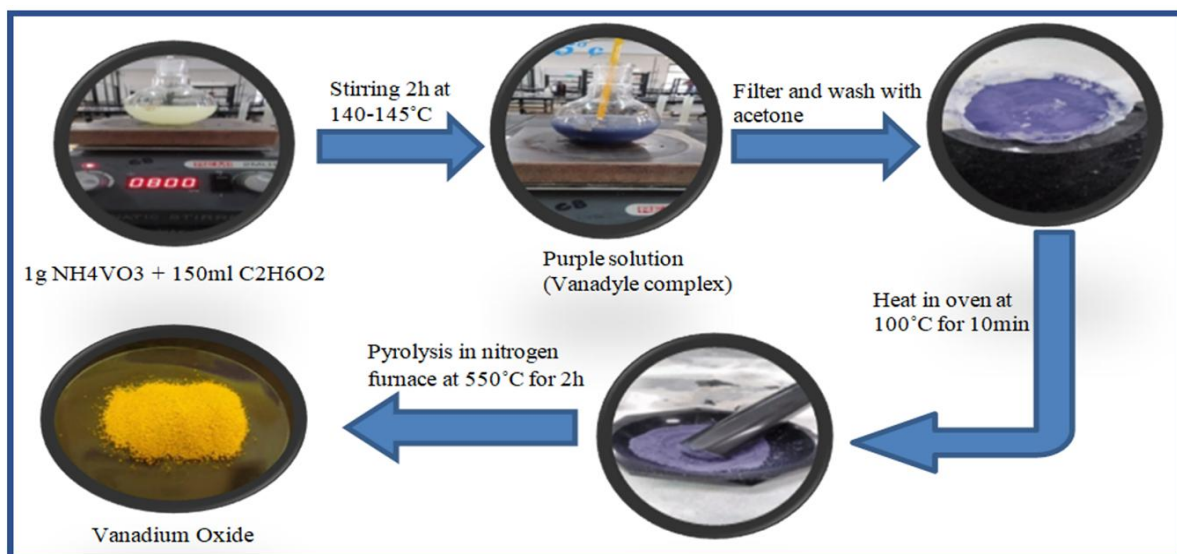


Figure 4.2 Flow chart of synthesis of V_2O_5 nanoparticles by mechanochemical method

4.2.3. Microwave Synthesis Technique

To Prepare the Vanadium oxide nanoparticles using microwave irradiation synthesis (as shown in Figure 4.3), 80mg of ammonium metavanadate was dissolved in ethylene glycol, and the mixture was stirred continuously for 30 min. After this, the mixture was ultrasonicated for 15 min to break down the aggregates and ensure the uniform distribution of the solute. The homogeneous suspension was then transferred to a microwave container at 600 watts for 6 min. This microwave heating step provided rapid and uniform heating, enhancing the reaction kinetics and promoting the formation of nanoparticles. The solution was washed numerous times with a suitable solvent to remove impurities. The washed precursor was then dried thoroughly to obtain a dry powder. For the annealing, dry precursor was placed in the muffle furnace at 500°C for 2h. This high temperature annealing step promoted crystallization and improved the structural properties of the nanoparticles. Finally, the product V_2O_5 nanoparticles were ready to use for the further application.

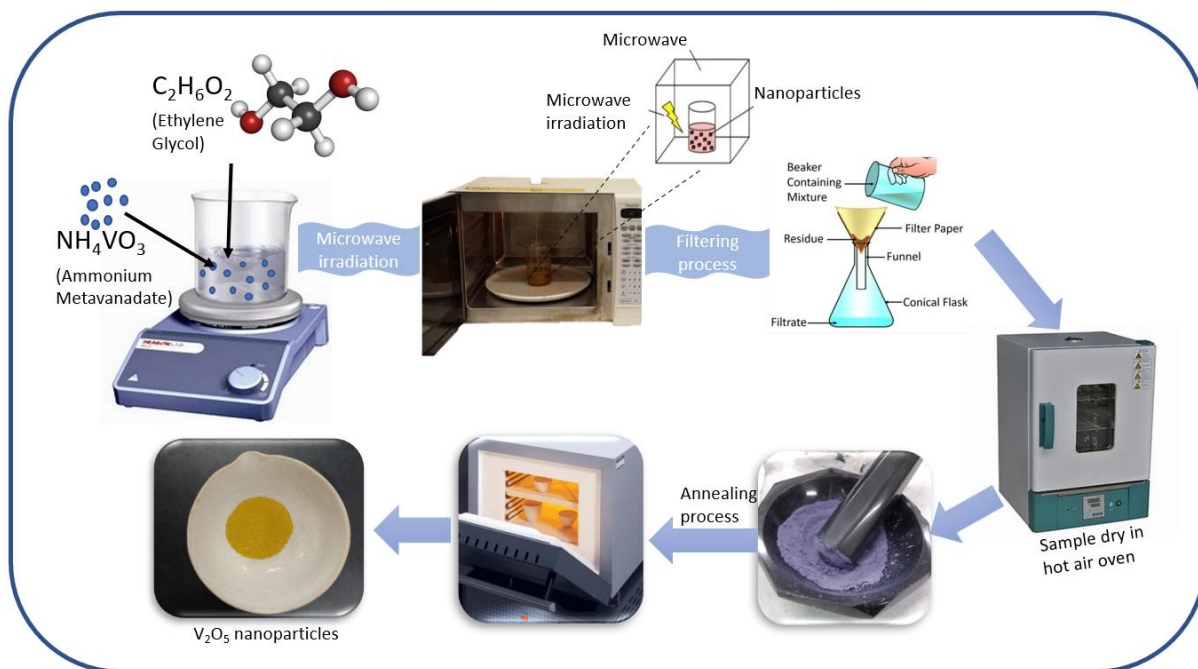


Figure 4.3 Flow chart of synthesis of V_2O_5 nanoparticles by microwave method

4.3. Characterization of synthesized V_2O_5 nanoparticles

The analysis of V_2O_5 nanoparticles prepared through hydrothermal, mechanochemical and microwave methods is illustrated in figure 4.4 (a), which shows the X-ray diffraction (XRD) patterns for these samples. The XRD analysis confirms that the prepared nanoparticles exhibit the orthorhombic phase of V_2O_5 . This is identified by the characteristic diffraction peaks corresponding to this crystal structure. These peaks have a small full width at half maximum (FWHM), indicating that the nanoparticles are highly crystalline, meaning they have well-ordered atomic structures with minimal defects [220]. The crystalline size (D) calculated by Debye-Scherrer formula for V_2O_5 are 61 nm ($2\theta=15.4$), 32 nm ($2\theta=15.34$) and 28 nm ($2\theta=15.4$) prepared by mechanochemical, hydrothermal and microwave method respectively. The XRD figure 4.4 (a) reveals a notable shift the peak positions towards lower angles for the V_2O_5 nanoparticles which was synthesized via the hydrothermal and mechanochemical method. This shift suggests an growth in the unit cell volume of the V_2O_5 produced by this method, indicating slight variations in the properties of crystal compared to the microwave method [221]. From the data of X-ray diffraction, a plot of $\beta \cos\theta$ and $\sin\theta$ is created; linear fit is given for the data points. The corresponding Williamson Hall plots are shown in the Figure 4.4 (b, c and d). From the W-H plot, the calculated value of the

average crystallite size is found to be 61 nm, 31 nm and 28 nm of the V_2O_5 prepared by mechanochemical method, hydrothermal method and microwave method.

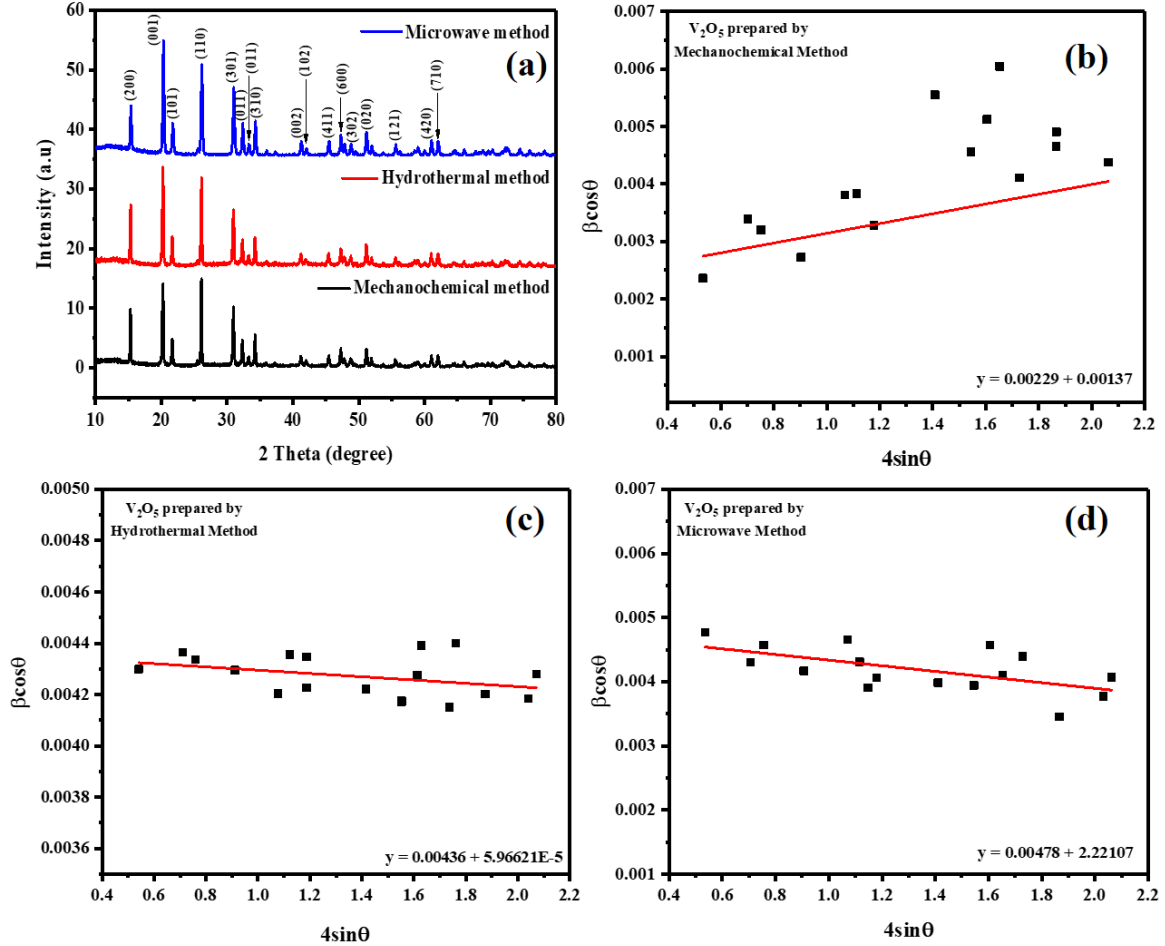


Figure 4.4 XRD data of hydrothermal, mechanochemical and microwave method of V_2O_5 .

The Fourier transform infrared (FTIR) spectra of V_2O_5 , obtained using three distinct methods, are shown in Figure 4.5. Two significant absorption bands about 845 cm^{-1} and 1012 cm^{-1} are visible in the FTIR spectra. These bands are important because they identify certain vibrational modes in the structure of V_2O_5 . The absorption band at 1012 cm^{-1} is due to vibrating of isolated $V=O$ vanadyl groups present in VO_5 trigonal-bipyramids. The stretching vibration of extra coordinated oxygen bonds ($V-O-V$), sometimes referred to as bridge oxygen, and is linked to the band at about 845 cm^{-1} . [222]. These vibrational signatures confirm the presence of the expected chemical bonds within the V_2O_5 nanoparticles.

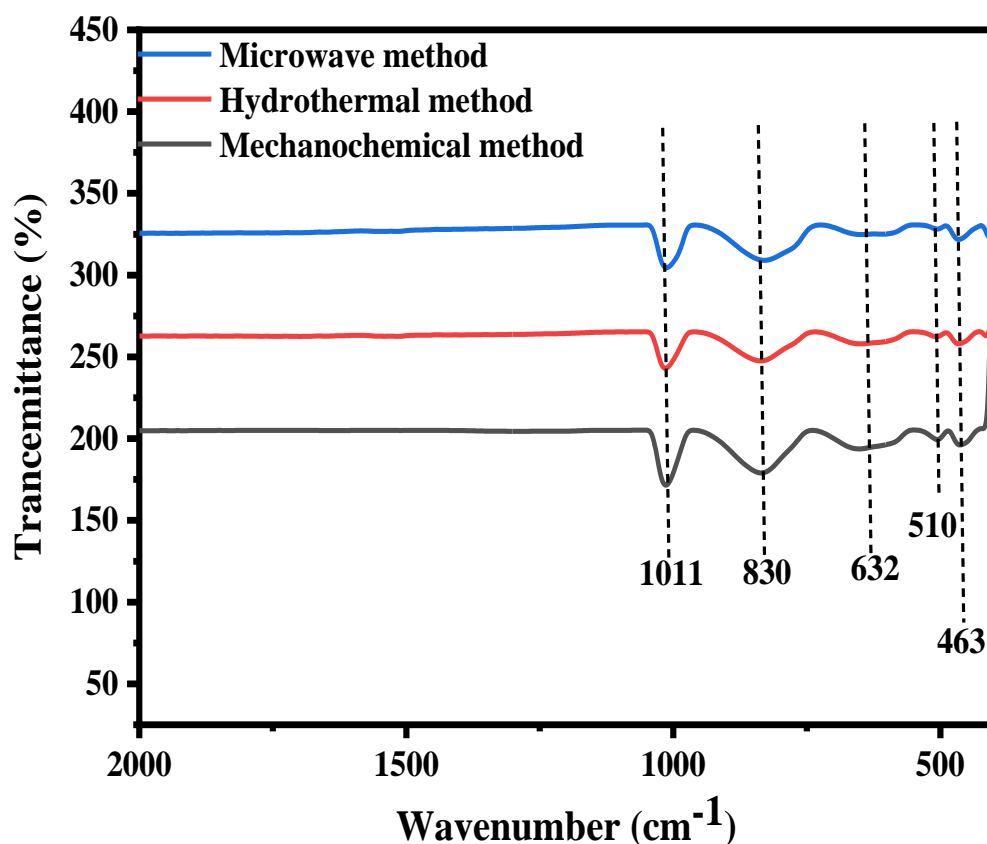


Figure 4.5 FTIR data of hydrothermal, mechanochemical and microwave method of V_2O_5 .

Figure 4.6 (a-c) displays the SEM image of V_2O_5 synthesized by the hydrothermal method mechanochemical method and the microwave method respectively. The morphology obtained of the V_2O_5 which is prepared by the mechanochemical method is nanoparticles like and as presented in fig 4.6(d) the particles size is around 198nm. Figure 4.6(e) illustrate the SEM image of nanostructured V_2O_5 particles which is fabricate by hydrothermal method and the particles size is around 175nm. Another finding is that the vanadium pentoxide which is prepared by the microwave method nanoparticles have a rod like morphology as shown in figure 4.6(f), and some neighbouring particles are iso-oriented with each other and the particle size is 145nm which is smaller than the V_2O_5 nanoparticles prepared by the mechanochemical and hydrothermal method. This difference in particle size can be recognized to the distinct synthesis conditions of each method.

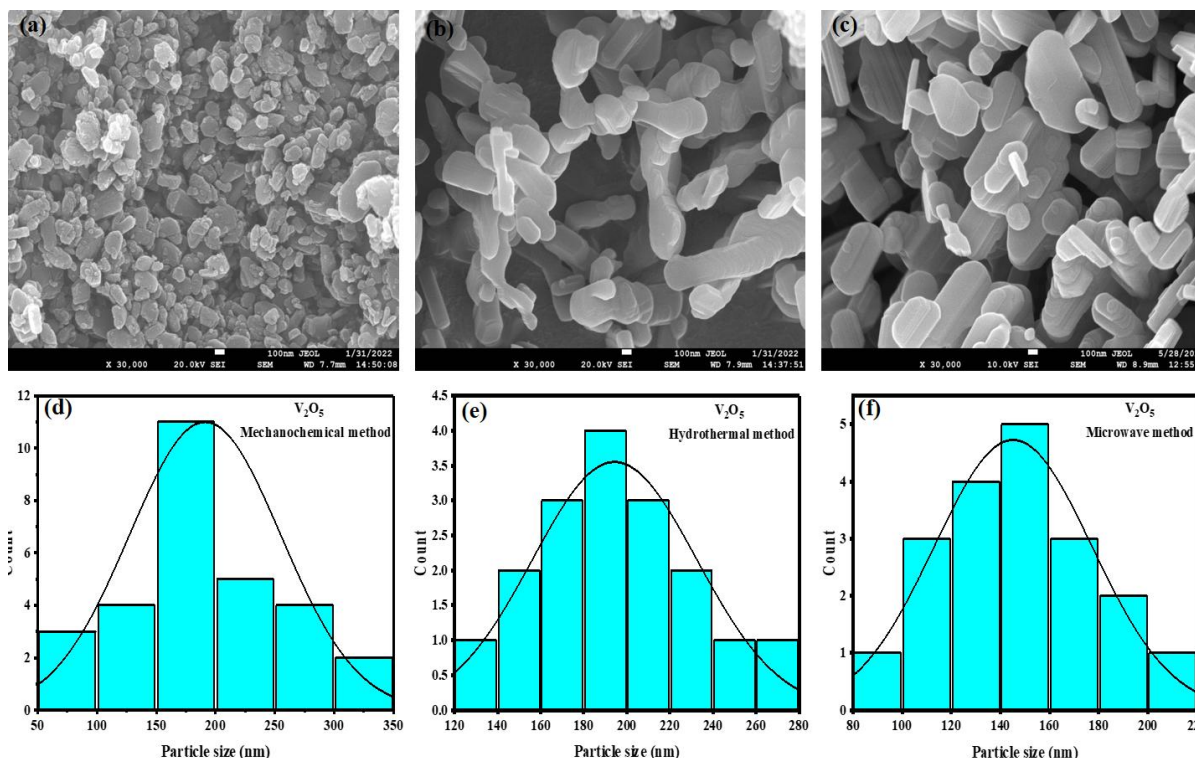


Figure 4.6 SEM and EDX data of V_2O_5 prepared by (a & d) hydrothermal method, (b & e) mechanochemical method and (c & f) microwave method

4.4. Electrochemical analysis of prepared Sample

The active material is applied on a 1 cm x 1 cm piece of nickel foam to produce the working electrode for an electrochemical cell. This process starts with the preparation of a homogeneous paste, which includes mixing activated carbon (AC), polyvinylidene fluoride (PVDF), and the solvent N-methyl-2-pyrrolidone (NMP) in a weight ratio of 8:1:1. The active material constitutes 80% of the total weight, while activated carbon and PVDF each account for 10%. The NMP solvent is added to dissolve the PVDF, ensuring that the mixture forms a uniform paste. Following the coating process, the nickel foam is dried at approximately 80°C in a vacuum oven. The vacuum environment ensures effective removal of the solvent and prevents oxidation or contamination, resulting in a well-adhered and functional electrode.

Figure 4.7 presents the cyclic voltammetry (CV) curves of V_2O_5 synthesized using hydrothermal, mechanochemical and microwave techniques, recorded at various scan rates ranging from 10 to 100 mV/s. The distinctive redox peaks on the CV curves point to the

faradic behaviour that characterizes the V_2O_5 material. This faradic pattern implies that redox processes as well as ion electrostatic interactions play a role in the charge storage device.

The peak currents in the CV curves reach in line with the scan rate. Higher scan rates cause an increase in peak current without significantly changing the overall shape of the CV curves. This behaviour indicates that the faster potential sweep rates enable a larger number of redox-active species to engage in the electrochemical reactions during each cycle [223]. This phenomenon reflects the pseudo-capacitive nature of V_2O_5 , where the faradic redox processes, involving intercalation-deintercalation and incomplete adsorption-desorption of ions on the electrode surface, contribute to the charge storage [224].

For the V_2O_5 synthesized via the hydrothermal and mechanochemical, the CV curves show a more pronounced cathodic peak compared to the anodic peak. This pronounced cathodic peak suggests a stronger reduction process relative to the oxidation process. This could be due to modifications on the electrode surface and the presence of impurities that enhance the reduction reactions [225].

In contrast, the CV curves for V_2O_5 prepared through the hydrothermal method exhibit two distinct oxidation peaks, which are associated with the intercalation or de-intercalation of potassium ions (K^+). The presence of these two oxidation peaks in the hydrothermal method's CV curves highlights specific electrochemical behaviour of the V_2O_5 material under these synthesis conditions. This does not necessarily indicate a greater number of phase transitions compared to the mechanochemical and microwave method but rather reflects differences in how the material interacts electrochemically [226].

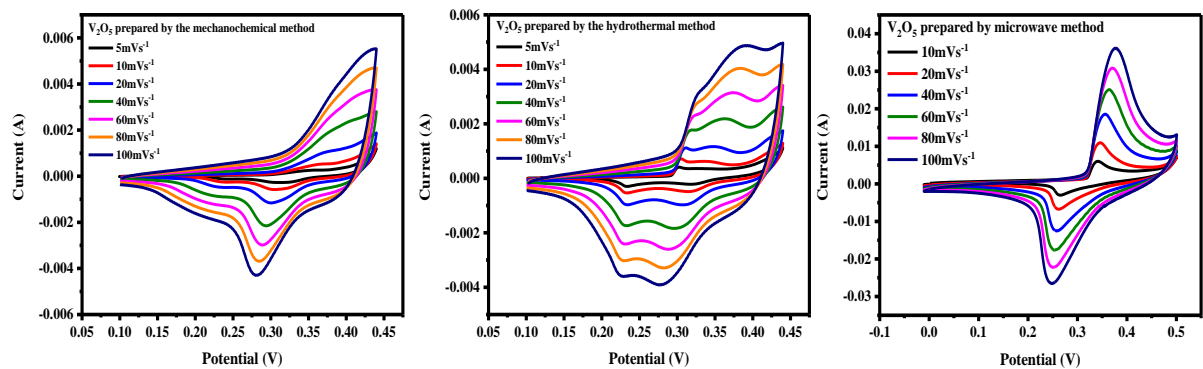


Figure 4.7 CV curve of the V_2O_5 electrode at different scan rates for mechanochemical, hydrothermal and microwave method.

The galvanostatic charge-discharge experiments, depicted in Figure 4.8, were conducted on V_2O_5 electrode materials of different method, at range of 1 A/g with the potential window of 0 V to 0.4 V. These experiments designed to evaluate for the specific capacitances (C_s) of the samples, which were calculated using a specific equation. The equation considers the current density (I_m), discharge time (Δt), and potential window (ΔV).

$$C_s = \frac{I_m * \Delta t}{\Delta V}$$

The specific capacitances (C_s) of V_2O_5 prepared by the mechanochemical, hydrothermal and the microwave methods was evaluated to be 75 Fg^{-1} , 77 Fg^{-1} and 122 Fg^{-1} respectively. The higher specific capacitance value for the microwave method indicates a superior electrochemical performance compared to the hydrothermal and mechanochemical method.

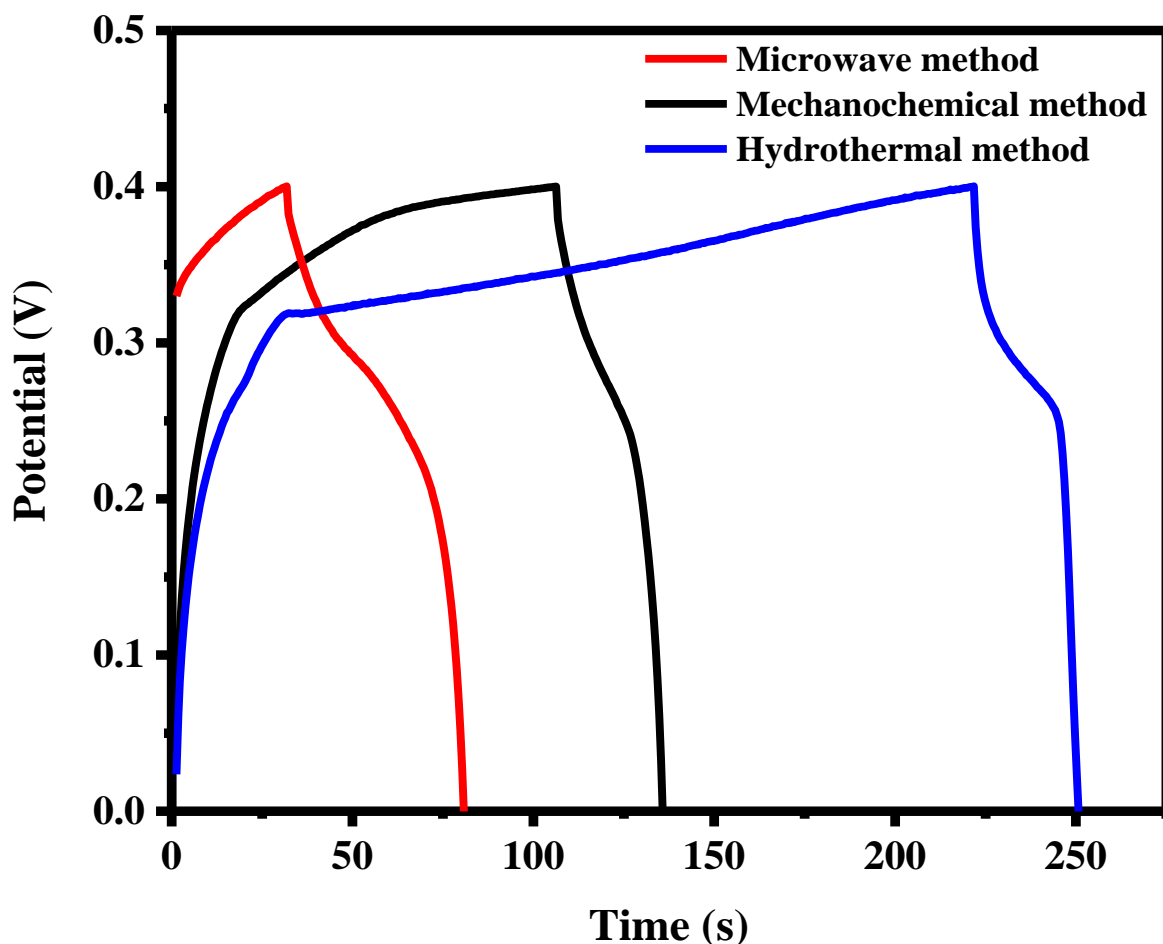


Figure 4.8 The GCD curves of the V_2O_5 electrodes are depicted for hydrothermal, mechanochemical and microwave method.

This discrepancy suggests that the V_2O_5 synthesized through the hydrothermal and mechanochemical method has a less favourable electrode surface, higher internal equivalent series resistance (ESR), and likely contains impurities, as inferred from the cyclic voltammetry (CV) curves [227]. Specific capacitance (C_s) declines as the current density rises because the V_2O_5 electrode's discharge time shortens. Diffusion constraints are the main cause of the drop in C_s at greater current densities. At higher current densities, the ions have less time to diffuse into the deeper parts of the electrode material, resulting in reduced charge storage efficiency [228].

Figure 4.9 shows the impedance curve exhibiting two typical components: a low-frequency straight line (between 400 Hz to 10 mHz) followed by a high-frequency semicircle (between 10 kHz to 400 Hz). These components correspond to the interfacial charge transfer resistance between the electrodes and electrolytes (R_{ct}), and electrode kinetics controlled by the diffusion, respectively [123].

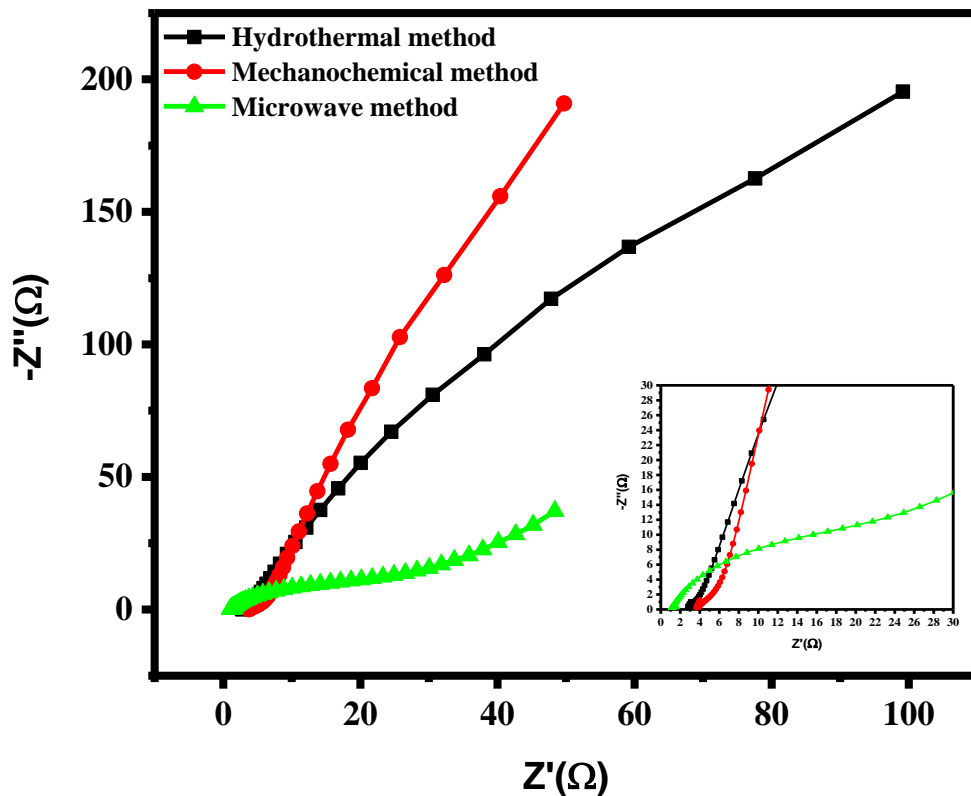


Figure 4.9 electrochemical impedance spectroscopy (EIS) plot of V_2O_5 electrode of different method.

Figure 4.9 shows the Nyquist plot for V_2O_5 electrode material prepared by the hydrothermal mechanochemical and microwave method. The microwave method resulted in a smaller

value of series resistance $R_s = 1 \, \Omega$ compared to $R_s = 2.5 \, \Omega$ and $R_s = 5 \, \Omega$ for the hydrothermal method and mechanochemical method. The presence of curved vertical lines along the imaginary axis ($-Z''$) at lower frequencies reveals the pseudocapacitive behavior of the electrode material due to significant ion diffusion limitations in the V_2O_5 electrode.

Chapter – 5

Properties and Performance of V_2O_5 as a Gas Sensor

Chapter – 5

Properties and Performance of V_2O_5 as a Gas Sensor

5.1. Introduction

Volatile organic compounds (VOCs) are prevalent in various industrial processes, household products, and automotive emissions, posing significant health risks even at low concentrations. In recent years, the harmful effects of volatile organic compounds (VOCs) on the health of people and the environment caused a great deal of attention being dedicated to their detection and monitoring. Consequently, the development of efficient sensing platforms capable of rapid and sensitive detection of VOCs is imperative for environmental and public health protection. Because of their high sensitivity, quick response, and ability to be included into portable devices, electrochemical sensors are one of the sensing technologies that are most suited for volatile organic compound (VOC) detection.

Gas sensors based on metal oxide have involved a lot of attention due to their improved chemical process control and potential medical uses. Zinc Oxide (ZnO), SnO_2 , and Fe_2O_3 are examples of binary metallic oxides that have excellent sensing properties [229], [230], [231], [232]. Vanadium pentoxide (V_2O_5), also known as vanadium (V) oxide, is an inorganic compound that can be used to develop sensors that detect volatile organic compounds. V_2O_5 shows n-type conductivity by nature, but when formed in a hydrated amorphous phase by atomic layer deposition, it can change to p-type conductivity. The surface of V_2O_5 can absorb more oxygen ions, which can lead to high sensing performance. Metal oxide-based gas sensors have produced a lot of research attention due to the increasing of environmental issues and medicinal applications. Among of the semiconductor materials and metal oxides, such as SnO_2 , ZnO and Fe_2O_3 , have great sensor abilities [233].

A gas sensor uses chemical procedures that transform into signals that can be observed analytically to detect different gases in different atmospheres. Although a sensor may produce many different types of outputs, electrical or optical signals are the most often used [234]. The particular type of gas, the amount present, the materials used to make the sensor, and the output produced when the gas interacts with the surface material of the sensor all affect how effective a gas sensor is [235]. When the chemical composition of the ambient

atmosphere changes, transition-metal oxides can sense gases by reversibly changing their electrical conductance; this method of gas detection relies on the interaction between the surface of the sensor element and the surrounding gaseous environment [236].

Semiconductors like SnO_2 , ZnO , and Fe_2O_3 are commonly employed for detecting ethanol gas. However, their limited sensitivity and high temperature of operation limit their use, requiring the search for innovative and possible alternative materials. As a result of its exceptional intrinsic features, vanadium pentoxide (V_2O_5) has been proposed for multiple optoelectronic applications primarily as a gas sensor. One-dimensional V_2O_5 has a potential future in the production of gas sensors which can work at ambient temperature. V_2O_5 is a transition-metal oxide semiconductor that has attracted a lot of interest over the years due to its unique layered structure, many valence states, and several uses [237], [238]. V_2O_5 is n-type semiconductor with high oxidation state and a high stability. Moreover, V_2O_5 has active areas for gaseous molecule adsorption on its surface. It has numerous intriguing properties, including a multilayer structure, multivalence, a large optical bandgap (2.44 eV), and strong chemical and thermal stability. Vanadium pentoxide is a great option for gas sensing because of its properties [239], [240].

V_2O_5 thin film prepared by several techniques such as electron beam evaporation, magnetron sputtering, spray pyrolysis, thermal evaporation, and sol-gel technique. In this study, the sol-gel technique was used to create V_2O_5 thin-film nanostructures from high-purity V_2O_5 powder mixed in distilled water and hydrogen peroxide as a precursor. XRD and FESEM were employed to analyze the nanoparticles. These techniques provided detailed information about the structural and morphological characteristics of the particles, allowing for a thorough examination of their properties. The performance of sensing and efficiency of the outcome V_2O_5 thin film gas sensor is described. This work focused on the response time and recovery time of the V_2O_5 thin film. Target gases have been determined to be Acetone, IPA and Methanol.

5.2. Materials and methods

For the synthesis of V_2O_5 , a Kenstar residential microwave oven (model No. OM 20 ESP; 1200 W) was utilized, capable of providing a power ranging from 0 to 1000 W. The key chemical reagents used in this process were ammonium metavanadate (NH_4VO_3 , > 99.0%

purity), hydrogen peroxide (H_2O_2), and ethylene glycol ($\text{C}_2\text{H}_6\text{O}_2$), all sourced from Loba Chemie, India.

The synthesis involved microwave irradiation; a technique known for its efficiency in producing various morphologies of vanadium oxide. This method leverages the rapid heating capabilities of microwave radiation to accelerate chemical reactions, leading to the formation of different nanostructures. To describe the morphology and microstructure of the synthesized vanadium oxide, SEM was employed. SEM analysis provides detailed images of the sample's surface, allowing for the examination of particle shapes, sizes, and distribution. The crystalline pattern and particle size of the vanadium oxide were assessed through XRD analysis. This technique provided detailed insights into the material's structural characteristics and allowed for precise measurement of the particle dimensions. The XRD investigation was conducted with a BRUKER diffractometer consuming Cu-K α radiation ($\lambda = 1.54 \text{ \AA}$). XRD is a crucial technique for identifying the phases present in the sample and measuring the crystallite size, as it provides diffraction patterns that can be interpreted to reveal the material's structural properties.

5.2.1. Synthesis of Vanadium Oxide by solvent-thermal and microwave method

To prepare vanadium oxide using both solvent-thermal and microwave methods (figure 5.1), 2.34 grams of ammonium metavanadate (NH_4VO_3) is dissolved in 60 ml of ethylene glycol. This mixture is stirred continuously for 20 minutes at temperature range of 50-60°C to ensure complete dissolution and homogeneity. After the initial stirring, the solution is divided into two equal parts to proceed with different synthesis methods.

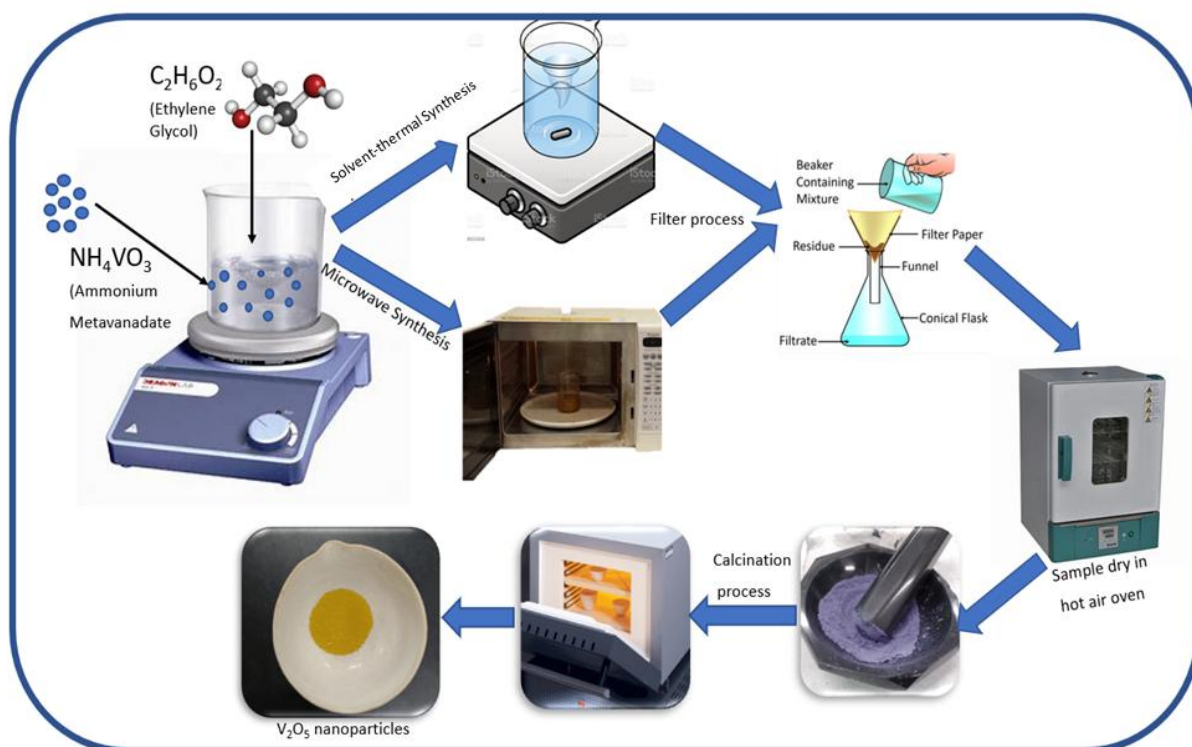


Figure 5.1 Flow diagram of V_2O_5 synthesized by Solvent-thermal and Microwave method

For the mechanochemical method, one part of the solution is continuously stirred for 2 hours at a temperature of 140°C . This prolonged stirring at elevated temperature promotes the reaction and formation of vanadium oxide nanoparticles through mechanical means.

The other part of the solution is subjected to the microwave method. Here, the solution is placed in the microwave oven and heated for 5 minutes at a power setting of 600 watts. The microwave energy rapidly heats the solution, facilitating the chemical reaction and formation of nanoparticles in a much shorter time compared to the mechanochemical method.

Following the reaction, both solutions are filtered to separate the solid nanoparticles from the liquid phase. The solid products are then thoroughly washed with ethanol and de-ionized water multiple times to remove any unreacted starting materials and by-products. After washing, the nanoparticles are dried in oven at 45°C for 30 minutes to eliminate any residual solvents and moisture. The final step involves calcining the dried vanadium oxide nanoparticles. Calcination is performed at 550°C for 2 hours, which helps to improve the crystallinity and phase purity of the vanadium oxide nanoparticles. This thermal treatment

ensures that the nanoparticles attain the desired structural and chemical properties suitable for various applications.

5.2.2. Thin film Preparation of Vanadium Oxide

The V_2O_5 thin films were fabricated using by the spin coating method (steps of method are shown in the Flow chart as Figure 5.2), a method that allows for precise control over film thickness and uniformity. The process began by dissolving 0.6 grams of synthetic V_2O_5 powder in 40 ml of a 5% hydrogen peroxide (H_2O_2) solution. This mixture was then heated in a water bath at a constant temperature of 70°C while being continuously stirred. Over a period of 20 minutes, the initially reddish-brown solution transformed into a viscous gel. The viscosity of the gel, which is crucial for the spin coating process, was monitored by observing the temperature of the water bath and the heating duration.

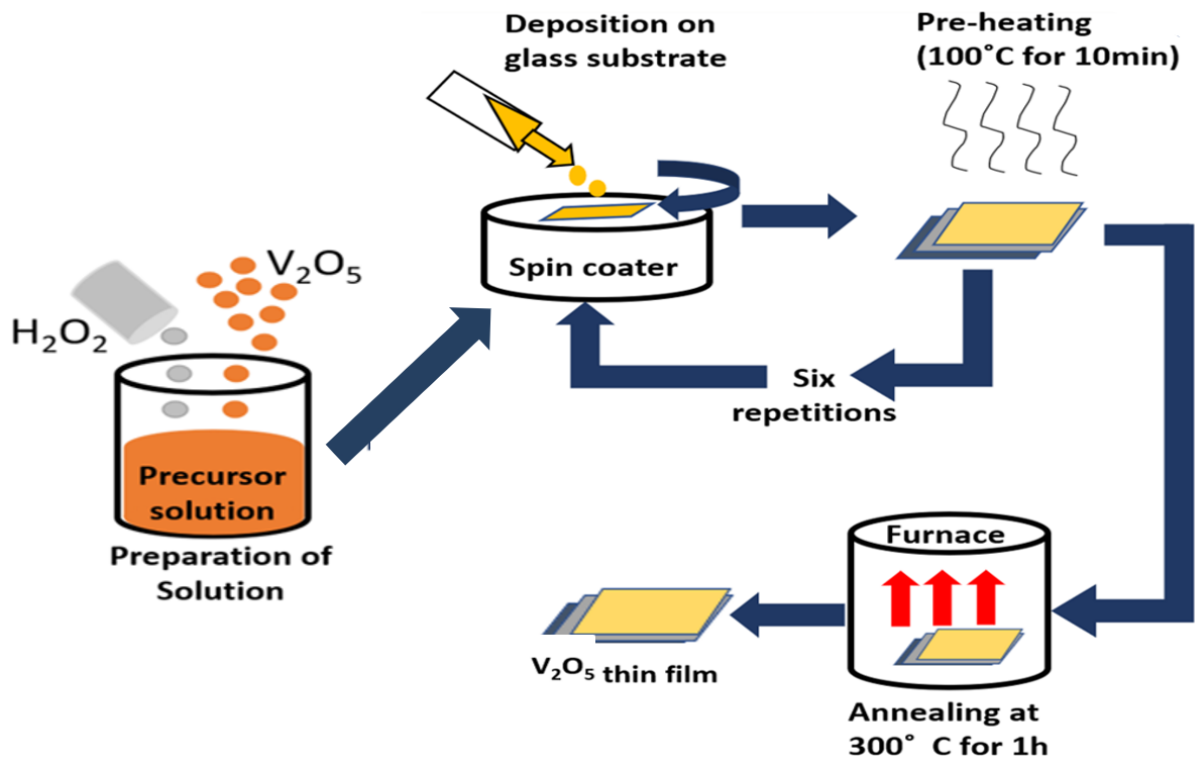


Figure 5.2 Flow chart of fabricate V_2O_5 thin films based on the sol gel spin coating process.

To create the thin films, a small amount of the viscous solution was deposited onto a glass substrate. The substrate was then spun at speeds ranging from 1500 to 6000 revolutions per minute (rpm). The spinning speed was adjusted depending on the desired thickness of the

film. This spinning process ensured that the solution spread evenly across the substrate, forming a uniform layer. Following each spin coating process, the samples were subjected to heating at 250°C for a duration of 10 minutes to ensure the films were thoroughly dried. This drying step helped to remove any residual solvents and solidify the coating. To achieve the desired film thickness, the spin coating and drying process was repeated six times. Each layer added to the previous one, gradually building up the thickness of the film. Once the desired thickness was achieved, the films underwent a final annealing process. The samples were heated at 500°C for two hours. This high-temperature treatment helped to crystallize the V_2O_5 , ensuring that the films had a good crystalline structure. The annealing process also improved the film's overall stability and adhesion to the substrate.

5.2.3. Gas sensing Measurement Technique

The prepared thin film was tested for its gas sensing capabilities for three different gases: acetone, isopropyl alcohol (IPA), and methanol. The testing was conducted using a custom-made sealed chamber to ensure a controlled environment. The whole system set up is as shown figure 5.3.

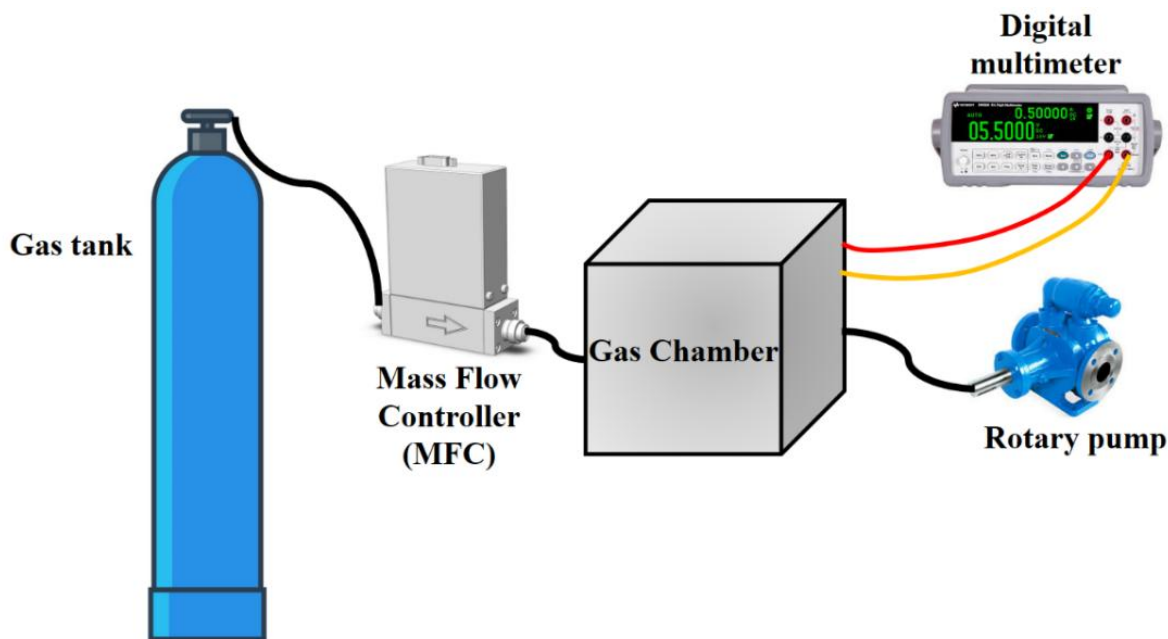


Figure 5.3 Experimental setup for the gas sensing measurement

The film was inserted into this chamber, and a mass flow controller controlled the gas flow into the chamber to ensure accurate gas flow rates. Each of the three gases was tested on the sensor at room temperature. The electrical resistance of the film was measured in relation to its non-exposure state in order to assess its gas sensing behaviour. The film was exposed to acetone, IPA, and methanol gases. A precise digital multimeter (Fluke 8846 A) was used to record these variations in resistance. For the purpose of getting clear of any unnecessary gases or impurities that may have affected the test findings, argon gas was pumped into the chamber for five minutes before to beginning the gas sensing studies for each gas. This procedure allowed researchers to accurately determine the film's response to acetone, IPA, and methanol gases, which is essential for understanding its gas sensing properties for these specific gases.

5.3. Result and discussion

5.3.1. Gas sensing Measurement

The gas sensitivity response (S) was calculated by using the formula

$$S = \frac{|R_{gas} - R_{air}|}{R_{air}} \times 100\%$$

Where,

R_{gas} = Resistance in vapor environment

R_{air} = Resistance in open environment

As shown in the table 5.1, the comparison between the gas sensors fabricated from V_2O_5 prepared via microwave and solvent-thermal techniques reveals significant differences in their gas response to various volatile organic compounds (VOCs) [241].

Table 5.1. Represent the response with different vapour of microwave and solvent-thermal method

Sample Name	Response (S) with different vapours		
	Acetone	IPA	Methanol
Microwave	78.94%	77.44%	32.29%
Solvent-thermal	17.91%	11.95%	18.86%

The microwave-assisted gas sensor shows the most significant response to acetone, with a peak value of 78.94%, outperforming its responses to isopropanol (IPA) and methanol. In contrast, the solvent-thermal method yields a gas sensor with the highest response to methanol, measuring 18.87%, followed by acetone and IPA. The sensor's high selectivity for acetone, compared to other test vapors can be attributed to its advantageous molecular profile relative to other test substances. In comparison with the other test vapors, acetone possesses a lower ionization energy (9.69 eV), facilitating charge transfer; a moderate bond dissociation energy (393 kJ mol⁻¹), balancing stability and reactivity; and a relatively large kinetic diameter (0.42 nm), potentially enhancing surface adsorption. This combination promotes preferential interaction with the V₂O₅ prepared by microwave method [242]. This indicates that the V₂O₅-based gas sensor prepared using the microwave method offers superior performance compared to the one made via the solvent-thermal approach. Additionally, further evaluations of the microwave gas sensor's response and recovery times were carried out to analyze its dynamic performance. The sensor exhibits remarkably fast response and recovery times across different VOCs [241]. For example, in acetone vapor, the sensor demonstrates the response time of 4 seconds and recovery time of 2 seconds, as described in figure 5.4 (a, b). Similarly, as figure 5.4 (c, d) illustrates the response and recovery periods in methanol vapor are 6 and 3 seconds, respectively. Figure 5.4 (e and f) shows the sensor's reaction and recovery times in the instance of IPA vapor, which are 12 seconds and 2 seconds, respectively.

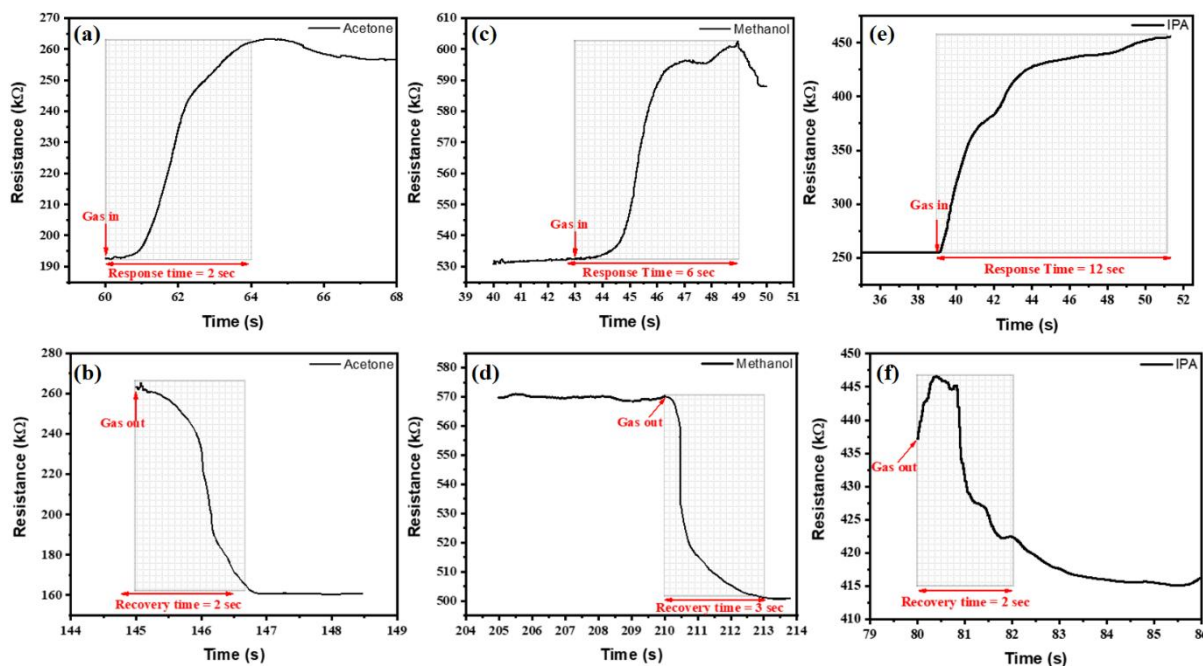


Figure 5.4 Response and Recovery time for the (a, b) Acetone, (c, d) Methanol and (e, f) IPA Vapour Gases.

These results demonstrate how well the microwave gas sensor performs in comparison to the solvent-thermal gas sensor in terms of both sensitivity and reaction time. The microwave sensor's quick recovery and reaction times make it an excellent choice for real-time monitoring applications where fast VOC analysis and detection are crucial.

5.4. Gas sensing Mechanism

The V_2O_5 -based gas sensors' gas detecting method is based on the way that the presence of the target gas changes the stability of surface chemisorbed oxygen processes. These sensors can be categorized into p-type and n-type semiconductors, each exhibiting distinct sensing behaviors towards the same detected gas. When exposed to oxidizing gases, n-type semiconductors experience an increase in resistance as the gas species act as acceptors, whereas p-type semiconductors undergo a resistance decrease. Conversely, when subjected to reducing gases, n-type semiconductors show a decrease in resistance, while p-type semiconductors display an increase in resistance due to the gas species acting as donors [243].

The p-type semiconductor oxide V_2O_5 utilised in this sensing mechanism is part of the surface-controlled model, which is based on a change in the semi conductive sensor's

resistance carried on by the adsorption and desorption of various gaseous molecules [244]. As illustrated in Fig 5.5, it is expected that the adsorbed oxygen and water molecules would function as electron acceptors when the sensor is exposed to air, resulting in an upward band bending at the surface that represents an electron-depleted but hole-enriched area.

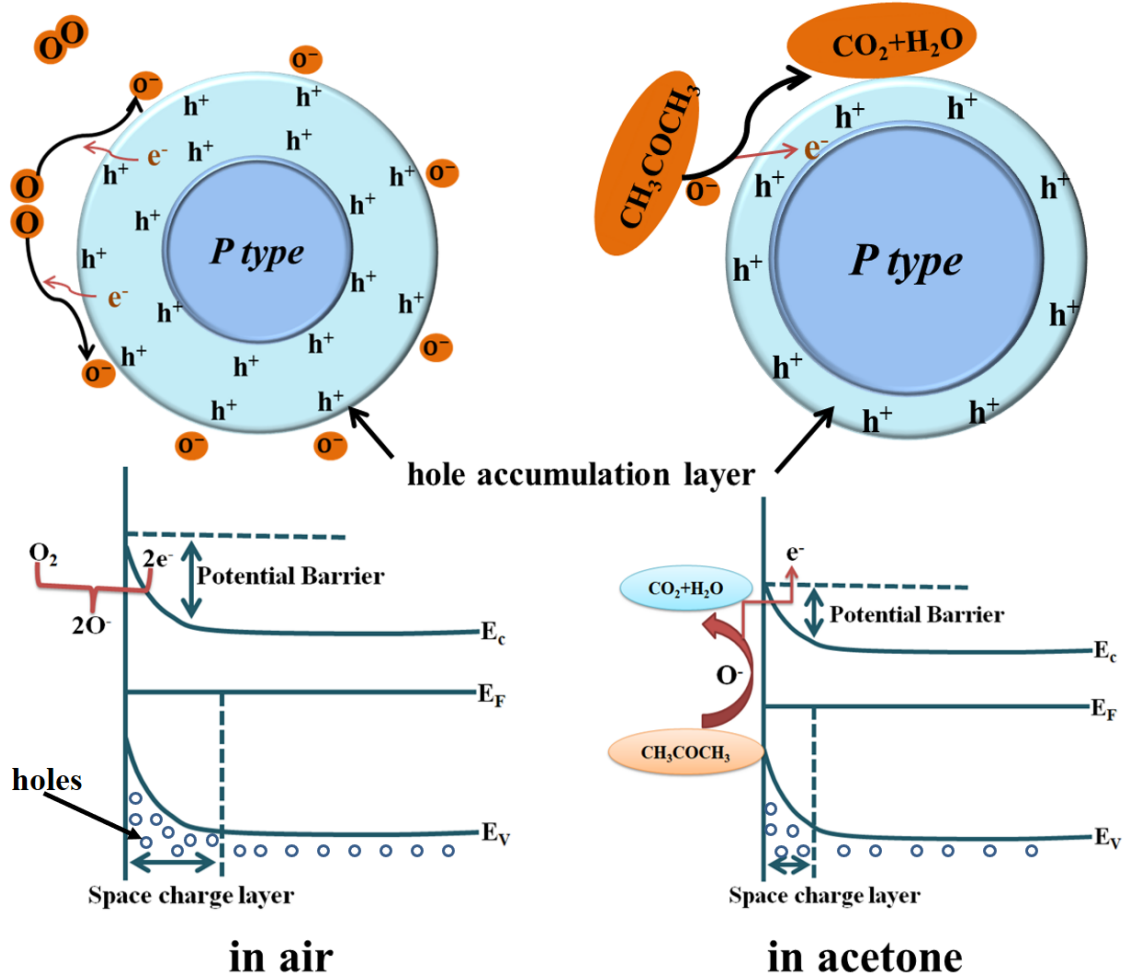
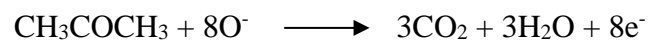


Figure 5.5 Gas sensing mechanism of V_2O_5 in air and in acetone.

Whereas, the conductivity increases in relation to nitrogen in a p-type semiconductor, as would be expected. On the other hand, in the presence of acetone, the valence band electrons are trapped on the surface, forming an accumulation layer of holes surrounding the p-type MOS core. As a result, the MOS acetone gas sensor's resistance rises [245].

The acetone molecules may react with O_2^- to produce CO_2 and H_2O on the surface (reaction no.). This process releases electrons into the material and causes electron-hole recombination, which lowers the concentration of holes in the material [246].



Therefore, when acetone is applied, the sensor resistance increases, the energy band bends lower as shown in Figure Acetone, and the density of absorbed O_2^- decreases. In a nanometric material, where the surface predominates over the bulk, this phenomenon is enhanced.

Chapter – 6

Electrochemical Applications of Microwave Assisted V₂O₅-Graphene Oxide Composites

6.1. Introduction

The advance of renewable energy storage technologies has been driven by the exhaustion of fossil fuels and the growing global demand for energy. Various energy sources are used to produce and store energy, leading to advancements in energy storage devices [247], [248], [249]. Supercapacitors, known for their rapid charging and discharging capabilities, are particularly suitable for powering portable devices and electric cars [250]. Research in supercapacitors aims to identify environmentally safe, high-performance electrolytes with increased energy density [251]. Improved electrode materials are essential for improving supercapacitors' effectiveness and performance. Transition metal oxides (TMOs) are frequently employed in this context due to their ability to connect with various metals and semiconductors with tunable nanostructures and techniques [252]. However, there is a need for more affordable and eco-friendly alternatives to materials like ruthenium oxide [253], [254].

Research on TMOs in binary and ternary compositions has shown that the addition of graphene oxide (GO) enhances optical and electrical characteristics [255], [256]. Combining iron-cobalt oxides with crumpled graphene oxide at low current densities improves specific capacitance and conductivity [257]. 1196.1 F/g capacitance and a 61% retention capacity after 4000 cycles have been obtained by wet chemical synthesis of nickel cobalt oxide/sulfide, whereas copper oxide electrodes in a 1 molar solution of Na₂SO₄ show improved specific capacitance [258]. GO's wide range of functional groups can serve as suitable sites for redox reactions, allowing different metal oxide ions to bind to its surface [259]. The electrochemical performance of composite electrodes can be improved by the complementary effects of metal ions and graphene oxide. For example, graphene/TiO₂ composites produced via atomic layer deposition show reduced specific capacitance, while a V₂O₅/graphene composite created using a laser exhibits increased specific capacitance [260]. The results of the current work are stable with Chen et al.'s hydrothermal techniques, which produced decreased GO/V₂O₅ with the specific capacitance of 438.5 F/g at 1 A/g [261].

This work proposes the development of a graphene/metal oxide nanocomposite with enhanced rate performance. Solid connections between the matrix and nanoparticles must be created to maintain the structure throughout cycle performance. The electrochemical performance of battery is enhanced when TMOs and 2D based materials are combined as anode materials. Key considerations in electrode fabrication and design include the charge transfer rate, ion exposure surface area, and the electrode-electrolyte interface [262]. Improved electrochemical performance can be achieved in composites made of MXene, a pseudocapacitive material [263].

We reported on the hydrothermal production of graphene oxide (GO) nanosheets incorporating vanadium pentoxide (V_2O_5). Samples were generated with different weight percentages of GO (5%, 10%, and 15%), designated as VG5, VG10, and VG15, respectively. Electrochemical testing confirmed that these composite samples were effective electrode materials. The VG10 composite, in particular, demonstrated an ideal composition with a high specific capacitance value. V_2O_5 is extensively studied for supercapacitor electrodes because of its high theoretical capacitance, strong conductivity, long cycle life, low cost, and simplicity of synthesis. It was selected for this purpose [264], [265]. Its stability in electrolyte solutions makes V_2O_5 a popular choice for electrochemical energy storage systems. The combination of GO and V_2O_5 in composites has been shown to improve conductivity and electrochemical performance. We aimed to create graphene-based V_2O_5 nanocomposites using hydrothermal process to improve the electrochemical properties of microwave-synthesized V_2O_5 with graphene oxide.

6.2. Materials and methods

Vanadium oxide was synthesized using a Kenstar microwave oven (model No. OM 20 ESP; 1200 W), which power range from 0 to 1000 W with adjustable settings for precise control. The synthesis process involved NH_4VO_3 , >99.0% and $C_2H_6O_2$, both sourced from Loba Chemie in India.

The synthesis procedure involved microwave irradiation synthesis, which facilitated the production of multiple types of vanadium oxide morphologies. Microwave irradiation synthesis is a technique wherein microwave energy is used to induce chemical reactions, offering advantages such as rapid heating, uniform heating, and enhanced reaction rates

compared to conventional heating methods. To produce graphene oxide from graphite, the Hummers technique oxidizes the graphite flakes and then exfoliates them to produce graphene oxide. When graphene oxide is reduced to reduced graphene oxide, oxygen-containing functional groups are eliminated, restoring a portion of the carbon network characteristic of graphene.

6.2.1. Synthesis of V_2O_5 microwave method

To Prepare the Vanadium oxide nanoparticles using microwave irradiation synthesis, 80mg of ammonium metavanadate was dissolve in ethylene glycol, and stirred the solution continuously for 40 min to ensure through mixing. After this, the mixed solution was sonicated for 15 min to break down the aggregates and ensure the uniform distribution of the solute. The homogenous suspension was then transferred to a microwave container at 600 watt for 6 min. this microwave heating step provided rapid and uniform heating, enhancing the reaction kinetics and promoting the formation of nanoparticles. After radiation, the mixture was filtered to remove the solid precursor and liquid precursor, and the solution was repeatedly cleaned with an appropriate solvent to get rid of contaminants. The washed precursor was then dried thoroughly to obtain a dry powder. For the annealing, dry precursor was placed in the furnace at 500°C for 2h. This high temperature annealing step promoted crystallization and improved the structural properties of the nanoparticles. Finally the product V_2O_5 nanoparticles was ready to use for the further application.

6.2.2. Synthesis of V_2O_5 -GO nanocomposite

The hydrothermal technique was employed to prepare a graphene oxide (GO) and vanadium pentoxide (V_2O_5) nanocomposite. Initially, 100 mg of V_2O_5 nanoparticles were suspended in 50 ml of deionized water, and the mixture was ultra-sonicated for 30 minutes while being vigorously stirred to ensure a uniform suspension. After this, varying amounts of GO (5 mg, 10 mg, and 15 mg) were added to separate batches of the suspension, resulting in samples designated as VG5, VG10, and VG15, respectively. The synthesis process is illustrated in figure 6.1.

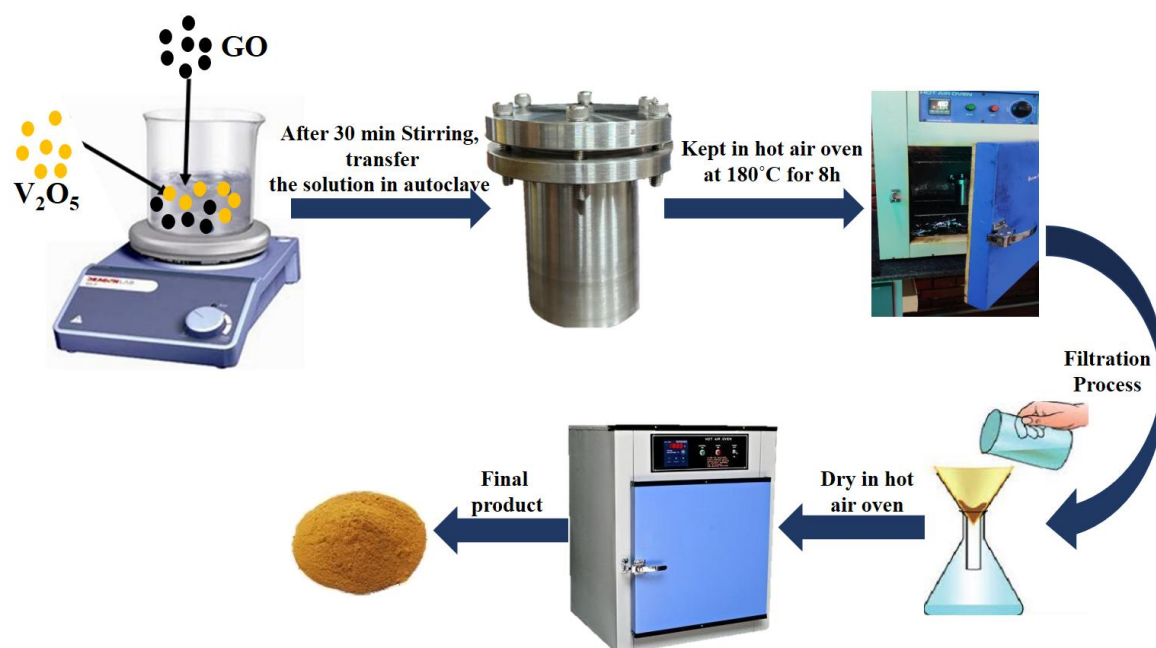


Figure 6.1 Flow chart of Synthesis of V₂O₅-graphene oxide composite by hydrothermal method.

Each mixture was then ultra-sonicated for an additional 30 minutes to integrate the GO thoroughly with the V₂O₅ nanoparticles. After the well-mixed solutions were transferred, they were heated at 180°C for 8 hours in a hot air oven to facilitate the production of the nanocomposite in a 100 ml Teflon-lined stainless-steel autoclave. The autoclave was then shut. After the heating stage, the autoclave was allowed to naturally cool to ambient temperature. After collecting the precipitate, any contaminants were removed with ethanol and deionized water, and the mixture was dried for 12 hours at 80°C in an oven.

6.3. Result and Discussion

SEM analysis is required to determine the morphology and microstructure (SEM, JOEL). Cu-K α radiation ($\lambda = 1.54$) was used to analyse the crystalline structure and particle size using X-ray diffraction (BRUKER). Fourier analysis was used to produce FTIR spectra of V₂O₅ produced by microwave processes in the wave number range 400–4000 cm⁻¹. At room temperature, use the PerkinElmer Spectrum IR Version 10.6.1 for transform infrared spectroscopy. For the electrochemical analysis of the prepared electrodes, the electrochemical workstation (METROHM) performed the CV, GCD, and EIS.

6.3.1. Crystallographic study

The crystalline structure of as-synthesized samples were investigated using X-ray diffraction (XRD), with the diffraction patterns displayed in figure 6.2. The XRD data of the as-prepared V_2O_5 , graphene oxide (GO), and the VG10 nanocomposite.

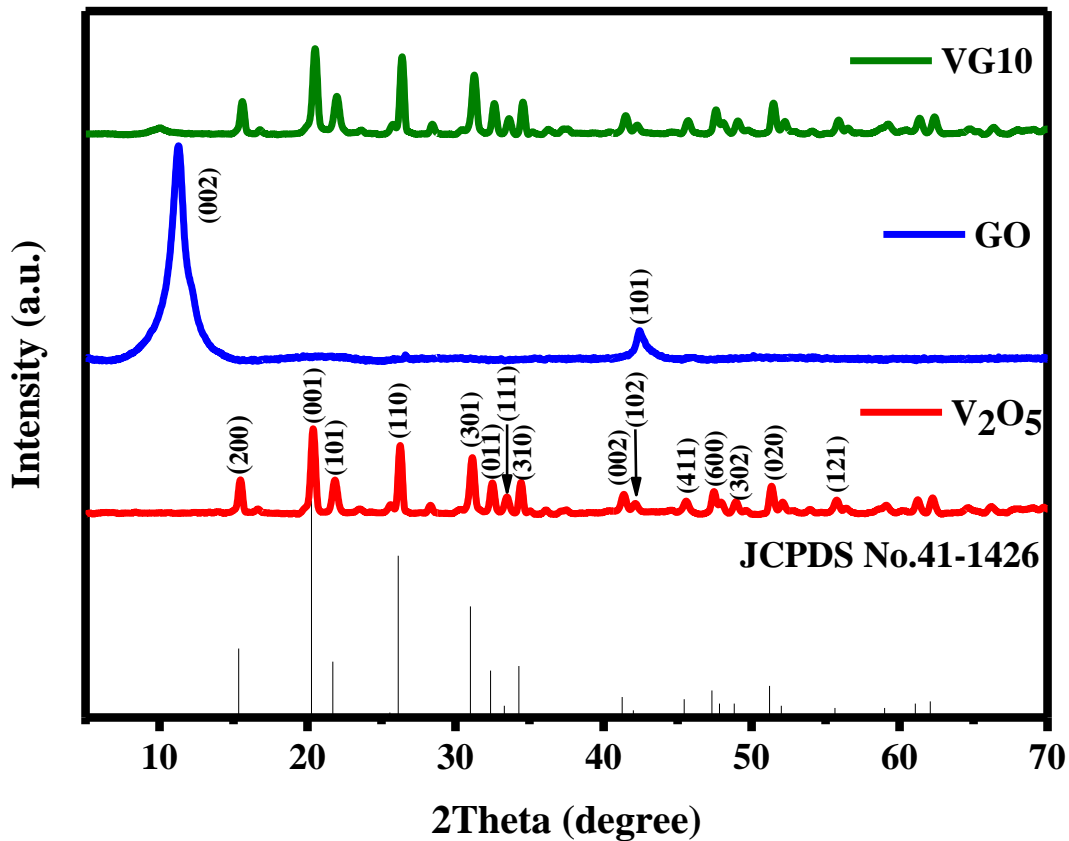


Figure 6.2 XRD pattern of V_2O_5 , GO and VG10.

The produced GO exhibits two strong peaks at 2θ values of approximately 11.46° and 42.55° , consistent to the (002) and (101) planes, respectively [266]. The peak at 11.46° shows a high degree of crystallinity in the GO structure, while the smaller peak at 42.55° suggests the presence of defects and disorders within the GO. For the VG10 nanocomposite and pure V_2O_5 samples, the XRD patterns reveal distinct peaks similar the (200), (001), (101), and (110) planes of V_2O_5 orthorhombic phase [267]. These peaks align with the standard data from the Joint Committee on Powder Diffraction Standards (JCPDS 41–1426), confirming the orthorhombic V_2O_5 phase with space group $Pmmn$ and lattice parameters $a = 11.494 \text{ \AA}$, $b = 4.369 \text{ \AA}$, and $c = 3.559 \text{ \AA}$. The absence of any impurity peaks indicates the high purity of the synthesized VG10 samples [268].

6.3.2. Morphological Study

Figure 6.3(a-c) depict the morphology of V_2O_5 , GO and VG10 as observed through different magnification SEM images. The V_2O_5 material consists of microspheres formed by the aggregation of V_2O_5 blocks. This aggregation results in a limited active surface area being exposed, which can restrict the material's overall effectiveness in applications. However, when a suitable amount of graphene oxide (GO) is introduced, the morphology changes significantly.

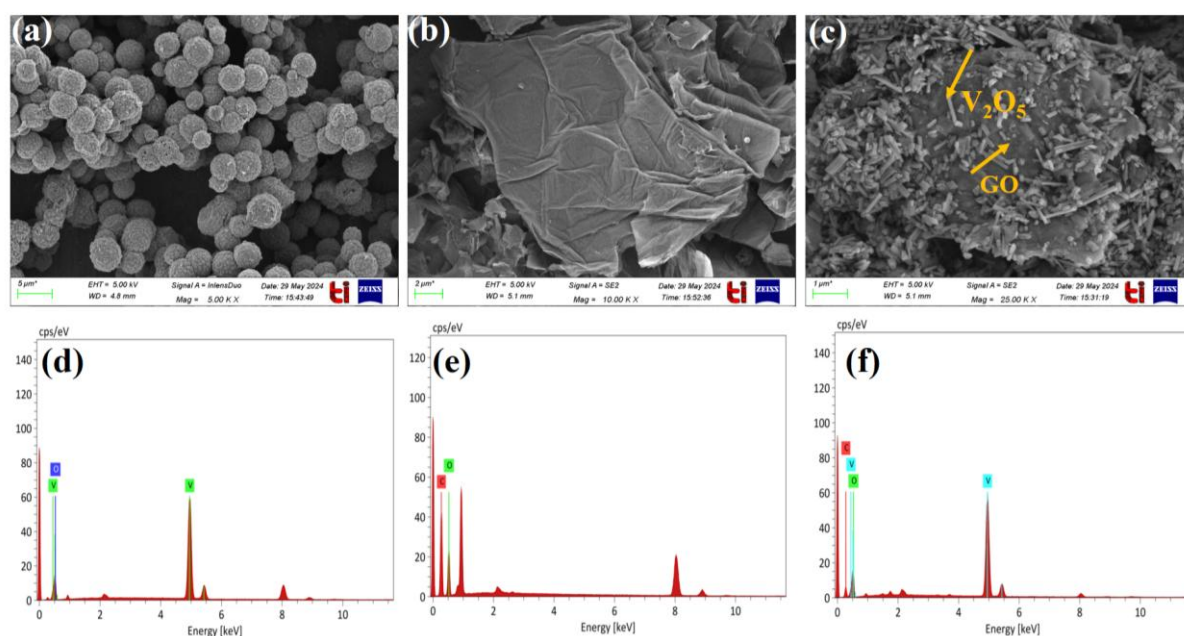


Figure 6.3 FESEM images and EDS analysis of (a, d) V_2O_5 microspheres, (b, e) GO nanosheets and (c, f) VG10 composite.

In VG10, the V_2O_5 is no longer present in block form but is instead dispersed as nanorods. This morphological change, brought about by the addition of GO, leads to a substantial increase in the specific surface area. The dispersion into nanorods also boosts of active sites available within the material. These enhancements are crucial as they can significantly improve the material's performance in applications such as energy storage, where a more active sites contribute to better efficiency and effectiveness [269].

The EDS method was used to assess the elemental composition and concentration of the produced samples, as shown in Figure 6.3(c-e). Figure 6.3(c) presents the EDS spectrum of

V_2O_5 , revealing a composition of 70% vanadium and 30% oxygen. Figure 6.3(d) illustrates the elemental distribution of GO, consisting of 52% carbon and 48% oxygen, with no detected impurities, representing the high purity of GO. The FTIR study confirms that the distribution of vanadium, oxygen, and carbon in figure 6.3(e) of the VG10 composite corresponds to surface functional groups containing these elements [270].

6.3.3. FTIR Spectra Analysis

Figure 6.4 displays the results of FTIR spectroscopy, which were conducted to identify and confirm the presence of functional groups on the surface of GO [271]. The vibrational modes present in graphene oxide (GO) include hydroxyl groups (O–H), carbonyl groups (C=O), aromatic carbon-carbon bonds (C=C), carboxyl groups (COOH), and epoxy groups.

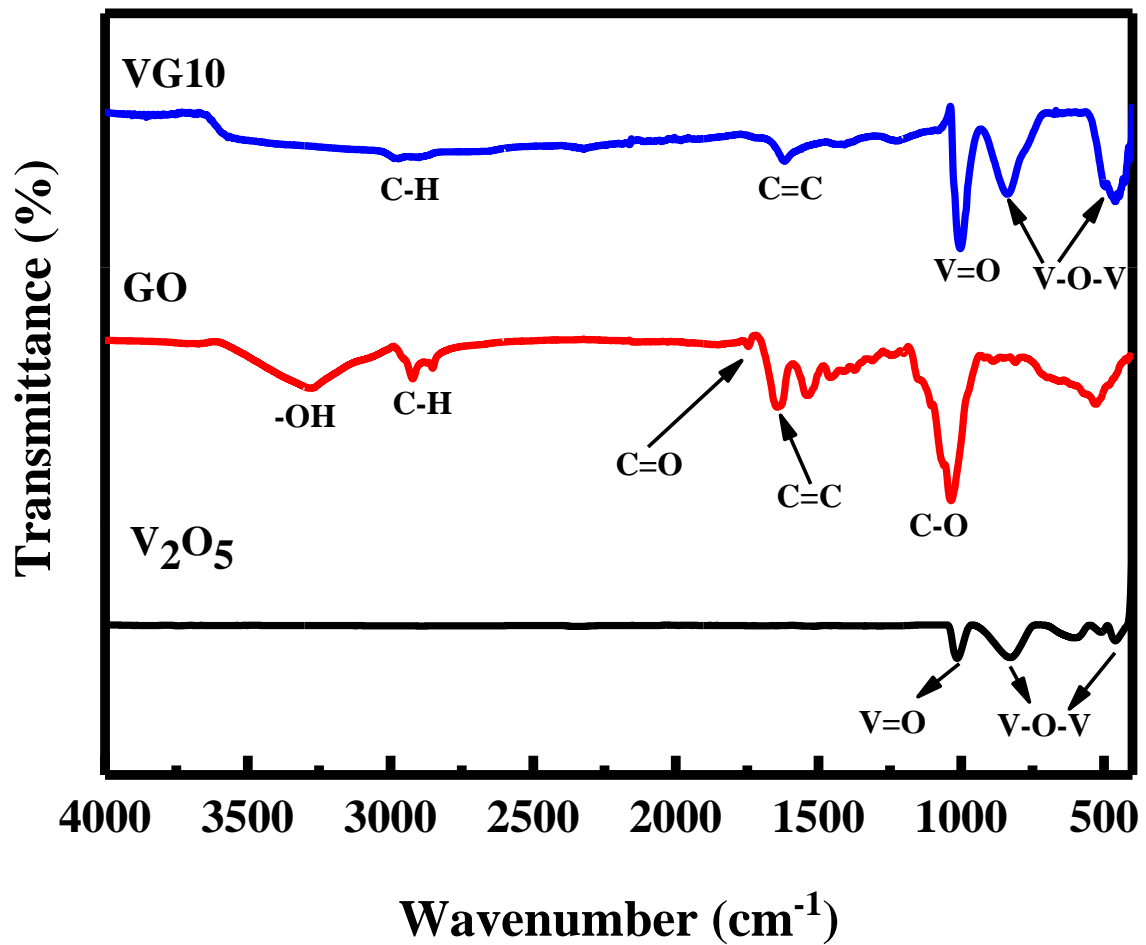


Figure 6.4 FTIR spectrum of V_2O_5 , GO and VG10 composite.

The peaks observed at 3300 cm^{-1} , 1744 cm^{-1} , and 1643 cm^{-1} are associated with the carboxyl groups, ketone groups, and primary graphitic domains, respectively, due to the sp^2 hybridization of the carbon atoms. [272]. The band seen in V_2O_5 at 825, 584, and 456 cm^{-1} is associated with the edge-sharing vibration and the V–O–V bending vibration, respectively. The V=O's terminal oxygen symmetric stretching vibration is responsible for the band at 1011 cm^{-1} . The VG10 sample exhibits some small differences in spectroscopy and displacements of the characteristic bands at 1000, 833, and 461 cm^{-1} , which might be explained by GO's interaction with the vanadyl groups of V_2O_5 . Additionally, the GO spectrum displays significant differences from the VG10 spectrum, including the distinctive peaks of C=O at 1744 cm^{-1} , C=C at 1639 cm^{-1} , and C–O at 1035 cm^{-1} . Water (H_2O) molecules' O–H stretching vibrations are attributed to the peak at 3300 cm^{-1} , while the bending of H–O–H vibrations is identified as the peak at 1624 cm^{-1} demonstrate that high-quality VG thin films were produced using the sol-gel technique [273].

6.3.4. Raman Analysis

Raman spectroscopy was used to identify the signature band for GO, V_2O_5 and VG10, as shown in figure 6.5 The VG10 sample exhibits two different types of peaks: External modes are defined as those that are found in the low-frequency domain area, while internal modes are defined as those that are found in the high-frequency domain [274].

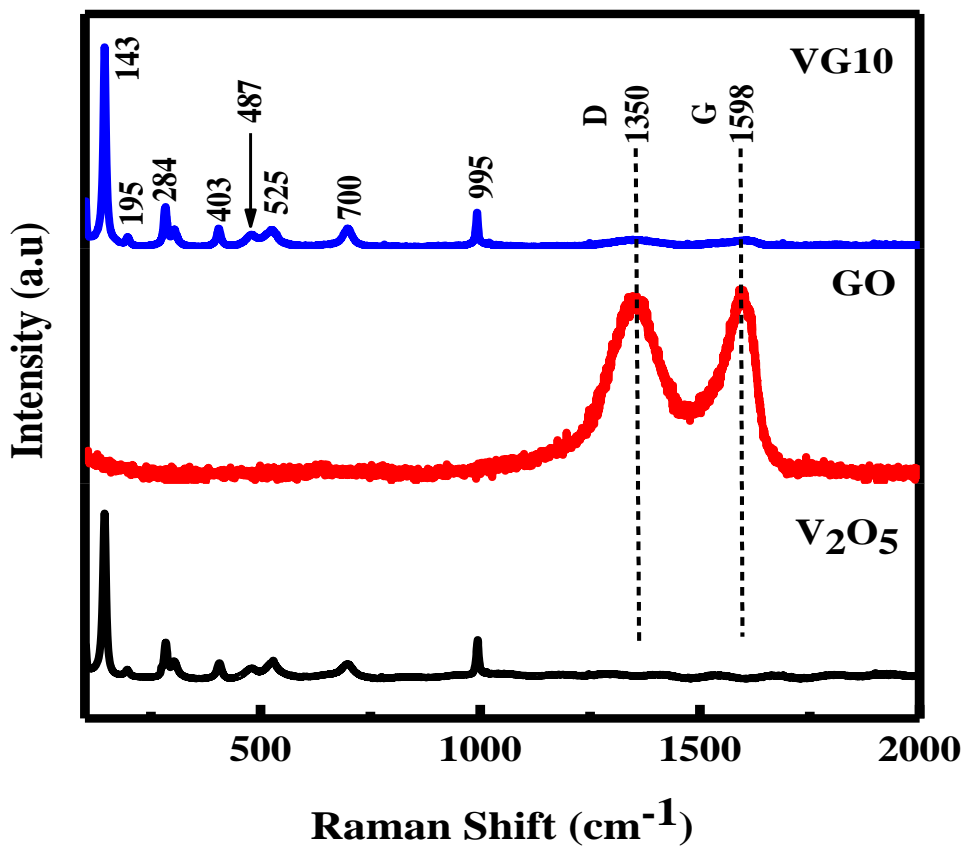


Figure 6.5 RAMAN spectrum of V_2O_5 , GO and VG10 composite.

Raman peaks at (143, 195, 284, 403, 487, 525, 700, and 995) cm^{-1} correspond to different vibration modes, were identified as orthorhombic phase of the V_2O_5 vibration modes [275]. As seen, the orthorhombic V_2O_5 layered structure is closely linked to 143 cm^{-1} , the low-frequency mode. The stretching mode of V-O is represented by the band seen at 190 cm^{-1} . The bond's V=O indicate the bending vibrations associated with symmetry vibrations are responsible for the peaks seen at 288 and 408 cm^{-1} , which have been confirmed by FTIR as well. The triple coordinated oxygen (V3-O) stretching modes linked to the vibration of A_g symmetry has the same Raman mode, which was discovered at 525 cm^{-1} [276]. The phases of double stretching and bending coordinate oxygen ($V_2\text{-O}$) were associated with the peak at the 706 cm^{-1} . The existence of V_2O_5 in the nanocomposite is shown by the band that is present at 995 cm^{-1} , this is aligned with the vanadium atoms' terminal oxygen stretching vibration when they are double-bonded to oxygen atom (V=O). The sp^2 of the graphitic carbon in the composite is responsible for the G band, while defects are usually responsible for the D band [277], [278].

6.3.5. Electrochemical Measurement

The electrochemical experiment was carried out at room temperature using a three-electrode setup. The working electrode for each of the three electrodes was ink-filled nickel foam, the reference electrode was Ag/AgCl, and the counter electrode was platinum wire. An electrolyte of 3M KOH was used in the experiment. The Ni foam was first cleaned many times using de-ionized water and ethanol to prepare electrodes, and after that it was dried in an oven. The active material, carbon black, and polyvinylidene fluoride (PVDF) binder were combined in a weight ratio of 80:10:10 to create a homogeneous paste, which was then used to create the working electrode. NMP (N-methyl-2-pyrrolidone) was utilized as a solvent for this process. The above paste was coated on Ni foam substrates in order to make an electrode and the nickel foam was dried at 70 °C for overnight. Using an electrochemical workstation (METROHM), experiments including (CV) cyclic voltammetry, (GCD) galvanostatic charging/discharging, and (EIS) electrochemical impedance spectroscopy were performed. The single electrode was tested using CV and EIS and charge-discharge characteristics were tested using galvanostatic charge-discharge (GCD).

Cyclic Voltammetry

The cyclic voltammetry of V_2O_5 and nanocomposites with graphene oxide was done using three electrode system. To fabricate the working electrode, Ni foam cut in the squares shape with the length of 1 cm. Using a microbalance, the weight of the V_2O_5 and VG composites was calculated by comparing the deposited material in the Ni foam with the uncovered Ni foam [279]. The CV was carried out through in an aqueous solution of 3 M KOH electrolyte at scanning rates of 5, 10, 20, 40, 60, 80 and 100 mV/s in the potential window of 0 to 0.7 V for V_2O_5 as shown in figure 6.6 (a) and 0 to 0.6 for the VG5, VG10 and VG15 as shown in figure 6.6 (b-d).

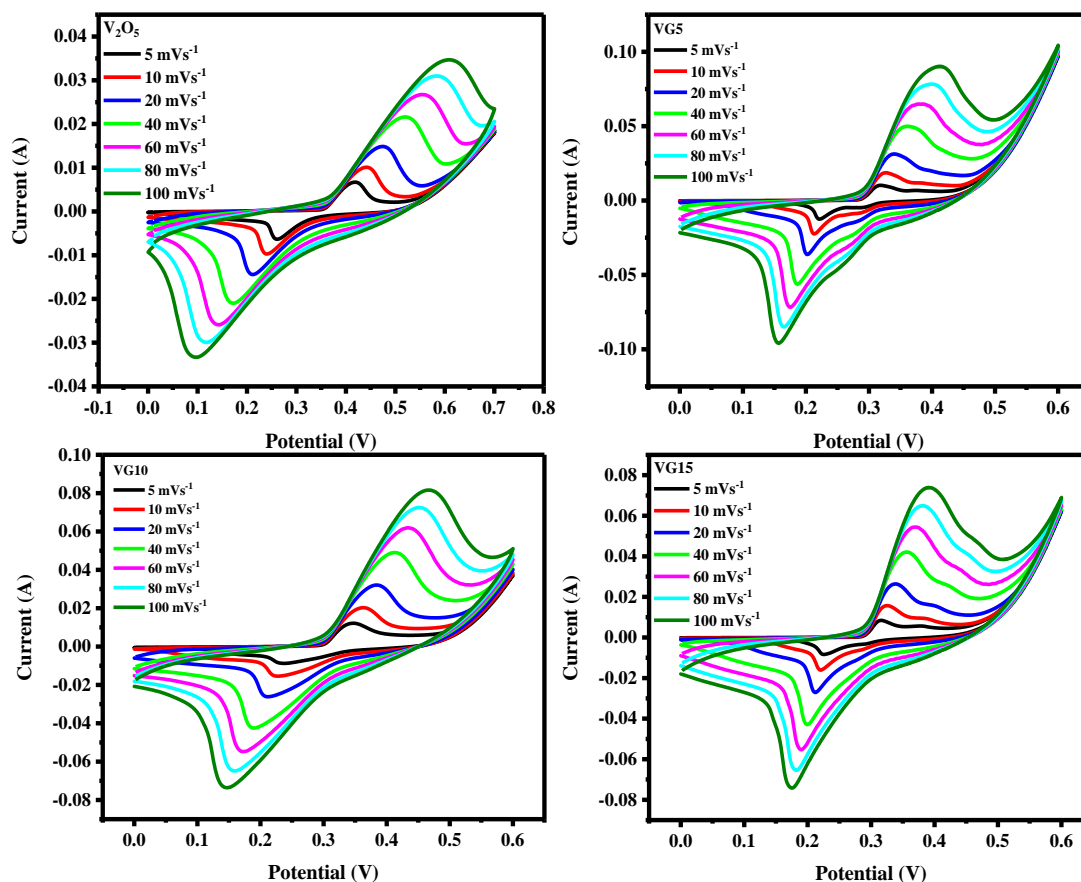


Figure 6.6 CV curve of (a) V_2O_5 , (b) VG5, (c) VG10 and (d) VG15.

The specific capacitance was evaluated by the equation no (1):

$$C_s = \frac{A}{m \cdot \text{scan rate} \cdot \text{potential window}} \quad \dots\dots\dots (1)$$

Where ‘ C_s ’ is the specific capacitance, the area inside the curve is ‘ A ’ and the mass loading of the active component is ‘ m ’. For the V_2O_5 , VG5, VG10, and VG15 electrodes, Based on the CV data, the specific capacitance calculate at the scan rate of 5 mVs^{-1} were 437, 750, 956, and 600 F/g, respectively [280]. The data shown in figure 6.7(d) confirmed these findings, demonstrating that the specific capacitance rises as the scan rate decreases in mVs^{-1} . The anodic/cathodic reaction showed redox peaks during the electrochemical process, this may be connected to the ions absorbed on the electrode surfaces and their subsequent intercalation and deintercalation [281].

The exceptional symmetry of the oxidation and reduction peaks in the CV curves indicates an elevated capacitance and a reversible faradaic process [282]. V_2O_5 provides pseudocapacitance, and graphene provides perfect electron conductivity. A notably high specific capacity is displayed by the composite [283]. Less ion migration to the carbon surface causes a decline in specific capacitance as scan rate rises, which is probably due to pores already present at the electrode's surface being inaccessible. These behaviors, which are often observed in all varieties of SCs, are a reflection of the porous electrode's restricted mass transfer kinetics [284].

Galvanostatic Charge/Discharge

The behaviour of V_2O_5 , V_2O_5 -GO nanocomposite with the current density 1 A/g and potential window 0-0.8V was examined using galvanic charge discharge. The charge/discharge patterns of composite electrodes and V_2O_5 are depicted in figure 6.7(a). A capacitive component displays a voltage change as a result of the energy within the capacitor changing and a resistive component, which occurs from rapid voltage drop and indicates a shift in voltage produced on by internal resistance, frequently create the discharge profile.

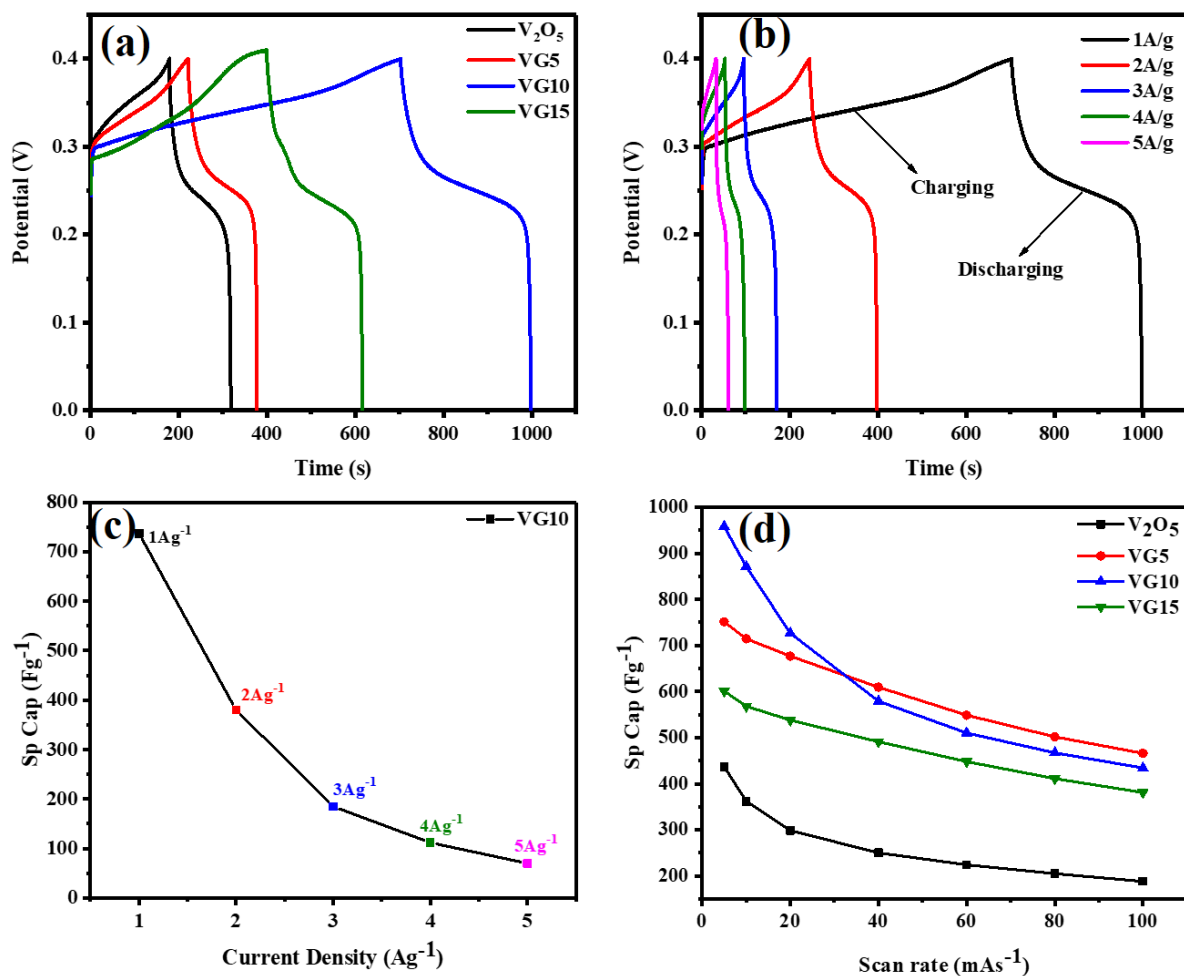


Figure 6.7 GCD curve of (a) V₂O₅, VG5, VG10 and VG15, (b) VG10 at the different current density (c) Specific capacitance of VG10 as a function of current density from GCD. (d) Specific capacitance of pure V₂O₅ and Composites as a function of scan rate from CV curves.

In addition, there is symmetric behaviour in the voltage-time curve. These nonlinear charge-discharge curves, which have a small curvature and a virtually triangular form, show that the electrodes have strong capacitive qualities. The longer charge/discharge duration of the VG10 electrode compared to the other electrodes confirms its higher specific capacitance [285]. The main cause of the VG10 electrode's higher specific capacitance is the uniform loading of V₂O₅ nanorods on GO nanosheets, This results in improved electrical conductivity and an ion-accessible surface area that is more efficient [286]. The formula used to obtain the specific capacitance values analytically is given by

$$Cs = \frac{I_m * \Delta t}{\Delta V} \dots\dots\dots(2)$$

Where I_m is the current, and discharge time for V_2O_5 , VG5, VG10, and VG15 samples is 138, 156, 295, and 216 s, with a potential window of 0.4 V for every electrode that has been formed. The value of the specific capacitance was determined to be (345, 390, 737 and 540) F/g, respectively. This data suggests that because VG10 has more active sites in the morphology of its wrinkles, it completes the proper usage of the active components.

Electrochemical impedance spectroscopy

As seen in Figure 6.8, the aqueous solution of 3 M KOH was examined the EIS curve at frequencies ranging from 1 to 100,000 Hz. The two Nyquist plot sections display a straight line in the low-frequency area and a semicircle loop in the high-frequency zone.

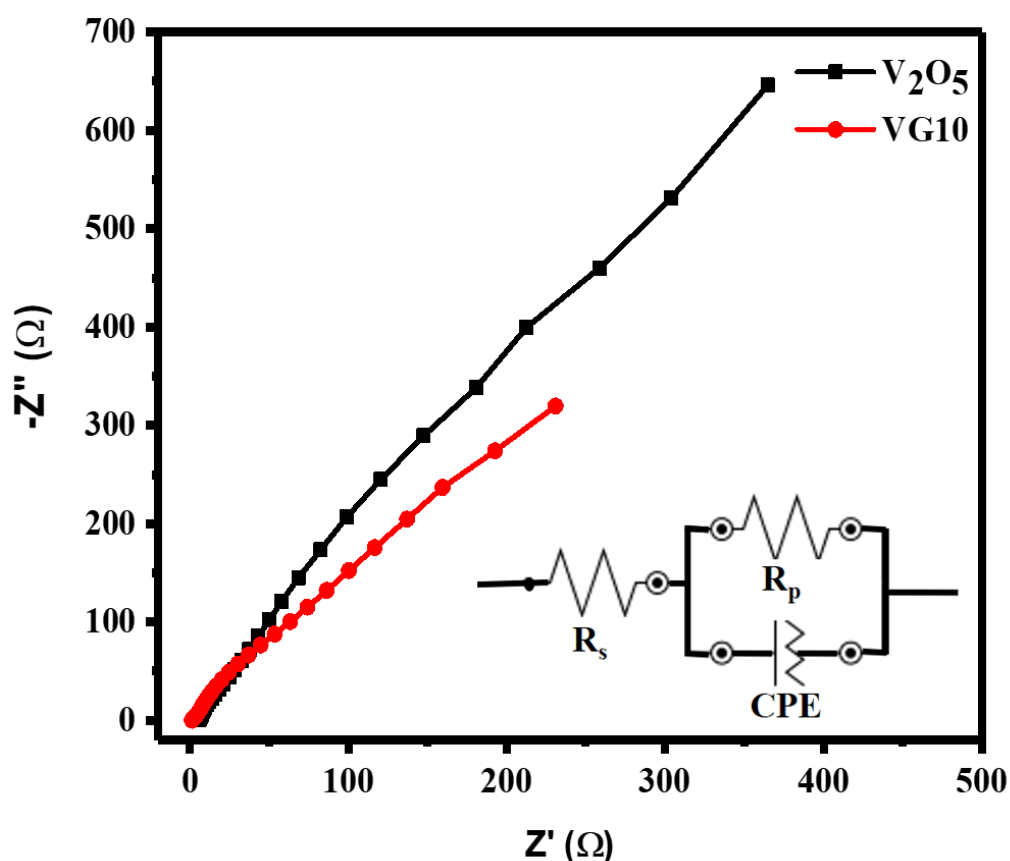


Figure 6.8 Nyquist plots of pure V_2O_5 and various VG10 electrode (insets are the corresponding equivalent circuits).

This suggests, there are regional differences in the electrochemical process at electrode/electrolyte contacts. Showing ion diffusion resistance and the charge transfer resistance (R_{ct}) respectively, are the semicircles and the linear graph. Substance intrinsic resistance, the contact resistance of active materials and resistance of electrolyte ionic combined represent the total resistance in the semicircle area, which is shown by the intersection with the real component (Z') [287]. Furthermore, the VG10 composite electrode exhibits a smaller series resistance ($R_s = 1.1\Omega$) than the bare V_2O_5 series resistance ($R_s = 5.5\Omega$). This can be explained by the Warburg impedance (Z_W), which is caused by the transfer of OH^- ions after the redox process. The lower frequency range of pseudocapacitive behavior of the electrode is shown by the vertical lines aligned with the imaginary axis ($-Z''$) [288].

6.3.6. Energy Storage Mechanism

We investigated into the created electrodes storage processes in order to gain further understanding of our electrochemical studies. Three main components include charge storage: the first two are ascribed to intercalating (diffusion) ways and faradic surface redox processes, which result in pseudo-capacitive behaviour. At the same time, the third element is connected to interfacial effects, which are ascribed to the development of an EDL (electric double layer). The connection between the CV peak current (i) and scan rate (v) was investigated to understand the contributions from equations 3 and 4.

$$i = av^b \quad \dots\dots\dots (3)$$

$$\log(i) = \log(a) + b\log(v) \quad \dots\dots\dots (4)$$

According to published reports, a 'b' value of 1 denotes pseudocapacitive behaviour, A diffusion-controlled mechanism similar to a battery is indicated by a value of 0.5 [289]. As can be seen in figure 6.9(a), the anode peaks of VG10 show "b" values 0.66 respectively. These result demonstrate that the specific capacitance of VG10 electrode are affected by both diffusion-controlled and pseudocapacitive behaviour. The percentage of these two contributions may be studied from the CV curves and equations (5 and 6) [290].

$$i(V) = K_1 v + K_2 v^{1/2} \quad \dots\dots\dots (5)$$

$$\frac{i(V)}{v^{1/2}} = K_1 v^{1/2} + K_2 \quad \dots\dots\dots (6)$$

The tuneable values measure for the K1 and K2 are obtained by using the y-axis and slope of curves between " $i v^{-1/2}$ " and " $v^{1/2}$." The " $K_1 v$ " and " $K_2 v^{1/2}$ " are the elements that indicate diffusion-controlled behaviour and capacitive behaviour, respectively.

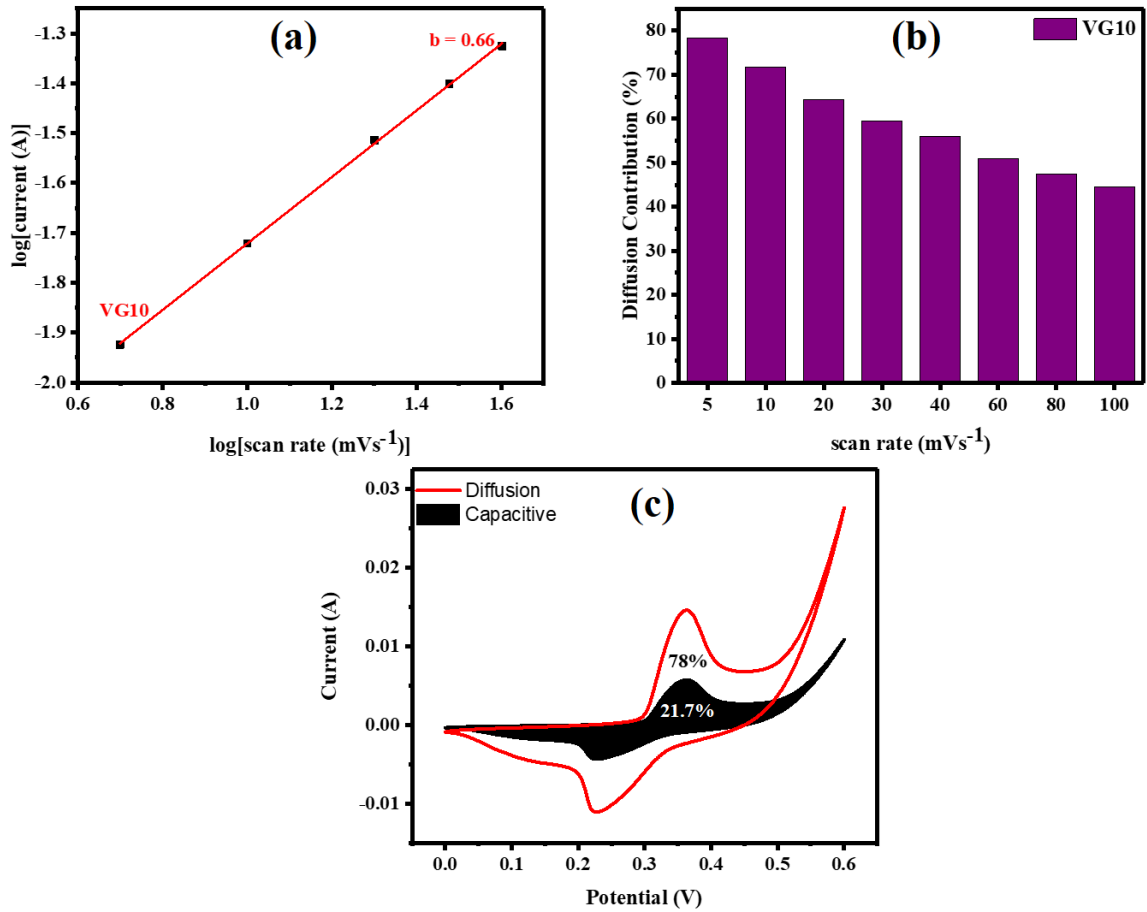


Figure 6.9 (a) the graph of relationship between the log of the peak current and the log of the scan rate of VG10 for the anodic peaks. (b) Percentage of diffusion contribution by VG10 at different scan rates. (c) The distribution of percentage contributions from capacitive and diffusion currents at a fixed scan rate of 10 mV/sec of VG10.

Figure 6.9(b) displays the fractions that represent the battery-type behavior of VG10. The diffusion contributions for VG10 are 78%, 71%, 64%, 59%, 50%, 47%, and 41% for scan rates of 5-100 mV/sec, according the above figures. A larger frequency of interaction between the electrolyte ions and at a lower scanning rate the electrode materials leads to a

significant output from faradaic interactions. However, Charge storage usually happens through non-faradaic mechanisms at faster scan rates because there is an ion of electrolyte for less time to interact with the materials of the electrode. The CV for VG10 electrode materials obtained at the scan rate of 10 mV/sec are shown in figure 6.9(c). The CV curve in red represent the current ascribed to diffusion kinetics, while the shaded CV curve in black constitute the current contribution from the capacitive kinetics. Therefore, it is visible from the above results that the battery-type (diffusion) mechanism of the V_2O_5 is significantly improved by the addition of GO.

Chapter: 7

Summary and Conclusion

The urgent need for alternative energy sources has become increasingly apparent in today's world. As we deplete our natural resources, it is imperative to explore sustainable and renewable alternatives. Energy storage systems play a pivotal role in harnessing the power of these renewable sources, ensuring a steady and reliable supply.

Supercapacitors stand out as promising energy storage devices due to their exceptional properties. Unlike traditional batteries, they boast a long cycle life, lightweight design, small footprint, and high power density. Their ability to be rapidly recharged makes them ideal for applications demanding quick bursts of energy. Metal oxide-based nanostructured materials and nanocomposites have garnered significant attention for their potential to enhance the performance of supercapacitors. These materials possess a high specific surface area, making them excellent candidates for electrode materials in electric double-layer capacitors (EDLCs). This study focused on doping graphene oxide with vanadium oxide to optimize the electrode material for supercapacitor applications. By modifying the chemical properties and band gap of graphene oxide through doping, the researchers aimed to significantly increase capacitance. This combination of double-layer and pseudocapacitance mechanisms resulted in a highly efficient and promising energy storage device.

In chapter 4, the electrode materials of V_2O_5 were successfully synthesized using hydrothermal, mechanochemical and microwave methods, allowing for a detailed comparison of their electrochemical properties. The synthesis of V_2O_5 was confirmed through comprehensive characterization techniques including XRD, FTIR, and SEM. These methods provided evidence of the formation and structural integrity of the V_2O_5 materials. The electrochemical characteristics of the synthesized V_2O_5 were thoroughly investigated using several advanced techniques. CV was employed to analyze the redox behavior and capacitance of the materials. GCD measurements were conducted to assess the charge storage capacity and cyclic stability of the electrodes. EIS was utilized to examine the charge transfer resistance and overall conductivity of the materials. The results from these electrochemical tests revealed significant differences the V_2O_5 synthesized by the hydrothermal, mechanochemical and microwave methods. The V_2O_5 produced through the microwave method displayed remarkably higher specific capacitance values, approximately twice those of the V_2O_5 synthesized via the hydrothermal and mechanochemical method.

Additionally, the V_2O_5 prepared by the microwave method demonstrated superior pseudo-capacitive behavior, indicating better performance in terms of energy storage and release. The study's findings highlight the benefits of the microwave method for producing V_2O_5 with enhanced electrochemical properties. The improved performance is attributed to the optimized structural and morphological characteristics of the microwave-synthesized V_2O_5 , which likely contribute to better ion diffusion and electron transport during electrochemical processes.

In chapter 5, we extensively investigated the gas sensing capabilities of pure V_2O_5 nanoparticles for detecting acetone, isopropanol (IPA), and methanol vapors. These nanoparticles were synthesized using two distinct techniques: microwave irradiation and solvent-thermal methods. Both synthesis methods yielded samples that displayed a well-defined crystalline structure characterized by an orthorhombic phase. The performance of gas sensing for the V_2O_5 nanoparticles was evaluated by measuring their response and recovery times when exposed to acetone, IPA, and methanol vapors. The response time and the recovery times for acetone vapor were found to be 4 seconds and 2 seconds, respectively. For IPA vapor, the response and recovery times were 12 seconds and 2 seconds, while for methanol vapor, they were 6 seconds and 3 seconds, respectively. Among the three vapors tested, the acetone vapor gas sensor demonstrated the most favourable sensing response, as well as the fastest response time and recovery times. This superior performance was observed in the sensor fabricated using V_2O_5 nanoparticles synthesized via the microwave technique. The comparison between the two syntheses methods revealed that the microwave-synthesized V_2O_5 nanoparticles provided a more effective gas sensor than those produced using the solvent-thermal method. The improved selectivity of the microwave gas sensor for acetone is due to the carbonyl group present in acetone. This group is polar and has a greater dipole moment compared to the functional groups found in methanol and IPA. This increased polarity likely facilitates stronger interactions with the V_2O_5 sensor material, leading to improved sensing performance.

This research presents a comprehensive study on the hydrothermal synthesis of V_2O_5 /GO nanocomposites. A combination of advanced analytical techniques was employed to thoroughly investigate the phase composition, elemental content, and morphological distribution of the synthesized materials. X-ray diffraction (XRD) analysis confirmed the successful formation of both pristine V_2O_5 and V_2O_5 /GO nanocomposites. Further evidence

was provided by scanning electron microscopy (SEM), which visualized the morphology and distribution of V_2O_5 and GO within the nanocomposites. To assess the electrochemical performance of the V_2O_5 /GO nanocomposites, a series of tests were conducted. Cyclic voltammetry (CV) was used to study redox behavior and capacitance, while galvanostatic charge-discharge (GCD) measurements evaluated charge storage capacity and cyclic stability. Electrochemical impedance spectroscopy (EIS) provided insights into charge transfer resistance and overall conductivity.

The results from these tests demonstrated a significant enhancement in the electrochemical properties of the V_2O_5 /GO nanocomposites compared to pristine V_2O_5 . The optimal integration of graphene oxide (GO) led to remarkable capacitance retention and a high specific capacitance of 737 Fg^{-1} . These findings underscore the potential of V_2O_5 /GO nanocomposites as promising electrode materials for next-generation energy storage systems.

Future Scope

The following outlines the challenges and possible benefits of using graphene with vanadium-based nanocomposites for supercapacitor applications.

1. Novel Synthesis Methods:

- Pursue innovative synthesis techniques to optimize the electrochemical and gas-sensing properties of V_2O_5 . Explore methods that can control the size, shape, and morphology of V_2O_5 nanostructures, leading to enhanced performance.
- Investigate alternative precursors or reaction conditions to tailor the properties of V_2O_5 for specific applications. For example, using different solvents or surfactants during synthesis can influence the crystal structure and surface chemistry.

2. Enhanced Gas Sensing Performance:

- Prioritize research on improving the sensitivity and selectivity of V_2O_5 -based gas sensors. Develop strategies to enhance the sensor's response to target gases while minimizing interference from other components in the environment.
- Explore novel fabrication methods to create more sensitive and selective gas sensing devices. Consider techniques like 3D printing or atomic layer deposition to engineer unique structures and optimize gas diffusion pathways.
- Integrate V_2O_5 with other sensing elements to create hybrid sensors with enhanced capabilities. Combining V_2O_5 with materials that exhibit different sensing mechanisms can broaden the detection range and improve overall performance.

3. Optimization of V_2O_5 -GO Composite Electrodes:

- Conduct in-depth studies on the composition and structure of V_2O_5 -GO composite electrodes. Investigate the effects of varying V_2O_5 and GO content on electrochemical properties, stability, and compatibility with different electrolytes.
- Explore different GO modification strategies to optimize its interaction with V_2O_5 and enhance the overall performance of the composite electrodes. For instance,

functionalizing GO with specific groups can improve its conductivity or affinity for V_2O_5 .

- Investigate the stability and compatibility of V_2O_5 -GO composites with various electrolytes and device architectures. Evaluate their performance in different operating conditions and identify potential challenges or limitations.

4. Advanced Characterization Techniques:

- Utilize a wide range of characterization techniques to gain a comprehensive understanding of the crystal phases, morphology, and composition of V_2O_5 and its composites. Techniques such as X-ray diffraction, transmission electron microscopy, and Raman spectroscopy can provide valuable insights into the structural and electronic properties of these materials.
- Employ advanced analytical tools to accurately characterize the gas sensing and electrochemical properties of V_2O_5 -based materials. This includes techniques like impedance spectroscopy, gas chromatography, and mass spectrometry.
- Correlate the results from characterization techniques with the observed performance of V_2O_5 -based devices to establish structure-property relationships and guide future research efforts.

Reference

- [1] P. Simon and Y. Gogotsi, “Materials for electrochemical capacitors,” *Nat. Mater.*, vol. 7, no. 11, pp. 845–854, Nov. 2008, doi: 10.1038/nmat2297.
- [2] L. L. Zhang and X. S. Zhao, “Carbon-based materials as supercapacitor electrodes,” *Chem. Soc. Rev.*, vol. 38, no. 9, p. 2520, 2009, doi: 10.1039/b813846j.
- [3] X. Zhao, B. M. Sánchez, P. J. Dobson, and P. S. Grant, “The role of nanomaterials in redox-based supercapacitors for next generation energy storage devices,” *Nanoscale*, vol. 3, no. 3, p. 839, 2011, doi: 10.1039/c0nr00594k.
- [4] M. V. Kiamahalleh, S. H. S. Zein, G. Najafpour, S. A. Sata, and S. Buniran, “MULTIWALLED CARBON NANOTUBES BASED NANOCOMPOSITES FOR SUPERCAPACITORS: A REVIEW OF ELECTRODE MATERIALS,” *Nano*, vol. 07, no. 02, p. 1230002, Apr. 2012, doi: 10.1142/S1793292012300022.
- [5] M. Hashemi, M. S. Rahmanifar, M. F. El-Kady, A. Noori, M. F. Mousavi, and R. B. Kaner, “The use of an electrocatalytic redox electrolyte for pushing the energy density boundary of a flexible polyaniline electrode to a new limit,” *Nano Energy*, vol. 44, pp. 489–498, Feb. 2018, doi: 10.1016/j.nanoen.2017.11.058.
- [6] T. C. Mendes, F. Zhou, A. J. Barlow, M. Forsyth, P. C. Howlett, and D. R. MacFarlane, “An ionic liquid based sodium metal-hybrid supercapacitor-battery,” *Sustain. Energy Fuels*, vol. 2, no. 4, pp. 763–771, 2018, doi: 10.1039/C7SE00547D.
- [7] A. G. Pandolfo and A. F. Hollenkamp, “Carbon properties and their role in supercapacitors,” *J. Power Sources*, vol. 157, no. 1, pp. 11–27, Jun. 2006, doi: 10.1016/j.jpowsour.2006.02.065.
- [8] L. Ren, G. Zhang, J. Lei, Y. Wang, and D. Hu, “Novel layered polyaniline-poly(hydroquinone)/graphene film as supercapacitor electrode with enhanced rate performance and cycling stability,” *J. Colloid Interface Sci.*, vol. 512, pp. 300–307, Feb. 2018, doi: 10.1016/j.jcis.2017.10.067.
- [9] A. Burke, “Ultracapacitors: why, how, and where is the technology,” *J. Power Sources*, vol. 91, no. 1, pp. 37–50, Nov. 2000, doi: 10.1016/S0378-7753(00)00485-7.

- [10] P. J. Hall *et al.*, “Energy storage in electrochemical capacitors: designing functional materials to improve performance,” *Energy Environ. Sci.*, vol. 3, no. 9, p. 1238, 2010, doi: 10.1039/c0ee00004c.
- [11] “Electrochemical supercapacitors: Energy storage beyond batteries,” 2024.
- [12] H. D. Abruña, Y. Kiya, and J. C. Henderson, “Batteries and electrochemical capacitors,” *Phys. Today*, vol. 61, no. 12, pp. 43–47, Dec. 2008, doi: 10.1063/1.3047681.
- [13] J. R. Miller and A. Burke, “Electrochemical Capacitors: Challenges and Opportunities for Real-World Applications,” *Electrochem. Soc. Interface*, vol. 17, no. 1, pp. 53–57, Mar. 2008, doi: 10.1149/2.F08081IF.
- [14] M. Jayalakshmi and K. Balasubramanian, “Solution Combustion Synthesis of Fe₂O₃/C, Fe₂O₃-SnO₂/C, Fe₂O₃-ZnO/C Composites and their Electrochemical Characterization in Non-Aqueous Electrolyte for Supercapacitor Application,” *Int. J. Electrochem. Sci.*, vol. 4, no. 6, pp. 878–886, Jun. 2009, doi: 10.1016/S1452-3981(23)15191-1.
- [15] D. P. Dubal, O. Ayyad, V. Ruiz, and P. Gómez-Romero, “Hybrid energy storage: the merging of battery and supercapacitor chemistries,” *Chem. Soc. Rev.*, vol. 44, no. 7, pp. 1777–1790, 2015, doi: 10.1039/C4CS00266K.
- [16] P. K. Katkar, S. J. Marje, S. S. Pujari, S. A. Khalate, A. C. Lokhande, and U. M. Patil, “Enhanced Energy Density of All-Solid-State Asymmetric Supercapacitors Based on Morphologically Tuned Hydrous Cobalt Phosphate Electrode as Cathode Material,” *ACS Sustain. Chem. Eng.*, vol. 7, no. 13, pp. 11205–11218, Jul. 2019, doi: 10.1021/acssuschemeng.9b00504.
- [17] G. Wang, L. Zhang, and J. Zhang, “A review of electrode materials for electrochemical supercapacitors,” *Chem Soc Rev*, vol. 41, no. 2, pp. 797–828, 2012, doi: 10.1039/C1CS15060J.
- [18] J. P. Zheng, J. Huang, and T. R. Jow, “The Limitations of Energy Density for Electrochemical Capacitors,” *J. Electrochem. Soc.*, vol. 144, no. 6, pp. 2026–2031, Jun. 1997, doi: 10.1149/1.1837738.
- [19] C. Zhong, Y. Deng, W. Hu, J. Qiao, L. Zhang, and J. Zhang, “A review of electrolyte materials and compositions for electrochemical supercapacitors,” *Chem. Soc. Rev.*, vol. 44, no. 21, pp. 7484–7539, 2015, doi: 10.1039/C5CS00303B.

- [20] Y.-G. Wang, Z.-D. Wang, and Y.-Y. Xia, "An asymmetric supercapacitor using RuO₂/TiO₂ nanotube composite and activated carbon electrodes," *Electrochimica Acta*, vol. 50, no. 28, pp. 5641–5646, Sep. 2005, doi: 10.1016/j.electacta.2005.03.042.
- [21] D.-W. Wang *et al.*, "Aligned Titania Nanotubes as an Intercalation Anode Material for Hybrid Electrochemical Energy Storage," *Adv. Funct. Mater.*, vol. 18, no. 23, pp. 3787–3793, Dec. 2008, doi: 10.1002/adfm.200800635.
- [22] J. W. Long, D. Bélanger, T. Brousse, W. Sugimoto, M. B. Sassin, and O. Crosnier, "Asymmetric electrochemical capacitors—Stretching the limits of aqueous electrolytes," *MRS Bull.*, vol. 36, no. 7, pp. 513–522, Jul. 2011, doi: 10.1557/mrs.2011.137.
- [23] W. Shimizu, S. Makino, K. Takahashi, N. Imanishi, and W. Sugimoto, "Development of a 4.2 V aqueous hybrid electrochemical capacitor based on MnO₂ positive and protected Li negative electrodes," *J. Power Sources*, vol. 241, pp. 572–577, Nov. 2013, doi: 10.1016/j.jpowsour.2013.05.003.
- [24] W. Lu, L. Hao, and Y. Wang, "Highly active N, S Co-Doped Ultramicroporous Carbon for High-Performance Supercapacitor Electrodes," *Micromachines*, vol. 13, no. 6, p. 905, Jun. 2022, doi: 10.3390/mi13060905.
- [25] G. Xu *et al.*, "Binder-free activated carbon/carbon nanotube paper electrodes for use in supercapacitors," *Nano Res.*, vol. 4, no. 9, pp. 870–881, Sep. 2011, doi: 10.1007/s12274-011-0143-8.
- [26] X. Li, C. Han, X. Chen, and C. Shi, "Preparation and performance of straw based activated carbon for supercapacitor in non-aqueous electrolytes," *Microporous Mesoporous Mater.*, vol. 131, no. 1–3, pp. 303–309, Jun. 2010, doi: 10.1016/j.micromeso.2010.01.007.
- [27] A. Alonso *et al.*, "Activated carbon produced from Sasol-Lurgi gasifier pitch and its application as electrodes in supercapacitors," *Carbon*, vol. 44, no. 3, pp. 441–446, Mar. 2006, doi: 10.1016/j.carbon.2005.09.008.
- [28] T. Chen and L. Dai, "Carbon nanomaterials for high-performance supercapacitors," *Mater. Today*, vol. 16, no. 7–8, pp. 272–280, Jul. 2013, doi: 10.1016/j.mattod.2013.07.002.

- [29] A. Ray *et al.*, “Correlation between the dielectric and electrochemical properties of TiO₂-V₂O₅ nanocomposite for energy storage application,” *Electrochimica Acta*, vol. 266, pp. 404–413, Mar. 2018, doi: 10.1016/j.electacta.2018.02.033.
- [30] J. Yu *et al.*, “Omnidirectionally Stretchable High-Performance Supercapacitor Based on Isotropic Buckled Carbon Nanotube Films,” *ACS Nano*, vol. 10, no. 5, pp. 5204–5211, May 2016, doi: 10.1021/acsnano.6b00752.
- [31] M. Lee *et al.*, “One-step hydrothermal synthesis of graphene decorated V₂O₅ nanobelts for enhanced electrochemical energy storage,” *Sci. Rep.*, vol. 5, no. 1, Art. no. 1, Jan. 2015, doi: 10.1038/srep08151.
- [32] R. N. A. R. Seman, M. A. Azam, and A. A. Mohamad, “Systematic gap analysis of carbon nanotube-based lithium-ion batteries and electrochemical capacitors,” *Renew. Sustain. Energy Rev.*, vol. 75, pp. 644–659, Aug. 2017, doi: 10.1016/j.rser.2016.10.078.
- [33] S. K. Simotwo, C. DelRe, and V. Kalra, “Supercapacitor Electrodes Based on High-Purity Electrospun Polyaniline and Polyaniline–Carbon Nanotube Nanofibers,” *ACS Appl. Mater. Interfaces*, vol. 8, no. 33, pp. 21261–21269, Aug. 2016, doi: 10.1021/acsami.6b03463.
- [34] R. Deka, S. Rathi, and S. M. Mobin, “Exploring the feasibility of a two-dimensional layered cobalt-based coordination polymer for supercapacitor applications: effect of electrolytic cations,” *Energy Adv.*, vol. 2, no. 12, pp. 2119–2128, 2023, doi: 10.1039/D3YA00378G.
- [35] W. K. Chee, H. N. Lim, Z. Zainal, N. M. Huang, I. Harrison, and Y. Andou, “Flexible Graphene-Based Supercapacitors: A Review,” *J. Phys. Chem. C*, vol. 120, no. 8, pp. 4153–4172, Mar. 2016, doi: 10.1021/acs.jpcc.5b10187.
- [36] J. Yu *et al.*, “Metallic Fabrics as the Current Collector for High-Performance Graphene-Based Flexible Solid-State Supercapacitor,” *ACS Appl. Mater. Interfaces*, vol. 8, no. 7, pp. 4724–4729, Feb. 2016, doi: 10.1021/acsami.5b12180.
- [37] C. Zhu *et al.*, “Supercapacitors Based on Three-Dimensional Hierarchical Graphene Aerogels with Periodic Macropores,” *Nano Lett.*, vol. 16, no. 6, pp. 3448–3456, Jun. 2016, doi: 10.1021/acs.nanolett.5b04965.
- [38] E. D. Walsh *et al.*, “Dry-Processed, Binder-Free Holey Graphene Electrodes for Supercapacitors with Ultrahigh Areal Loadings,” *ACS Appl. Mater. Interfaces*, vol. 8, no. 43, pp. 29478–29485, Nov. 2016, doi: 10.1021/acsami.6b09951.

- [39] Y. Shi *et al.*, “Nanostructured conductive polypyrrole hydrogels as high-performance, flexible supercapacitor electrodes,” *J Mater Chem A*, vol. 2, no. 17, pp. 6086–6091, 2014, doi: 10.1039/C4TA00484A.
- [40] P. R. Deshmukh, S. N. Pusawale, N. M. Shinde, and C. D. Lokhande, “Growth of polyaniline nanofibers for supercapacitor applications using successive ionic layer adsorption and reaction (SILAR) method,” *J. Korean Phys. Soc.*, vol. 65, no. 1, pp. 80–86, Jul. 2014, doi: 10.3938/jkps.65.80.
- [41] T. Liu *et al.*, “Polyaniline and Polypyrrole Pseudocapacitor Electrodes with Excellent Cycling Stability,” *Nano Lett.*, vol. 14, no. 5, pp. 2522–2527, May 2014, doi: 10.1021/nl500255v.
- [42] N. Kurra, J. Park, and H. N. Alshareef, “A conducting polymer nucleation scheme for efficient solid-state supercapacitors on paper,” *J Mater Chem A*, vol. 2, no. 40, pp. 17058–17065, Aug. 2014, doi: 10.1039/C4TA03603D.
- [43] J. Li, Z. Ren, S. Wang, Y. Ren, Y. Qiu, and J. Yu, “MnO₂ Nanosheets Grown on Internal Surface of Macroporous Carbon with Enhanced Electrochemical Performance for Supercapacitors,” *ACS Sustain. Chem. Eng.*, vol. 4, no. 7, pp. 3641–3648, Jul. 2016, doi: 10.1021/acssuschemeng.6b00092.
- [44] Z. Peng *et al.*, “Design and Tailoring of the 3D Macroporous Hydrous RuO₂ Hierarchical Architectures with a Hard-Template Method for High-Performance Supercapacitors,” *ACS Appl. Mater. Interfaces*, vol. 9, no. 5, pp. 4577–4586, Feb. 2017, doi: 10.1021/acsami.6b12532.
- [45] C.-C. Hu, C.-W. Wang, K.-H. Chang, and M.-G. Chen, “Anodic composite deposition of RuO₂/reduced graphene oxide/carbon nanotube for advanced supercapacitors,” *Nanotechnology*, vol. 26, no. 27, p. 274004, Jul. 2015, doi: 10.1088/0957-4484/26/27/274004.
- [46] S. Maitra, R. Mitra, and T. K. Nath, “Investigation of electrochemical performance of sol-gel derived MgFe₂O₄ nanospheres as aqueous supercapacitor electrode and bi-functional water splitting electrocatalyst in alkaline medium,” *Curr. Appl. Phys.*, vol. 27, pp. 73–88, Jul. 2021, doi: 10.1016/j.cap.2021.04.009.
- [47] N. Thongyong, S. Siriroj, J. Padchasri, N. Chanlek, S. Kheawhom, and P. Kidkhunthod, “Effect of recycled glass-V₂O₅ composite for stabilizing cathode

- capacity of lithium-ion batteries,” *Materialia*, vol. 35, p. 102132, Jun. 2024, doi: 10.1016/j.mtla.2024.102132.
- [48] K. Xu, X. Zhu, P. She, Y. Shang, H. Sun, and Z. Liu, “Macroscopic porous MnO₂ aerogels for supercapacitor electrodes,” *Inorg. Chem. Front.*, vol. 3, no. 8, pp. 1043–1047, 2016, doi: 10.1039/C6QI00110F.
- [49] Y. Huang *et al.*, “Enhanced Tolerance to Stretch-Induced Performance Degradation of Stretchable MnO₂-Based Supercapacitors,” *ACS Appl. Mater. Interfaces*, vol. 7, no. 4, pp. 2569–2574, Feb. 2015, doi: 10.1021/am507588p.
- [50] R. B. Rakhi, B. Ahmed, D. Anjum, and H. N. Alshareef, “Direct Chemical Synthesis of MnO₂ Nanowhiskers on Transition-Metal Carbide Surfaces for Supercapacitor Applications,” *ACS Appl. Mater. Interfaces*, vol. 8, no. 29, pp. 18806–18814, Jul. 2016, doi: 10.1021/acsami.6b04481.
- [51] M. Le Thai, G. T. Chandran, R. K. Dutta, X. Li, and R. M. Penner, “100k Cycles and Beyond: Extraordinary Cycle Stability for MnO₂ Nanowires Imparted by a Gel Electrolyte,” *ACS Energy Lett.*, vol. 1, no. 1, pp. 57–63, Jul. 2016, doi: 10.1021/acsenergylett.6b00029.
- [52] S. Nagamuthu, S. Vijayakumar, and G. Muralidharan, “Biopolymer-Assisted Synthesis of λ-MnO₂ Nanoparticles As an Electrode Material for Aqueous Symmetric Supercapacitor Devices,” *Ind. Eng. Chem. Res.*, vol. 52, no. 51, pp. 18262–18268, Dec. 2013, doi: 10.1021/ie402661p.
- [53] G. Godillot, P.-L. Taberna, B. Daffos, P. Simon, C. Delmas, and L. Guerlou-Demourgues, “High power density aqueous hybrid supercapacitor combining activated carbon and highly conductive spinel cobalt oxide,” *J. Power Sources*, vol. 331, pp. 277–284, Nov. 2016, doi: 10.1016/j.jpowsour.2016.09.035.
- [54] M. Z. Iqbal, J. Khan, H. T. A. Awan, M. Alzaid, A. M. Afzal, and S. Aftab, “Cobalt–manganese-zinc ternary phosphate for high performance supercapattery devices,” *Dalton Trans.*, vol. 49, no. 46, pp. 16715–16727, 2020, doi: 10.1039/D0DT03313H.
- [55] Y. Xu, L. Wang, P. Cao, C. Cai, Y. Fu, and X. Ma, “Mesoporous composite nickel cobalt oxide/graphene oxide synthesized via a template-assistant co-precipitation route as electrode material for supercapacitors,” *J. Power Sources*, vol. 306, pp. 742–752, Feb. 2016, doi: 10.1016/j.jpowsour.2015.12.106.

- [56] Y. Ding *et al.*, “Cellulose Tailored Anatase TiO₂ Nanospindles in Three-Dimensional Graphene Composites for High-Performance Supercapacitors,” *ACS Appl. Mater. Interfaces*, vol. 8, no. 19, pp. 12165–12175, May 2016, doi: 10.1021/acsami.6b02164.
- [57] C. Yu *et al.*, “Integration of mesoporous nickel cobalt oxide nanosheets with ultrathin layer carbon wrapped TiO₂ nanotube arrays for high-performance supercapacitors,” *New J. Chem.*, vol. 40, no. 8, pp. 6881–6889, 2016, doi: 10.1039/C6NJ00359A.
- [58] L. S. Aravinda, K. K. Nagaraja, H. S. Nagaraja, K. U. Bhat, and B. R. Bhat, “Fabrication and performance evaluation of hybrid supercapacitor electrodes based on carbon nanotubes and sputtered TiO₂,” *Nanotechnology*, vol. 27, no. 31, p. 314001, Aug. 2016, doi: 10.1088/0957-4484/27/31/314001.
- [59] K. K. Purushothaman, I. Manohara Babu, B. Sethuraman, and G. Muralidharan, “Nanosheet-Assembled NiO Microstructures for High-Performance Supercapacitors,” *ACS Appl. Mater. Interfaces*, vol. 5, no. 21, pp. 10767–10773, Nov. 2013, doi: 10.1021/am402869p.
- [60] S. Vijayakumar, S. Nagamuthu, and G. Muralidharan, “Supercapacitor Studies on NiO Nanoflakes Synthesized Through a Microwave Route,” *ACS Appl. Mater. Interfaces*, vol. 5, no. 6, pp. 2188–2196, Mar. 2013, doi: 10.1021/am400012h.
- [61] F. Cao, G. X. Pan, X. H. Xia, P. S. Tang, and H. F. Chen, “Synthesis of hierarchical porous NiO nanotube arrays for supercapacitor application,” *J. Power Sources*, vol. 264, pp. 161–167, Oct. 2014, doi: 10.1016/j.jpowsour.2014.04.103.
- [62] P. M. Kulal, D. P. Dubal, C. D. Lokhande, and V. J. Fulari, “Chemical synthesis of Fe₂O₃ thin films for supercapacitor application,” *J. Alloys Compd.*, vol. 509, no. 5, pp. 2567–2571, Feb. 2011, doi: 10.1016/j.jallcom.2010.11.091.
- [63] G. Binitha *et al.*, “Electrospun α -Fe₂O₃ nanostructures for supercapacitor applications,” *J. Mater. Chem. A*, vol. 1, no. 38, p. 11698, 2013, doi: 10.1039/c3ta12352a.
- [64] J. Huang *et al.*, “Fe₂O₃ sheets grown on nickel foam as electrode material for electrochemical capacitors,” *J. Electroanal. Chem.*, vol. 713, pp. 98–102, Jan. 2014, doi: 10.1016/j.jelechem.2013.12.009.

- [65] B. Sethuraman, K. K. Purushothaman, and G. Muralidharan, "Synthesis of mesh-like $\text{Fe}_2\text{O}_3/\text{C}$ nanocomposite via greener route for high performance supercapacitors," *RSC Adv*, vol. 4, no. 9, pp. 4631–4637, 2014, doi: 10.1039/C3RA45025B.
- [66] Z. Lu, Z. Chang, W. Zhu, and X. Sun, "Beta-phased $\text{Ni}(\text{OH})_2$ nanowall film with reversible capacitance higher than theoretical Faradic capacitance," *Chem. Commun.*, vol. 47, no. 34, p. 9651, 2011, doi: 10.1039/c1cc13796d.
- [67] M. Aghazadeh, A. N. Golikand, and M. Ghaemi, "Synthesis, characterization, and electrochemical properties of ultrafine $\beta\text{-Ni}(\text{OH})_2$ nanoparticles," *Int. J. Hydrog. Energy*, vol. 36, no. 14, pp. 8674–8679, Jul. 2011, doi: 10.1016/j.ijhydene.2011.03.144.
- [68] T. Xue and J.-M. Lee, "Capacitive behavior of mesoporous $\text{Co}(\text{OH})_2$ nanowires," *J. Power Sources*, vol. 245, pp. 194–202, Jan. 2014, doi: 10.1016/j.jpowsour.2013.06.135.
- [69] J. Tang, D. Liu, Y. Zheng, X. Li, X. Wang, and D. He, "Effect of Zn-substitution on cycling performance of $\alpha\text{-Co}(\text{OH})_2$ nanosheet electrode for supercapacitors," *J. Mater. Chem. A*, vol. 2, no. 8, p. 2585, 2014, doi: 10.1039/c3ta14042c.
- [70] Y. Wang *et al.*, "Recent progress in carbon-based materials for supercapacitor electrodes: a review," *J. Mater. Sci.*, vol. 56, no. 1, pp. 173–200, Jan. 2021, doi: 10.1007/s10853-020-05157-6.
- [71] F. Béguin, V. Presser, A. Balducci, and E. Frackowiak, "Carbons and Electrolytes for Advanced Supercapacitors," *Adv. Mater.*, vol. 26, no. 14, pp. 2219–2251, Apr. 2014, doi: 10.1002/adma.201304137.
- [72] Q. Qu *et al.*, "Electrochemical Performance of MnO_2 Nanorods in Neutral Aqueous Electrolytes as a Cathode for Asymmetric Supercapacitors," *J. Phys. Chem. C*, vol. 113, no. 31, pp. 14020–14027, Aug. 2009, doi: 10.1021/jp8113094.
- [73] C. A. C. Sequeira and D. M. F. Santos, "Electrochemical routes for industrial synthesis," *J. Braz. Chem. Soc.*, vol. 20, no. 3, pp. 387–406, 2009, doi: 10.1590/S0103-50532009000300002.
- [74] V. L. Patil, S. A. Vanalakar, P. S. Patil, and J. H. Kim, "Fabrication of nanostructured ZnO thin films based NO_2 gas sensor via SILAR technique," *Sens. Actuators B Chem.*, vol. 239, pp. 1185–1193, Feb. 2017, doi: 10.1016/j.snb.2016.08.130.
- [75] Y. Luo, C. Zhang, B. Zheng, X. Geng, and M. Debligny, "Hydrogen sensors based on noble metal doped metal-oxide semiconductor: A review," *Int. J. Hydrog. Energy*, vol. 42, no. 31, pp. 20386–20397, Aug. 2017, doi: 10.1016/j.ijhydene.2017.06.066.

- [76] W. L. Suchanek, J. M. Garcés, P. F. Fulvio, and M. Jaroniec, “Hydrothermal Synthesis and Surface Characteristics of Novel Alpha Alumina Nanosheets with Controlled Chemical Composition,” *Chem. Mater.*, vol. 22, no. 24, pp. 6564–6574, Dec. 2010, doi: 10.1021/cm102158w.
- [77] R. Varma and D. R. Varma, “The Bhopal Disaster of 1984,” *Bull. Sci. Technol. Soc.*, vol. 25, no. 1, pp. 37–45, Feb. 2005, doi: 10.1177/0270467604273822.
- [78] H. Ji, W. Zeng, and Y. Li, “Gas sensing mechanisms of metal oxide semiconductors: a focus review,” *Nanoscale*, vol. 11, no. 47, pp. 22664–22684, 2019, doi: 10.1039/C9NR07699A.
- [79] S. Sharma and M. Madou, “A new approach to gas sensing with nanotechnology,” *Philos. Trans. R. Soc. Math. Phys. Eng. Sci.*, vol. 370, no. 1967, Art. no. 1967, May 2012, doi: 10.1098/rsta.2011.0506.
- [80] M. S. B. De Castro, C. L. Ferreira, and R. R. De Aveliz, “Vanadium oxide thin films produced by magnetron sputtering from a V₂O₅ target at room temperature,” *Infrared Phys. Technol.*, vol. 60, pp. 103–107, Sep. 2013, doi: 10.1016/j.infrared.2013.03.001.
- [81] W. Yan, M. Hu, D. Wang, and C. Li, “Room temperature gas sensing properties of porous silicon/V₂O₅ nanorods composite,” *Appl. Surf. Sci.*, vol. 346, pp. 216–222, Aug. 2015, doi: 10.1016/j.apsusc.2015.01.020.
- [82] L. Francioso, A. Taurino, A. Forleo, and P. Siciliano, “TiO₂ nanowires array fabrication and gas sensing properties,” *Sens. Actuators B Chem.*, vol. 130, no. 1, Art. no. 1, Mar. 2008, doi: 10.1016/j.snb.2007.07.074.
- [83] F. Gyger, M. Hübner, C. Feldmann, N. Barsan, and U. Weimar, “Nanoscale SnO₂ Hollow Spheres and Their Application as a Gas-Sensing Material,” *Chem. Mater.*, vol. 22, no. 16, Art. no. 16, Aug. 2010, doi: 10.1021/cm1011235.
- [84] M. S. Patil *et al.*, “Gas Sensing Properties of Hydrothermally Synthesized Button Rose-Like WO₃ Thin Films,” *J. Electron. Mater.*, vol. 48, no. 1, Art. no. 1, Jan. 2019, doi: 10.1007/s11664-018-6756-x.
- [85] J. Huotari, R. Bjorklund, J. Lappalainen, and A. Lloyd Spetz, “Pulsed Laser Deposited Nanostructured Vanadium Oxide Thin Films Characterized as Ammonia Sensors,” *Sens. Actuators B Chem.*, vol. 217, pp. 22–29, Oct. 2015, doi: 10.1016/j.snb.2015.02.089.

- [86] V. L. Patil *et al.*, “Gas sensing properties of 3D mesoporous nanostructured ZnO thin films,” *New J. Chem.*, vol. 42, no. 16, Art. no. 16, 2018, doi: 10.1039/C8NJ01242C.
- [87] S. Islam *et al.*, “Recent Advancements in Electrochemical Deposition of Metal-Based Electrode Materials for Electrochemical Supercapacitors,” *Chem. Rec.*, vol. 22, no. 7, p. e202200013, Jul. 2022, doi: 10.1002/tcr.202200013.
- [88] J. W. Ross, J. H. Riseman, and J. A. Krueger, “POTENTIOMETRIC GAS SENSING ELECTRODES,” in *International Symposium on Selective Ion-Sensitive Electrodes*, Elsevier, 1973, pp. 473–487. doi: 10.1016/B978-0-408-70562-2.50008-7.
- [89] Z. Luo, Q. Tang, S. Su, and J. Hu, “A high-performance structure for the bulk acoustic wave metal oxide semiconductor gas sensor,” *Smart Mater. Struct.*, vol. 28, no. 10, p. 105015, Oct. 2019, doi: 10.1088/1361-665X/ab360c.
- [90] Z. Li *et al.*, “Advances in designs and mechanisms of semiconducting metal oxide nanostructures for high-precision gas sensors operated at room temperature,” *Mater. Horiz.*, vol. 6, no. 3, Art. no. 3, 2019, doi: 10.1039/C8MH01365A.
- [91] T. Becker, S. Ahlers, C. Bosch-v.Braunmühl, G. Müller, and O. Kiesewetter, “Gas sensing properties of thin- and thick-film tin-oxide materials,” *Sens. Actuators B Chem.*, vol. 77, no. 1–2, Art. no. 1–2, Jun. 2001, doi: 10.1016/S0925-4005(01)00672-4.
- [92] V. Mounasamy, G. K. Mani, and S. Madanagurusamy, “Vanadium oxide nanostructures for chemiresistive gas and vapour sensing: a review on state of the art,” *Microchim. Acta*, vol. 187, no. 4, Art. no. 4, Apr. 2020, doi: 10.1007/s00604-020-4182-2.
- [93] S. T. Shishiyanu, T. S. Shishiyanu, and O. I. Lupan, “Sensing characteristics of tin-doped ZnO thin films as NO₂ gas sensor,” *Sens. Actuators B Chem.*, vol. 107, no. 1, Art. no. 1, May 2005, doi: 10.1016/j.snb.2004.10.030.
- [94] M. A. Basyooni, S. E. Zaki, S. Ertugrul, M. Yilmaz, and Y. R. Eker, “Fast response of CO₂ room temperature gas sensor based on Mixed-Valence Phases in Molybdenum and Tungsten Oxide nanostructured thin films,” *Ceram. Int.*, vol. 46, no. 7, Art. no. 7, May 2020, doi: 10.1016/j.ceramint.2019.12.259.
- [95] H. Zhang *et al.*, “A cost-effective method to fabricate VO₂ (M) nanoparticles and films with excellent thermochromic properties,” *J. Alloys Compd.*, vol. 636, pp. 106–112, Jul. 2015, doi: 10.1016/j.jallcom.2015.01.277.

- [96] X. Liu, G. Xie, C. Huang, Q. Xu, Y. Zhang, and Y. Luo, "A facile method for preparing VO₂ nanobelts," *Mater. Lett.*, vol. 62, no. 12–13, Art. no. 12–13, Apr. 2008, doi: 10.1016/j.matlet.2007.10.022.
- [97] X. Wu, X. Weng, L. Yuan, J. Zhang, L. Qi, and B. Wei, "Phase- and shape-controlled synthesis of VO₂ by a hydrothermal-calcination method," *Vacuum*, vol. 176, p. 109352, Jun. 2020, doi: 10.1016/j.vacuum.2020.109352.
- [98] O. Karahan, A. Tufani, S. Unal, I. B. Misirlioglu, Y. Z. Menciloglu, and K. Sendur, "Synthesis and Morphological Control of VO₂ Nanostructures via a One-Step Hydrothermal Method," *Nanomaterials*, vol. 11, no. 3, Art. no. 3, Mar. 2021, doi: 10.3390/nano11030752.
- [99] Y. Chen *et al.*, "Synthesis, characterization and electromagnetic absorbing performance of multi-step petaloid morphology VO₂(M)," *Ceram. Int.*, vol. 46, no. 16, Art. no. 16, Nov. 2020, doi: 10.1016/j.ceramint.2020.07.020.
- [100] M. Li, S. Magdassi, Y. Gao, and Y. Long, "Hydrothermal Synthesis of VO₂ Polymorphs: Advantages, Challenges and Prospects for the Application of Energy Efficient Smart Windows," *Small*, vol. 13, no. 36, Art. no. 36, Sep. 2017, doi: 10.1002/smll.201701147.
- [101] C. Wang *et al.*, "Preparation of VO₂ (M) nanoparticles with exemplary optical performance from VO₂ (B) nanobelts by Ball Milling," *J. Alloys Compd.*, vol. 877, p. 159888, Oct. 2021, doi: 10.1016/j.jallcom.2021.159888.
- [102] S. R. Popuri, M. Miclau, A. Artemenko, C. Labrugere, A. Villesuzanne, and M. Pollet, "Rapid Hydrothermal Synthesis of VO₂ (B) and Its Conversion to Thermochromic VO₂ (M1)," *Inorg. Chem.*, vol. 52, no. 9, Art. no. 9, May 2013, doi: 10.1021/ic301201k.
- [103] S. Wang, C. Li, S. Tian, B. Liu, and X. Zhao, "Facile synthesis of VO₂ (D) and its transformation to VO₂(M) with enhanced thermochromic properties for smart windows," *Ceram. Int.*, vol. 46, no. 10, Art. no. 10, Jul. 2020, doi: 10.1016/j.ceramint.2020.02.278.
- [104] H. Zhu, Z. Zhang, and X. Jiang, "Glycothermal Synthesis of VO₂ (B) Nanoparticles for Gas Sensing Application," *J. Nanosci. Nanotechnol.*, vol. 20, no. 3, Art. no. 3, Mar. 2020, doi: 10.1166/jnn.2020.17167.

- [105] A. Simo, K. Kaviyarasu, B. Mwakikunga, M. Mokwena, and M. Maaza, "Room temperature volatile organic compound gas sensor based on vanadium oxide 1-dimension nanoparticles," *Ceram. Int.*, vol. 43, no. 1, Art. no. 1, Jan. 2017, doi: 10.1016/j.ceramint.2016.10.091.
- [106] J. Pan, L. Zhong, M. Li, Y. Luo, and G. Li, "Microwave-Assisted Solvothermal Synthesis of VO₂ Hollow Spheres and Their Conversion into V₂O₅ Hollow Spheres with Improved Lithium Storage Capability," *Chem. – Eur. J.*, vol. 22, no. 4, Art. no. 4, Jan. 2016, doi: 10.1002/chem.201504259.
- [107] A. Simo, B. Mwakikunga, B. T. Sone, B. Julies, R. Madjoe, and M. Maaza, "VO₂ nanostructures based chemiresistors for low power energy consumption hydrogen sensing," *Int. J. Hydrog. Energy*, vol. 39, no. 15, Art. no. 15, May 2014, doi: 10.1016/j.ijhydene.2014.03.037.
- [108] J. Liang, W. Wu, Q. Lou, K. Wang, and C. Xuan, "Room temperature NO₂ sensing performance of Ag nanoparticles modified VO₂ nanorods," *J. Alloys Compd.*, vol. 890, p. 161837, Jan. 2022, doi: 10.1016/j.jallcom.2021.161837.
- [109] G. T. Chandrappa, N. Steunou, S. Cassaignon, C. Bauvais, and J. Livage, "Hydrothermal synthesis of vanadium oxide nanotubes from V₂O₅ gels," *Catal. Today*, vol. 78, no. 1–4, Art. no. 1–4, Feb. 2003, doi: 10.1016/S0920-5861(02)00298-5.
- [110] S. Kamila, B. Chakraborty, S. Basu, and B. K. Jena, "Combined Experimental and Theoretical Insights into Energy Storage Applications of a VO₂ (D)–Graphene Hybrid," *J. Phys. Chem. C*, vol. 123, no. 39, Art. no. 39, Oct. 2019, doi: 10.1021/acs.jpcc.9b03563.
- [111] W. G. Menezes *et al.*, "V₂O₅ nanoparticles obtained from a synthetic bariandite-like vanadium oxide: Synthesis, characterization and electrochemical behavior in an ionic liquid," *J. Colloid Interface Sci.*, vol. 337, no. 2, pp. 586–593, Sep. 2009, doi: 10.1016/j.jcis.2009.05.050.
- [112] Z. Zhang, Y. V. Kaneti, X. Jiang, and A. Yu, "Hydrothermal synthesis of sodium vanadium oxide nanorods for gas sensing application," *Sens. Actuators B Chem.*, vol. 202, pp. 803–809, Oct. 2014, doi: 10.1016/j.snb.2014.05.064.
- [113] J. Chu *et al.*, "Hydrothermal synthesis of vanadium oxide nanorods and their electrochromic performance," *Mater. Lett.*, vol. 166, pp. 179–182, Mar. 2016, doi: 10.1016/j.matlet.2015.12.067.

- [114] M. Li *et al.*, “Synthesis and electrochemical performance of V₂O₅ nanosheets for supercapacitor,” *AIP Adv.*, vol. 12, no. 5, Art. no. 5, May 2022, doi: 10.1063/5.0086344.
- [115] S. Sutrave *et al.*, “A simple solution combustion method for the synthesis of V₂O₅ nanostructures for supercapacitor applications,” *Appl. Surf. Sci. Adv.*, vol. 12, p. 100331, Dec. 2022, doi: 10.1016/j.apsadv.2022.100331.
- [116] N. Shah, H. Nawaz, S. M. Abbas, A. Khesro, and K. Ullah, “Enhanced electrochemical properties of (V₂O₅/GO) composite electrodes for high-performance supercapacitor applications,” *J. Mater. Res.*, vol. 38, no. 7, Art. no. 7, Apr. 2023, doi: 10.1557/s43578-023-00936-8.
- [117] S. N. Chanu, P. S. Devi, and B. P. Swain, “Photoluminescence, phonon vibrations and structural properties of electrospun V₂O₅/rGO/PCL nanofibers and their application for supercapacitor electrode material,” *Inorg. Chem. Commun.*, vol. 155, p. 110978, Sep. 2023, doi: 10.1016/j.inoche.2023.110978.
- [118] S. Gupta, B. Aberg, and S. B. Carrizosa, “Hydrothermal Synthesis of Vanadium Pentoxides–Reduced Graphene Oxide Composite Electrodes for Enhanced Electrochemical Energy Storage,” *MRS Adv.*, vol. 1, no. 45, Art. no. 45, Sep. 2016, doi: 10.1557/adv.2016.480.
- [119] B. Hu *et al.*, “In Situ Constructing Flexible V₂O₅@GO Composite Thin Film Electrode for Superior Electrochemical Energy Storage,” *J. Electrochem. Soc.*, vol. 165, no. 16, Art. no. 16, 2018, doi: 10.1149/2.0341816jes.
- [120] T. B. Naveen, D. Durgalakshmi, J. Mohanraj, A. K. Kunhiraman, S. Balakumar, and R. A. Rakkesh, “Insights on the electrochemical properties of lattice strain induced layered V₂O₃–Al₂O₃ nanocomposites derived from the carbonization process,” *J. Mater. Sci. Mater. Electron.*, vol. 34, no. 22, Art. no. 22, Aug. 2023, doi: 10.1007/s10854-023-11082-6.
- [121] Q. T. Qu *et al.*, “V₂O₅·0.6H₂O nanoribbons as cathode material for asymmetric supercapacitor in K₂SO₄ solution,” *Electrochem. Commun.*, vol. 11, no. 6, Art. no. 6, Jun. 2009, doi: 10.1016/j.elecom.2009.05.003.
- [122] G. Wee, H. Z. Soh, Y. L. Cheah, S. G. Mhaisalkar, and M. Srinivasan, “Synthesis and electrochemical properties of electrospun V₂O₅ nanofibers as supercapacitor electrodes,” *J. Mater. Chem.*, vol. 20, no. 32, Art. no. 32, 2010, doi: 10.1039/c0jm00059k.

- [123] L.-M. Chen, Q.-Y. Lai, Y.-J. Hao, Y. Zhao, and X.-Y. Ji, "Investigations on capacitive properties of the AC/V₂O₅ hybrid supercapacitor in various aqueous electrolytes," *J. Alloys Compd.*, vol. 467, no. 1–2, Art. no. 1–2, Jan. 2009, doi: 10.1016/j.jallcom.2007.12.017.
- [124] B. Wang, K. Konstantinov, D. Wexler, H. Liu, and G. Wang, "Synthesis of nanosized vanadium pentoxide/carbon composites by spray pyrolysis for electrochemical capacitor application," *Electrochimica Acta*, vol. 54, no. 5, Art. no. 5, Feb. 2009, doi: 10.1016/j.electacta.2008.09.028.
- [125] S. D. Perera, B. Patel, J. Bonso, M. Grunewald, J. P. Ferraris, and K. J. Balkus, "Vanadium Oxide Nanotube Spherical Clusters Prepared on Carbon Fabrics for Energy Storage Applications," *ACS Appl. Mater. Interfaces*, vol. 3, no. 11, Art. no. 11, Nov. 2011, doi: 10.1021/am2011965.
- [126] B.-H. Kim, K. S. Yang, and D. J. Yang, "Electrochemical behavior of activated carbon nanofiber-vanadium pentoxide composites for double-layer capacitors," *Electrochimica Acta*, vol. 109, pp. 859–865, Oct. 2013, doi: 10.1016/j.electacta.2013.07.180.
- [127] B.-H. Kim, C. H. Kim, K. S. Yang, A. Rahy, and D. J. Yang, "Electrospun vanadium pentoxide/carbon nanofiber composites for supercapacitor electrodes," *Electrochimica Acta*, vol. 83, pp. 335–340, Nov. 2012, doi: 10.1016/j.electacta.2012.07.093.
- [128] Z. Chen *et al.*, "Design and Synthesis of Hierarchical Nanowire Composites for Electrochemical Energy Storage," *Adv. Funct. Mater.*, vol. 19, no. 21, Art. no. 21, Nov. 2009, doi: 10.1002/adfm.200900971.
- [129] Y. Yang, D. Kim, M. Yang, and P. Schmuki, "Vertically aligned mixed V₂O₅–TiO₂ nanotube arrays for supercapacitor applications," *Chem. Commun.*, vol. 47, no. 27, Art. no. 27, 2011, doi: 10.1039/c1cc11811k.
- [130] M. Jayalakshmi, M. M. Rao, N. Venugopal, and K.-B. Kim, "Hydrothermal synthesis of SnO₂–V₂O₅ mixed oxide and electrochemical screening of carbon nanotubes (CNT), V₂O₅, V₂O₅–CNT, and SnO₂–V₂O₅–CNT electrodes for supercapacitor applications," *J. Power Sources*, vol. 166, no. 2, Art. no. 2, Apr. 2007, doi: 10.1016/j.jpowsour.2006.11.025.
- [131] L. Hao, J. Wang, L. Shen, J. Zhu, B. Ding, and X. Zhang, "Synthesis and electrochemical performances of mixed-valence vanadium oxide/ordered mesoporous

- carbon composites for supercapacitors,” *RSC Adv.*, vol. 6, no. 30, Art. no. 30, 2016, doi: 10.1039/C5RA22520E.
- [132] I. Shakir *et al.*, “Ultra-thin and uniform coating of vanadium oxide on multiwall carbon nanotubes through solution based approach for high-performance electrochemical supercapacitors,” *Electrochimica Acta*, vol. 111, pp. 400–404, Nov. 2013, doi: 10.1016/j.electacta.2013.07.156.
- [133] S. D. Perera, A. D. Liyanage, N. Nijem, J. P. Ferraris, Y. J. Chabal, and K. J. Balkus, “Vanadium oxide nanowire – Graphene binder free nanocomposite paper electrodes for supercapacitors: A facile green approach,” *J. Power Sources*, vol. 230, pp. 130–137, May 2013, doi: 10.1016/j.jpowsour.2012.11.118.
- [134] H. Zhao, L. Pan, S. Xing, J. Luo, and J. Xu, “Vanadium oxides–reduced graphene oxide composite for lithium-ion batteries and supercapacitors with improved electrochemical performance,” *J. Power Sources*, vol. 222, pp. 21–31, Jan. 2013, doi: 10.1016/j.jpowsour.2012.08.036.
- [135] X.-B. Li, S.-Y. Xie, H. Zheng, W. Q. Tian, and H.-B. Sun, “Boron based two-dimensional crystals: theoretical design, realization proposal and applications,” *Nanoscale*, vol. 7, no. 45, Art. no. 45, 2015, doi: 10.1039/C5NR04359J.
- [136] M. Li, G. Sun, P. Yin, C. Ruan, and K. Ai, “Controlling the Formation of Rodlike V_2O_5 Nanocrystals on Reduced Graphene Oxide for High-Performance Supercapacitors,” *ACS Appl. Mater. Interfaces*, vol. 5, no. 21, Art. no. 21, Nov. 2013, doi: 10.1021/am403739g.
- [137] Q. Qu, Y. Zhu, X. Gao, and Y. Wu, “Core–Shell Structure of Polypyrrole Grown on V_2O_5 Nanoribbon as High Performance Anode Material for Supercapacitors,” *Adv. Energy Mater.*, vol. 2, no. 8, Art. no. 8, Aug. 2012, doi: 10.1002/aenm.201200088.
- [138] M.-H. Bai, L.-J. Bian, Y. Song, and X.-X. Liu, “Electrochemical Codeposition of Vanadium Oxide and Polypyrrole for High-Performance Supercapacitor with High Working Voltage,” *ACS Appl. Mater. Interfaces*, vol. 6, no. 15, Art. no. 15, Aug. 2014, doi: 10.1021/am502630g.
- [139] J. Yang, T. Lan, J. Liu, Y. Song, and M. Wei, “Supercapacitor electrode of hollow spherical V_2O_5 with a high pseudocapacitance in aqueous solution,” *Electrochimica Acta*, vol. 105, pp. 489–495, Aug. 2013, doi: 10.1016/j.electacta.2013.05.023.

- [140] K. Jeyalakshmi, S. Vijayakumar, K. K. Purushothaman, and G. Muralidharan, "Nanostructured nickel doped β -V₂O₅ thin films for supercapacitor applications," *Mater. Res. Bull.*, vol. 48, no. 7, Art. no. 7, Jul. 2013, doi: 10.1016/j.materresbull.2013.03.007.
- [141] Yiyang Wei, Jianguo Zhu, and Guoxiu Wang, "High-Specific-Capacitance Supercapacitor Based on Vanadium Oxide Nanoribbon," *IEEE Trans. Appl. Supercond.*, vol. 24, no. 5, Art. no. 5, Oct. 2014, doi: 10.1109/TASC.2014.2340453.
- [142] L. Cao *et al.*, "Ultrathin single-crystalline vanadium pentoxide nanoribbon constructed 3D networks for superior energy storage," *J Mater Chem A*, vol. 2, no. 32, Art. no. 32, 2014, doi: 10.1039/C4TA02229G.
- [143] J. Zhu *et al.*, "Building 3D Structures of Vanadium Pentoxide Nanosheets and Application as Electrodes in Supercapacitors," *Nano Lett.*, vol. 13, no. 11, Art. no. 11, Nov. 2013, doi: 10.1021/nl402969r.
- [144] Y. Wu, G. Gao, and G. Wu, "Self-assembled three-dimensional hierarchical porous V₂O₅/graphene hybrid aerogels for supercapacitors with high energy density and long cycle life," *J. Mater. Chem. A*, vol. 3, no. 5, Art. no. 5, 2015, doi: 10.1039/C4TA05537C.
- [145] X. Wu, Y. Tao, L. Dong, and J. Hong, "Synthesis and characterization of self-assembling (NH₄)_{0.5}V₂O₅ nanowires," *J. Mater. Chem.*, vol. 14, no. 5, Art. no. 5, 2004, doi: 10.1039/b314775d.
- [146] H. Qiao, X. Zhu, Z. Zheng, L. Liu, and L. Zhang, "Synthesis of V₃O₇·H₂O nanobelts as cathode materials for lithium-ion batteries," *Electrochem. Commun.*, vol. 8, no. 1, Art. no. 1, Jan. 2006, doi: 10.1016/j.elecom.2005.10.021.
- [147] Z. Peng, W. Jiang, and H. Liu, "Synthesis and Electrical Properties of Tungsten-Doped Vanadium Dioxide Nanopowders by Thermolysis," *J. Phys. Chem. C*, vol. 111, no. 3, Art. no. 3, Jan. 2007, doi: 10.1021/jp066342u.
- [148] S. Gao, Z. Chen, M. Wei, K. Wei, and H. Zhou, "Single crystal nanobelts of V₃O₇·H₂O: A lithium intercalation host with a large capacity," *Electrochimica Acta*, vol. 54, no. 3, Art. no. 3, Jan. 2009, doi: 10.1016/j.electacta.2008.08.043.
- [149] T. Zhai *et al.*, "Centimeter-Long V₂O₅ Nanowires: From Synthesis to Field-Emission, Electrochemical, Electrical Transport, and Photoconductive Properties," *Adv. Mater.*, vol. 22, no. 23, Art. no. 23, Jun. 2010, doi: 10.1002/adma.200903586.

- [150] L. Mai *et al.*, “Electrospun Ultralong Hierarchical Vanadium Oxide Nanowires with High Performance for Lithium Ion Batteries,” *Nano Lett.*, vol. 10, no. 11, Art. no. 11, Nov. 2010, doi: 10.1021/nl103343w.
- [151] Y. Zhang *et al.*, “Hydrothermal synthesis, characterization, formation mechanism and electrochemical property of $V_3O_7 \cdot H_2O$ single-crystal nanobelts,” *Mater. Sci. Eng. B*, vol. 175, no. 2, Art. no. 2, Nov. 2010, doi: 10.1016/j.mseb.2010.07.023.
- [152] M. Li, F. Kong, H. Wang, and G. Li, “Synthesis of vanadium pentoxide (V_2O_5) ultralong nanobelts via an oriented attachment growth mechanism,” *CrystEngComm*, vol. 13, no. 17, Art. no. 17, 2011, doi: 10.1039/c1ce05477e.
- [153] Y. Zhang *et al.*, “Improvement of the electrochemical properties of $V_3O_7 \cdot H_2O$ nanobelts for Li battery application through synthesis of $V_3O_7 @ C$ core-shell nanostructured composites,” *Curr. Appl. Phys.*, vol. 11, no. 5, pp. 1159–1163, Sep. 2011, doi: 10.1016/j.cap.2011.02.010.
- [154] Y. Zhang *et al.*, “Controlled synthesis and electrochemical properties of vanadium oxides with different nanostructures,” *Bull. Mater. Sci.*, vol. 35, no. 3, Art. no. 3, Jun. 2012, doi: 10.1007/s12034-012-0311-9.
- [155] J. Shao, X. Li, Q. Qu, and H. Zheng, “One-step hydrothermal synthesis of hexangular starfruit-like vanadium oxide for high power aqueous supercapacitors,” *J. Power Sources*, vol. 219, pp. 253–257, Dec. 2012, doi: 10.1016/j.jpowsour.2012.07.045.
- [156] Y. Zhang *et al.*, “Facile hydrothermal synthesis of vanadium oxides nanobelts by ethanol reduction of peroxovanadium complexes,” *Ceram. Int.*, vol. 39, no. 1, Art. no. 1, Jan. 2013, doi: 10.1016/j.ceramint.2012.06.001.
- [157] M. Shahid, J. Liu, Z. Ali, I. Shakir, and M. F. Warsi, “Structural and electrochemical properties of single crystalline MoV_2O_8 nanowires for energy storage devices,” *J. Power Sources*, vol. 230, pp. 277–281, May 2013, doi: 10.1016/j.jpowsour.2012.12.033.
- [158] Y. Tang *et al.*, “Vanadium pentoxide cathode materials for high-performance lithium-ion batteries enabled by a hierarchical nanoflower structure via an electrochemical process,” *J Mater Chem A*, vol. 1, no. 1, Art. no. 1, 2013, doi: 10.1039/C2TA00351A.
- [159] Y. Sun *et al.*, “A composite film of reduced graphene oxide modified vanadium oxide nanoribbons as a free standing cathode material for rechargeable lithium

- batteries,” *J. Power Sources*, vol. 241, pp. 168–172, Nov. 2013, doi: 10.1016/j.jpowsour.2013.04.093.
- [160] I. Mjejri, N. Etteyeb, and F. Sediri, “Hydrothermal synthesis of mesoporous rod-like nanocrystalline vanadium oxide hydrate $V_3O_7 \cdot H_2O$ from hydroquinone and V_2O_5 ,” *Mater. Res. Bull.*, vol. 48, no. 9, Art. no. 9, Sep. 2013, doi: 10.1016/j.materresbull.2013.05.051.
- [161] F. K. Butt *et al.*, “Synthesis of Novel ZnV_2O_4 Hierarchical Nanospheres and Their Applications as Electrochemical Supercapacitor and Hydrogen Storage Material,” *ACS Appl. Mater. Interfaces*, vol. 6, no. 16, Art. no. 16, Aug. 2014, doi: 10.1021/am503136h.
- [162] C. Cheng, A. Amini, C. Zhu, Z. Xu, H. Song, and N. Wang, “Enhanced photocatalytic performance of TiO_2 - ZnO hybrid nanostructures,” *Sci. Rep.*, vol. 4, no. 1, Art. no. 1, Feb. 2014, doi: 10.1038/srep04181.
- [163] M. Qin *et al.*, “Template-free synthesis of vanadium oxides nanobelt arrays as high-rate cathode materials for lithium ion batteries,” *J. Power Sources*, vol. 268, pp. 700–705, Dec. 2014, doi: 10.1016/j.jpowsour.2014.06.103.
- [164] C. Zhu, J. Shu, X. Wu, P. Li, and X. Li, “Electrospun V_2O_5 micro/nanorods as cathode materials for lithium ion battery,” *J. Electroanal. Chem.*, vol. 759, pp. 184–189, Dec. 2015, doi: 10.1016/j.jelechem.2015.11.013.
- [165] S. Ni, J. Ma, J. Zhang, X. Yang, and L. Zhang, “Electrochemical performance of cobalt vanadium oxide/natural graphite as anode for lithium ion batteries,” *J. Power Sources*, vol. 282, pp. 65–69, May 2015, doi: 10.1016/j.jpowsour.2015.01.187.
- [166] Q. An *et al.*, “Graphene decorated vanadium oxide nanowire aerogel for long-cycle-life magnesium battery cathodes,” *Nano Energy*, vol. 18, pp. 265–272, Nov. 2015, doi: 10.1016/j.nanoen.2015.10.029.
- [167] M. Chiku, H. Takeda, S. Matsumura, E. Higuchi, and H. Inoue, “Amorphous Vanadium Oxide/Carbon Composite Positive Electrode for Rechargeable Aluminum Battery,” *ACS Appl. Mater. Interfaces*, vol. 7, no. 44, Art. no. 44, Nov. 2015, doi: 10.1021/acsami.5b06420.
- [168] X. Wang *et al.*, “Self-Assembled Sandwich-like Vanadium Oxide/Graphene Mesoporous Composite as High-Capacity Anode Material for Lithium Ion Batteries,” *Inorg. Chem.*, vol. 54, no. 24, Art. no. 24, Dec. 2015, doi: 10.1021/acs.inorgchem.5b01914.

- [169] Y. Li *et al.*, “Synthesis and electrochemical performance of lithium vanadium phosphate and lithium vanadium oxide composite cathode material for lithium ion batteries,” *J. Power Sources*, vol. 282, pp. 100–108, May 2015, doi: 10.1016/j.jpowsour.2015.02.051.
- [170] H. Song, C. Zhang, Y. Liu, C. Liu, X. Nan, and G. Cao, “Facile synthesis of mesoporous V₂O₅ nanosheets with superior rate capability and excellent cycling stability for lithium ion batteries,” *J. Power Sources*, vol. 294, pp. 1–7, Oct. 2015, doi: 10.1016/j.jpowsour.2015.06.055.
- [171] Y. Su *et al.*, “Template-assisted formation of porous vanadium oxide as high performance cathode materials for lithium ion batteries,” *J. Power Sources*, vol. 295, pp. 254–258, Nov. 2015, doi: 10.1016/j.jpowsour.2015.06.137.
- [172] D.-H. Wei *et al.*, “Tuning Surface Plasmonic Resonance and Surface Wettability of Au/CrN Films Using Nitrogen-Containing Gas,” *Nanomaterials*, vol. 12, no. 15, Art. no. 15, Jul. 2022, doi: 10.3390/nano12152575.
- [173] E. Umeshbabu and G. Ranga Rao, “Vanadium pentoxide nanochains for high-performance electrochemical supercapacitors,” *J. Colloid Interface Sci.*, vol. 472, pp. 210–219, Jun. 2016, doi: 10.1016/j.jcis.2016.03.050.
- [174] Z. Li, G. Liu, M. Guo, L.-X. Ding, S. Wang, and H. Wang, “Electrospun porous vanadium pentoxide nanotubes as a high-performance cathode material for lithium-ion batteries,” *Electrochimica Acta*, vol. 173, pp. 131–138, Aug. 2015, doi: 10.1016/j.electacta.2015.05.057.
- [175] B. M. Babar *et al.*, “V₂O₅-rGO based chemiresistive gas sensor for NO₂ detection,” *Mater. Sci. Eng. B*, vol. 298, p. 116827, Dec. 2023, doi: 10.1016/j.mseb.2023.116827.
- [176] Z.-K. Wang *et al.*, “Graphene-nanosheet-wrapped LiV₃O₈ nanocomposites as high performance cathode materials for rechargeable lithium-ion batteries,” *J. Power Sources*, vol. 307, pp. 426–434, Mar. 2016, doi: 10.1016/j.jpowsour.2016.01.005.
- [177] K. Tang *et al.*, “Self-reduced VO/VO_x/carbon nanofiber composite as binder-free electrode for supercapacitors,” *Electrochimica Acta*, vol. 209, pp. 709–718, Aug. 2016, doi: 10.1016/j.electacta.2016.05.051.
- [178] Q. Wang *et al.*, “High-performance supercapacitor based on V₂O₅/carbon nanotubes-super activated carbon ternary composite,” *Ceram. Int.*, vol. 42, no. 10, Art. no. 10, Aug. 2016, doi: 10.1016/j.ceramint.2016.04.145.

- [179] G. P. Pandey *et al.*, “Mesoporous Hybrids of Reduced Graphene Oxide and Vanadium Pentoxide for Enhanced Performance in Lithium-Ion Batteries and Electrochemical Capacitors,” *ACS Appl. Mater. Interfaces*, vol. 8, no. 14, Art. no. 14, Apr. 2016, doi: 10.1021/acsami.6b02372.
- [180] Y. Zhang and Y. Huang, “Facile synthesis and characterization of rough surface V_2O_5 nanomaterials for pseudo-supercapacitor electrode material with high capacitance,” *Bull. Mater. Sci.*, vol. 40, no. 6, Art. no. 6, Oct. 2017, doi: 10.1007/s12034-017-1470-5.
- [181] H. Li *et al.*, “All solid-state V_2O_5 -based flexible hybrid fiber supercapacitors,” *J. Power Sources*, vol. 371, pp. 18–25, Dec. 2017, doi: 10.1016/j.jpowsour.2017.10.031.
- [182] Y. Yang *et al.*, “Silicon-nanoparticle-based composites for advanced lithium-ion battery anodes,” *Nanoscale*, vol. 12, no. 14, Art. no. 14, 2020, doi: 10.1039/C9NR10652A.
- [183] S. Xu, D. Cen, P. Gao, H. Tang, and Z. Bao, “3D Interconnected V_6O_{13} Nanosheets Grown on Carbonized Textile via a Seed-Assisted Hydrothermal Process as High-Performance Flexible Cathodes for Lithium-Ion Batteries,” *Nanoscale Res. Lett.*, vol. 13, no. 1, Art. no. 1, Dec. 2018, doi: 10.1186/s11671-018-2469-6.
- [184] Y. Park, “Electrochemical properties of vanadium oxide thin film deposited by R.F. sputtering,” *Solid State Ion.*, vol. 154–155, pp. 229–235, Dec. 2002, doi: 10.1016/S0167-2738(02)00437-X.
- [185] G. López-Calzada *et al.*, “Optical characterization of novel matrix glasses based on a $\text{CdO}:\text{ZnO}:\text{V}_2\text{O}_5$ ternary system,” *J. Non-Cryst. Solids*, vol. 356, no. 6–8, Art. no. 6–8, Mar. 2010, doi: 10.1016/j.jnoncrysol.2009.11.033.
- [186] Y. Wang and G. Cao, “ Li^+ -intercalation electrochemical/electrochromic properties of vanadium pentoxide films by sol electrophoretic deposition,” *Electrochimica Acta*, vol. 51, no. 23, Art. no. 23, Jun. 2006, doi: 10.1016/j.electacta.2006.01.026.
- [187] A. Gies *et al.*, “Effect of silver co-sputtering on V_2O_5 thin films for lithium microbatteries,” *Thin Solid Films*, vol. 516, no. 21, Art. no. 21, Sep. 2008, doi: 10.1016/j.tsf.2007.12.165.
- [188] D. M. Yu *et al.*, “Effect of manganese doping on Li-ion intercalation properties of V_2O_5 films,” *J. Mater. Chem.*, vol. 20, no. 48, Art. no. 48, 2010, doi: 10.1039/c0jm01252a.

- [189] Q. Shi, R. Hu, M. Zeng, M. Dai, and M. Zhu, "The cycle performance and capacity fading mechanism of a LiV_3O_8 thin-film electrode with a mixed amorphous-nanocrystalline microstructure," *Electrochimica Acta*, vol. 56, no. 25, Art. no. 25, Oct. 2011, doi: 10.1016/j.electacta.2011.08.007.
- [190] J. Wu *et al.*, "Influence of Hydrofluoric Acid Formation on Lithium Ion Insertion in Nanostructured V_2O_5 ," *J. Phys. Chem. C*, vol. 116, no. 40, Art. no. 40, Oct. 2012, doi: 10.1021/jp305937b.
- [191] S. Boukhalifa, K. Evanoff, and G. Yushin, "Atomic layer deposition of vanadium oxide on carbon nanotubes for high-power supercapacitor electrodes," *Energy Environ. Sci.*, vol. 5, no. 5, Art. no. 5, 2012, doi: 10.1039/c2ee21110f.
- [192] M. Mousavi, A. Kompany, N. Shahtahmasebi, and M.-M. Bagheri-Mohagheghi, "Effect of S-doping on structural, optical and electrochemical properties of vanadium oxide thin films prepared by spray pyrolysis," *Phys. Scr.*, vol. 88, no. 6, Art. no. 6, Dec. 2013, doi: 10.1088/0031-8949/88/06/065701.
- [193] K. Jeyalakshmi, K. K. Purushothaman, and G. Muralidharan, "Thickness dependent supercapacitor behaviour of sol-gel spin coated nanostructured vanadium pentoxide thin films," *Philos. Mag.*, vol. 93, no. 13, Art. no. 13, May 2013, doi: 10.1080/14786435.2012.745654.
- [194] K. H. Krishna and O. M. Hussain, "Tailoring of electrochemical properties of V_2O_5 thin films grown on flexible substrates using plasma-assisted activated reactive evaporation," *Ionics*, vol. 19, no. 10, Art. no. 10, Oct. 2013, doi: 10.1007/s11581-013-0862-9.
- [195] H. Yin *et al.*, "Influence of morphologies and pseudocapacitive contributions for charge storage in V_2O_5 micro/nano-structures," *Electrochimica Acta*, vol. 111, pp. 762–770, Nov. 2013, doi: 10.1016/j.electacta.2013.08.005.
- [196] D. Yu *et al.*, "Mica-like vanadium pentoxide-nanostructured thin film as high-performance cathode for lithium-ion batteries," *J. Power Sources*, vol. 266, pp. 1–6, Nov. 2014, doi: 10.1016/j.jpowsour.2014.04.099.
- [197] H.-Y. Li *et al.*, "Electrochemically grown nanocrystalline V_2O_5 as high-performance cathode for sodium-ion batteries," *J. Power Sources*, vol. 285, pp. 418–424, Jul. 2015, doi: 10.1016/j.jpowsour.2015.03.086.

- [198] J. I. Goldstein *et al.*, *Scanning Electron Microscopy and X-ray Microanalysis: Third Edition*. Boston, MA: Springer US, 2003. doi: 10.1007/978-1-4615-0215-9.
- [199] M. Aliofkhazraei, Ed., *Handbook of Nanoparticles*. Cham: Springer International Publishing, 2016. doi: 10.1007/978-3-319-15338-4.
- [200] P. B. Hirsch, “Elements of X-Ray Diffraction,” *Phys. Bull.*, vol. 8, no. 7, Art. no. 7, Jul. 1957, doi: 10.1088/0031-9112/8/7/008.
- [201] J. K. Cooper, A. M. Franco, S. Gul, C. Corrado, and J. Z. Zhang, “Characterization of Primary Amine Capped CdSe, ZnSe, and ZnS Quantum Dots by FT-IR: Determination of Surface Bonding Interaction and Identification of Selective Desorption,” *Langmuir*, vol. 27, no. 13, Art. no. 13, Jul. 2011, doi: 10.1021/la201273x.
- [202] S. Bharti, G. Kaur, S. Gupta, and S. K. Tripathi, “Pegylated CdSe/ZnS core/shell nanoparticles for controlled drug release,” *Mater. Sci. Eng. B*, vol. 243, pp. 115–124, Apr. 2019, doi: 10.1016/j.mseb.2019.03.015.
- [203] S. Bharti, G. Kaur, S. Gupta, and S. K. Tripathi, “PEGylation of CdSe/ZnS core/shell nanoparticles and its behavior at different pH,” *J. Lumin.*, vol. 181, pp. 459–466, Jan. 2017, doi: 10.1016/j.jlumin.2016.09.005.
- [204] R. S. Das and Y. K. Agrawal, “Raman spectroscopy: Recent advancements, techniques and applications,” *Vib. Spectrosc.*, vol. 57, no. 2, Art. no. 2, Nov. 2011, doi: 10.1016/j.vibspec.2011.08.003.
- [205] G. S. Bumbrah and R. M. Sharma, “Raman spectroscopy – Basic principle, instrumentation and selected applications for the characterization of drugs of abuse,” *Egypt. J. Forensic Sci.*, vol. 6, no. 3, Art. no. 3, Sep. 2016, doi: 10.1016/j.ejfs.2015.06.001.
- [206] A.-S. Feiner and A. J. McEvoy, “The Nernst Equation,” *J. Chem. Educ.*, vol. 71, no. 6, Art. no. 6, Jun. 1994, doi: 10.1021/ed071p493.
- [207] N. Elgrishi, K. J. Rountree, B. D. McCarthy, E. S. Rountree, T. T. Eisenhart, and J. L. Dempsey, “A Practical Beginner’s Guide to Cyclic Voltammetry,” *J. Chem. Educ.*, vol. 95, no. 2, Art. no. 2, Feb. 2018, doi: 10.1021/acs.jchemed.7b00361.
- [208] R. Datt, J. Gangwar, S. K. Tripathi, R. K. Singh, and A. Kumar Srivastava, “Porous Nickel Oxide Nanostructures for Supercapacitor Applications,” *Quantum Matter*, vol. 5, no. 3, Art. no. 3, Jun. 2016, doi: 10.1166/qm.2016.1323.

- [209] C. Young *et al.*, “High energy density supercapacitors composed of nickel cobalt oxide nanosheets on nanoporous carbon nanoarchitectures,” *J. Mater. Chem. A*, vol. 5, no. 23, Art. no. 23, 2017, doi: 10.1039/C7TA01362K.
- [210] J. Zang *et al.*, “Well-Aligned Cone-Shaped Nanostructure of Polypyrrole/RuO₂ and Its Electrochemical Supercapacitor,” *J. Phys. Chem. C*, vol. 112, no. 38, Art. no. 38, Sep. 2008, doi: 10.1021/jp8049558.
- [211] H. Liu, P. He, Z. Li, Y. Liu, and J. Li, “A novel nickel-based mixed rare-earth oxide/activated carbon supercapacitor using room temperature ionic liquid electrolyte,” *Electrochimica Acta*, vol. 51, no. 10, Art. no. 10, Feb. 2006, doi: 10.1016/j.electacta.2005.06.034.
- [212] J. Zhao, X. Zhang, M. Li, S. Lu, and P. Yang, “Synthesis of precursor-derived 1D to 2D Co₃O₄ nanostructures and their pseudo capacitance behaviour,” *CrystEngComm*, vol. 18, no. 41, Art. no. 41, 2016, doi: 10.1039/C6CE01676F.
- [213] M. Aadil *et al.*, “Gadolinium doped zinc ferrite nanoarchitecture reinforced with a carbonaceous matrix: a novel hybrid material for next-generation flexible capacitors,” *RSC Adv.*, vol. 13, no. 40, pp. 28063–28075, 2023, doi: 10.1039/D3RA05290G.
- [214] S. Rafiq *et al.*, “NiO nanoparticles and their nanohybrid with flat rGO sheets: As an ideal electroactive material for hybrid capacitor applications,” *Ceram. Int.*, vol. 48, no. 10, pp. 14596–14605, May 2022, doi: 10.1016/j.ceramint.2022.01.353.
- [215] M. Mahmood *et al.*, “Nanostructured V₂O₅ and its nanohybrid with MXene as an efficient electrode material for electrochemical capacitor applications,” *Ceram. Int.*, vol. 48, no. 2, pp. 2345–2354, Jan. 2022, doi: 10.1016/j.ceramint.2021.10.014.
- [216] K. Panigrahi, P. Howli, and K. K. Chattopadhyay, “3D network of V₂O₅ for flexible symmetric supercapacitor,” *Electrochimica Acta*, vol. 337, p. 135701, Mar. 2020, doi: 10.1016/j.electacta.2020.135701.
- [217] Y.-C. Si, L.-F. Jiao, H.-T. Yuan, H.-X. Li, and Y.-M. Wang, “Structural and electrochemical properties of LiV₃O₈ prepared by combustion synthesis,” *J. Alloys Compd.*, vol. 486, no. 1–2, pp. 400–405, Nov. 2009, doi: 10.1016/j.jallcom.2009.06.188.
- [218] D. Wei, M. R. J. Scherer, C. Bower, P. Andrew, T. Ryhänen, and U. Steiner, “A Nanostructured Electrochromic Supercapacitor,” *Nano Lett.*, vol. 12, no. 4, pp. 1857–1862, Apr. 2012, doi: 10.1021/nl2042112.

- [219] G. R. Patzke, Y. Zhou, R. Kontic, and F. Conrad, "Oxide Nanomaterials: Synthetic Developments, Mechanistic Studies, and Technological Innovations," *Angew. Chem. Int. Ed.*, vol. 50, no. 4, pp. 826–859, Jan. 2011, doi: 10.1002/anie.201000235.
- [220] M. Rashid *et al.*, "Solar-light-driven and magnetically recoverable doped nano-ferrite: An ideal photocatalyst for water purification applications," *Opt. Mater.*, vol. 135, p. 113192, Jan. 2023, doi: 10.1016/j.optmat.2022.113192.
- [221] Z. S. Iro, C. Subramani, and S. S. Dash, "A Brief Review on Electrode Materials for Supercapacitor," *Int. J. Electrochem. Sci.*, vol. 11, no. 12, pp. 10628–10643, Dec. 2016, doi: 10.20964/2016.12.50.
- [222] C. Tsang and A. Manthiram, "Synthesis of Nanocrystalline VO₂ and Its Electrochemical Behavior in Lithium Batteries," *J. Electrochem. Soc.*, vol. 144, no. 2, pp. 520–524, Feb. 1997, doi: 10.1149/1.1837442.
- [223] S. Munir, M. Aadil, M. F. Warsi, H. H. Somaily, N. U. Ain, and M. Shahid, "Synergistic effect of noble metal doping and composite formation to boost the electrochemical properties of vanadium pentoxide," *Ceram. Int.*, vol. 48, no. 22, pp. 33306–33314, Nov. 2022, doi: 10.1016/j.ceramint.2022.07.273.
- [224] A. M. Mangan, S. P. Voinigescu, Ming-Ta Yang, and M. Tazlauanu, "De-embedding transmission line measurements for accurate modeling of IC designs," *IEEE Trans. Electron Devices*, vol. 53, no. 2, pp. 235–241, Feb. 2006, doi: 10.1109/TED.2005.861726.
- [225] F. Mao, H. Lu, D. Liu, K. Guo, F. Tang, and X. Song, "Structural stability and magnetic properties of SmCo₅ compounds doped with transition metal elements," *J. Alloys Compd.*, vol. 810, p. 151888, Nov. 2019, doi: 10.1016/j.jallcom.2019.151888.
- [226] Y. Li, F. Zhang, W. Gao, and Z. Zhan, "A high-performance Cu-doped vanadium pentoxide thin-film cathode for lithium-ion batteries," *Ionics*, vol. 27, no. 6, pp. 2335–2344, Jun. 2021, doi: 10.1007/s11581-021-04003-2.
- [227] M. Jin, G. Zhang, F. Yu, W. Li, W. Lu, and H. Huang, "Sponge-like Ni(OH)₂–NiF₂ composite film with excellent electrochemical performance," *Phys Chem Chem Phys*, vol. 15, no. 5, pp. 1601–1605, 2013, doi: 10.1039/C2CP43357E.
- [228] J. Pan *et al.*, "Microwave-assisted hydrothermal synthesis of V₂O₅ nanorods assemblies with an improved Li-ion batteries performance," *Mater. Res. Bull.*, vol. 74, pp. 90–95, Feb. 2016, doi: 10.1016/j.materresbull.2015.10.020.

- [229] T. A.-H. Abbas, "Light-Enhanced Vanadium Pentoxide (V₂O₅) Thin Films for Gas Sensor Applications," *J. Electron. Mater.*, vol. 47, no. 12, pp. 7331–7342, Dec. 2018, doi: 10.1007/s11664-018-6673-z.
- [230] K. Schneider, M. Lubecka, and A. Czapla, "V₂O₅ thin films for gas sensor applications," *Sens. Actuators B Chem.*, vol. 236, pp. 970–977, Nov. 2016, doi: 10.1016/j.snb.2016.04.059.
- [231] D. Machado *et al.*, "Graphene Based Sensors for Air Quality Monitoring - Preliminary Development Evaluation," *J. Coat. Sci. Technol.*, vol. 6, no. 1, pp. 10–21, Oct. 2019, doi: 10.6000/2369-3355.2019.06.01.2.
- [232] X. H. Yang, H. Xie, H. T. Fu, X. Z. An, X. C. Jiang, and A. B. Yu, "Synthesis of hierarchical nanosheet-assembled V₂O₅ microflowers with high sensing properties towards amines," *RSC Adv.*, vol. 6, no. 90, pp. 87649–87655, 2016, doi: 10.1039/C6RA18848F.
- [233] N. M. Abd-Alghafour, G. A. Naeem, N. M. Ahmed, N. Afzal, and R. F. Muslim, "Thermal evaporation based V₂O₅ thin film for extended gate field effect transistor pH sensor," *Mater. Res. Express*, vol. 6, no. 12, p. 125423, Jan. 2020, doi: 10.1088/2053-1591/ab5df5.
- [234] R. Wang *et al.*, "Enhanced gas sensing properties of V₂O₅ nanowires decorated with SnO₂ nanoparticles to ethanol at room temperature," *RSC Adv.*, vol. 5, no. 51, pp. 41050–41058, 2015, doi: 10.1039/C5RA00530B.
- [235] A. Dhayal Raj, T. Pazhanivel, P. Suresh Kumar, D. Mangalaraj, D. Nataraj, and N. Ponpandian, "Self assembled V₂O₅ nanorods for gas sensors," *Curr. Appl. Phys.*, vol. 10, no. 2, pp. 531–537, Mar. 2010, doi: 10.1016/j.cap.2009.07.015.
- [236] X. Liu, S. Cheng, H. Liu, S. Hu, D. Zhang, and H. Ning, "A Survey on Gas Sensing Technology," *Sensors*, vol. 12, no. 7, pp. 9635–9665, Jul. 2012, doi: 10.3390/s120709635.
- [237] A. Bhatnagar *et al.*, "Fe₃O₄@graphene as a superior catalyst for hydrogen de/absorption from/in MgH₂/Mg," *J. Mater. Chem. A*, vol. 4, no. 38, pp. 14761–14772, 2016, doi: 10.1039/C6TA05998H.
- [238] M. Abbasi, S. M. Rozati, R. Irani, and S. Beke, "Synthesis and gas sensing behavior of nanostructured V₂O₅ thin films prepared by spray pyrolysis," *Mater. Sci. Semicond. Process.*, vol. 29, pp. 132–138, Jan. 2015, doi: 10.1016/j.mssp.2014.01.008.

- [239] “VO nanofibres: novel gas sensors with extremely high sensitivity and selectivity to amines,” *Sens. Actuators B Chem.*, vol. 106, no. 2, pp. 730–735, May 2005, doi: 10.1016/j.snb.2004.09.024.
- [240] J. Liu *et al.*, “Controllable synthesis of In_2O_3 octodecahedra exposing {110} facets with enhanced gas sensing performance,” *RSC Adv.*, vol. 5, no. 55, pp. 44306–44312, 2015, doi: 10.1039/C5RA05212B.
- [241] Q. Rong *et al.*, “Design of ultrasensitive Ag-LaFeO₃ methanol gas sensor based on quasi molecular imprinting technology,” *Sci. Rep.*, vol. 8, no. 1, p. 14220, Sep. 2018, doi: 10.1038/s41598-018-32113-x.
- [242] M. Ezhilan, A. J. Jbb, and J. B. Balaguru Rayappan, “Influence of PVA templates on the synthesis of interconnected and long-winded electrospun V₂O₅ nanowires – Acetone sensor,” *Mater. Res. Bull.*, vol. 139, p. 111276, Jul. 2021, doi: 10.1016/j.materresbull.2021.111276.
- [243] J. Zhang, Z. Qin, D. Zeng, and C. Xie, “Metal-oxide-semiconductor based gas sensors: screening, preparation, and integration,” *Phys. Chem. Chem. Phys.*, vol. 19, no. 9, pp. 6313–6329, 2017, doi: 10.1039/C6CP07799D.
- [244] X.-Z. Song, Y.-L. Meng, Z. Tan, L. Qiao, T. Huang, and X.-F. Wang, “Concave ZnFe_2O_4 Hollow Octahedral Nanocages Derived from Fe-Doped MOF-5 for High-Performance Acetone Sensing at Low-Energy Consumption,” *Inorg. Chem.*, vol. 56, no. 22, pp. 13646–13650, Nov. 2017, doi: 10.1021/acs.inorgchem.7b02425.
- [245] B. Wang, L. Sun, M. Schneider-Ramelow, K.-D. Lang, and H.-D. Ngo, “Recent Advances and Challenges of Nanomaterials-Based Hydrogen Sensors,” *Micromachines*, vol. 12, no. 11, p. 1429, Nov. 2021, doi: 10.3390/mi12111429.
- [246] L. Han *et al.*, “A novel redox bromide-ion additive hydrogel electrolyte for flexible Zn-ion hybrid supercapacitors with boosted energy density and controllable zinc deposition,” *J. Mater. Chem. A*, vol. 8, no. 30, pp. 15042–15050, 2020, doi: 10.1039/D0TA03547E.
- [247] S. Z. Hussain, M. Ihrar, S. B. Hussain, W. C. Oh, and K. Ullah, “A review on graphene based transition metal oxide composites and its application towards supercapacitor electrodes,” *SN Appl. Sci.*, vol. 2, no. 4, p. 764, Apr. 2020, doi: 10.1007/s42452-020-2515-8.

- [248] J. Zhang, J. Jiang, H. Li, and X. S. Zhao, "A high-performance asymmetric supercapacitor fabricated with graphene-based electrodes," *Energy Environ. Sci.*, vol. 4, no. 10, p. 4009, 2011, doi: 10.1039/c1ee01354h.
- [249] B. Ding and X. Wu, "Transition metal oxides anchored on graphene/carbon nanotubes conductive network as both the negative and positive electrodes for asymmetric supercapacitor," *J. Alloys Compd.*, vol. 842, p. 155838, Nov. 2020, doi: 10.1016/j.jallcom.2020.155838.
- [250] M. Fu *et al.*, "Facile synthesis of V₂O₅/graphene composites as advanced electrode materials in supercapacitors," *J. Alloys Compd.*, vol. 862, p. 158006, May 2021, doi: 10.1016/j.jallcom.2020.158006.
- [251] N. Devi, S. Sahoo, R. Kumar, and R. K. Singh, "A review of the microwave-assisted synthesis of carbon nanomaterials, metal oxides/hydroxides and their composites for energy storage applications," *Nanoscale*, vol. 13, no. 27, pp. 11679–11711, 2021, doi: 10.1039/D1NR01134K.
- [252] S. Sahoo, R. Kumar, E. Joanni, R. K. Singh, and J.-J. Shim, "Advances in pseudocapacitive and battery-like electrode materials for high performance supercapacitors," *J. Mater. Chem. A*, vol. 10, no. 25, pp. 13190–13240, 2022, doi: 10.1039/D2TA02357A.
- [253] H. Qu *et al.*, "A review of graphene-oxide/metal–organic framework composites materials: characteristics, preparation and applications," *J. Porous Mater.*, vol. 28, no. 6, pp. 1837–1865, Dec. 2021, doi: 10.1007/s10934-021-01125-w.
- [254] M. Li *et al.*, "Flower-like Nitrogen-co-doped MoS₂@RGO Composites with Excellent Stability for Supercapacitors," *ChemElectroChem*, vol. 8, no. 15, pp. 2903–2911, Aug. 2021, doi: 10.1002/celec.202100401.
- [255] R. Kumar and R. Thangappan, "Electrode material based on reduced graphene oxide (rGO)/transition metal oxide composites for supercapacitor applications: a review," *Emergent Mater.*, vol. 5, no. 6, pp. 1881–1897, Dec. 2022, doi: 10.1007/s42247-021-00339-7.
- [256] C. Yan *et al.*, "Hydrothermal synthesis of vanadium doped nickel sulfide nanoflower for high-performance supercapacitor," *J. Alloys Compd.*, vol. 928, p. 167189, Dec. 2022, doi: 10.1016/j.jallcom.2022.167189.

- [257] C. Lee, S. K. Kim, J.-H. Choi, H. Chang, and H. D. Jang, "Electrochemical performances of iron-cobalt oxides nanoparticles loaded crumpled graphene for supercapacitor," *J. Alloys Compd.*, vol. 735, pp. 2030–2037, Feb. 2018, doi: 10.1016/j.jallcom.2017.11.393.
- [258] F. Zhao, W. Huang, and D. Zhou, "Chemical bath deposition synthesis of nickel cobalt oxides/sulfides for high-performance supercapacitors electrode materials," *J. Alloys Compd.*, vol. 755, pp. 15–23, Jul. 2018, doi: 10.1016/j.jallcom.2018.04.304.
- [259] S. K. Shinde *et al.*, "Using chemical bath deposition to create nanosheet-like CuO electrodes for supercapacitor applications," *Colloids Surf. B Biointerfaces*, vol. 181, pp. 1004–1011, Sep. 2019, doi: 10.1016/j.colsurfb.2019.05.079.
- [260] E. Aawani, N. Memarian, and H. R. Dizaji, "Synthesis and characterization of reduced graphene oxide–V₂O₅ nanocomposite for enhanced photocatalytic activity under different types of irradiation," *J. Phys. Chem. Solids*, vol. 125, pp. 8–15, Feb. 2019, doi: 10.1016/j.jpcs.2018.09.028.
- [261] Y. Chen *et al.*, "Tailoring defective vanadium pentoxide/reduced graphene oxide electrodes for all-vanadium-oxide asymmetric supercapacitors," *Chem. Eng. J.*, vol. 429, p. 132274, Feb. 2022, doi: 10.1016/j.cej.2021.132274.
- [262] M. Kandasamy, S. Sahoo, S. K. Nayak, B. Chakraborty, and C. S. Rout, "Recent advances in engineered metal oxide nanostructures for supercapacitor applications: experimental and theoretical aspects," *J. Mater. Chem. A*, vol. 9, no. 33, pp. 17643–17700, 2021, doi: 10.1039/D1TA03857E.
- [263] N. M. Abbasi *et al.*, "Heterostructures of titanium-based MXenes in energy conversion and storage devices," *J. Mater. Chem. C*, vol. 9, no. 27, pp. 8395–8465, 2021, doi: 10.1039/D1TC00327E.
- [264] D. Leistenschneider, Z. Abedi, D. G. Ivey, and W. Chen, "Coating of Low-Cost Asphaltenes-Derived Carbon Fibers with V₂O₅ for Supercapacitor Application," *Energy Fuels*, vol. 36, no. 6, pp. 3328–3338, Mar. 2022, doi: 10.1021/acs.energyfuels.2c00066.
- [265] Z. Feng, Y. Zhang, X. Yu, Y. Yu, C. Huang, and C. Meng, "Aluminum-ion intercalation and reduced graphene oxide wrapping enable the electrochemical properties of hydrated V₂O₅ for Zn-ion storage," *Colloids Surf. Physicochem. Eng. Asp.*, vol. 641, p. 128473, May 2022, doi: 10.1016/j.colsurfa.2022.128473.

- [266] Y. J. Oh *et al.*, “Oxygen functional groups and electrochemical capacitive behavior of incompletely reduced graphene oxides as a thin-film electrode of supercapacitor,” *Electrochimica Acta*, vol. 116, pp. 118–128, Jan. 2014, doi: 10.1016/j.electacta.2013.11.040.
- [267] G. Huang *et al.*, “Lithiophilic V₂O₅ nanobelt arrays decorated 3D framework hosts for highly stable composite lithium metal anodes,” *Chem. Eng. J.*, vol. 384, p. 123313, Mar. 2020, doi: 10.1016/j.cej.2019.123313.
- [268] W. Sun, G. Gao, Y. Du, K. Zhang, and G. Wu, “A facile strategy for fabricating hierarchical nanocomposites of V₂O₅ nanowire arrays on a three-dimensional N-doped graphene aerogel with a synergistic effect for supercapacitors,” *J. Mater. Chem. A*, vol. 6, no. 21, pp. 9938–9947, 2018, doi: 10.1039/C8TA01448E.
- [269] H. Liu, W. Zhu, D. Long, J. Zhu, and G. Pezzotti, “Porous V₂O₅ nanorods/reduced graphene oxide composites for high performance symmetric supercapacitors,” *Appl. Surf. Sci.*, vol. 478, pp. 383–392, Jun. 2019, doi: 10.1016/j.apsusc.2019.01.273.
- [270] P. Sehrawat, A. Abid, S. S. Islam, A. Mauger, and C. M. Julien, “Nanostructured Graphene Oxide-Based Hybrids as Anodes for Lithium-Ion Batteries,” *C*, vol. 6, no. 4, p. 81, Dec. 2020, doi: 10.3390/c6040081.
- [271] A. Qian *et al.*, “Capacitance enhancement in supercapacitors by incorporating ultra-long hydrated vanadium-oxide nanobelts into graphene,” *J. Alloys Compd.*, vol. 688, pp. 814–821, Dec. 2016, doi: 10.1016/j.jallcom.2016.07.222.
- [272] Y. Chen, Z. Zhang, Z. Huang, and H. Zhang, “Effects of oxygen-containing functional groups on the supercapacitor performance of incompletely reduced graphene oxides,” *Int. J. Hydrog. Energy*, vol. 42, no. 10, pp. 7186–7194, Mar. 2017, doi: 10.1016/j.ijhydene.2016.08.054.
- [273] Y. Guo, J. Li, M. Chen, and G. Gao, “Facile synthesis of vanadium pentoxide@carbon core-shell nanowires for high-performance supercapacitors,” *J. Power Sources*, vol. 273, pp. 804–809, Jan. 2015, doi: 10.1016/j.jpowsour.2014.09.118.
- [274] T. K. Le, M. Kang, and S. W. Kim, “A review on the optical characterization of V₂O₅ micro-nanostructures,” *Ceram. Int.*, vol. 45, no. 13, pp. 15781–15798, Sep. 2019, doi: 10.1016/j.ceramint.2019.05.339.
- [275] T. K. Le, M. Kang, V. T. Tran, and S. W. Kim, “Relation of photoluminescence and sunlight photocatalytic activities of pure V₂O₅ nanohollows and V₂O₅/RGO

- nanocomposites,” *Mater. Sci. Semicond. Process.*, vol. 100, pp. 159–166, Sep. 2019, doi: 10.1016/j.mssp.2019.04.047.
- [276] K. Ullah, A. Ullah, A. Aldalbahi, J. Chung, and W.-C. Oh, “Enhanced visible light photocatalytic activity and hydrogen evolution through novel heterostructure AgI–FG–TiO₂ nanocomposites,” *J. Mol. Catal. Chem.*, vol. 410, pp. 242–252, Dec. 2015, doi: 10.1016/j.molcata.2015.09.024.
- [277] K. Ullah, S. Ye, Z. Lei, K.-Y. Cho, and W.-C. Oh, “Synergistic effect of PtSe₂ and graphene sheets supported by TiO₂ as cocatalysts synthesized via microwave techniques for improved photocatalytic activity,” *Catal. Sci. Technol.*, vol. 5, no. 1, pp. 184–198, 2015, doi: 10.1039/C4CY00886C.
- [278] Z. Liu, H. Zhang, Q. Yang, and Y. Chen, “Graphene / V₂O₅ hybrid electrode for an asymmetric supercapacitor with high energy density in an organic electrolyte,” *Electrochimica Acta*, vol. 287, pp. 149–157, Oct. 2018, doi: 10.1016/j.electacta.2018.04.212.
- [279] T. Liu *et al.*, “Boosting zinc ion storage performance of sandwich-like V₂O₅/graphene composite by effectively inhibiting vanadium dissolution,” *J. Colloid Interface Sci.*, vol. 613, pp. 524–535, May 2022, doi: 10.1016/j.jcis.2022.01.057.
- [280] N. Aliahmad, Y. Liu, J. Xie, and M. Agarwal, “V₂O₅/Graphene Hybrid Supported on Paper Current Collectors for Flexible Ultrahigh-Capacity Electrodes for Lithium-Ion Batteries,” *ACS Appl. Mater. Interfaces*, vol. 10, no. 19, pp. 16490–16499, May 2018, doi: 10.1021/acsami.8b02721.
- [281] D. Su *et al.*, “High N-doped hierarchical porous carbon networks with expanded interlayers for efficient sodium storage,” *Nano Res.*, vol. 13, no. 10, pp. 2862–2868, Oct. 2020, doi: 10.1007/s12274-020-2944-0.
- [282] L. Gong, Y. Zhang, and Z. Li, “V-MOF@graphene derived two-dimensional hierarchical V₂O₅@graphene as high-performance cathode for aqueous zinc-ion batteries,” *Mater. Today Chem.*, vol. 23, p. 100731, Mar. 2022, doi: 10.1016/j.mtchem.2021.100731.
- [283] Y. Liu *et al.*, “Graphene-based interlayer for high-performance lithium–sulfur batteries: A review,” *Mater. Des.*, vol. 211, p. 110171, Dec. 2021, doi: 10.1016/j.matdes.2021.110171.

- [284] S. Zhu *et al.*, “Vanadium pentoxide nanosheets with rich oxygen vacancies as a high-performance electrode for supercapacitors,” *Ionics*, vol. 28, no. 6, pp. 2931–2942, Jun. 2022, doi: 10.1007/s11581-022-04541-3.
- [285] D. J. Ahirrao, K. Mohanapriya, and N. Jha, “V₂O₅ nanowires-graphene composite as an outstanding electrode material for high electrochemical performance and long-cycle-life supercapacitor,” *Mater. Res. Bull.*, vol. 108, pp. 73–82, Dec. 2018, doi: 10.1016/j.materresbull.2018.08.028.
- [286] P. Asen, S. Shahrokhian, and A. Iraj Zad, “One step electrodeposition of V₂O₅/polypyrrole/graphene oxide ternary nanocomposite for preparation of a high performance supercapacitor,” *Int. J. Hydrog. Energy*, vol. 42, no. 33, pp. 21073–21085, Aug. 2017, doi: 10.1016/j.ijhydene.2017.07.008.
- [287] M. S. Javed *et al.*, “Faradic redox active material of Cu₇S₄ nanowires with a high conductance for flexible solid state supercapacitors,” *Nanoscale*, vol. 7, no. 32, pp. 13610–13618, 2015, doi: 10.1039/C5NR03363B.
- [288] Z.-Q. Hou, Z.-G. Yang, and Y.-P. Gao, “Synthesis of vanadium oxides nanosheets as anode material for asymmetric supercapacitor,” *Chem. Pap.*, vol. 72, no. 11, pp. 2849–2857, Nov. 2018, doi: 10.1007/s11696-018-0504-9.
- [289] J. Ning *et al.*, “Superior Pseudocapacitive Storage of a Novel Ni₃Si₂/NiOOH/Graphene Nanostructure for an All-Solid-State Supercapacitor,” *Nano-Micro Lett.*, vol. 13, no. 1, p. 2, Dec. 2021, doi: 10.1007/s40820-020-00527-w.
- [290] S. Wang, Y. Shao, W. Liu, Y. Wu, and X. Hao, “Elastic sandwich-type GaN/MnO₂/MnON composites for flexible supercapacitors with high energy density,” *J. Mater. Chem. A*, vol. 6, no. 27, pp. 13215–13224, 2018, doi: 10.1039/C8TA04182B.

Chapter-9

List of publications and conferences attended

9.1. List of publication

- **Vishwakarma, N.**, Mashangva, T. T., Kumar, M., Srivastava, A., & Sharma, A. (2024). Impact of hydrothermal and solvent-thermal synthesis on the electrochemical performance of V₂O₅. *Materials Letters*, 136137.
- **Vishwakarma, N.**, Remadevi, A. A., Kumar, D., Solanki, A., Rana, A. S., & Srivastava, A. (2024). Metastable marvels: Navigating VO₂ polymorphs for next-gen electronics and energy solutions. *Journal of Applied Physics*, 135(2).
- **Vishwakarma, N.**, Sindhu, M., Maan, K. S., Tabasum, S., Rani, S., Patel, V., & Sharma, A. K. (2023, September). Preparation of vanadium oxide from various route of synthesis process for energy storage application. In *AIP Conference Proceedings* (Vol. 2800, No. 1). AIP Publishing.
- **Vishwakarma, N.**, Mashangva, T. T., Rajput, S., Pham, T. D., Kumar, M., & Sharma, A. (2024). Unlocking the potential for revolutionary energy storage capabilities of V₂O₅/GO nanocomposites synthesized under microwave irradiation. *Journal of Energy Storage*, 103, 114405.
- Sindhu, M., Singh, A., Kumar, Y. P., Vishwakarma, N., Wani, A. H., & Sharma, A. (2025). Nutshell-Derived Efficient Carbon Nanomaterials as a Potential Smart Electrode Material for Electrocatalytic Hydrogen Production. In *Waste-Derived Carbon Nanostructures: Synthesis and Applications* (pp. 193-212). Cham: Springer Nature Switzerland.
- Maan, K. S., Vishwakarma, N., Sharma, A., Sanghi, R., & Singh, P. P. (2025). Microbial fuel cells with polyaniline nanofiber/nanoparticle electrodes: a promising

approach for sustainable electricity generation. Chemical Engineering Communications, 1-12.

9.2. Conferences and Workshops

- Presented paper on “Preparation of Vanadium Oxide (VO_2) for energy storage application” in International Conference on Materials for Emerging Technologies (ICMET-21) held at lovely Professional University.
- Presented paper on “Effect on Mechanochemical and Hydrothermal Assisted synthesis on electrochemical performance in V_2O_5 based nanomaterial” in International Chemical Engineering Conference 2022 held at IIT Patna.
- Presented paper on “Synthesis of V_2O_5 nanomaterials by various route of synthesis method and their sensitivity towards Acetone, IPA and Methanol” in International Conference on Recent Advances in Fundamental and Applied Sciences” (RAFAS-2023) held at lovely Professional University.
- Presented paper on “ V_2O_5 nanomaterials based highly sensitive sensors towards electrochemical volatile organic comp various route of synthesis method and their sensitivity towards Acetone, IPA and Methanol” in International Conference on Recent Advances in Fundamental and Applied Sciences” (RAFAS-2024) held at lovely Professional University.
- Presented paper on “Synthesis and electrochemical characterization of vanadium oxide based nanoparticles for supercapacitor application” in International Conclave on Materials, Energy and Climates held at Indra Gandhi Delhi Technical University from 12-14 December 2022.
- Participated KARYASHALA (High-End workshop) on “Renewable Energy: Production and Storage” from September 24-30, 2022, held at and organized by IIT Ropar and sponsored under the Accelerate Vigyan Program of SERB, Government of India.
- Certificate of International Association of Advance Material from 11-14 October 2022 which is held by Stockholm, Sweden.
- Certificate of the Next Generation of STEM Scientist (NGSS-2022) organized by Marwadi University, Rajkot, Gujarat from 4th-6th Augut,2022
- Participated the advanced instrumentation training on “High Value Scientific

Equipment” organized by IIT Kanpur and sponsored by the DST under the Synergistic Training Programme Utilizing Scientific Technological Infrastructure (STUTI) from 16-20 January 2023.

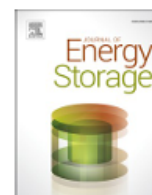
9.3. Award

- Best Poster Presentation Award in International Chemical Engineering Conference 2022 held at IIT Patna.



Contents lists available at ScienceDirect

Journal of Energy Storage

journal homepage: www.elsevier.com/locate/est

Research papers

Unlocking the potential for revolutionary energy storage capabilities of V₂O₅/GO nanocomposites synthesized under microwave irradiationNeetu Vishwakarma^{a,*}, Tim Tim Mashangva^a, Shubham Rajput^b, Thanh-Dong Pham^c, Mukesh Kumar^{a,*}, Ajit Sharma^{d,e,**}^a Department of Physics, School of Chemical Engineering and Physical Sciences, Lovely Professional University, Punjab 144001, India^b Department of Physics and Materials Science, Thapar Institute of Engineering and Technology, Punjab, India^c Faculty of Chemistry, Vietnam National University, VNU University of Science, Hanoi, Vietnam^d Department of Chemistry, School of Chemical Engineering and Physical Science, Lovely Professional University, Punjab 144411, India^e Centre for Nanoscience and Nano bioelectronics, School of Chemical Engineering and Physical Sciences, Lovely Professional University, Phagwara, Punjab 144411, India

ARTICLE INFO

Keywords:

Vanadium pentoxide
Supercapacitor
Electrochemical properties
Graphene oxide
Nanocomposite

ABSTRACT

A microwave-assisted synthesis process was used to prepare the nanocomposite material by doping graphene oxide into vanadium pentoxide (V₂O₅). The composite's enhanced hybrid super capacitive performance has been investigated. When the graphene oxide was added to V₂O₅, the electrochemical performance of the nanocomposite significantly improved. Following optimization, 10 % of GO-doped into V₂O₅ was used as a positive electrode and showed improved performance with a specific capacitance of 737 F/g at 1 A/g within a broad working potential window of 0.0–0.4 V in a 3 M KOH aqueous electrolyte. The addition of GO to the composites created a highly conductive route and functional surface on which V₂O₅ nanoparticles could attach, increasing the surface area. The VG10 sample electrode maintained excellent electrochemical performance. Based on these results, composites of vanadium pentoxide and graphene oxide (VG) may represent an excellent active material for supercapacitor electrodes.

1. Introduction

The fossil fuel depletion and increasing demands for the energy worldwide have promoted to the advancement of green and renewable energy storage technologies. Various energy sources are used to produce and store energy, leading to advancements in energy storage devices [1–3]. Supercapacitors, known for their rapid charging and discharging capabilities, are particularly suitable for powering portable devices and electric cars [4]. Research in supercapacitors aims to identify environmentally safe, high-performance electrolytes with increased energy density [5]. Three key factors determine a supercapacitors capacitance characteristics: the synthesis technique, the electrolyte, and the electrode material. In order to achieve exceptional electrochemical performance, research efforts have recently focused more and more on the design of electrode materials [6].

To enhance the efficiency and performance of supercapacitors,

innovative electrode materials are crucial. Transition metal oxides (TMOs) are frequently employed in this context due to their ability to connect with various metals and semiconductors with tunable nanostructures and techniques [7]. However, there is a need for more affordable and eco-friendly alternatives to materials like ruthenium oxide [8,9]. Research on TMOs in binary and ternary compositions has shown that the addition of graphene oxide (GO) enhances optical and electrical characteristics [10,11]. The combination of crumpled iron-cobalt oxides along with graphene oxide at low current densities improves specific capacitance and conductivity [12]. Wet chemical synthesis of nickel cobalt oxide/sulfide has resulted in the specific capacitance of 1196 Fg^{−1} and the capacity of retention 61 % after 4000 cycles, while the electrodes of copper oxide in a 1 M solution of Na₂SO₄ exhibit increased specific capacitance [13]. GO's wide range of functional groups can serve as suitable sites for redox reactions, allowing different metal oxide ions to bind to its surface [14]. The

* Corresponding author.

** Correspondence to: A. Sharma, Department of Chemistry, School of Chemical Engineering and Physical Science, Lovely Professional University, Punjab 144411, India.

E-mail addresses: moka.esh9@gmail.com (M. Kumar), ajitsharma2003@gmail.com (A. Sharma).<https://doi.org/10.1016/j.est.2024.114405>

Received 10 July 2024; Received in revised form 15 October 2024; Accepted 26 October 2024

Available online 31 October 2024

2352-152X/© 2024 Elsevier Ltd. All rights are reserved, including those for text and data mining, AI training, and similar technologies.



Impact of hydrothermal and solvent-thermal synthesis on the electrochemical performance of V_2O_5

Neetu Vishwakarma^a, Tim Tim Mashangva^a, Mukesh Kumar^a, Amar Srivastava^{a,*},
Ajit Sharma^{b,*}

^a Department of Physics, School of Chemical Engineering and Physical Science, Lovely Professional University, Jalandhar, Punjab 14411, India

^b Department of Chemistry, School of Chemical Engineering and Physical Science, Lovely Professional University, Jalandhar, Punjab 14411, India

ARTICLE INFO

Keywords:

V_2O_5
Hydrothermal method
Nanoparticles
X-ray techniques
Electrochemical study

ABSTRACT

This research focuses on synthesizing vanadium oxide through hydrothermal and solvent-thermal methods, to explore their potential application in supercapacitors. X-ray diffraction (XRD) and Fourier transform infrared spectroscopy (FT-IR) are used to determine the crystalline size and functional group, while scanning electron microscopy (SEM) is used to investigate their morphologies. The electrochemical performance was evaluated through cyclic voltammetry (CV), galvanostatic charge-discharge (GCD), and electrochemical impedance spectroscopy (EIS). The results demonstrated that the V_2O_5 synthesized by the hydrothermal method exhibited two-fold increases in specific capacitance compared to those produced by the solvent-thermal method. Experimental results also indicate that nanoparticles V_2O_5 by hydrothermal can deliver a capacitance of 121 Fg^{-1} and solvent-thermal deliver a capacitance of 72 Fg^{-1} at the current density of 1 Ag^{-1} in the potential range from 0 to 0.45 V in a 3 M KOH aqueous electrolyte.

1. Introduction

Energy storage has become increasingly important in recent years in diverse domains of modern existence. This includes using renewable energy, powering electric vehicles, generating electricity, and ensuring the efficient operation of portable electronic devices such as computers and mobile phones [1]. Supercapacitors (SCs), on the other hand, known as electrochemical capacitors (ECs), are among the emerging energy storage technologies due to their high energy density, quick charging/discharging process, and long lifespan [2]. Advanced materials are playing a crucial role in the development of these energy storage technologies. Among the diverse array of materials investigated, metal oxides like Co_3O_4 , RuO_2 , MnO_2 , CuO , NiO , and V_2O_5 emerge as exceedingly promising candidates due to their remarkable electrochemical properties and potential uses in energy storage devices [1–3]. V_2O_5 , in particular, is considered the best choice for pseudocapacitor application owing to its inherent properties: multiple valence, high potential window, low cost, multiple structures, and toxicity [4,5]. To harness these advantageous characteristics, different methods have been utilized to synthesize vanadium oxide nanoparticles, including sol-gel methods, hydrothermal synthesis, microwave processes, and solvent-

thermal processes. Recent results on V_2O_5 nanofibers, produced through the electro spinning method, exhibit a significant capacitance of 190 F/g [6]. Another study demonstrates that a V_2O_5 nanostructure can attain a maximum capacitance of 155 F/g [7]. Challenges such as inadequate conductivity and the inability to precisely control the morphology shape, and valences of V_2O_5 contribute to its low specific capacitance values. Addressing these challenges could lead to the development of more efficient and durable energy storage technologies. This research investigates the electrochemical characteristics of V_2O_5 , synthesized with distinct morphologies through both hydrothermal and solvent-thermal methods, aiming to assess and compare their performance.

2. Materials and characterization

V_2O_5 was synthesized via two different approaches, hydrothermal and solvent-thermal shown in Fig. S1. The details of the synthesis procedure are discussed in the Supplementary file.

* Corresponding authors.

E-mail addresses: amariitk09@gmail.com (A. Srivastava), ajitsharma2003@gmail.com (A. Sharma).

Metastable Marvels: Navigating VO₂ Polymorphs for Next-Gen Electronics and Energy Solutions

Neetu Vishwakarma¹, Abhijith Ambadi Remadevi¹, Deepak Kumar², Ankur Solanki³, Abhimanyu Singh Rana⁴, Amar Srivastava^{1,*}

Affiliations:

¹Department of Physics, School of Chemical Engineering and Physical Sciences, Lovely Professional University, Phagwara, Panjab 144411, India

²Department of Chemistry, School of Chemical Engineering and Physical Sciences, Lovely Professional University, Phagwara, Panjab 144411, India

³Department of Physics, School of Technology, Pandit Deendayal Energy University, Gandhinagar, Gujarat, 382421, India


⁴Centre for Advanced Materials and Devices, School of Engineering and Technology, BML Munjal University, Sidhrawali, Gurgaon 122413, India

Corresponding Author E-mail: [*amariitk09@gmail.com](mailto:amariitk09@gmail.com)

ABSTRACT: VO₂ polymorphs present a unique opportunity to unravel diverse electronic properties possessed by their metastable phases. A highly reproducible, single-phase and inexpensive synthesis method is challenging for obtaining VO₂ polymorphs. Recent years have witnessed some exciting success in the growth and application of a wide range of VO₂ polymorphs. This comprehensive review article delves into the different polymorphs, including VO₂(x) (x = A, B, M, R, C, P, and D), and investigates their distinct physical attributes. The primary focus of this article centers on providing a thorough overview of the recent progress made in stabilizing VO₂(A) and VO₂(B) polymorphs, emphasizing the significance of the coexistence of nanodomains at the film-substrate interface in stabilizing specific metastable phases. Additionally, the review article delves into advancements in understanding the phase transition mechanism, adjusting the order parameter in resistivity, and modifying the MIT (Metal-Insulator Transition) temperature through doping. It also summarizes the structural, optical, electronic, and interface properties of these polymorphs and highlights their potential applications in next-generation electronic devices, particularly in the fields of sensing and energy storage.

RESEARCH ARTICLE | SEPTEMBER 08 2023

Preparation of vanadium oxide from various route of synthesis process for energy storage application

Neetu Vishwakarma ; Monika Sindhu; Karan Singh Maan; Sahima Tabasum; Suman Rani; Vijay Patel; Jashanpreet Singh; Amar Srivastava; Ajit Kumar Sharma



AIP Conf. Proc. 2800, 020075 (2023)

<https://doi.org/10.1063/5.0163546>



View
Online



Export
Citation

CrossMark

Articles You May Be Interested In

A functional integral formalism for quantum spin systems

J. Math. Phys. (July 2008)



Microbial fuel cells with polyaniline nanofiber/nanoparticle electrodes: a promising approach for sustainable electricity generation

Karan Singh Maan^a, Neetu Vishwakarma^b, Ajit Sharma^c, Rashmi Sanghi^d, and Prabal Pratap Singh^e

^aDepartment of Chemical Engineering, School of Chemical Engineering and Physical Sciences, Lovely Professional University, Jalandhar, India; ^bDepartment of Physics, School of Chemical Engineering and Physical Sciences, Lovely Professional University, Punjab, India; ^cDepartment of Chemistry, School of Chemical Engineering and Physical Sciences, Lovely Professional University, Jalandhar, India; ^dAmity School of Chemical Sciences, Amity University Punjab, India; ^eDepartment of Chemistry, GLA University, Mathura, UP, India

ABSTRACT

Electrode modifications employing conductive and nanostructured polyaniline (PANI) have been acknowledged as an effective strategy to enhance the interaction between electrode surfaces and bacteria, thereby augmenting the performance of Microbial Fuel Cells (MFCs). However, the specific influence of PANI morphology on power generation in MFCs remains unknown. In this study, two nanostructures of polyaniline, viz., polyaniline nanofiber (PANI-NF) and polyaniline nanoparticle (PANI-NP), were electro-polymerized on a peanut shell biochar (PSB) electrode by chronoamperometry. The physico-chemical properties of PSB, PSB/PANI-NF, and PSB/PANI-NP were analyzed using scanning electron microscopy (SEM), X-ray diffraction spectroscopy (XRD), and Fourier transform infrared spectroscopy (FT-IR). The electrochemical performance of the electrodes was investigated using cyclic voltammetry (CV) and electrochemical impedance spectroscopy (EIS) techniques. Remarkably, the PSB/PANI-NP composite exhibited notably heightened electrochemical activity and superior electrode-electrolyte interaction, leading to a significant enhancement in MFC performance. MFCs equipped with PSB/PANI-NP electrodes achieved a power output of 600 mW/m² surpassing the performance of MFCs utilizing PSB/PANI-NF and PSB electrodes by 2.8 and 25 times, respectively. This investigation elucidates the pivotal role of PANI morphology on power production in MFC.

HIGHLIGHTS

- The application of electrodes in microbial fuel cell was successfully demonstrated.
- Polyaniline NFs and NPs were electropolymerized on the surface peanut shell biochar electrode.
- Polyaniline NPs exhibited superior electrochemical activity and interfacial properties.
- MFCs equipped with PSB/PANI-NP electrodes achieved a power output of 600 mW/m².

KEYWORDS

Microbial fuel cell; power production; polyaniline; nanofiber; nanoparticle; nanostructure

1. Introduction

The growing global need for sustainable and ecologically friendly energy options has catalyzed research on renewable energy sources. Among renewable sources like hydropower, wind, solar, tidal and geothermal, bioenergy is distinctive in its ability to produce power from biological matter. Bio-energy is commonly obtained through the production of bioethanol, although other forms such as biodiesel, bio-oil, biogas, and bio hydrogen are also

prevalent in solid, liquid, and gaseous states (Sintayehu 2018; Cherwoo et al. 2023; Kumar et al. 2025).

In contrast, Microbial Fuel Cells (MFCs) present another alternative for bio-energy production, converting waste biomass directly into electricity (Magotra et al. 2021; Devi et al. 2025). There are different configurations of MFCs, such as up flow MFC, single-chamber MFC, dual-chamber MFC, and stacked MFC. However, the dual-chamber MFC has been widely used. This configuration

[Home](#) > [Waste-Derived Carbon Nanostructures](#) > Chapter

Nutshell-Derived Efficient Carbon Nanomaterials as a Potential Smart Electrode Material for Electrocatalytic Hydrogen Production

Chapter | First Online: 10 January 2025

pp 193–212 | [Cite this chapter](#)

[Monika Sindhu](#), [Arshjeet Singh](#), [Yarramsetti Praveen Kumar](#), [Neetu Vishwakarma](#), [Afshan Hassan Wani](#) & [Ajit Sharma](#) 

 Part of the book series: [Nanostructure Science and Technology \(\(NST\)\)](#) 89 Accesses  1 [Altmetric](#)

Abstract

As part of ongoing exertions by scientists to develop alternative solutions to curtail the issue of continuous emissions of greenhouse gases by the use of fossil fuels, attention has been directed toward biomass (organic matter that can be turned into useful energy). Green nanotechnology is advancing to address society's global sustainability disquiets by recycling a variety of industrial and bio-wastes to generate functional carbonaceous nanomaterials that include biochar and activated carbon. Biomass can be the primary source of bio-based carbon nanomaterials for electrochemical energy production and storage technologies. Carbon nanomaterials derived from biomass possess diverse chemical, structural, and mechanical characteristics that have been investigated as a carbon source due to their high surface area, configurable structure, abundance, cost-effectiveness, and cyclic and environmentally friendly nature. In this chapter, various nutshells are used as a green carbon source for the electrode to produce the electrocatalytic hydrogen. This chapter aims to provide a thorough understanding and perspective on all of the potential uses of nutshell biomass for energy generation. We explore the latest advancements and current obstacles and possibilities for biomass materials in energy generation.



सत्यमेव जयते



प्रमाणपत्र सं. / Certificate No.:
LD-20250165064

प्रतिलिप्याधिकार कार्यालय, भारत सरकार | Copyright Office, Government Of India

प्रतिलिप्याधिकार प्रमाणपत्र | Copyright Certificate

प्रतिलिप्याधिकार नियम का नियम 70 | Rule 70 of The Copyright Rules

प्रतिलिप्याधिकार रजिस्टर से उद्धरण | Extracts from the Register of Copyrights

आवेदन सं. / Application No.: 40761/2024-CO/L दायित्व करने की तिथि/ Date of Filing: 23/12/2024

एतद्वारा यह प्रमाणित किया जाता है कि प्रतिलिप्याधिकार अधिनियम, 1957 के प्रावधानों के अनुसार, उपर्युक्त आवेदन में प्रकट किए गए "Synthesis And Characterization Of V2o5 By Various Route For Energy And Sensing Application" नामक कार्य के लिए प्रतिलिप्याधिकार प्रदान किया गया है।

This is to certify that a copyright has been registered for the work titled "Synthesis And Characterization Of V2o5 By Various Route For Energy And Sensing Application" as disclosed in the below mentioned application in accordance with the provisions of the Copyright Act, 1957.

रचयिता / Authors:

सं. / SNO. नाम / Name

पता / Address

1 Neetu Vishwakarma

Lovely Professional University Jalandhar
Delhi-Gt Road Phagwara Punjab-144411

2 Mukesh Kumar

Lovely Professional University Jalandhar
Delhi-Gt Road Phagwara Punjab-144411

3 Ajit Sharma

Lovely Professional University Jalandhar
Delhi-Gt Road Phagwara Punjab-144411

स्वामी / Owners:

सं. / SNO. नाम / Name

पता / Address

1 Lovely Professional University

Lovely Professional University Jalandhar
Delhi-Gt Road Phagwara Punjab-144411

प्रकाशक विवरण /

Publisher Details: N.A.

कार्य की भाषा / English

Language of

the Work:

कार्य का विवरण / N.A.

Description of

the Work:

(शर्तें/टिप्पणियाँ, N.A.

यदि कोई हो) /

(Conditions/

Remarks,

if any):

आर. ओ. सी. जारी होने की तिथि /

Date of ROC: 21/05/2025

Registrar of Copyrights

IIT Patna Best Presentation award





International Chemical Engineering Conference 2022

November 12-13, 2022

Department of Chemical and Biochemical Engineering, IIT Patna
In Association with IChE Patna Regional Centre



THIS CERTIFICATE IS PROUDLY PRESENTED FOR HONORABLE ACHIEVEMENT TO

Neetu Vishwakarma

For the best ORAL / POSTER PRESENTATION of the paper titled

Effect of Mechanochemical and Hydrothermal assisted synthesis on
electrochemical performance in V_2O_5 Based Nanomaterial
at IChEC 2022 held at Department of Chemical and Biochemical Engineering, IIT
Patna on 12 and 13 November, 2022

Dr. NITIN D. CHATURVEDI
Co-CONVENER, IChEC 2022

S. K. Samanta
12/11/2022
Dr. S. K. SAMANTA
CHAIRMAN Cum CONVENER,
IChEC 2022

Sushant Kumar
12.11.22
Dr. SUSHANT KUMAR
HOD, Dept. of Chemical &
Biochemical Eng.

CERTIFICATE

This is to certify that

Ms. Neetu Vishwakarma

Lovely Professional University, India

Delivered **Poster Presentation**

On

“Synthesis and Electrochemical characterization of Vanadium Oxide based Nanoparticles for Supercapacitor Application”

In the

International Conclave on Materials, Energy & Climate,

12 December to 14 December 2022

ONSITE - ONLINE LIVE

Onsite Venue

Indira Gandhi Delhi Technical University for Women, Delhi, India

Organized by



IAAM[®]
International Association of
Advanced Materials



Date:
14 December 2022

Place and Country
New Delhi, India

International Association of
Advanced Materials
Org. 802503-6784

Gammalkilsvägen 18
Ulrika 590 53, Sweden

Web : www.iaamonline.org
Tel. : (+46) 1313-2424
E-mail : contact@iaamonline.org



Secretary General